Regionale Wasserversorgung Basel-Landschaft 21

Trinkwasseraufbereitung Hardwald

Tony Merle, Minju Lee, Urs von Gunten

BASEL LANDSCHAFT

eawag aquatic research

Universität Basel

ETH zürich

EPFL ÉCOLE POLYTECHNIQUE FÉDÉRALE DE LAUSANNE

u^b UNIVERSITÄT BERN

Impressum

Teilprojekt 4: Trinkwasseraufbereitung Hardwald

Leitung:

Prof. Dr. Urs von Gunten, Eawag und EPFL
Dr. Wouter Pronk, Eawag
Thomas Meier,Hardwasser AG

Verfasser:

Dr. Tony Merle, Eawag
Dr. Minju Lee, EPFL
Prof. Dr. Urs von Gunten, Eawag und EPFL

In Zusammenarbeit mit:

Dr. Marc Bourgin, Emy Cretegny, Thomas Gabriel, Dr. Frederik Hammes, Prof. Dr. Juliane Hollender, Andreas Maccagnan, Patrick Messmer, Adrian Pulgarin, Dr. Judith Rothardt, Elisabeth Salhi, Heinz Singer, Brian Sinnet, Philippe Stolz, Bernadette Vogler

Titelbild:

Dr. Tony Merle

Projekt Regionale Wasserversorgung Basel-Landschaft 21

Gesamtprojektleitung:

Dr. Adrian Auckenthaler, Amt für Umweltschutz und Energie Basel-Landschaft
Prof. Dr. Urs von Gunten, Eawag und EPFL

Projektkoordination:

Dr. Paul Borer, Eawag
Dr. Sebastian Stoll, Eawag

Steuerungsgruppe:

Dr. Alberto Isenburg, Amt für Umweltschutz und Energie Basel-Landschaft
Dr. Tove Larsen, Eawag
Prof. Dr. Hansruedi Siegrist, Eawag
Dr. Peter Wenk, Amt für Lebensmittelsicherheit und Veterinärwesen

Begleitgruppe:

Dr. Richard Hürzeler, F. Hoffmann-La Roche AG
Dr. Kurt Rüegg, Energie Wasser Luzern und SVGW
Dr. Andreas Peter, Wasserversorgung Zürich
Dr. Michael Schärer, Bundesamt für Umwelt
Pierre Studer, Bundesamt für Lebensmittelsicherheit und Veterinärwesen

Liestal, Dübendorf, Oktober 2016

INHALTSVERZEICHNIS

1 Einführung 1

2 Micropollutant adsorption – RSSCT and kinetic experiments 2
2.1 Materials and methods 2
2.1.1 Feed water quality and spiked micropollutants 2
2.1.2 Activated carbon 3
2.1.3 Micropollutant analyses 5
2.1.4 Rapid Small-Scale Column Tests 5
2.1.4.1 Concept 5
2.1.4.2 Set-up 5
2.1.4.3 RSSCT data modeling using the software AdDesignS™ 7
2.1.5 Adsorption kinetics experiments with differing water qualities 10
2.1.5.1 Set-up 10
2.1.5.2 Data Analysis 10
2.2 Results and discussion 11
2.2.1 RSSCT 11
2.2.1.1 Micropollutant breakthrough for RSSCT 11
2.2.1.2 Comparison between RSSCT and full-scale data 15
2.2.2 Adsorption kinetics with powdered activated carbon (PAC) 15
2.2.2.1 Determination of pseudo first order rate constants and prediction of PAC dosage 15
2.2.2.2 Role of initial micropollutant concentrations in adsorption experiments 19
2.3 Practical significance of adsorption experiments 20
2.4 References 21

3 Evaluation of O_3/H_2O_2 and UV/H_2O_2 as additional treatment before or after the adsorption process - laboratory-scale experiments 23
3.1 Materials and methods 23
3.1.1 Feed water quality and spiked micropollutants 23
3.1.2 Set-up 24
3.1.2.1 O_3/H_2O_2 24
3.1.2.2 UV/H_2O_2 24
3.1.3 Analytical methods 24
3.2 Results and discussion 25
3.2.1 Abatement of pCBA using O_3/H_2O_2 or UV/H_2O_2 treatment 25
3.2.2 Application of O_3/H_2O_2 treatment for the removal of five selected micropollutants and the formation of transformation products 26
3.2.2.1 Determination of the ozone doses required to remove 50, 80 and 90% of the five selected micropollutants 26
3.2.2.2 Formation of transformation products for an abatement of parent compounds of 50% and 90% 28
3.3 Practical significance of oxidation experiments 33
3.4 References 34

4 Abatement of polychoro-1,3-butadienes in aqueous solution by ozone, UV-photolysis, and advanced oxidation processes 36
4.1 Materials and methods 37
4.1.1 Standards and reagents 37
4.1.2 Analytical methods 37
4.1.3 Determination of second-order rate constants for the reactions of CBDs with ozone (k_{O3}) and hydroxyl radicals ($k_{\bullet OH}$) 37
4.1.4 Quantum chemical computations for the prediction of k_{O3} of CBDs 38
4.1.5 Kinetic modeling 38

4.2 Results and discussion 39
4.2.1 Kinetics of the reactions of CBDs with ozone ($k_{O3,exp}$) 39
4.2.2 Prediction of rate constants for the reactions of CBDs with ozone ($k_{O3,pred}$) 39
4.2.3 Kinetics for the reaction of CBDs with hydroxyl radical ($k_{\bullet OH}$) 41
4.2.4 Determination of fluence-based first-order rate constants (k'), molar absorption coefficients (ε), and quantum yields (Φ) 41
4.2.4.1 Fluence-based first-order rate constants (k') and photoisomerization processes. 41
4.2.4.2 Molar absorption coefficients (ε). 43
4.2.4.3 Quantum yields (Φ). 43
4.2.5 Abatement of CBDs and micropollutants and bromate formation in a natural groundwater during ozonation, direct UV photolysis, and the AOPs O_3/H_2O_2 and UV/H_2O_2 43
4.2.5.1 Ozonation and O_3/H_2O_2. 43
4.2.5.2 Direct UV photolysis and UV/H_2O_2. 44
4.2.6 Practical implications 45
4.3 References 46
4.4 Supporting information 49
4.5 References (supporting information) 59

5 Pilot-scale testing 61
5.1 Materials and methods 61
5.1.1 Description of the Pilot-plant 61
5.1.1.1 Long-term experiments 64
5.1.1.2 Short-term experiments 65
5.1.2 Analytical methods 66
5.1.2.1 Long-term experiments 66
5.1.2.2 Short-term experiments 66
5.2 Results and discussion 66
5.2.1 Long-term experiments with advanced oxidation processes as pre-treatment 66
5.2.1.1 Water qualities of Hardwald groundwater before and after advanced oxidation 66
5.2.1.2 Micropollutant abatement after AOPs 67
5.2.1.3 Adsorption of micropollutants with and without pre-oxidation treatment using small-scale columns in series 72
5.2.1.4 Adsorption of chlorobutadienes without pre-oxidation treatment using small-scale columns in series 76
5.2.1.5 Adsorption of dissolved organic carbon (DOC) with and without pre-oxidation treatment using small-scale columns in series 77
5.2.1.6 Elimination of H_2O_2 residual in the small-scale columns in series 78
5.2.2 Long-term experiments with advanced oxidation as post-treatment 78
5.2.3 Short-term experiments 79
5.2.3.1 Optimisation of the peroxone process (O_3/H_2O_2) 79
5.2.3.2 Optimisation of the UV/H_2O_2 process 85
5.2.3.3 Combination of AOPs and PAC adsorption to remove micropollutants 87
5.2.3.4 Formation of transformation products during AOP treatments 90
5.2.3.5 Adsorption of transformation products on PAC 104
5.2.3.6 Biodegradation of transformation products during sand filtration 105
5.3 References 105

6 A novel oxidation process for micropollutant abatemnet under minimal formation of bromate: O_3/H_2O_2/membrane 106
6.1 Materials and methods 106
6.1.1 O_3/H_2O_2 106
6.1.2 O_3/H_2O_2/membrane 106
6.2 Results and discussion 108

7 Comparison of the treatability of Hardwald groundwater and Rhine river water using AOPs 109
7.1 O_3/H_2O_2 109
7.2 UV/H_2O_2 110
7.3 O_3/H_2O_2/Membrane 110

1 EINFÜHRUNG

Das Trinkwasser aus dem Hardwald stammt aus infiltriertem Rheinwasser. Der Rhein in Basel führt ca. 70% des Wassers aus der Schweiz ab und damit auch rund 70% des gereinigten Abwassers. Im Rheinwasser ist somit eine Vielzahl von Spurenstoffen vorhanden, die im Trinkwasser unerwünscht sind. Die Bodenpassage und der vorhandene Aktivkohlefilter, welcher aufgrund von historischen Belastungen mit Tetrachlorbutadienen installiert wurde, sind geeignet, eine grosse Anzahl an Substanzen aus dem Wasser zu entfernen. Jedoch kann eine Aktivkohlefiltration nicht alle möglichen vorhandenen Substanzen mit gleicher Effizienz zurückhalten, insbesondere bei längeren Laufzeiten. Im vorliegenden Projekt wurde untersucht wie gut die granulierten Aktivkohlefilter die Spurenstoffe zurückhalten und ob allenfalls eine vor oder nachgeschaltete Oxidation zu einer längeren Laufzeit je Spurenstoff und/oder einer besseren Entfernung einer breiten Palette von Spurenstoffen führen kann.

In diesem Teilprojekt wurden folgende Aspekte im Labor- und Pilotmassstab untersucht:

Labor:

- Prognose des Durchbruchs von 20 Substanzen für den Aktivkohlefilter im Hardwald mittels „Rapid Small Scale Column Tests (RSSCT)“
- Vergleich der Wasseraufbereitung mit Pulveraktivkohle und Oxidation für Hardwald Grundwasser und Rheinwasser
- Effizienz verschiedener Prozesse der weitergehenden Oxidation zum Abbau von polaren Spurenstoffen und Polychor-1,3-butadienen in Hardwald Grundwasser
- Entwicklung eines neuen Ozon-Membranverfahren zur weitergehenden Oxidation unter minimaler Bromatbildung (Hardwald Grundwasser, Rheinwasser)

Pilotanlage:

- Kurzzeitexperimente zum Abbau ausgewählter Spurenstoffe (inkl. Polychlor-1,3-butadiene) mit dem Ozon/Wasserstoffperoxid Prozess
- Kurzzeitexperimente zum Abbau ausgewählter Spurenstoffe (inkl. Polychlor-1,3-butadiene) mit dem UV/Wasserstoffperoxid Prozess
- Kurzeitexperimente zur Bildung von Transformationsprodukten für die Prozesse Ozon/ Wasserstoffperoxid und UV/Wasserstoffperoxid und die Kombination mit Pulveraktivkohle
- Langzeitexperimente zur Adsorption von Spurenstoffen an granulierter Aktivkohle und deren Vergleich mit der Aktivkohlefiltration in der Grossanlage
- Langzeitexperimente zum Abbau von iodierten Röntgenkontrastmitteln, künstlichen Süssstoffen, Pestiziden, Arzneimitteln und Industriechemikalien mit Prozessen der weitergehenden Oxidation (Ozon/Wasserstoffperoxid, UV/Wasserstoffperoxid) und deren Auswirkung auf die nachfolgende Filtration über granulierte Aktivkohle

2 MICROPOLLUTANT ADSORPTION – RSSCT AND KINETIC EXPERIMENTS

The understanding of the Hardwasser full-scale granular activated carbon (GAC) filters is a crucial point to decide whether or not an improvement of the current drinking water treatment strategy is necessary. The efficiency of GAC filters can be tested by small-scale adsorption set-ups, namely "Rapid Small Scale Column Tests (RSSCT)", considering the full-scale hydraulic conditions. The advantage of RSSCT is its capability to accelerate the adsorption process and predict in advance the performances of real GAC filters.

*The first part of this chapter aimed to compare the **RSSCT data with the full-scale data** recorded between January 2014 and March 2016. From these results, a **prediction of the full-scale GAC filter performance** was estimated until 2020. The results were extracted from the master theses of Philippe Stolz (2014) and Emy Cretegny (2015).*

*In the second part, **kinetic adsorption experiments** were performed with powdered activated carbon (PAC) to compare the adsorption **performances** when treating **Rhine river water before and after sand filtration** and **Hardwald groundwater**. Philippe Stolz performed the corresponding modeling during his master project.*

2.1 MATERIALS AND METHODS

2.1.1 FEED WATER QUALITY AND SPIKED MICROPOLLUTANTS

For RSSCT, Hardwald groundwater (HGW) was collected at least once per month at the Hardwasser drinking water treatment plant located in the Hardwald forest near Basel (**Fig. 2.1**) before the full-scale GAC filters. Water containers were stored at 4°C without any pre-filtration prior to use.

Some of the spiked 20 compounds are weakly soluble in water and for this reason micropollutant stock solutions were prepared in ethanol. However, ethanol is an organic compound leading to adsorption competition with the target compounds and microbial growth. Therefore, prior to the mixing with Hardwald groundwater, micropollutant stock solutions were placed in a 1 L amber glass bottle with a large opening and placed at ambient temperature during 24 hours to evaporate the ethanol. Afterwards, approximately 1 L of Hardwald groundwater was added to the amber bottle and stirred during 30 minutes to dissolve the micropollutant, which was crystallized inside the bottle. The solution was weighed and added to a 25 L glass bottle, which was cleaned with nanopure water beforehand. The amber glass bottle was flushed several times with Hardwald groundwater and then poured in the 25 L glass bottle until the RSSCT feed solution reached 20 kg. The solution was stored at 4 °C and used within 10 days.

Fig. 2.1: *Location of the Hardwasser drinking water plant in the Hardwald forest.*

Tab. 2.1: *Characteristics of the 20 compounds spiked to Hardwald groundwater (HGW), Rhine river water (RRW) and Rhine river water after sand filtration (SFW) for RSSCT and adsorption kinetic tests.*

			Concentrations (ng/L)			
			RSSCT	Kinetic experiments (KE)		
Compound	**Log D (@ pH 8)[(1)]**	**MW (g/mol)**	**HGW**	**HGW**	**RRW**	**SFW**
Iohexol	-1.95	821.14	3208 ± 367	3418	3469	3789
Iomeprol	-1.45	777.09	3342 ± 282	3745	3697	4031
Iopamidol	-0.74	777.09	3274 ± 303	3468	3351	4208
Diatrizoate	-0.63	613.91	3345 ± 414	3494	3338	3766
Iopromide	-0.45	791.11	3252 ± 285	3266	3244	3972
Sucralose	-0.47	397.63	350 ± 42	n.a.	n.a.	n.a.
Deisopropylatrazine	1.12	173.60	51 ± 6	57	52	51
Desethylatrazine	1.54	187.63	48 ± 7	57	56	51
Simazine	1.78	201.66	32 ± 16	52	65	55
2,6-Dichlorobenzamide	2.03	190.03	57 ± 8	54	57	58
Atrazine	2.20	215.68	49 ± 9	54	64	56
Diuron	2.53	233.09	51 ± 6	51	61	60
Metolachlor	3.45	283.79	55 ± 20	52	56	52
Atenolol	-1.24	266.43	51 ± 14	57	n.a.	n.a.
Sulfamethoxazole	-0.11	253.28	59 ± 11	71	55	51
Metoprolol	0.09	267.36	76 ± 30	56	55	61
Diclofenac	0.85	296.15	52 ± 12	55	69	70
Carbamazepine	2.77	236.27	60 ± 15	54	62	59
Benzotriazole	1.21	119.12	267 ± 35	267	448	389
5-Methylbenzotriazole	1.76	133.15	303 ± 34	311	397	434

[(1)] calculated with the software *MarvinSketch.*

Tab. 2.2: *Water quality parameters for Hardwald groundwater (HGW), Rhine River Water (RRW) and Sand Filtered Water Rhine River Water (SFW) used for RSSCT and kinetic experiments (KE).*

Parameter	**HGW_RSSCT**	**HGW_KE**	**RRW_KE**	**SFW_KE**
pH	8.05 +/- 0.10	8.09	7.92	7.94
DOC (mgC/L)	0.49 +/- 0.07	0.50	1.62	1.56

For adsorption kinetic tests, the HGW quality was the same as for RSSCT. Rhine river water (RRW) and Rhine river water after sand filtration (SFW) were sampled at the Hardwasser water treatment plant in Pratteln. Waters were stored at 4°C and used for the experiments within two weeks. As shown in **Tab. 2.2**, the main difference in terms of water quality was the DOC concentration, which was at least 3 times higher for RRW and SFW than for HGW.

2.1.2 ACTIVATED CARBON

The activated carbon used for the tests is the bituminous coal Calgon Filtrasorb® 400 (F400) provided by Chemviron Carbon Corporation and activated by steam. Its surface area is 1050 m^2/g (i.e., an average value for activated carbon) and the porosity is distributed between mesopores and micropores (**Tab. 2.3**). This adsorbent is the same as currently utilized at the Hardwasser treatment plant.

Tab. 2.3: *Physical properties of the Calgon F400 granular activated carbon.*

Parameter	Value
Mean Particle Diameter (µm)	1'000
Apparent Density (kg/m^3)	440-540
BET Surface Area (m^2/g)	1'050
DFT Micropore Volume (0-2 nm) (cm^3/g)	0.382
DFT Mesopore Volume (2-36 nm) (cm^3/g)	0.203

For RSSCT, the granular adsorbent was crushed with a mortar and pestle and the fraction between 63 and 100 µm was collected with sieves. Then, the activated carbon was washed with nanopure water to ensure the removal of fine particles and dried at 105°C.

The particle size distribution was determined with a Mastersizer 2000 instrument and the average size was 94.3 µm (**Fig. 2.2**).

For the adsorption kinetics with PAC, the fraction below 63 µm was selected and used without any cleaning. A slurry of 10 g/L PAC was prepared in nanopure water prior to performing the tests.

According to Patni et al. (2008), the grinding of GAC to lower particle diameters does not change its adsorptive characteristics. This implies that the physical and chemical properties of activated carbon do not vary within the particles.

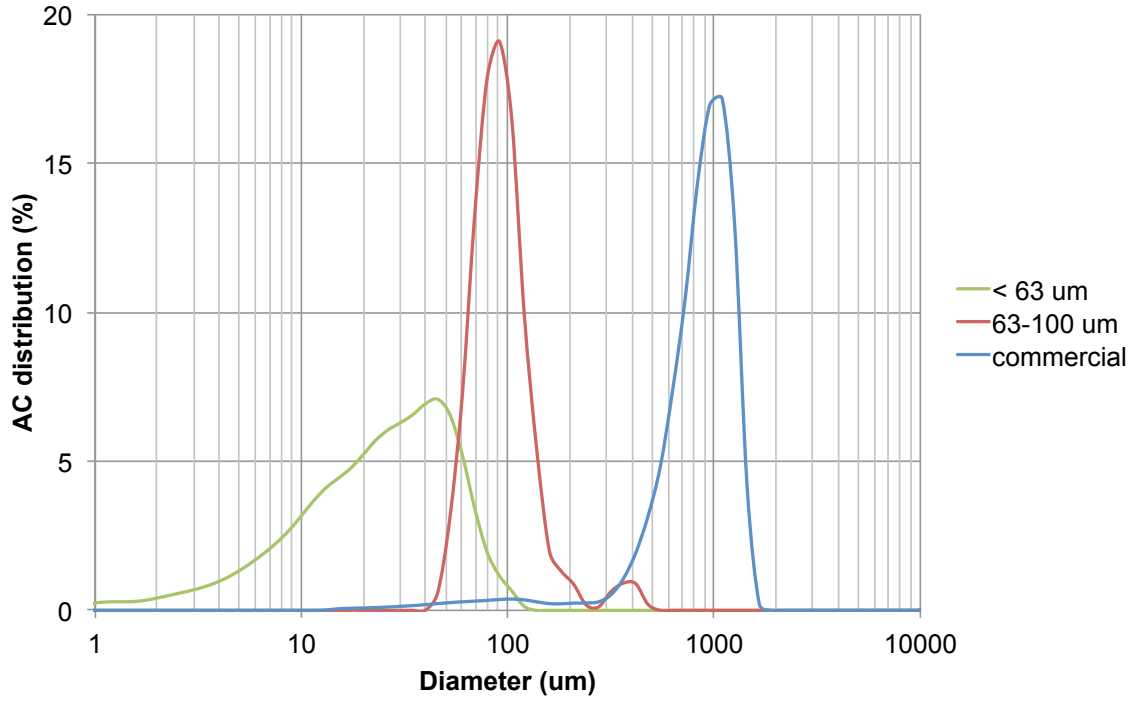

Fig. 2.2: *Particule size distribution of Calgon F-400 granular activated carbon and powdered activated carbon (after crushing and sieving). The commercial activated carbon particles were grinded and segregated with two sieves. The green curve represents the fraction below < 63 µm, the red one represents the fraction between 63 and 100 µm and the blue curve is the particle size disctribution of the non-grinded activated carbon.*

2.1.3 MICROPOLLUTANT ANALYSES

The 20 micropollutants were quantified by a fully automated online solid phase extraction/liquid chromatography/mass spectrometry (online SPE/LC/MS/MS). In a first step, 20 mL of a sample was loaded with a solution of acidic nanopure water (0.1 % formic acid) on a 2-layer extraction cartridge made of 8 mg OASIS HLB (15 µm, Waters) and 14 mg Isolute ENV+ (70 µm, Biotage). The separation was performed at ambient temperature using an Atlantis T3 column (3.0 x 150 mm, 3 µm particle size) with a HPLC gradient containing acidic nanopure water (0.1% formic acid) and methanol. The detection was performed with a Thermo TSQ-Vantage equipped with an electrospray ionization probe (ESI).

Calibration curves were established with standards prepared in Milli-Q water. The concentrations of standards ranged from 1 to 1000 ng/L for industrial compounds, pharmaceuticals and pesticides. For the X-ray contrast agents the concentrations were ten times higher, because of lower sensitivity of the analytical method for this class of compounds. The calibration standards were analyzed at the beginning and at the end of the sequence to check a potential drift of the analytical instrument. Every ten samples, a blank containing only the internal standards and a blank sample were analyzed to control a possible cross-contamination.

2.1.4 RAPID SMALL-SCALE COLUMN TESTS

2.1.4.1 CONCEPT

The concept of Rapid Small-Scale Column Tests was developed by Crittenden in 1986 to quickly assess the lifetime and effectiveness of GAC at laboratory-scale. RSSCT presents three main advantages: (i) it is completed in a fraction of the time required for full-scale filters, (ii) no additional isotherms or kinetic studies are necessary to predict the performance of a full-scale filter and (iii) it does not require large amounts of water. Nevertheless, it does not reflect long-term filtration at full-scale if the organic content is too high. Furthermore, it is difficult to model the biological removal of micropollutants and the effect of seasonal trends.

Two RSSCT design approaches are commonly used: the constant diffusivity (CD-RSSCT) approach and the proportional diffusivity (PD-RSSCT) approach (Crittenden et al., 2005). The CD-RSSCT is applied when the concentrations of target compounds are high with a low background of natural organic matter (NOM), whereas the PD-RSSCT simulates the removal of small micropollutant concentrations in presence of a substantial amount of NOM. The PD-RSSCT approach was used in this study since the micropollutants are present in water at ng/L levels. For PD-RSSCT, intra-particle diffusivity is assumed to be directly proportional to the size of GAC particles and the empty bed contact time in the small column ($EBCT_{SC}$) was calculated by Equation 1.

$$EBCT_{SC} = EBCT_{LC} \times \frac{d_{p,SC}}{d_{p,LC}} \qquad \textit{Equation 1}$$

with $EBCT_{SC}$ the empty bed contact time for the small column (min), $EBCT_{LC}$ the empty bed contact time for the large column (min), $d_{p,SC}$ the particle diameter for the small column (µm) and $d_{p,LC}$ the particle diameter for the large column (µm).

As a second condition, the ratio between the diameter of the small column (D_{SC}) and $d_{p,LC}$ must be higher than 10.

2.1.4.2 SET-UP

The set-up presented in **Fig. 2.3** ran from January 2014 to March 2016 at 12°C (i.e., temperature close to the Hardwald groundwater) under exclusion of light to avoid photodegradation of micropollutants and the development of algae. The experimental conditions are presented in

Tab. ***2.4***.

The RSSCT feed solution was kept in a 25 L glass bottle (1) equipped on the top with a glass tube containing GAC (2) to avoid any pollution from the outside air. This solution was injected with a HPLC pump (3) at a flow rate of 3.1 mL/min into two columns (6) and (7) assembled in series and filled with 3 g of crushed GAC (i.e., average particle size of 94.3 µm). A pressure gauge was connected after the pump (4) to make sure that the pressure does not exceed 3.5 bar, which is the maximum pressure allowed in the columns. Moreover, a relief valve (5) was installed as an additional security to protect the columns against overpressure. The treated water was collected in a tank (8).

As shown in **Fig. 2.3**, three sampling points were selected. The inlet point (A) was directly after the HPLC pump, an intermediate sampling point (B) between the two columns and one sampling point (C) after the second column to quantify micropollutant concentration after treatment. The intermediate point was useful to understand whether or not the micropollutant adsorption is proportional to the column length.

Twice a week, the flow rate and pressure were monitored. At the same time, samples at the inlet, intermediate and outlet sampling points were collected in glass beakers. A glass bottle of 250 mL was filled with 50.0 g of the sample and immediately spiked with 50 µL of an internal standard solution. These samples were frozen at -20 °C prior to analyses of the micropollutants.

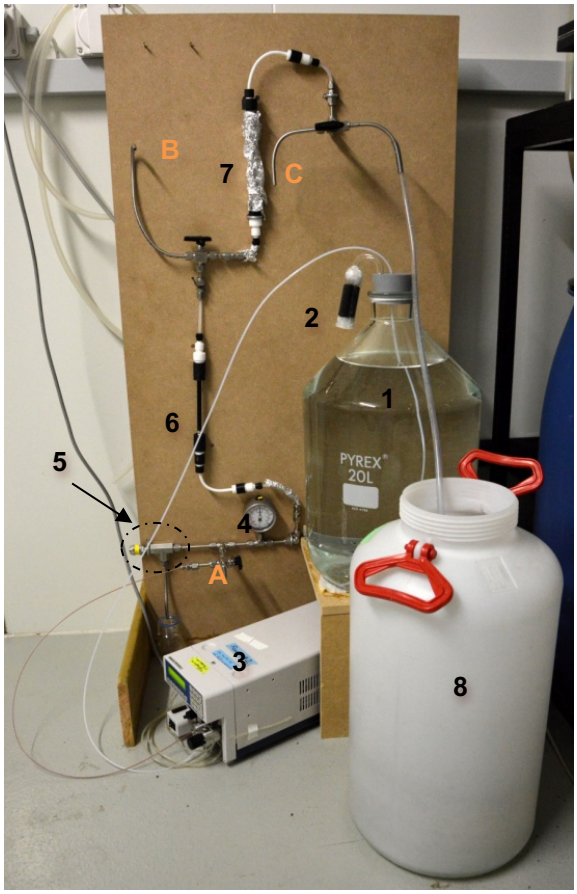

Fig. 2.3: *Experimental set-up of RSSCT – (A) Inlet, (B) Intermediate and (C) outlet sampling points – (1) 25 L glass bottle containing the feed solution, (2) glass tube containing GAC to avoid the contamination of the feed solution with volatile organic compounds, (3) HPLC pump feeding the RSSCT, (4) pressure gauge connected to a (5) relief valve to keep the pressure below 3.5 bar, (6) and (7) GAC columns and (8) dumping tank.*

Tab. 2.4: *Operating parameters of RSSCT and full-scale filters*

Parameters	RSSCT	Full-scale
GAC particle size diameter - d_p (µm)	94.3	1100
Weight of GAC (g)	3.31	80 x 10^6
Filter dimension (cm)	25.8 x 0.6 (D x d)	1350 x 525 x 250 (L x W x D)
Hydraulic loading rate (m/h)	6.6 (+/- 0.2)	7.7 (+/- 1.6)
Empty Bed Contact Time - EBCT (min)	2.3 (+/- 0.1)	19.5 (+/- 4.1)
Flow rate (mL/min)	3.2 (+/- 0.1)	32.7 (+/- 6.8) x 10^6
Experiment duration (days)	700	800*

* Duration of data collection in full-scale filter

2.1.4.3 RSSCT DATA MODELING USING THE SOFTWARE ADDESIGNS™

The software "Adsorption Design Software" (AdDesignS^{TM}) was developed by the Michigan Technology University to evaluate fixed-bed adsorption processes for the removal of contaminants from air and water. It can calculate the breakthrough parameters and predict the behavior of micropollutants at a larger scale. AdDesignS^{TM} includes three models: Equilibrium Column Model (ECM), Constant Pattern Homogeneous Surface Diffusion Model (CPHSDM) and Pore and Surface Diffusion Model (PSDM).

The ECM is designed for a step-increase in influent concentration (Crittenden et al., 1991). This model uses the Ideal Adsorb Solution Theory (IAST) to predict competitive adsorption effects in multi-component mixtures. It can be used to determine the elution order of the adsorbing compounds. The CPHSDM model is used for single compounds, which can be represented by the Freundlich isotherm equation.

The PSDM model is a dynamic fixed-bed model that incorporates various mechanisms (Crittenden et al., 1991). For instance, the flow rate should be constant and the adsorption of individual compounds is represented by a Freundlich isotherm equation. In PSDM, both pore and surface diffusion can contribute to the diffusive adsorbate flux inside a GAC particle. This model was chosen to model the results obtained with the RSSCT.

AdDesignS^{TM} contains the chemical and physical properties of many compounds and commercial activated carbon. The GAC (i.e., Calgon F-400) used in this study was included and all required informations are reported in **Tab. 2.5**.

First, the Freundlich coefficients K and 1/n were specified. An initial value of K was estimated by calculating the apparent Freundlich capacity parameter (K*) according to

$$K^* = \frac{BV_{50\%}}{\rho_{app}} \qquad \textit{Equation 2}$$

with K being the Freundlich capacity parameter, BV50% the breakthrough at 50% determined visually with RSSCT data and ρ_{app} the GAC apparent bed density.*

The coefficient 1/n was set equal to 1 because natural organic matter was present in the system and target compounds occur at low concentrations. The K value was optimized depending on the fitting

between model and experimental data (**Fig. 2.4**a). When K < K*, the breakthrough curves occur faster but the curve shape does not significantly change whereas it occurs more slowly when K > K*.

Secondly, two parameters can be adjusted to improve the slope fitting between the model and the experimental data. These two parameters are the tortuosity (τ) and the Surface-To-Pore Diffusion Flux Ratio (SPDFR) (**Fig. 2.4**b and c). The tortuosity factor is defined as the ratio of the real capillary length to the idealized straight capillary length. A tortuosity value of 1 corresponds to the maximum pore diffusion flux. A higher tortuosity value means that the diffusive path length increases and the pore diffusion flux decreases. Consequently, the duration of the breakthrough is much longer since the path to reach the middle of the particle is farther. The SPDFR coefficient is a ratio between the surface and the pore diffusion. The minimal SPDFR value can be set to 10^{-30}, which corresponds to an insignificant surface diffusion. If the tortuosity value increases, the slope decreases. If the model is too flat for a tortuosity of 1, the SPDFR value can be increased involving surface diffusion in addition of the pore diffusion.

Fouling induced by the presence of NOM should be also considered since it reduces the adsorption capacity of the adsorbent. Indeed, Corwin and Summers (2010) hypothesized that pore blockage and adsorption competition are the two main factors responsible for the decrease of the GAC efficiency. Therefore, they proposed to correct RSSCT data taking into account a fouling index linked to the scaling factor according to Equation 3:

$$FI = \frac{d_{p,SC}}{d_{p,LC}}^{Y} = SF^{Y} \qquad \textit{Equation 3}$$

with FI being the fouling index, SF the scaling factor and Y the fouling factor.

Hence, to compare full-scale and RSSCT data, the modeled breakthrough curves were divided by the fouling index and the full-scale filter performances were calculated until 2020.

Tab. 2.5: *Liquid, fixed bed and adsorbent properties used to model the intermediate and outlet points with AdDesignS™*

	Parameter	**Value**
Liquid properties	Pressure (atm)	2.5
	Temperature (°C)	12.0
Fixed bed properties	Bed length (intermediate/outlet) (cm)	12.9 / 25.8
	Bed diameter (cm)	0.6
	Adsorbent weight (g)	1.5/ 3.0
	Flow rate (mL/min)	3.2
Adsorbent properties	Name	Calgon F400 (12 x 40)
	Apparent Density (g/mL)	0.803
	Particle radius (m)	4.70×10^{-5}
	Porosity	0.641
	Particle shape factor	1.00
Simulation parameters	Total run time (intermediate/outlet) (d)	399 / 590
	First point displayed (d)	6.94×10^{-8}
	Time steps (intermediate/outlet) (d)	1.0 / 1.5
	Number of axial elements	10

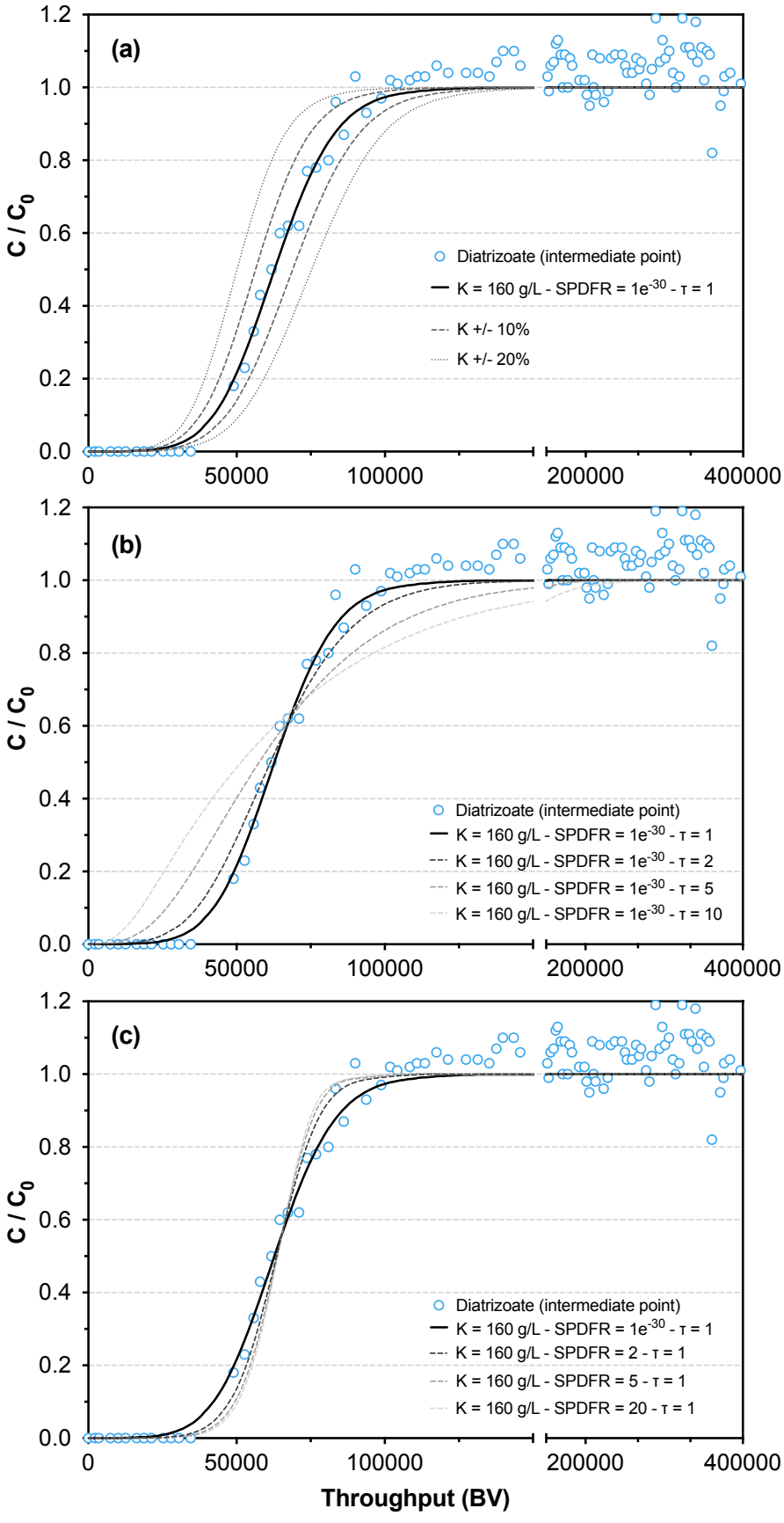
(a)
C / C0
Diatrizoate (intermediate point)
K = 160 g/L - SPDFR = 1e-30 - τ = 1
K +/- 10%
K +/- 20%
(b)
C / C0
Diatrizoate (intermediate point)
K = 160 g/L - SPDFR = 1e-30 - τ = 1
K = 160 g/L - SPDFR = 1e-30 - τ = 2
K = 160 g/L - SPDFR = 1e-30 - τ = 5
K = 160 g/L - SPDFR = 1e-30 - τ = 10
(c)
C / C0
Diatrizoate (intermediate point)
K = 160 g/L - SPDFR = 1e-30 - τ = 1
K = 160 g/L - SPDFR = 2 - τ = 1
K = 160 g/L - SPDFR = 5 - τ = 1
K = 160 g/L - SPDFR = 20 - τ = 1
0.0
0.2
0.4
0.6
0.8
1.0
1.2
0
50000
100000
200000
400000
Throughput (BV)

Fig. 2.4: *Experimental and modeled (AdDesignS^{TM}) breakthrough of diatrizoate at the intermediate sampling point of the RSSCT. Variation effects of (a) the Freundlich coefficient K, (b) tortuosity τ and (c) the Surface-to-Pore Diffusion Ratio SPDFR values on the breakthrough curve prediction of diatrizoate.*

2.1.5 ADSORPTION KINETICS EXPERIMENTS WITH DIFFERING WATER QUALITIES

2.1.5.1 SET-UP

Batch experiments were performed to investigate the adsorption kinetics of micropollutants onto powdered activated carbon (PAC) with Rhine river water (RRW), Rhine river water after sand filtration (SFW) and Hardwald groundwater (HGW). These experiments were carried out in a climate chamber at 12 °C. Glass bottles with Teflon-coated lids were filled with 1 L of water spiked with micropollutants (see section 2.1.1 for the preparation). A blank sample of this solution was taken for the quantification of the initial concentrations of micropollutants.

At the beginning of the experiments, differing volumes of a PAC slurry (10 g/L PAC in nanopure water) were added to the solutions to obtain PAC doses of 1, 5, 10, 20, and 50 mg/L. The bottles were then placed on a shaker at 180 rpm, which was sufficient to keep the PAC suspended. Samples were taken at pre-defined time steps, ranging from 2 min to 24 h. A solution volume of about 80 mL was poured in a glass beaker at every sampling time and was then immediately filtered through a 60 mL plastic syringe equipped with a 0.45 µm regenerated cellulose filter to remove the PAC. The filters were washed with deionised water before the experiments and a new filter was used for each sample. The syringe was rinsed with deionised water between the samples. Two distinct samples were taken at every time step. First, exactly 50 mL of a sample was weighed in 250 mL glass bottles for the analyses of MP concentrations by online SPE-LC-MS/MS. These samples were immediately spiked with 50 µL of the internal standard solution containing the isotope-labelled micropollutants in ethanol. The samples were stored at -20°C in the dark prior to analyses.

Additional adsorption kinetics experiments were carried out to examine if the adsorption kinetics depends on the initial concentrations of the micropollutants. This question was important since the concentrations of the micropollutants spiked are significantly above the concentrations measured in Hardwald groundwater, particularly for the X-ray contrast media. For instance, the maximum concentration of iopamidol in Hardwald groundwater measured during this study was 170 ng/L whereas the spiked iopamidol concentration used in most adsorption experiments was about 3000 ng/L.

To investigate the influence of the initial concentration on the adsorption kinetics, solutions of Hardwald groundwater were prepared as described in section 2.1.1 but the concentrations of X-ray contrast agents were 300 ng/L and 1000 ng/L instead of 3000 ng/L. The concentrations of all other micropollutants were the same as usual. The PAC dosages used in this experiment were 10 and 50 mg/L. The experiment was conducted under the same conditions as described previously.

2.1.5.2 DATA ANALYSIS

The data obtained from the adsorption kinetics experiments were fitted to a first order kinetic model.

Since the PAC usually gets saturated with NOM and micropollutants after a certain period of time, only measurements up to 60 min after the start of the experiment were considered for the modelling. The first order adsorption rate constant, $k_{ads.}$, was determined from the regression of $\log(c/c_0)$ versus time (t), where c_0 is the initial concentration of the substance and c is the concentration of a substance at time t. A quadratic relationship was found between the pseudo first order rate constant k_{ads} and the PAC dose m_{PAC}:

$$k_{ads}=a\cdot m_{PAC}^2+b\cdot m_{PAC}+c \qquad \textit{Equation 4}$$

A 90 % removal of the micropollutants was assumed as the treatment goal. The first order adsorption rate constant required to meet this objective for a given contact time could be calculated by Equation 5:

$$k_{ads} = \frac{ln(\frac{C_0}{C})}{t} = \frac{ln(10)}{t} \qquad \textit{Equation 5}$$

The PAC dose required to remove 90 % of a micropollutant for a given contact time could then be determined by solving Equation 4 for m_{PAC}:

$$m_{PAC} = \frac{-b+\sqrt{b^2-4\cdot a\cdot(c-k_{ads})}}{2a} \qquad \textit{Equation 6}$$

Equation 5 and Equation 6 were solved for differing contact times between 0 and 90 min for all micropollutants.

2.2 RESULTS AND DISCUSSION

2.2.1 RSSCT

2.2.1.1 MICROPOLLUTANT BREAKTHROUGH FOR RSSCT

During the 2-year running time of RSSCT, a breakthrough was observed only for six compounds at the intermediate and outlet sampling points: the five X-ray contrast media (i.e. diatrizoate, iohexol, iomeprol, iopamidol and iopromide) and sucralose. This list of compounds was expected since they present both high molecular weights and low values of log D at pH 8. Indeed, compounds with high molecular weight would not be able to diffuse in the smaller pores of GAC particles. Moreover, a low value of log D induces a higher hydrophilicity and therefore, a lower affinity with GAC adsorption sites.

Fig. 2.5 and **Fig. 2.6** show the breakthrough curves determined with RSSCT for both the intermediate and outlet sampling points for the five X-ray contrast media and sucralose, respectively. Results for the full-scale filters are also added to the figures but only for diatrizoate, iopamidol and sucralose, because the other compounds were not detected in Hardwald groundwater. Moreover, RSSCT data were corrected taking into account the fouling index defined in section 2.1.4.3. A fouling index of 5 gave the best fitting. The X-ray contrast media broke through the GAC columns before sucralose in the following order, diatrizoate, iohexol, iomeprol, iopamidol, iopromide, which is consistent with the log D values, except for diatrizoate. Although diatrizoate is the smallest molecule and could potentially diffuse more easily inside the small micropores, it is also the only compound dissociated and negatively charged at pH 8 because of a pK_a of 2.2. Therefore, the adsorption of diatrizoate is expected to be weaker than other X-ray contrast media. The four other compounds are eluted according to their log D values.

Furthermore, the breakthrough curves are proportional to the bed length. The curves obtained for the intermediate point overlay with the ones at the outlet point. Even though this observation is less pronounced for sucralose, this finding shows that RSSCT could be shortened for further tests using a smaller GAC column.

In addition, six pesticides were detected and quantified after the intermediate sampling point. The breakthrough curves are presented in **Fig. 2.7** and the micropollutant elution was in the order 2,6-dichlorobenzamide, desethylatrazine, metolachlor, atrazine, deisopropylatrazine, simazine. Neither the molecular weight nor the log D values can explain this order but it might be a combination of these two parameters that leads to this observation.

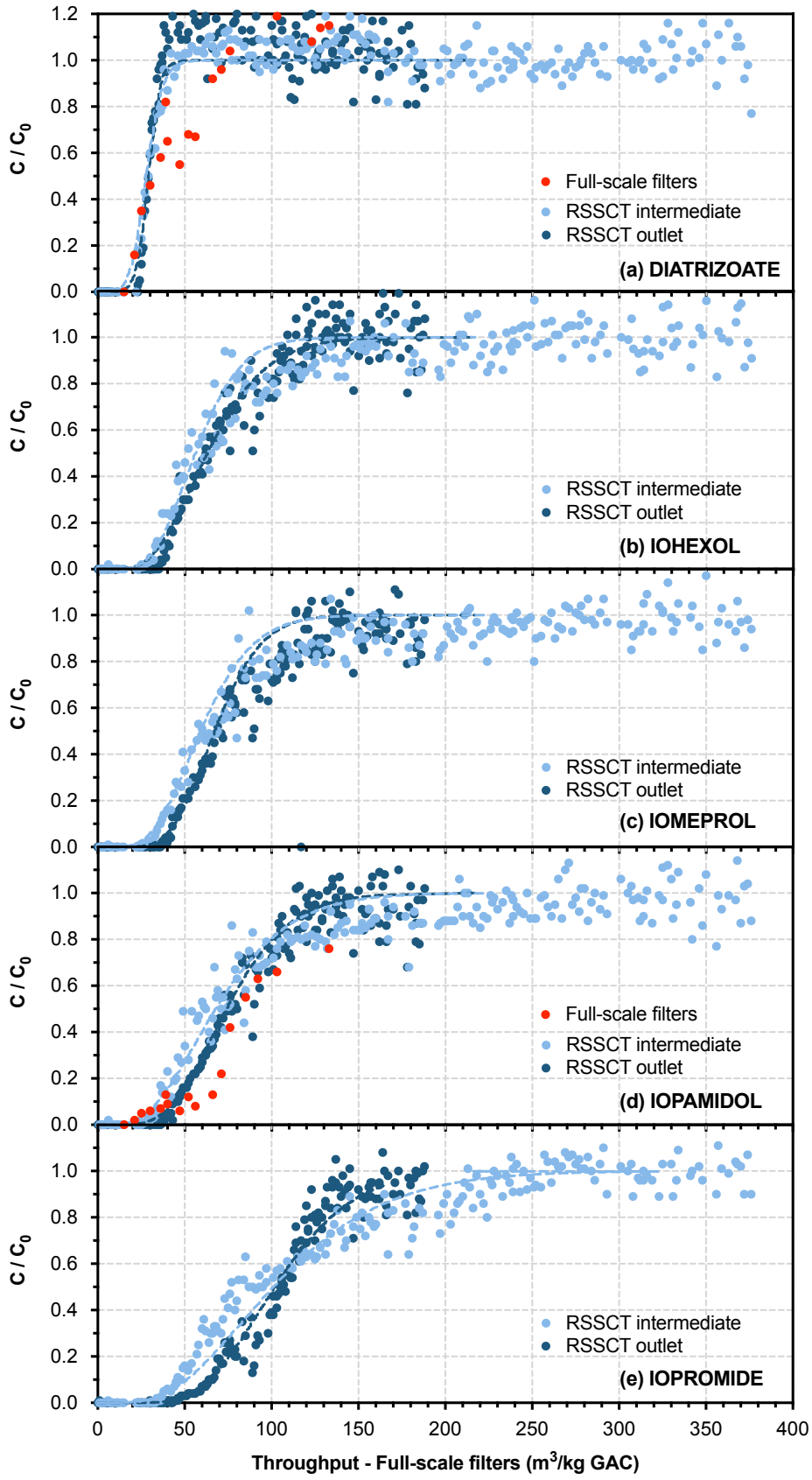

Fig. 2.5: *Breakthrough curves for five X-ray contrast media: (a) diatrizoate, (b) iohexol, (c) iomeprol, (d) iopamidol and (e) iopromide. RSSCT data were corrected with the Fouling Index to be comparable with the full-scale data set (light blue circles for intermediate, dark blue circles for outlet sampling point). Model prediction (dashed lines) are plotted for the intermediate and outlet points. The full-scale data are shown in red circles.*

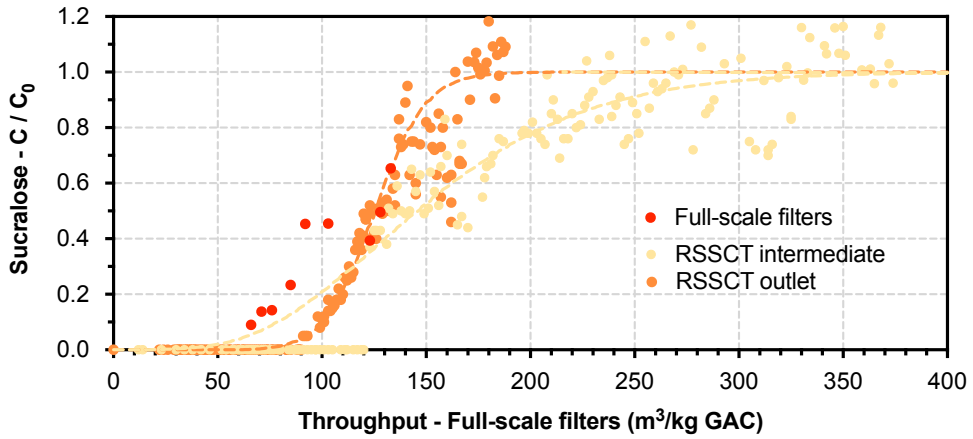

Fig. 2.6: *Breakthrough curves for sucralose. Corrected RSSCT data with fouling index (yellow circles for intermediate, orange circles for outlet sampling point) and model prediction (dashed lines) for the intermediate and outlet points. Full-scale data are shown in red circles.*

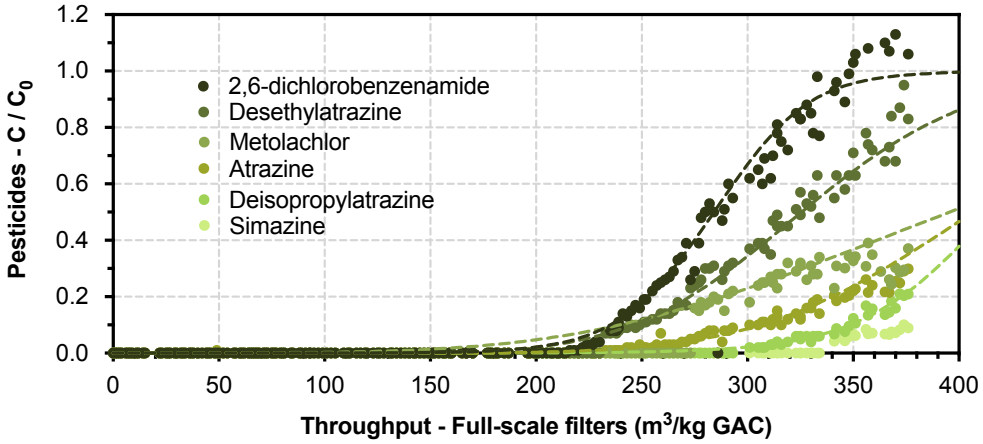

Fig. 2.7: *Breakthrough curves for the six selected pesticides at the intermediate sampling point. Corrected RSSCT data with fouling index and model prediction (dashed lines) for the intermediate sampling point.*

The breakthrough curves were modeled using the software AdDesignS™. The modeling was performed by using a throughput in bed volumes and the results were normalized to make a comparison between the intermediate and the outlet breakthrough curves. The SPDFR coefficient was set to 10^{-30} for all the micropollutants except for 2,6-dichlorobenzamide and deisopropropylatrazine. For some compounds such as iopromide, the prediction was not accurate for the entire breakthrough curve, but the area of interest is for c/c_0 values <0.5, which corresponds to the beginning of the breakthrough. Indeed, it is most important to know when the micropollutants will start to be released by the column.

The Freundlich coefficient (K), the SPDFR value and the porosity (τ) were extracted and are shown in **Tab. 2.6**. They were determined as explained in **Fig. 2.4**. Overall, the maximum difference for the K values for the intermediate and outlet sampling point was 19% for sucralose whereas a difference below 11% was observed for the X-ray contrast media. This confirms the proportionality between the adsorption phenomena and the length of the column. These results were used to make predictions for the breakthrough in the full-scale filter.

Tab. 2.6: *Modeling parameters calculated with AdDesignS™ for the intermediate and outlet sampling points.*

Molecule	K (L/g) (int./out.)[(1)]	SPDFR (int./out.)[(1)]	τ (int./out.)[(1)]
Diatrizoate	155 / 160	10^{-30} / 10^{-30}	1.0 / 1.0
Iohexol	320 / 340	10^{-30} / 10^{-30}	2.5 / 4.0
Iomeprol	340 / 380	10^{-30} / 10^{-30}	2.8 / 4.0
Iopamidol	360 / 410	10^{-30} / 10^{-30}	3.0 / 4.5
Iopromide	490 / 550	10^{-30} / 10^{-30}	4.0 / 4.0
Sucralose	850 / 690	10^{-30} / 10^{-30}	5.0 / 1.0
2,6-dichlorobenzamide	1560	5	1.0
Desethylatrazine	1800	10^{-30}	1.0
Metolachlor	2100	10^{-30}	2.0
Atrazine	2250	10^{-30}	1.0
Deisopropylatrazine	2275	10	1.0

[(1)]int.: intermediate; out.: outlet

To highlight the relationship between the molecular weights or log D values with the breakthrough curves, the K values at the intermediate sampling point were plotted against these two parameters (**Fig. 2.8**). The compounds with no available RSSCT data are presented in the zone at the righthand side of the dashed line. These compounds also need to be considered to get an overall picture. Based on these data, it appears that the breakthrough of micropollutants occurs faster when the molecular weight increases, due to a lack of pore accessibility, or when the log D value decreases (i.e., increase in hydrophilicity). However, it seems that molecular weights have a stronger influence on the micropollutant adsorption than the log D value because the molecules with a K value higher than 2400 L/g have a molecular weight around 200 g/mol whereas the log D value are widely spread between -1.24 for atenolol and 2.77 for carbamazepine

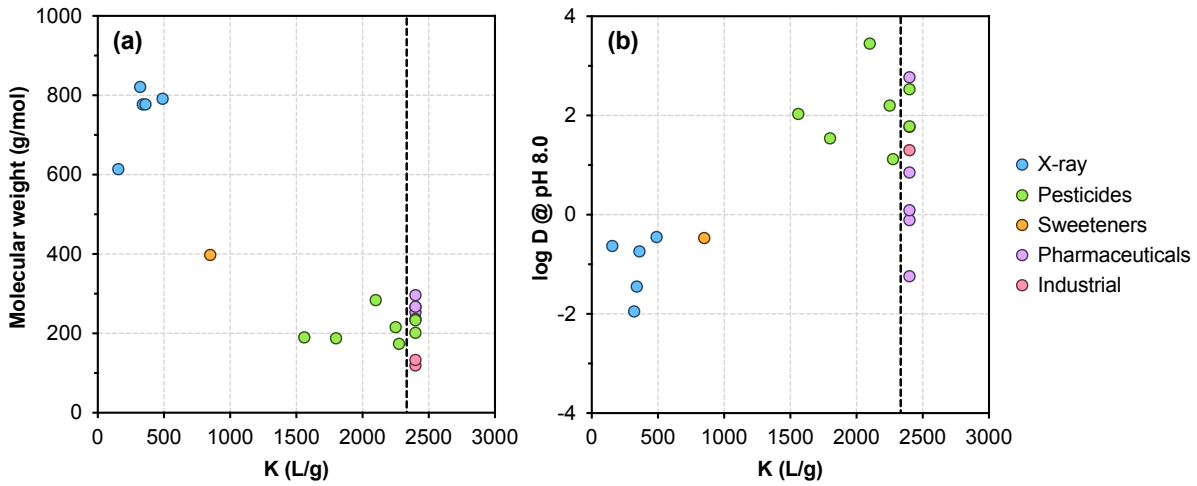

Fig. 2.8: *Relationship between (a) the molecular weight or (b) log D at pH 8.0 with the calculated Freundlich coefficient (K).*

2.2.1.2 COMPARISON BETWEEN RSSCT AND FULL-SCALE DATA

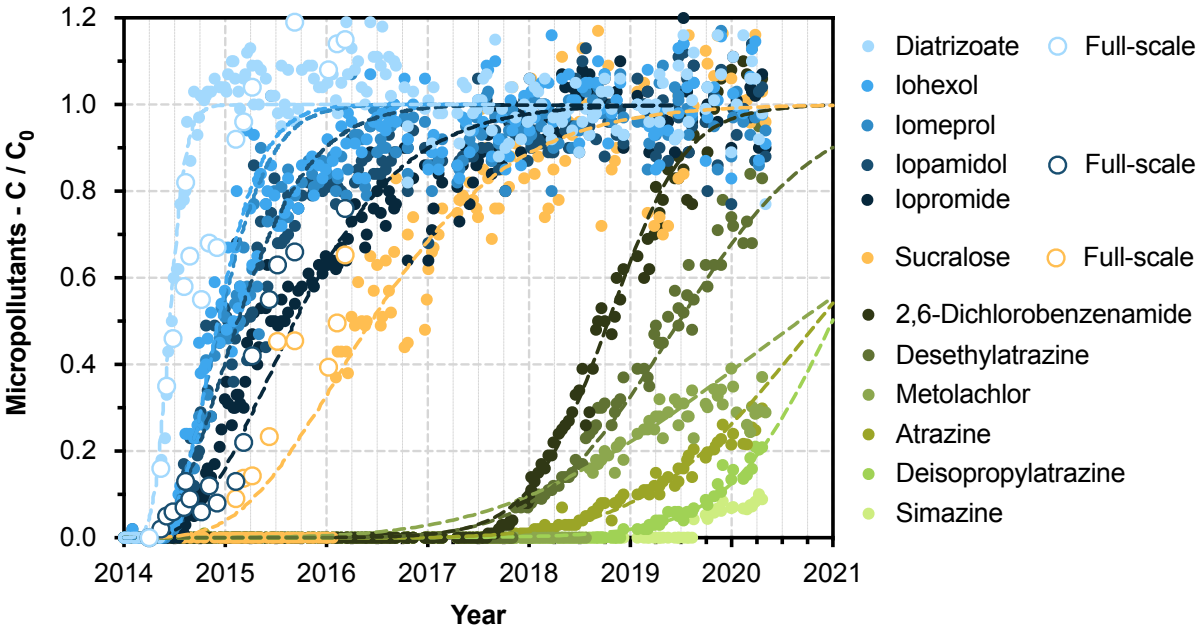

Fig. 2.9: *Comparison of the breakthrough prediction curves for 12 micropollutants determined with RSSCT for the period from 2014 to 2020 (filled circles) with the available full-scale data (open circles).*

In **Fig. 2.9**, RSSCT data at the intermediate sampling point and the corresponding modeled breakthrough curves are plotted as a function of time for 12 micropollutants. This time, the filter throughput was replaced by the treatment duration determined with the daily hydraulic rate provided by Hardwasser AG. According to this prediction, it appears that the retention of X-ray contrast media on the full-scale filters is less than 20% in June 2016 whereas the breakthrough of sucralose is 50% and all pesticides are retained on the filters. End of 2017, 2,6-dichlorobenzamide, desethylatrazine and metolachlor concentrations should be detected in the treated drinking water and the performances of the filters are expected to be good enough to adsorb more than 70% of atrazine, deisopropylatrazine and simazine at the beginning of 2020.

Unfortunately, it was not possible to integrate chlorobutadienes to the RSSCT experiments due to the difficulty to purchase these compounds, their high prize and their volatility. Nevertheless, some results will be discussed in section 5.2.1.3 for the pilot plant.

2.2.2 ADSORPTION KINETICS WITH POWDERED ACTIVATED CARBON (PAC)

2.2.2.1 DETERMINATION OF PSEUDO FIRST ORDER RATE CONSTANTS AND PREDICTION OF PAC DOSAGE

Adsorption kinetics were performed with the 18 micropollutants presented in **Tab. 2.1** and three water matrices (i.e., Hardwald groundwater (HGW), Rhine river water (RRW) and sand filtered water (SFW)). To simplify the discussion, three representative compounds out of the differing classes, namely atrazine, diclofenac, and iomeprol were selected but modeling for all compounds is presented in **Tab. 2.7**.

Fig. 2.10 shows the adsorption kinetics for the three compounds in Hardwald groundwater. At a PAC dosage of 50 mg/L, atrazine and diclofenac were completely adsorbed within 10 min but approximately 10 % of iomeprol is still present in solution after this time. The adsorption kinetics is much slower when 10 mg/L PAC are applied to Hardwald groundwater: 96 % and 91 % of atrazine and diclofenac are removed in the first 60 min of the experiment, respectively and up to 99% after 3 h. In the case of iomeprol, only 52 % are adsorbed within 60 min and 80 % after 3 h.

A first order kinetic model was fitted for the first 60 min. The correlation coefficients for the fitting were generally > 0.9, but it was lower for many X-ray contrast agents and for most of the substances at the lowest PAC concentration of 1 mg/L PAC because the amount of micropollutants adsorbed was very low. The first order kinetic model for iomeprol shows that the aqueous concentration tends to be overestimated at the beginning but underestimated after about 60 min. A more sophisticated model that considers the individual steps in the adsorption process would probably be able to better predict the adsorption kinetics of the different substances. The first order kinetic model only takes the transport of the micropollutant in the bulk solution and the diffusion through the boundary layer of the adsorbent particle into account. The intra-particle transport in the pores, which is often the rate-limiting step in the adsorption onto PAC (Summers et al., 2010), is inadequately considered in a simple first order approach.

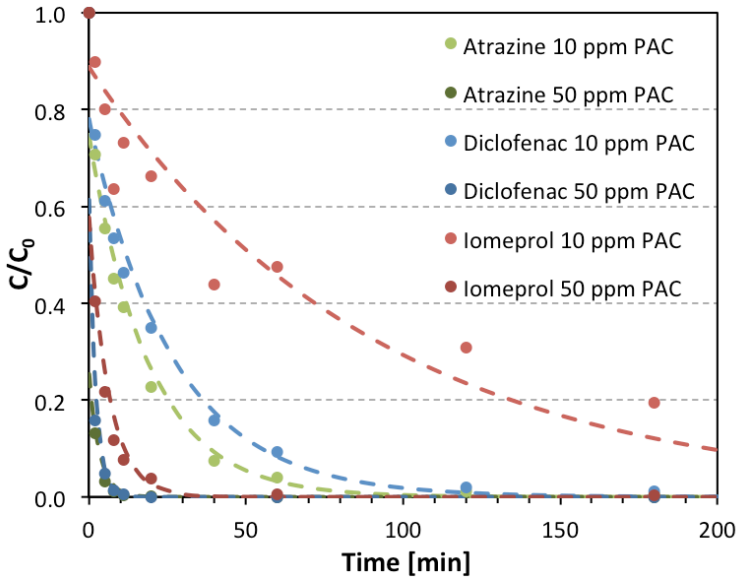

Fig. 2.10: *Adsorption kinetics of atrazine, diclofenac, and iomeprol in Hardwald groundwater for a PAC dosage of 10 and 50 mg/L – experimental data (circles) and first order kinetic modelling (dashed lines). T = 11 °C, $[atrazine]_0$ = 54 ng/L, $[diclofenac]_0$ = 55 ng/L, $[iomeprol]_0$ = 3745 ng/L.*

The first order adsorption rate constants of the micropollutants studied are summarized in **Tab. 2.6** for the three waters at PAC doses of 10 and 50 mg/L. When 10 mg/L PAC is applied to HGW, k_{ads} values are in the order of 10^{-3} s^{-1} for most pesticides, pharmaceuticals, and industrial chemicals, whereas they are approximately a factor of 4 lower for X-ray contrast agents. A PAC dosage of 50 mg/L generally results in an increase of k_{ads} by one order of magnitude. The first order adsorption rate constants are higher by up to a factor of 6.9 for the adsorption kinetics in HGW as compared to RRW. The only exception is metoprolol, which exhibits a similar k_{ads} in both waters. The data compiled in **Tab. 2.7** also show that adsorption kinetics vary only slightly between RRW and SFW, which was expected based on the small difference in the DOC concentration.

Tab. 2.7: *Kinetics of the adsorption of micropollutants on PAC. Pseudo first order rate constant (k_{ads}) for the adsorption of micropollutants on PAC in Hardwald groundwater (HGW), Rhine river water (RRW) and Rhine river water after sand filtration (SFW) for 10 and 50 mg/L PAC.*

		k_{ads} ($x10^3$ s^{-1})					
		10 mgPAC/L			50 mgPAC/L		
Compounds	**Log D[(1)]**	**HGW**	**RRW**	**SFW**	**HGW**	**RRW**	**SFW**
Iohexol	-1.95	0.20	0.10	0.08	2.36	0.55	0.52
Iomeprol	-1.45	0.20	0.16	0.09	2.70	0.69	0.60
Iopamidol	-0.74	0.30	0.11	0.10	2.51	0.54	0.60
Diatrizoate	-0.63	0.10	0.02	0.05	0.93	0.23	0.27
Iopromide	-0.45	0.27	0.08	0.09	2.56	0.56	0.68
Deisopropylatrazine	1.12	0.88	0.50	0.57	12.82	6.82	9.32
Desethylatrazine	1.54	0.77	0.40	0.42	9.20	4.71	5.36
Simazine	1.78	1.01	0.48	0.52	11.03	7.01	5.93
2,6-Dichlorobenzamide	2.03	0.93	0.38	0.40	9.39	5.65	6.79
Atrazine	2.20	0.89	0.35	0.39	7.37	4.85	4.96
Diuron	2.53	1.83	0.86	1.02	14.81	9.46	9.87
Metolachlor	3.45	0.87	0.27	0.28	8.28	4.48	1.07
Sulfamethoxazole	-0.11	0.39	0.11	0.16	8.02	1.86	1.48
Metoprolol	0.09	1.00	0.95	0.95	13.29	16.84	10.81
Diclofenac	0.85	0.62	0.15	0.22	8.69	1.70	1.88
Carbamazepine	2.77	1.06	0.51	0.53	10.55	6.78	5.88
Benzotriazole	1.21	1.04	0.71	0.98	18.39	8.28	9.01
5-Methylbenzotriazole	1.76	1.20	0.78	0.90	17.30	9.59	10.08

[(1)] calculated at pH 8 with the software *MarvinSketch.*

In practice, two main parameters can be changed to control the adsorption of micropollutants onto PAC: the PAC dose and the contact time. From the kinetic parameters presented here, a relationship between these two parameters for a micropollutant removal of 90% was established, which was assumed as the treatment objective in this study. **Fig. 2.11** shows the contact times and PAC doses required to achieve a 90% removal of micropollutants in HGW. The calculations are most reliable in the range of 0–60 min and for 1–50 mg/L PAC, for which the experiments were conducted and the regression was performed. These conditions are close to the operating conditions in practice, where the contact times are usually between 0.5 and 2 h and the PAC dosages ranges from 5 to 25 mg/L (Crittenden et al., 2005). In HGW, 90% of atrazine and diclofenac can be removed within 30 min with approximately 12 or 15 mg/L PAC, respectively. Under the same conditions, 33 mg/L PAC is required to adsorb 90% of iomeprol. Ridder et al. (2010) found that the equilibrium solid-phase concentration of a substance on activated carbon increases with increasing logD values. A reduced removal of iomeprol by PAC as compared to atrazine was therefore anticipated based on its low log D of -1.45.

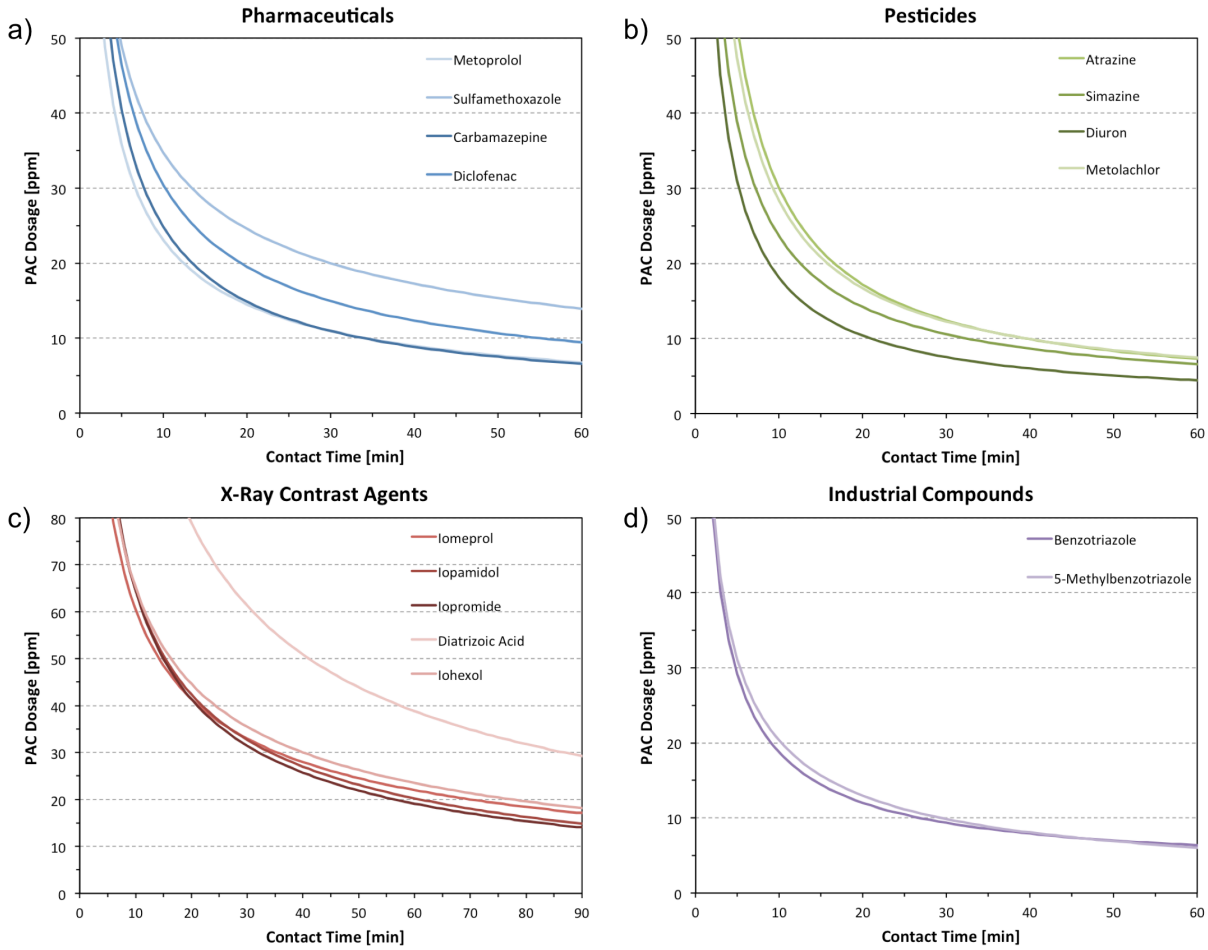

Fig. 2.11: *Relationships between PAC dose and contact time to remove 90% of (a) pharmaceuticals, (b) pesticides, (c) X-ray contrast agents, and (d) industrial compounds from Hardwald groundwater.*

Considering the removal of atrazine, diclofenac, and iomeprol in RRW, the contact time and PAC dose have to be increased considerably to adsorb 90 % of the substances compared to HGW (**Fig. 2.12**). Assuming a contact time of 60 min, the PAC dosage should be at least 16, 27, and 48 mg/L to achieve a 90 % removal of atrazine, diclofenac, and iomeprol, respectively. This suggests that the two substances are not equally affected by the differing NOM concentration and that the competition of NOM with diclofenac is stronger than with atrazine (Matsui, 2002).

In addition, the calculations demonstrate that the removal objective of 90 % can be achieved for all pesticides, pharmaceuticals, and industrial compounds considered if HGW is treated with 20 mg/L of PAC for a contact time of 30 min. When increasing the contact time to 60 min, a PAC dosage of 14 mg/L is sufficient to remove 90 % of the selected pesticides, pharmaceuticals, and industrial compounds. Higher PAC dosages and contact times are required to reach the treatment objective for X-ray contrast media, namely 36 and 24 mg/L PAC for a contact time of 30 and 60 min, respectively. Diatrizoate was not taken into account, because it would lead to a considerable increase of these operating parameters.

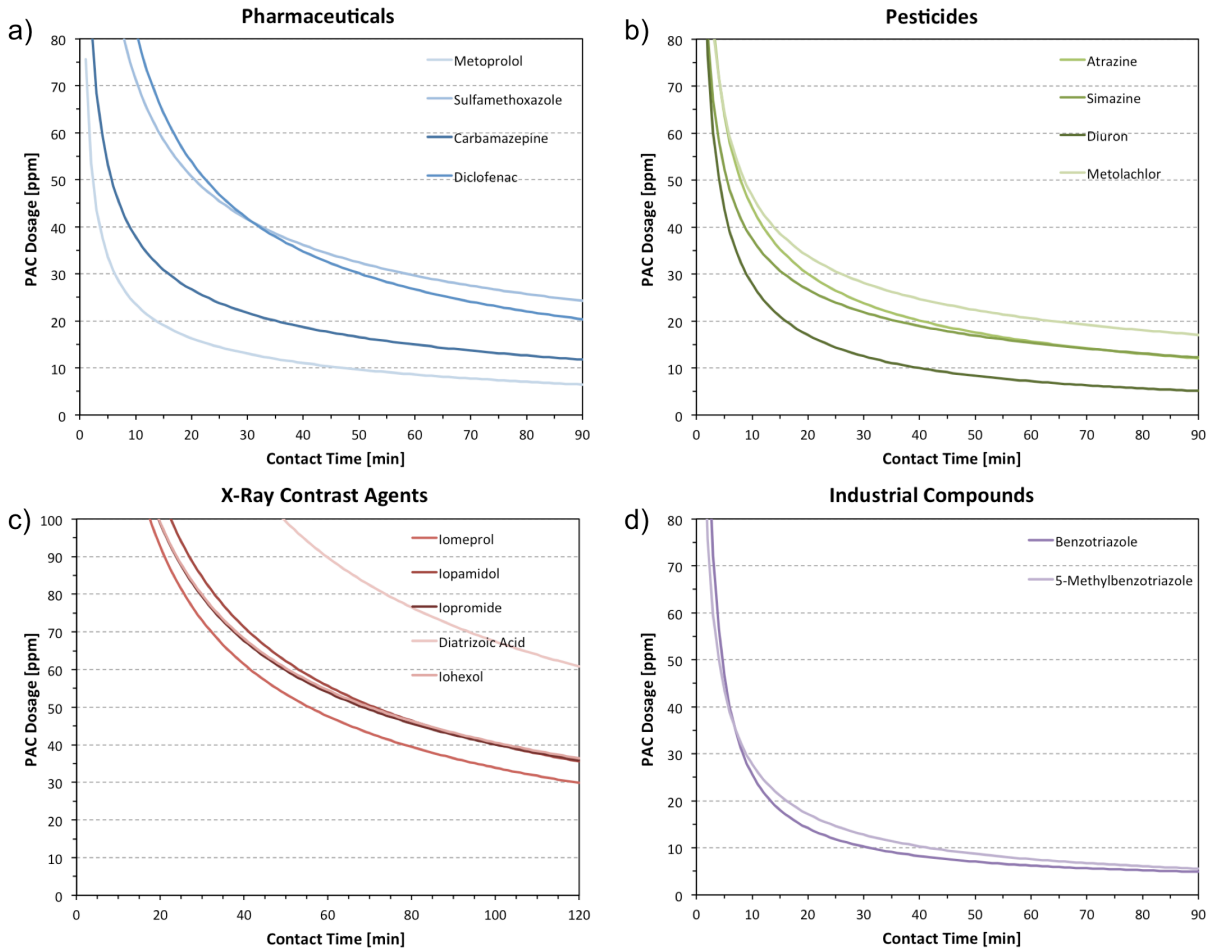

Fig. 2.12: *Relationships between PAC dose and contact time to remove 90% of (a) pharmaceuticals, (b) pesticides, (c) X-ray contrast agents, and (d) industrial compounds from Rhine river water (RRW).*

2.2.2.2 ROLE OF INITIAL MICROPOLLUTANT CONCENTRATIONS IN ADSORPTION EXPERIMENTS

The micropollutant concentrations spiked to the HGW were significantly higher than in the raw water. Therefore, it is important to check if the results presented in section 2.2.2.1 are applicable to lower micropollutant concentrations. **Fig. 2.13** shows the results of adsorption kinetics experiments conducted with initial iomeprol concentrations of 241, 1'031, and 3'746 ng/L. The agreement between the adsorption kinetics for the three initial concentrations is very good for both 10 and 50 mg/L PAC. There is some variation in the first order adsorption rate constants for the other X-ray contrast media (**Tab. 2.8**), which might rather be caused by slight differences in the experimental conditions. Therefore, it can be concluded that the adsorption kinetics of micropollutants do not depend on the initial concentrations if the normalized concentrations are considered. Hence, the results obtained in the adsorption kinetics experiments are transferable to lower concentrations.

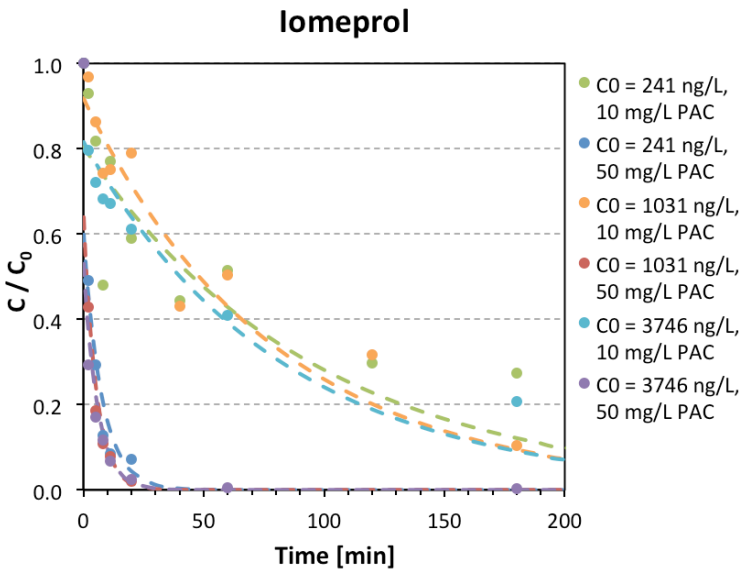

Fig. 2.13: *Adsorption kinetics in HGW for three initial concentrations of iomeprol and PAC doses of 10 and 50 mg/L, respectively - experimental data (circles) and first order kinetic modelling (dashed lines). T = 11 °C.*

Tab. 2.8: *Pseudo first order rate constant k_{ads} for the adsorption of X-ray contrast media on PAC in Hardwald groundwater (HGW), for 10 and 50 mg/L PAC.*

	k_{ads} (x10^3 s^{-1})					
	10 mgPAC/L			50 mgPAC/L		
	300 ng/L	1000 ng/L	3000 ng/L	300 ng/L	1000 ng/L	3000 ng/L
Iomeprol	0.18	0.21	0.20	2.18	3.11	2.82
Iopamidol	0.39	0.30	0.20	1.54	3.38	2.61
Iopromide	0.25	0.32	0.24	3.03	1.17	3.48
Diatrizoic acid	0.09	0.12	0.10	0.87	0.97	0.95
Iohexol	0.27	0.13	0.19	2.25	2.38	2.44

2.3 PRACTICAL SIGNIFICANCE OF ADSORPTION EXPERIMENTS

The adsorption of 20 compounds with a large range of adsorbability was tested at laboratory experiments with rapid small-scale column tests (RSSCTs) to predict their breakthrough in the full-scale filters currently operated by Hardwasser AG. The prediction provided by RSSCT shows that X-ray contrast media and sucralose are weakly retained on the filters and break through quite early. The first pesticides will start to be released at the end of 2017, after 4 years of operation. The release of pharmaceutical and industrial compounds was not observed in RSSCT meaning that they should not break through the full-scale filters before 2020, after about six years of opreation. Chlorobutadienes were unfortunately not tested in RSSCT for the reasons given above but their adsorption will be discussed later in section 5.2.1.4.

Tab. 2.9: *PAC doses required to adsorb 90% of the micropollutant concentration in HGW, RRW or SFW for contact times of 20 or 60 min.*

	PAC dose required (mgPAC/L) to adsorb 90 %					
	Contact time – 20 min			Contact time – 60 min		
Compounds	**HGW**	**RRW**	**SFW**	**HGW**	**RRW**	**SFW**
Iohexol	44.6	99.1	118.5	23.5	54.5	58.1
Iomeprol	41.4	92.7	110.1	22.0	47.6	52.6
Iopamidol	42.4	107.0	110.9	20.2	55.6	52.6
Diatrizoate	79.0	163.1	207.1	38.8	89.8	97.8
Iopromide	41.4	98.9	98.7	19.1	53.9	47.9
Deisopropylatrazine	14.1	25.5	22.7	7.0	13.5	12.6
Desethylatrazine	17.5	30.1	29.3	8.0	15.2	15.9
Simazine	14.2	26.7	27.0	6.6	15.4	13.7
2,6-Dichlorobenzamide	16.9	29.4	26.4	7.5	16.9	14.7
Atrazine	17.2	30.1	30.3	7.3	15.7	16.3
Diuron	10.4	17.0	15.1	4.4	7.2	6.3
Metolachlor	16.7	33.9	n.a.	7.5	20.6	22.2
Sulfamethoxazole	24.6	50.7	58.6	13.9	29.6	29.4
Metoprolol	14.5	16.3	16.9	6.8	8.6	7.4
Diclofenac	19,5	53.8	50.6	9.4	26.7	23.4
Carbamazepine	14.9	26.7	26.9	6.6	15.0	13.5
Benzotriazole	12.0	14.2	17.2	6.4	6.2	7.1
5-Methylbenzotriazole	13.0	17.2	15.8	6.1	7.6	6.7

Adsorption kinetic experiments were performed with the same selection of compounds (except sucralose and atenolol) using Hardwald groundwater (HGW), Rhine river water (RRW) and sand filtered water (SFW) as water matrices. Due to a difference of dissolved organic matter content (i.e., DOC was three times lower in HGW than in RRW and SFW), the adsorption of micropollutants required less PAC when they are present in HGW. **Tab. 2.9** shows the PAC doses necessary to remove 90% of micropollutants for contact times of 20 min or 60 min. For example, for atrazine a PAC dose of 17.2 mg/L is required to achieve 90% removal in 20 min in HGW while the dose needs to be increased to 30.1 mg/L for RRW. Consequently, the operational cost will increase by almost a factor of 2 when directly treating RRW. The sand filtration applied in Pratteln helps to remove turbidity but only a small fraction of micropollutants or organic matter is retained during this operation. Therefore, the PAC adsorption treatment is the same for RRW and SFW.

2.4 REFERENCES

AdDesignS™ - https://lc.cx/ocf5 - dwhand@mtu.edu

Corwin, C.J., Summers, R.S., 2010. Scaling trace organic contaminant adsorption capacity by granular activated carbon. Environ. Sci. Technol. 44, 5403–8. doi:10.1021/es9037462

Cretegny, E., 2015, Assessment of adsorption and ozone-based oxidation treatments for the removal of micropollutants in the Hardwald Groundwater: Bench-scale testing to predict pilot plant performances, Master thesis, Université Joseph Fourier, 2015.

Crittenden, J.C., Reddy, P.S., Arora, H., Trynoski, J., Hand, D.W., Perram, D.L., Summers, R.S., 1991. Predicting Gac Performance with Rapid Small-Scale Column Tests. J. Am. Water Work. Assoc. 83, 77–87.

Crittenden, J.C.J., Trussell, R.R., Hand, D.D.W., Howe, K.J., Tchobanoglous, G., Crittenden, John C.; Trussel, R. Rohdes; Hand, David W.; Howe, Kerry J.; Tchobanoglous, G., 2005. Water Treatment: Principles and Design, 2Nd. doi:10.1016/S0021-9673(00)90243-7

Matsui, Y., 2002. Pesticide Adsorption by Granular Activated Carbon Adsorbers . 1 . Effect of Natural Organic Matter Preloading on Removal Rates and Model Simplification. Environ. Sci. Technol. 36, 3426–3431.

Patni, A.G., Ludlow, D.K., Adams, C.D., 2008. Characteristics of Ground Granular Activated Carbon for Rapid Small-Scale Column Tests. Sect. Title Waste Treat. Dispos. 134, 216–221. doi:10.1061/(ASCE)0733-9372(2008)134:3(216)

Ridder, D.J. De, Villacorte, L., Verliefde, A.R.D., Verberk, J.Q.J.C., Heijman, S.G.J., Amy, G.L., Dijk, J.C. Van, 2010. Modeling equilibrium adsorption of organic micropollutants onto activated carbon. Water Res. 44, 3077–3086. doi:10.1016/j.watres.2010.02.034

Stolz, P., 2014, Performance of Activated Carbon Adsorption and the Combined Use of Activated Carbon and Ozone in the Removal of Micropollutants and Natural Organic Matter from Hardwald Groundwater, Master Thesis, ETH Zürich, 2014.

Summers, R.S., Knappe, D.R.U., Snoeyink, V.L., 2010. Adsorption of organic compounds by activated carbon.

3 EVALUATION OF O_3/H_2O_2 AND UV/H_2O_2 AS ADDITIONAL TREATMENT BEFORE OR AFTER THE ADSORPTION PROCESS - LABORATORY-SCALE EXPERIMENTS

To optimize the construction of a pilot plant, tests were performed at laboratory-scale to evaluate the efficiency of two advanced oxidation processes (AOPs) to abate micropollutants. First, p-chlorobenzoic acid (p-CBA) was used as target compound to compare the capability of O_3/H_2O_2 and UV/H_2O_2 to produce °OH radicals. Further, ozonation experiments were run with five micropollutants (carbamazepine, tramadol, benzotriazole, acesulfame and iopamidol) and a preliminary study was performed on the detection of transformation products. In addition, the oxidation of chlorobutadienes by O_3, O_3/H_2O_2, UV and UV/H_2O_2 was investigated in chapter 4. Finally, the formation of bromate, a potentially carcinogenic oxidation by-product formed during ozonation of bromide-containing waters was always assessed. Most of the results provided in this section were collected during the master thesis of Emy Cretegny (2015).

3.1 MATERIALS AND METHODS

3.1.1 FEED WATER QUALITY AND SPIKED MICROPOLLUTANTS

In the first experiments, Hardwald groundwater (HGW_LE1) was spiked with 0.5 µM of *p*-chlorobenzoic acid (*p*CBA) and 100 µg/L of bromide to evaluate the efficiency of the O_3/H_2O_2 and UV/H_2O_2 processes to produce °OH and the effect on bromate formation.

In a second series of experiments Hardwald groundwater (HGW_LE2) was spiked with 1 µM each of five micropollutants, namely acesulfame, benzotriazole, carbamazepine, iopamidol and tramadol. These experiments were performed to investigate the formation of the transformation products during the advanced oxidation of Hardwald groundwater

The characteristics of the two Hardwald groundwaters are presented in **Tab. 3.1**.

Tab. 3.1: *Water quality of Hardwald groundwater (HGW) for the two series of laboratory experiments (LE) performed in this chapter.*

Parameter	Unit	HGW_LE1	HGW_LE2
pH		8.13	8.08
DOC	mgC/L	0.48	0.52
Alcalinity	mg HCO_3^-/L	184	180
Br^-	µg/L	170[(1)]	35.8
BrO_3^-	µg/L	< 0.5	< 0.5
pCBA	µg/L (µM)	78 (0.5)[(2)]	n.a.
Acesulfame	µg/L (µM)	n.a.	221 (1.1)[(2)]
Benzotriazole	µg/L (µM)	n.a.	144 (1.2)[(2)]
Carbamazepine	µg/L (µM)	n.a.	229 (1.0)[(2)]
Iopamidol	µg/L (µM)	n.a.	717 (0.9)[(2)]
Tramadol	µg/L (µM)	n.a.	300 (1.1)[(2)]

[(1)] spiked with bromide, [(2)] spiked with compounds

3.1.2 SET-UP

3.1.2.1 O_3/H_2O_2

Batch experiments were conducted in the same manner with HGW_LE1 and HGW_LE2. For O_3/H_2O_2 experiments, H_2O_2 was added before O_3 to limit direct ozone reactions as much as possible.

The experiments were carried out in amber glass vials with 20 mL solution. Two ozone stock solutions (i.e., 15 or 60 mg/L) were prepared and the required volumes were added to result in the targeted ozone doses. Small volumes of the ozone stock solution were added to the glass vials under stirring with a magnetic stirrer. The total volume added represented at most 2.5% of the total volume.

After ozone addition, the vials were closed with a Teflon stopper and placed in the dark at ambient temperature for at least 12 hours for complete ozone consumption. Samples were stored at 4°C prior to analyses.

3.1.2.2 UV/H_2O_2

UV photolysis was carried out with a merry-go-round photoreactor equipped with a low pressure mercury lamp emitting monochromatic UV light at 254 nm with or without H_2O_2 (0 to 35 mg/L) applying UV doses from 400 to 10000 J/m^2. Because the light screening by the groundwater matrix components was negligible (<2%), no light screening correction for the UV experiments was applied.

3.1.3 ANALYTICAL METHODS

*p*CBA was quantified using a high-performance liquid chromatography (HPLC) (Dionex Ultimate 3000) at 240 nm with an eluent of methanol and 20 mM phosphate buffer (pH 2) (60:40, v:v) (Huber et al., 2003).

Bromate was measured by capillary ion chromatography (Thermo Dionex ICS-4000) coupled with tandem mass spectrometry (Thermo TSQ-Vantage). The water samples were diluted 10 times prior to analysis and the measurement detection limit was 0.5 µg/L (Shah et al., 2015).

The five selected micropollutants (i.e. carbamazepine, tramadol, benzotriazole, acesulfame, iopamidol) were analysed by liquid chromatography with high-resolution mass spectroscopy (Thermo QExactivePlus). For the sample preparation, 60 mL of a sample was spiked with an internal standard mixture and concentrated under vacuum and reflux to a volume of 300 µL using a Büchi Evaporator (Büchi Syncore Polyvap). The samples were reconstituted to 400 µL using nanopure water and were centrifuged at 10'000 rpm for 2 min at room temperature to remove particles. Afterwards, 100 µL of the concentrated sample was injected and separated on a reversed phase column (Atlantis T3C, 3 µm, 3x150 mm). The following gradient of water (Solvent A) and methanol (solvent B) both acidified with 0.1% formic acid at a flow rate of 300 µL/min was used: 0-1.5 min 5% B, 1.5-17.5 min linear gradient to 95% B, 17.5 – 25 min kept at 95% B, 25-25.1 min switch to 5% B, and 25.1-29 min kept at 5% B. Analyte detection was performed with electrospray ionization (spray voltage: 5/-3.5 kV, sheath gas flow: 50, auxiliary gas flow: 10, capillary temperature 380°C, S-lens RF level: 100/50, Probe Heater Temperature: 500/250°C) by separate measurements in positive and negative ionization mode. Full scan MS (mass range: 100-1000 m/z, mass resolution R: 140'000 at m/z 200) followed by five data-dependent MS/MS scans (R:17'500, normalized collision energy NCE: 50) were acquired using the exact masses of the protonated and deprotonated target molecules as trigger criteria for the data-dependent MS/MS in positive and negative ionization mode, respectively. The mass accuracy was determined to be < 5ppm for all measurements.

3.2 RESULTS AND DISCUSSION

3.2.1 ABATEMENT OF *P*CBA USING O_3/H_2O_2 OR UV/H_2O_2 TREATMENT

Two advanced oxidation processes were selected for the abatement of micropollutants in Hardwald groundwater (i.e., O_3/H_2O_2 or UV/H_2O_2). The main advantage of these processes is the formation of hydroxyl radicals, which are relatively non-selective oxidants. However, when O_3-based processes are applied to bromide-containing water, bromate (BrO_3^-) formation is always a potential problem. The Swiss drinking water standard for BrO_3^- is 10 µg/L (Verordnung des EDI über Fremd- und Inhaltsstoffe in Lebensmitteln). In the UV/H_2O_2 process, BrO_3^- is not formed (von Gunten and Oliveras, 1998) but the energy demand is significantly higher than for O_3/H_2O_2 (Katsoyiannis et al., 2011).

To assess the efficiency of advanced oxidation processes, *p*CBA is commonly used as a hydroxyl radical probe (Elovitz and von Gunten, 1999). It is well-known that *p*CBA reacts fast with hydroxyl radical ($k_{HO^\bullet}$ = 5×10^9 $M^{-1}s^{-1}$) and only slowly with O_3 (k_{O3} = ≤ 0.15 $M^{-1}s^{-1}$) (Elovitz and von Gunten, 1999).

The elimination of *p*CBA and the formation of BrO_3^- are presented in **Fig. 3.1** for the O_3/H_2O_2 process. The treatment conditions assessed during the experiments (i.e., 0.2 < ozone dose < 2.0 mg/L) are sufficient to remove at least 70% of the micropollutant with or without H_2O_2. The addition of the later is important since only 0.30 mg/L is required to achieve a pCBA degradation of 80% in the peroxone process (O_3/H_2O_2), while the ozone dose must be increased to 0.63 mg/L for the same abatement without H_2O_2. An increase of the H_2O_2 concentration did not show an important benefit for *p*CBA abatement. However, it minimizes the bromate formation. For a H_2O_2 dose of 5.67 mg/L, the ozone dose can be increased up to 1.7 mg/L without exceeding 10 µg/L for bromate. Without H_2O_2, 148 µg/L of BrO_3^- is formed, which is 15 times higher than the tolerance value of 10µg/L, with an ozone dose of 1.0 mg/L. Consequently, despite the similar efficience of micropollutant abatement, conventional ozonation should not be applied to Hardwald groundwater to abate micropollutants. The combined processes O_3/H_2O_2 leads to a slightly better abatement of micropollutants with a much lower bromate formation.

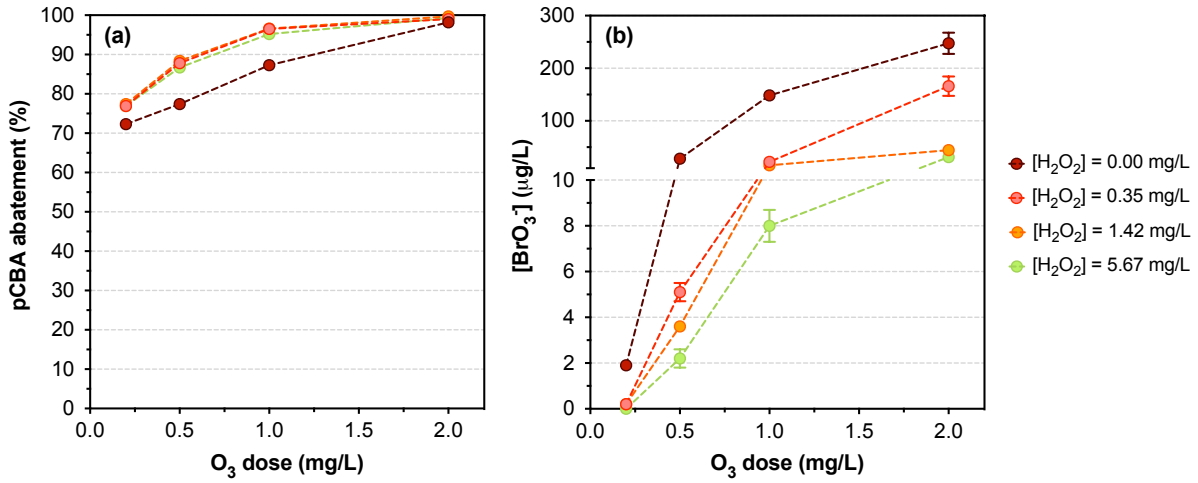

Fig. 3.1: *Conventional ozonation (O_3) and the ozone-based advanced oxidation (O_3/H_2O_2) of Hardwald Groundwater (HGW_LE1) spiked with bromide. (a) Removal of pCBA and (b) bromate formation - pH = 8.13, [Br⁻] = 170 µg/L.*

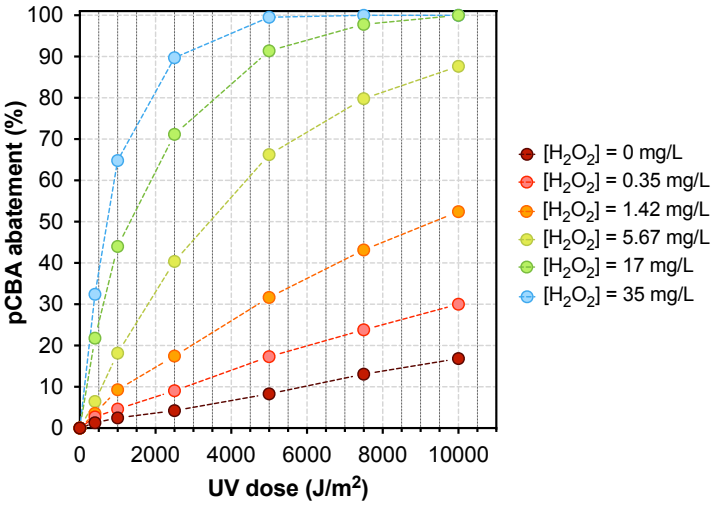

Fig. 3.2 – UV/H_2O_2 treatment of Hardwald Groundwater (HGW_LE1). Influence of the UV and H_2O_2 doses on pCBA abatement - pH = 8.13, [Br⁻] = 170 µg/L.

The abatement of pCBA was also studied with the UV/H_2O_2 treatment. The influence of UV and H_2O_2 doses is depicted in Fig. 3.2. An 80% abatement of *p*CBA cannot be reached with a H_2O_2 dose ≤ 1.42 mg/L and a maximum UV dose of 10000 J/m^2. However, this goal can be achieved if the H_2O_2 concentration is 5.67 mg/L with a UV dose of 7500 J/m^2. If the H_2O_2 concentration is increased to 17 or 35 mg/L, UV doses of only 3500 or 1900 J/m^2 are required, respectively. However, H_2O_2 is also an expensive chemical and it is not recommended to use it at such high concentrations. Based on these experiments a UV dose between 6000 and 8000 J/m^2 with a H_2O_2 concentration of 5 mg/L seems to be reasonable.

3.2.2 Application of O_3/H_2O_2 treatment for the removal of five selected micropollutants and the formation of transformation products

3.2.2.1 Determination of the ozone doses required to remove 50, 80 and 90% of the five selected micropollutants

The abatement of five micropollutants (i.e., carbamazepine, tramadol, benzotriazole, acesulfame and iopamidol) during ozonation with or without addition of H_2O_2 and the required ozone doses for an elimination of 50, 80 and 90% were investigated.

Fig. 3.3 shows the oxidation of the five micropollutants as a function of the ozone dose and the H_2O_2/O_3 mass ratio in Hardwald groundwater. Tramadol and carbamazepine are easily oxidizable by ozone directly. For an ozone dose of 0.1 mg/L, 95% of the initial concentration is abated for both compounds while only 25% of benzotriazole is abated for the same ozone dose. For acesulfame and iopamidol, the abatement does not reach 10% for these conditions. An ozone dose of 1.1 mg/L is required if the treatment objective is set to at least 80% abatement. As expected, iopamidol is the limiting compound because of its resistance to ozone and has a relatively low second order rate constant for the reaction with hydroxyl radicals.

The results obtained for the five micropollutants are consistent with the second order rate constants for the reactions with ozone. At pH 8.08, carbamazepine and tramadol have high apparent second order rate constants, namely k_{O3} = 3.0 x 10^5 M^{-1}s^{-1} and k_{O3} = 4.4 x 10^4 M^{-1}s^{-1}, respectively. Benzotriazole has an apparent second order rate constant for the reaction with ozone of 1.2 x 10^3 M^{-1}s^{-1} (Lee et al., 2014)(Hammes et al., 2006). Acesulfame and iopamidol have the lowest second order rate constants for their reactions with ozone, 88 M^{-1}s^{-1} (Kaiser et al., 2013) and 0.8 M^{-1}s^{-1} (Huber et al., 2003), respectively.

Interestingly, the addition of hydrogen peroxide with a H_2O_2/O_3 mass ratio of 0.5 and 4.0 does not improve the elimination of the five micropollutants For an ozone dose of 0.5 mg/L, the oxidation efficiency for acesulfame is reduced by 19% for a dose of 2 mg/L of H_2O_2. This difference is caused by a partial loss of the direct ozone reaction due to its lower stability. For compounds with a lower ozone reactivity, this difference is expected to be smaller.

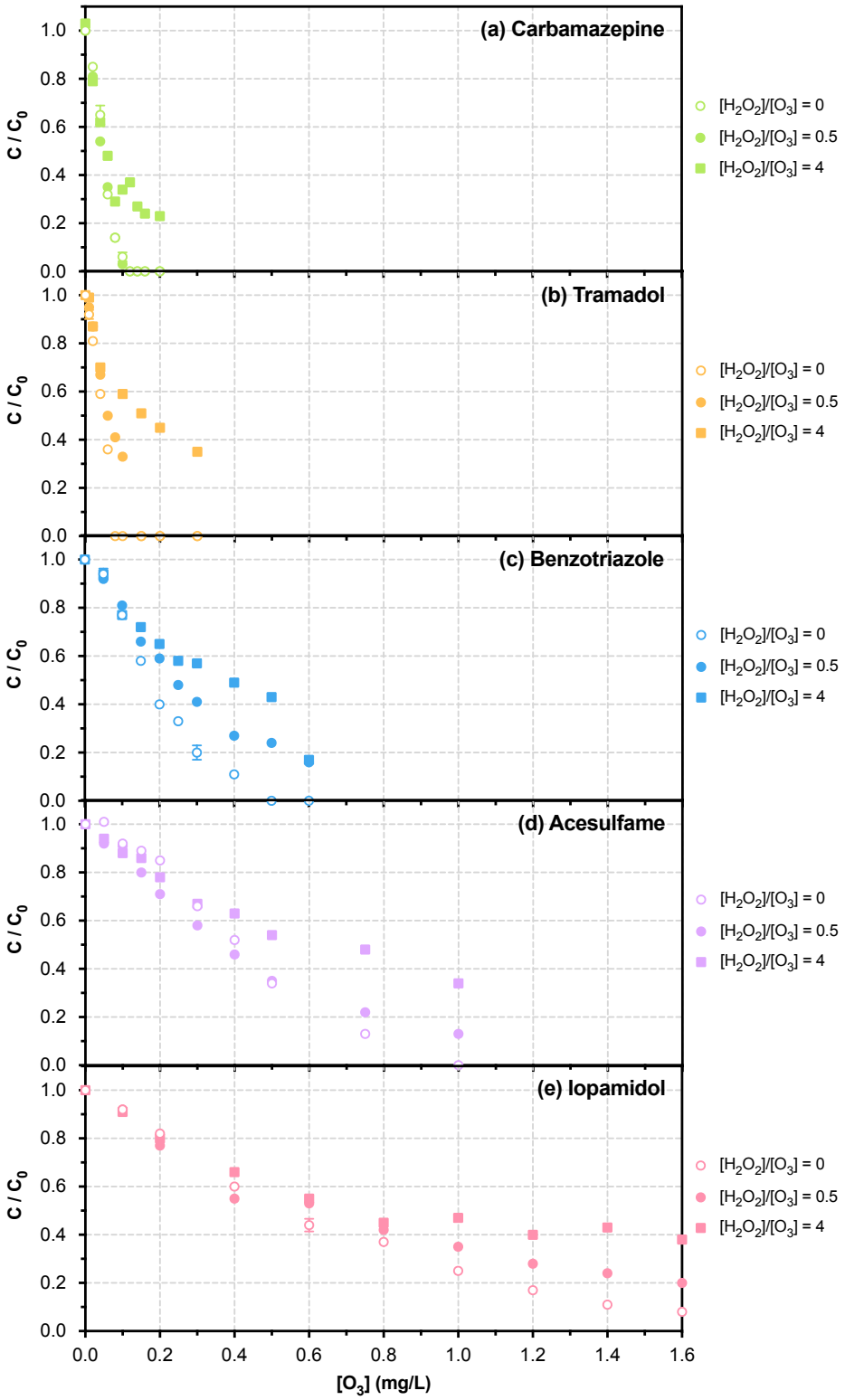

Fig. 3.3: *Bench-scale oxidation of five spiked micropollutants in Hardwald groundwater (HGW_LE2) with O_3 and the AOP O_3/H_2O_2. (a) carbamazepine, (b) tramadol, (c) benzotriazole,(d) acesulfame and (e) iopamidol - pH = 8.08, [Br⁻] = 35.8 µg/L. H_2O_2/O_3 are given as mass ratios.*

Tab. 3.2: *Ozone doses required to abate 50, 80 and 90% of five micropollutant in Hardwald groundwater.*

	Ozone dose required (mg/L) for x% abatement		
Compound	**50%**	**80%**	**90%**
Carbamazepine	0.05	0.07	0.09
Tramadol	0.05	0.06	0.07
Benzotriazole	0.17	0.30	0.40
Acesulfame	0.38	0.66	0.80
Iopamidol	0.50	1.10	1.40

Tab. 3.2 summarizes the ozone doses necessary to abate 50%, 80% and 90% of each micropollutant. It reveals that an ozone dose of 0.5 mg/L is sufficient to guarantee at least 50% abatement for the five compounds. If this dose is increased to 1.4 mg/L, the abatement will raise to at least 90%.

3.2.2.2 FORMATION OF BROMATE AND TRANSFORMATION PRODUCTS FOR AN ABATEMENT OF PARENT COMPOUNDS OF 50% AND 90%

The same experiments were repeated for the 3 ozone doses of each compound shown in **Tab. 3.2** but this time, the focus was on bromate formation and transformation products (reported in literature). As shown in **Fig. 3.4**, the abatement obtained without addition of H_2O_2 (blue sticks) is slightly different than expected. For instance, the abatements of carbamazepine were 72%, 98% and 100% for ozone doses of 0.05, 0.07 and 0.09 mg/L instead of 50%, 80% and 90%. The targeted values were also exceeded for acesulfame while they were inferior for tramadol and iopamidol and exact for benzotriazole. Nevertheless, the results were consistent because the micropollutant abatement efficiency increased with increasing ozone doses as expected.

As previously depicted in **Fig. 3.3**, the abatement of some micropollutant is attenuated when H_2O_2 is added to the water. One of the major reasons of H_2O_2 addition is a mitigation of bromate formation. While the bromate concentration exceeded 10 µg/L during conventional ozonation with an ozone dose above about 0.4 mg/L, H_2O_2 helps to keep the bromate concentration below this limit for O_3 doses up to 1.4 mg/L even with a low H_2O_2/O_3 mass ratio of 0.5. **Fig. 3.5** summarizes the bromate formation as a function of the ozone and hydrogen peroxide doses. These results highlight the necessity to perform ozone-based advanced oxidation instead of single ozonation for ozone doses > 0.3-0.4 mg/L. An increase of the H_2O_2/O_3 mass ratio to 4 does not significantly improve the mitigation of bromate formation. Therefore, an ozone dose ranging from 0.5 to 1.1 mg/L and an H_2O_2/O_3 mass ratio of 0.5 might be close to the optimum treatment conditions to ensure a relative abatement of > 80% for the five selected compounds and a bromate concentration of about 5 µg/L.

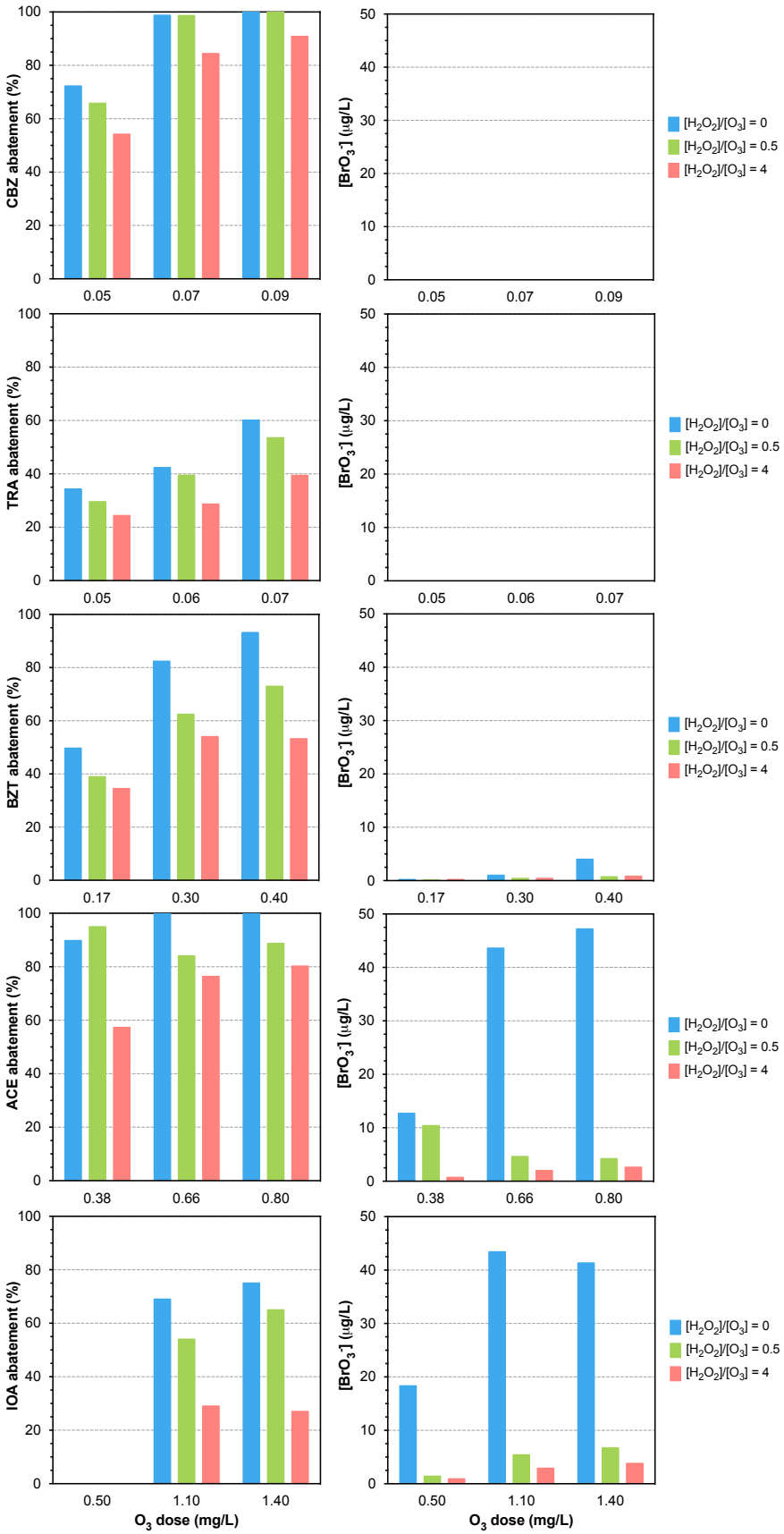

Fig. 3.4: *Abatement of five micropollutants (left column) (carbamazepine (CBZ), tramadol (TRA), benzotriazole (BZT), acesulfame (ACE) and iopamidol (IOA)) spiked in Hardwald groundwater (HGW_LE2) and bromate formation (right column) using O_3 and O_3/H_2O_2 in batch conditions – data were sorted from the most to the least reactive compound with O_3 (top to bottom) – pH = 8.08, [Br⁻] = 35.8 µg/L.*

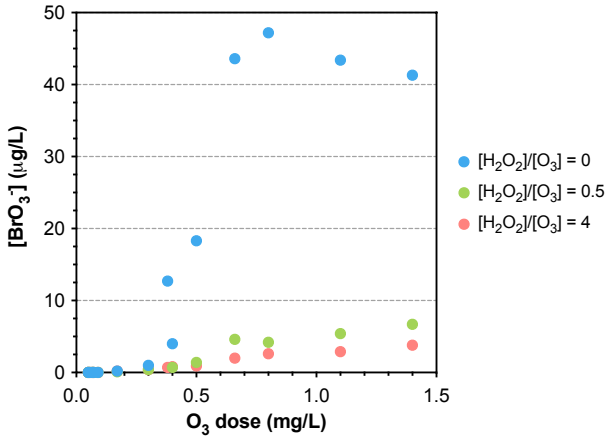

Fig. 3.5: *Bromate formation during the ozonation of Hardwald groundwater (HGW_LE2) as a function of the ozone dose with or without addition of H_2O_2. pH = 8.08, [Br⁻] = 35.8 µg/L.*

Transformation products, previously selected in literature, were measured semi-quantitatively with a LC/MS/MS instrument using the area ratio between the transformation products and the corresponding internal standard of the parent compounds as summarized. Results presented in **Table. 3.3** were measured with oxidation conditions selected for the elimination of 50% and 90% of the parent compounds without H_2O_2. It is important to underline that the area ratios are not directly comparable from one transformation product to another since their responses in the mass spectrometer are different. All the selected compounds were taken from previous publications and their formation pathways are shown in **Table. 3.3**. 15 out of the 20 transformation products targeted are more abundant when a parent compound abatement of 90% is achieved.

For **carbamazepine**, Hübner et al. (2014) showed that CBZ_TP1 and CBZ_TP4 are firstly formed during ozone-based oxidation in two different pathways (**Fig. 3.6**). CBZ_TP1 will be further transformed in CBZ_TP2, while CBZ_TP5 results from CBZ_TP4. CBZ_TP3 might result from the oxidation of both CBZ_TP1 and CBZ_TP4. An increase in the carbamazepine abatement to 90% will lead to a higher formation of transformation products, especially for CBZ_TP2. Nevertheless, the ozone dose applied to achieve such an effect (i.e., 0.09 mg/L) is very low and we can assume that the overall concentration of the selected transformation products would decrease with increasing ozone doses.

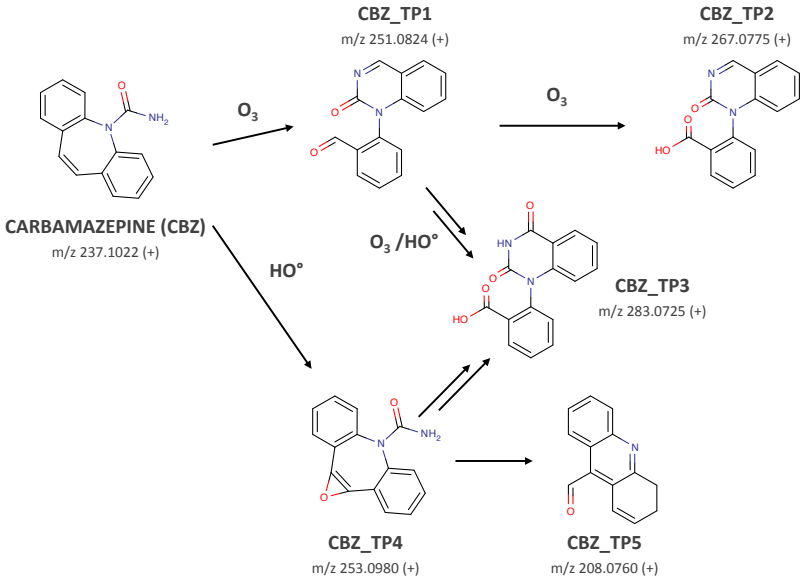

Fig. 3.6: *Carbamezepine. Transformation products from literature (Hübner et al., 2014) and semi-quantified after the oxidation of carbamazepine (CBZ) by O_3/H_2O_2 according to the treatment conditions in **Fig. 3.4**.*

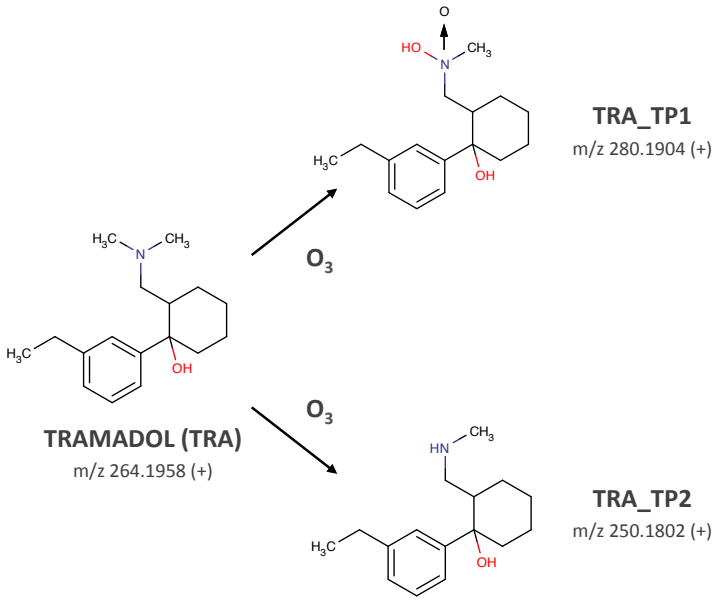

Fig. 3.7: *Tramadol. Transformation products from literature (Zimmermann et al., 2012) and semi-quantified after the oxidation of tramadol (TRA) by O_3/H_2O_2 according to the treatment conditions in* ***Fig. 3.4****.*

Zimmermann et al. (2012) elucidated **tramadol** transformation products and identified mainly the two products presented in **Table. 3.3**. TRA_TP1 resulted from the direct oxidation of tramadol by ozone and is considered as the most abundant one (**Fig. 3.7**). Its formation increased with increasing ozone doses.

Benzotriazole is transformed to BZT_TP2 in a first step (**Fig. 3.8**), which will further lead to the formation of both BZT_TP3 and BZT_TP4 (Benitez et al., 2015). An increase of the ozone dose might lead to a higher abatement of transformation products. The peak area ratio measured for BTZ_TP2 is reduced from 40.2 to 2.2 while it slightly increased for BZT_TP3 and BZT_TP4.

According to the study of Scheurer et al. (2012), ACE_TP1 and ACE_TP2 are the two main transformation products detected after ozonation of **acesulfame** (**Fig. 3.9**). We observed that ACE_TP1 is abated when increasing the ozone dose to 0.8 mg/L while the formation of ACE_TP2 increases.

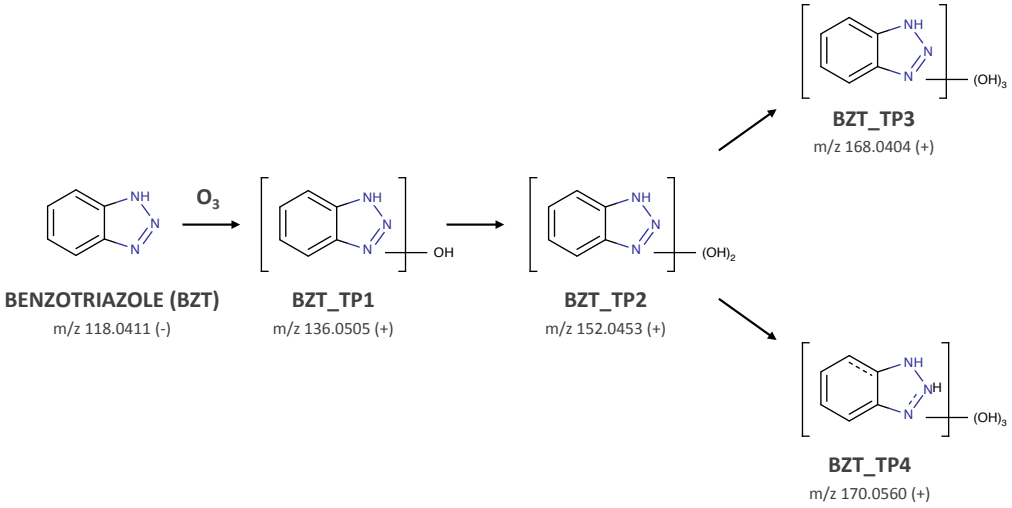

Fig. 3.8: *Benzotriazole. Transformation products from literature (Benitez et al., 2015) and semi-quantified after the oxidation of benzotriazole (BZT) by O3/H2O2 according to the treatment conditions in* ***Fig. 3.4****.*

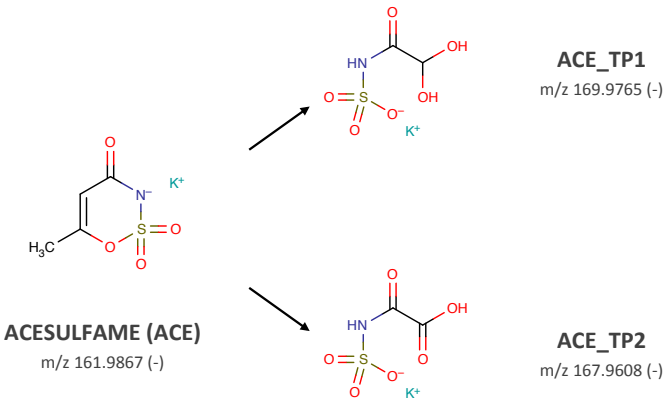

Fig. 3.9: *Acesulfame. Transformation products from literature (Scheurer et al., 2012) and semi-quantified after the oxidation of acesulfame (ACE) by O_3/H_2O_2 according to the treatment conditions in* ***Fig. 3.4****.*

Iopamidol, which is the least reactive compound, is transformed in IOA_TP1 and IOA_TP4 (**Fig. 3.10**) when reacting with °OH. IOA_TP1 will be further oxidized to IOA_TP2 and then into IOA_TP3. IOA_TP5 originates from the oxidation of IOA_TP4. All transformation products show a higher concentration when the ozone dose is set to 1.4 mg/L.

For micropollutants reacting fast with ozone (i.e., carbamazepine and tramadol), the composition of transformation products is quite similar with or without H_2O_2. However, for acesulfame and iopamidol, the concentration of the identified transformation product is lower when H_2O_2 is added to the solution.

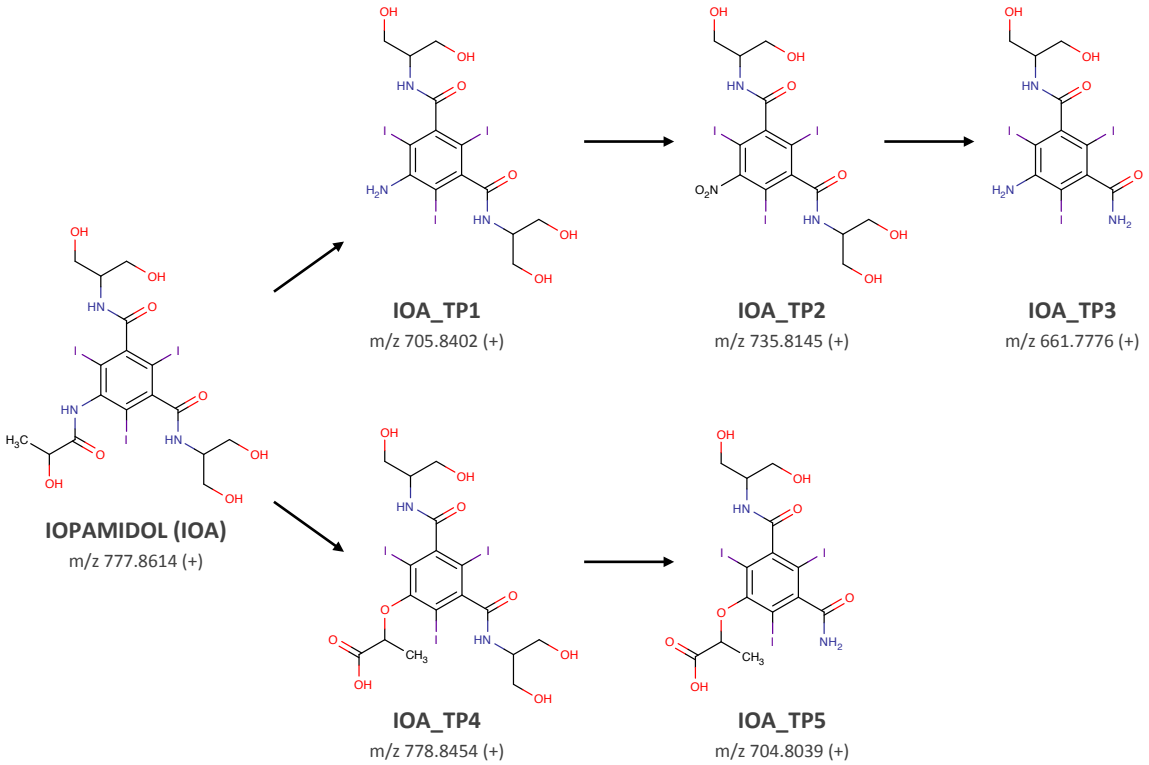

Fig. 3.10: *Iopamidol. Transformation products from literature (Singh et al., 2015; Wendel et al., 2014) and semi-quantified after the oxidation of iopamidol (IOA) by O_3/H_2O_2 according to the treatment conditions in Fig. 3.4.*

Table. 3.3: *Formation of transformation products (according to the literature) during the oxidation of five micropollutants during conventional ozonation and the peroxone process. Oxidation conditions were selected for an expected 50% and 90% abatement of the parent compounds without H_2O_2. Bold values reflect the dominant transformation products.*

		Transformation product peak area/parent ISTD peak area (x10^8)			
Compound	**m/z (polarity)**	**[H_2O_2]/[O_3] = 0**		**[H_2O_2]/[O_3] = 0.5**	
CBZ abatement	*237.1022 (+)*	*72%*	*100%*	*72%*	*100%*
CBZ_TP1	251.0824 (+)	4.1	**6.0**	6.6	**7.9**
CBZ_TP2	267.0775 (+)	37.8	**176.4**	42.3	**143.2**
CBZ_TP3	283.0725 (+)	3.2	**20.0**	3.3	**16.9**
CBZ_TP4	253.0980 (+)	**17.6**	15.3	**16.7**	15.1
CBZ_TP5	208.0760 (+)	11.9	**13.0**	14.1	**18.7**
TRA abatement	*264.1958 (+)*	*34%*	*60%*	*30%*	*53%*
TRA_TP1	280.1904 (+)	9348	**14199**	8560	**12912**
TRA_TP2	250.1802 (+)	103.6	**137.2**	97.3	**133.5**
TRA_TP3	278.1751 (+)	8.5	**14.6**	8.2	**13.3**
TRA_TP4	264.1594 (-)	**1.4**	0.1	**1.3**	0.1
BZT abatement	*118.0411 (-)*	*50%*	*93%*	*39%*	*73%*
BZT_TP1	136.0505 (+)	**0.2**	0	**0.2**	0
BZT_TP2	152.0453 (+)	**40.2**	2.2	**88.1**	69.4
BZT_TP3	168.0404 (+)	26.0	**29.5**	32.3	**49.8**
BZT_TP4	170.0560 (+)	1.8	**2.6**	2.8	**7.8**
ACE abatement	*161.9867 (-)*	*89%*	*100%*	*95%*	*89%*
ACE_TP1	169.9765 (-)	**81.3**	7.8	**0.5**	0.3
ACE_TP2	167.9608 (-)	16.1	**37.2**	**27.1**	13.6
IOA abatement	*777.8614 (+)*	*0%*	*75%*	*0%*	*65%*
IOA_TP1	705.8402 (+)	8.7	**19.1**	35.4	**61.5**
IOA_TP2	735.8145 (+)	177.9	**372.9**	2.5	**27.8**
IOA_TP3	661.7776 (+)	0	**0.1**	0.1	**0.3**
IOA_TP4	778.8454 (+)	11.7	**114.6**	0.8	**2.8**
IOA_TP5	704.8039 (+)	0.7	**9.1**	0.5	**7.1**

3.3 PRACTICAL SIGNIFICANCE OF OXIDATION EXPERIMENTS

In this chapter, it was clearly shown that conventional ozonation should not be applied to Hardwald groundwater because there is a risk to exceed the Swiss tolerance value of 10 µg/L for bromate if the ozone dose is > 0.4 mg/L. The application of a H_2O_2/O_3 mass ratio between 0.5 and 1 seems to be a good compromise because a higher ratio does not significantly change the removal of micropollutants and the bromate formation is under control. The optimum range for the ozone doses is between 0.5 - 1.1 mg/L.

For UV/H_2O_2 treatment, 80% of pCBA can be abated with a UV dose of 7500 J/m^2 and a H_2O_2 concentration of 5.67 mg/L. These treatment conditions are realistic. It would be possible to reach the same abatement by lowering the UV dose and increasing the H_2O_2 concentration but the H_2O_2 residual

would be too high after the UV reactor. By contrast, increasing the UV dose and decreasing the H_2O_2 concentration would be another solution but this requires much more energy.

3.4 REFERENCES

Benitez, F.J., Acero, J.L., Real, F.J., Roldán, G., Rodríguez, E., 2015. Ozonation of benzotriazole and methylindole: Kinetic modeling, identification of intermediates and reaction mechanisms. J. Hazard. Mater. 282, 224–232. doi:10.1016/j.jhazmat.2014.05.085

Cretegny, E., 2015, Assessment of adsorption and ozone-based oxidation treatments for the removal of micropollutants in the Hardwald Groundwater: Bench-scale testing to predict pilot plant performances, Master thesis, Université Joseph Fourier, 2015.

Elovitz, M.S., von Gunten, U., 1999. Hydroxyl Radical/Ozone Ratios During Ozonation Processes. I. The R ct Concept. Ozone Sci. Eng. 21, 239–260. doi:10.1080/01919519908547239

Hammes, F., Salhi, E., Köster, O., Kaiser, H.-P., Egli, T., von Gunten, U., 2006. Mechanistic and kinetic evaluation of organic disinfection by-product and assimilable organic carbon (AOC) formation during the ozonation of drinking water. Water Res. 40, 2275–86. doi:10.1016/j.watres.2006.04.029

Huber, M.M.M., Canonica, S., Park, G.-Y., von Gunten, U., 2003. Oxidation of Pharmaceuticals during Ozonation and Advanced Oxidation Processes. Environ. Sci. Technol. 37, 1016–1024. doi:10.1021/es025896h

Hübner, U., Seiwert, B., Reemtsma, T., Jekel, M., 2014. Ozonation products of carbamazepine and their removal from secondary effluents by soil aquifer treatment - Indications from column experiments. Water Res. 49, 34–43. doi:10.1016/j.watres.2013.11.016

Kaiser, H.-P., Köster, O., Gresch, M., Périsset, P.M.J., Jäggi, P., Salhi, E., von Gunten, U., 2013. Process Control For Ozonation Systems: A Novel Real-Time Approach. Ozone Sci. Eng. 35, 168–185. doi:10.1080/01919512.2013.772007

Katsoyiannis, I. a, Canonica, S., von Gunten, U., 2011. Efficiency and energy requirements for the transformation of organic micropollutants by ozone, O3/H2O2 and UV/H2O2. Water Res. 45, 3811–22. doi:10.1016/j.watres.2011.04.038

Lee, Y., Kovalova, L., McArdell, C.S., von Gunten, U., 2014. Prediction of micropollutant elimination during ozonation of a hospital wastewater effluent. Water Res. 64, 134–148. doi:10.1016/j.watres.2014.06.027

Scheurer, M., Godejohann, M., Wick, A., Happel, O., Ternes, T.A., Brauch, H., Ruck, W.K.L., 2012. Structural elucidation of main ozonation products of the artificial sweeteners cyclamate and acesulfame 1107–1118. doi:10.1007/s11356-011-0618-x

Shah, A.D., Liu, Z.-Q., Salhi, E., Höfer, T., Werschkun, B., Von Gunten, U., 2015. Formation of disinfection by-products during ballast water treatment with ozone, chlorine, and peracetic acid: influence of water quality parameters. Environ. Sci. Water Res. Technol. Environ. Sci. Water Res. Technol. View J. | View Issue Environ. Sci. Water Res. Technol 1, 465–465. doi:10.1039/c5ew00061k

Singh, R.R., Lester, Y., Linden, K.G., Love, N.G., Atilla-Gokcumen, G.E., Aga, D.S., 2015. Application of metabolite profiling tools and time-of-flight mass spectrometry in the identification of transformation products of iopromide and iopamidol during advanced oxidation. Environ. Sci. Technol. 49, 2983–2990. doi:10.1021/es505469h

von Gunten, U., Oliveras, Y., 1998. Advanced Oxidation of Bromide-Containing Waters: Bromate Formation Mechanisms. Environ. Sci. Technol. 32, 63–70. doi:10.1021/es970477j

Wendel, F.M., Lütke Eversloh, C., Machek, E.J., Duirk, S.E., Plewa, M.J., Richardson, S.D., Ternes, T.A., 2014. Transformation of iopamidol during chlorination. Environ. Sci. Technol. 48, 12689–12697. doi:10.1021/es503609s

Zimmermann, S.G., Schmukat, A., Schulz, M., Benner, J., von Gunten, U., Ternes, T.A., 2012. Kinetic and Mechanistic Investigations of the Oxidation of Tramadol by Ferrate and Ozone. Environ. Sci. Technol. 46, 876–84. doi:10.1021/es203348q

4 ABATEMENT OF POLYCHORO-1,3-BUTADIENES IN AQUEOUS SOLUTION BY OZONE, UV-PHOTOLYSIS, AND ADVANCED OXIDATION PROCESSES

This chapter is part of the Minju Lee's PhD thesis and was published in Environ. Sci. Technol. DOI: 10.1021/acs.est.6b04506

Poly-chloro-1,3-butadiene (CBD) congeners (i.e., tetra-, penta-, hexa-CBD) have been detected over the last four decades in river water (Burkhard et al., 1997; G. Oliver, Barry, L.E. Kaiser, 1986; Goldbach et al., 1976; Laska et al., 1976; Nikolaou et al., 2002) groundwater (Botta et al., 1996; Brüschweiler, 2010; Fattore et al., 1996) and wastewater (Barco-Bonilla et al., 2011; Nikolaou et al., 2002) worldwide in the concentration range of tens of ng/L to a few µg/L. Among CBDs, hexa-chloro-1,3-butadiene (HCBD) has various industrial applications such as an intermediate in manufacturing rubber compounds, as a solvent, as a fumigant, etc.(Agency for Toxic Substances and Disease Registry (ATSDR), 1994) Moreover, HCBD is inadvertently produced as a by-product from the manufacturing of chlorinated hydrocarbons such as trichloroethene (TCE) and tetrachloroethene (PCE).(Agency for Toxic Substances and Disease Registry (ATSDR), 1994) Due to the potential hazardous impacts on humans and aquatic organisms,(Agency for Toxic Substances and Disease Registry (ATSDR), 1994; *Hexachlorobutadiene in Drinking-water, Background document for development of WHO Guidelines for Drinking-water Quality, WHO/SDE/WSH/03.04/101*, 2004, "Stockholm Convention on Persistent Organic Pollutants," n.d.) HCBD has been subject to environmental guidelines worldwide: 0.6 µg/L for drinking water by World Health Organization(*Hexachlorobutadiene in Drinking-water, Background document for development of WHO Guidelines for Drinking-water Quality, WHO/SDE/WSH/03.04/101*, 2004) and an environmental quality standard value of 0.1 µg/L for inland surface water by the European Commission have been set. In contrast, little attention was drawn to other CBDs such as pentachloro-1,3-butadienes (PCBDs) and tetrachloro-1,3-butadienes (TCBDs).(Botta et al., 1996; Brüschweiler, 2010; Burkhard et al., 1997; Fattore et al., 1996) Such CBDs are known to be formed from reductive microbial dechlorination of HCBD under anaerobic conditions.(Booker and Pavlostathis, 2000; Bosma et al., 1994) Dechlorinated products are not necessarily less harmful, e.g., vinyl chloride, which is carcinogenic,(Atlanta, GA: U.S. Department of Health and Human Services, 2006) is produced from the reductive dechlorination of PCE and TCE.(Vogel and McCarty, 1985) Therefore, the ecotoxicological impact of other CBDs than HCBD should not be overlooked. A positive clastogenic activity was recently reported for 3 TCBDs and 2 PCBDs and a target value of 75 ng/L as the sum of TCBDs and PCBDs was proposed for drinking water using the threshold of toxicological concern (TTC) concept.(Brüschweiler, 2010)

Physical treatment technologies such as activated carbon and air stripping are commonly applied for eliminating highly chlorinated butadienes due to high hydrophobicity and volatility (e.g., $\log K_{ow}$=4.78(Banerjee et al., 1980) and Henry's Law Constant = 15.3×10^{-3} atm m^3/mol at 25°C(Dewulf et al., 1999) for HCBD). Alternatively, other treatment techniques such as ozonation, UV photolysis, or their combination with H_2O_2, i.e., O_3/H_2O_2 or UV/H_2O_2, also known as advanced oxidation processes (AOPs), can be potentially considered. AOPs are chemical treatment processes in which hydroxyl radicals ($^{\cdot}OH$) are produced *in situ*.(Glaze et al., 1987) However, the current lack of information on key parameters for such treatment options hampers the assessment of the abatement efficiency for CBDs, namely, second-order rate constants for the reaction of CBDs with ozone (k_{O3}) or hydroxyl radicals ($k_{\cdot OH}$) for ozonation, O_3/H_2O_2, and UV/H_2O_2(von Gunten, 2003; von Sonntag and von Gunten, 2012) and a photon fluence-based pseudo first-order rate constant (k') for UV-based processes such as UV photolysis or UV/H_2O_2,(Bolton and Stefan, 2002; Canonica et al., 2008) respectively.

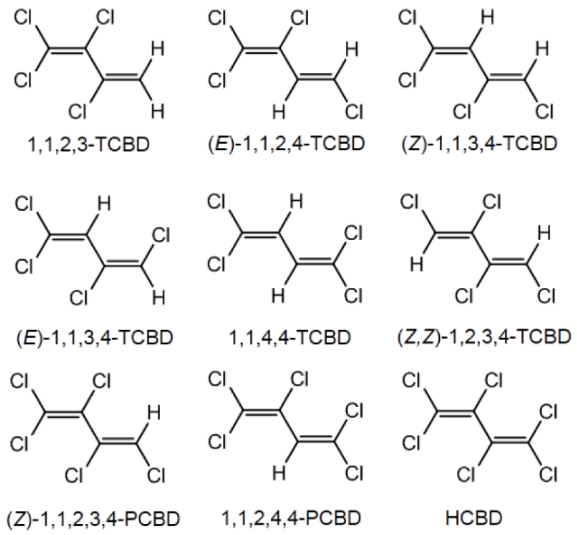

Fig. 4.1: *The selected 9 tetra-, penta-, and hexa-chlorobutadienes (TCBD, PCBD, and HCBD, respectively) for this study.*

In the present study, k_{O3}, $k_{\bullet OH}$, and k' for UV photolysis at 254 nm were experimentally determined for 9 CBDs, i.e., 6 TCBD isomers (1,1,2,3-, (*E*)-1,1,2,4-, (*Z*)-1,1,3,4-, (*E*)-1,1,3,4-, 1,1,4,4-, and (*Z*,*Z*)-1,2,3,4-), 2 PCBD isomers ((*Z*)-1,1,2,3,4- and 1,1,2,4,4-), and HCBD (**Fig. 4.1**). Moreover, a previously developed quantum chemical model(Lee et al., 2015) was applied to predict k_{O3}-values for 9 CBDs, which were then compared to the experimental k_{O3}-values. Finally, the treatment efficacy for the selected CBDs by ozonation, direct UV photolysis, and the AOPs O_3/H_2O_2 and UV/H_2O_2 was evaluated in a natural groundwater matrix. For ozonation and O_3/H_2O_2, the abatement of other common micropollutants and bromate formation was also evaluated.

4.1 MATERIALS AND METHODS

4.1.1 STANDARDS AND REAGENTS

All chemicals used are summarized in Text S1 in the Supporting Information.

4.1.2 ANALYTICAL METHODS

9 CBDs, *p*-chlorobenzoic acid (*p*CBA), atrazine, 5 micropollutants (benzotriazole, carbamazepine, diatrizoate, iopamidol, and tramadol), bromate, ozone, and H_2O_2 were quantified using appropriate analytical methods (Text S2).

4.1.3 DETERMINATION OF SECOND-ORDER RATE CONSTANTS FOR THE REACTIONS OF CBDS WITH OZONE (K_{O3}) AND HYDROXYL RADICALS ($K_{\bullet OH}$)

k_{O3} for CBDs was determined by simultaneously measuring the abatement of CBDs and the ozone decay using Eq. S1 in Text S3. Determination of $k_{\bullet OH}$ for CBDs was performed by competition kinetics (Eqs. S2-S4) using *p*CBA as a competitor. $^{\bullet}OH$ were produced by photolysis of H_2O_2. More details about analytical instruments and experimental procedures are provided in Text S3**.**

Determination of photon fluence-based first-order rate constants (k'), molar absorption coefficients (ε), and quantum yields (Φ) for phototransformation of CBDs at UV 254 nm

k' (m^2 $einstein^{-1}$) for 9 CBDs for UV irradiation at 254 nm were determined according to Eq. 1.

$$k' = \frac{k_{CBD,254nm}}{E_p^0} = \frac{2.303 \Phi_{ATZ,254nm} \varepsilon_{ATZ,254nm} k_{CBD,254nm}}{k_{ATZ,254nm}} \quad (1)$$

$k_{CBD,254nm}$ and $k_{ATZ,254nm}$ (s^{-1}) are a time-based pseudo first-order rate constant (s^{-1}) for the phototransformation of a CBD and atrazine at 254 nm, respectively, E_p^0 is a photon fluence rate (einstein m^{-2} s^{-1}) derived based on actinometry using atrazine (ATZ),(Canonica et al., 2008) and $\varepsilon_{ATZ,254nm}$ and $\Phi_{ATZ,254nm}$ are 386 m^2 mol^{-1} and 0.046 mol $einstein^{-1}$ for atrazine at 254nm, respectively.(Canonica et al., 2008) Direct UV photolysis to obtain $k_{CBD,254nm}$ was measured using the same photoreactor used for the $k_{\bullet OH}$ determination (Text S3), but employing a low pressure (LP) mercury lamp (model TNN 15/32, Heraus Noblelight, Hanau, Germany) emitting monochromatic UV light at 254 nm and a quartz cooling jacket. Sample solutions containing individual CBDs (1.0–3.5 µM, pH 7, 5mM phosphate buffer) prepared in quartz tubes were subject to UV irradiation. 5 µM of an atrazine solution at pH 7 (5 mM phosphate buffer) separately prepared was irradiated simultaneously to obtain the corresponding $k_{ATZ,254nm}$. $\varepsilon_{CBD,254nm}$ for the 9 CBDs were determined based on the Beer-Lambert law by monitoring the absorbance at 254 nm using a quartz cuvette (l = 10 cm) for various concentrations of CBDs (0.3 - 6 µM). $\Phi_{CBD,\ 254nm}$ was calculated according to Eq. 2.(Bolton and Stefan, 2002)

$$\Phi_{CBD,\ 254nm} = k'/(2.303 \varepsilon_{CBD,\ 254nm}) \quad (2)$$

Ozonation, direct UV photolysis (254nm), and advanced oxidation processes of the selected CBDs and micropollutants in a natural groundwater

A natural groundwater was sampled from the Hardwald site (Latitude 47°32′ N and Longitude 7°37′ E) in Switzerland (pH = 7.95 – 8.05, DOC = 0.5 mgC/L, alkalinity as HCO_3^- = 2.84 mM, and bromide = 48 µg/L). For ozonation, the groundwater was spiked with a mixture of the selected CBDs ((*E*)-1,1,2,4-, (*E*)-1,1,3,4-, (*Z*)-1,1,3,4-, 1,1,4,4-, and (*Z*,*Z*)-1,2,3,4-TCBDs, (*Z*)-1,1,2,3,4-PCBD, and HCBD, 5 - 9 µg/L) and 5 micropollutants (2 µg/L each). Varying ozone doses (0.25, 0.5, 1, 2, and 4 mg/L) were investigated in the absence and presence of H_2O_2 with ratios O_3:H_2O_2 (w/w) of 0.5, 1, and 2. UV photolysis for the selected CBDs was carried out in the absence and presence of H_2O_2 (0, 2.5, and 5.0 mg/L) up to a UV dose of 8600 J/m^2. Light screening by groundwater matrix components, estimated as a light attenuation factor as described elsewhere,(Wenk et al., 2011) was negligible (<2%). Therefore, no light screening correction for the UV dose was applied.

4.1.4 QUANTUM CHEMICAL COMPUTATIONS FOR THE PREDICTION OF K_{O3} OF CBDS

Quantum chemical computations were conducted using Gaussian 09 (Revision C.01).(Trucks et al., 2009) *Ab initio* Hartree-Fock (HF) and the Density Functional Theory (DFT)-B3LYP method with the 6-311++G** basis set were used. The integral equation formalism polarizable continuum model (IEF-PCM)(Tomasi et al., 2005) was used for all the computations to account for the solvent effect applying a dielectric constant of 78.3 for water. Natural bond orbital (NBO) analyses were conducted using the NBO 3.1 program(E. D. Glendening, A. E. Reed, J. E. Carpenter, n.d.) to obtain a NBO energy ($E_{NBO,\ C\text{-}C(\pi)}$) corresponding to the π orbital of a C-C double bond of the CBDs. More details about the model development and the application procedure are given elsewhere.(Lee et al., 2015)

4.1.5 KINETIC MODELING

Kinetic simulations using Kintecus 5.00(Ianni, 2014) were performed to derive the respective k' for photoisomerization and other phototransformation processes of (*Z*)-1,1,3,4- and (*E*)-1,1,3,4-TCBDs in a mixture (Text S5) and to derive a simulated abatement of CBDs based on derived k'-values.

4.2 RESULTS AND DISCUSSION

4.2.1 KINETICS OF THE REACTIONS OF CBDS WITH OZONE ($K_{O3,EXP}$)

The experimentally determined k_{O3} ($k_{O3,exp}$) are shown in **Tab. 4.1**. Overall, $k_{O3,exp}$-values for the 9 CBDs ranged over more than 4 orders of magnitude: TCBDs (1.6×10^2–7.8×10^3 $M^{-1}s^{-1}$), PCBDs (1–10 $M^{-1}s^{-1}$), and HCBD (< 0.1 $M^{-1}s^{-1}$). Note that (*E*)-1,1,3,4-TCBD and (*Z*)-1,1,3,4-TCBD was ozonated as a mixture as received from the supplier. Nonetheless, the obtained $k_{O3,exp}$-values are considered to be valid because the ozone concentration is in excess (>15 fold) to 1,1,3,4-TCBDs ensuring that each isomer degrades independently of the other isomer. $k_{O3,exp}$ for HCBD could not be determined because no appreciable degradation was observed under the experimental conditions. Thus, $k_{O3,exp}$ for HCBD was estimated to be < 0.1 $M^{-1}s^{-1}$ which is the reported $k_{O3,exp}$ range for PCE.(Hoigné and Bader, 1983)

Tab. 4.1: *Experimental k_{O3} ($k_{O3,exp}$) and predicted k_{O3} ($k_{O3,pred}$) or experimental $k_{\cdot OH}$ for the reactions of CBDs with ozone or hydroxyl radicals.*

Compound	$k_{O3,exp}$[a] (N[b])	$k_{O3,pred}$[c]		$k_{\cdot OH}$[a] (N[b]), $\times10^9$ $M^{-1}s^{-1}$
		HF/6-311++G**	B3LYP/6-311++G**	
1,1,2,3-TCBD	$(3.0\pm0.6)\times10^2$ (*4*)	1.4×10^3	1.6×10^3	3.4±0.5 (*4*)
(*E*)-1,1,2,4-TCBD	$(7.8\pm1.0)\times10^3$ (*4*)	2.2×10^3	2.5×10^3	6.0±1.6 (*6*)
(*E*)-1,1,3,4-TCBD	$(1.1\pm0.2)\times10^3$ (*3*)	3.4×10^2	5.0×10^2	5.3±1.8 (*3*)
(*Z*)-1,1,3,4-TCBD	$(4.0\pm2.4)\times10^2$ (*3*)	3.6×10^2	5.7×10^2	5.7±3.2 (*3*)
1,1,4,4-TCBD	$(2.7\pm0.4)\times10^2$ (*3*)	6.9×10^2	1.0×10^3	5.4±0.8 (*5*)
(*Z*,*Z*)-1,2,3,4-TCBD	$(1.6\pm0.3)\times10^2$ (*3*)	4.2×10^2	6.0×10^2	7.1±1.5 (*6*)
(*Z*)-1,1,2,3,4-PCBD	0.8±0.3 (*4*)	1.5×10^2	2.4×10^2	2.1±0.8 (*3*)
1,1,2,4,4-PCBD	10.0±2.3 (*5*)	1.5×10^2	1.8×10^2	3.9±0.9 (*5*)
HCBD	< 0.1	25	47	0.9±0.7 (*3*)

[a]Experimental *k-values* ($M^{-1}s^{-1}$) for ozone and hydroxyl radicals given as a mean value (±95% confidence interval determined by the Student's *t* test), [b]number of replicates, [c]predicted k_{O3}-value ($M^{-1}s^{-1}$) derived from Eq. S6 in SI. The experimental data used to determine k_{O3} and $k_{\cdot OH}$ are presented in Figures S2 and S3.

Overall, with increasing chlorine substituents on CBDs from four to six, the $k_{O3,exp}$-values decrease. This suggests the electron-withdrawing effect of chlorine substituents on $k_{O3,exp}$ for CBDs is additive, which is in agreement with previous observations for chlorinated ethenes.(Dowideit and von Sonntag, 1998) The range of $k_{O3,exp}$ for TCBD and PCBD is similar to the range of $k_{O3,exp}$ for dichloroethenes (DCEs) (1.1×10^2–7.9×10^3 $M^{-1}s^{-1}$)(Dowideit and von Sonntag, 1998) and TCE (14 $M^{-1}s^{-1}$),(Dowideit and von Sonntag, 1998) respectively.

Differences in $k_{O3,exp}$-values were noticeable between isomers with the same number of chlorine substituents: ~10-fold or ~50-fold for the two PCBD isomers or the six TCBDs isomers, respectively. This indicates that differing positions of the chlorine substituents influence electronic interactions of CBDs with ozone. Although this variation is not well understood, the *cis* effect may explain the specific observation that $k_{O3,exp}$ for *cis*- or (*Z*)-1,1,3,4-TCBD was lower than $k_{O3,exp}$ for *trans*- or (*E*)-1,1,3,4-TCBD by a factor of ~2.4. The *cis* effect is a phenomenon that the *cis*-isomer is more stable compared to the *trans*-isomer for 1,2-difluoroethene and 1,2-DCE(Chaudhuri et al., 2008; Craig et al., 1992; Pitzer and Hollenberg, 1954) and was also observed in k_{O3} for 1,2-DCE: k_{O3} for (*Z*)-1,2-DCE (5.4×10^2 $M^{-1}s^{-1}$) is ten times lower than k_{O3} for (*E*)-1,2-DCE (6.5×10^3 $M^{-1}s^{-1}$).(Dowideit and von Sonntag, 1998)

4.2.2 PREDICTION OF RATE CONSTANTS FOR THE REACTIONS OF CBDS WITH OZONE ($K_{O3,PRED}$)

k_{O3}-values for CBDs were predicted by taking into account (non)-planar CBD conformers using the previously developed quantum chemical model for olefins (**Tab. 4.1**).(Lee et al., 2015) Detailed procedures and discussion for deriving a predicted k_{O3} are presented in Text S4. A k_{O3} prediction procedure is briefly demonstrated for (*E*)-1,1,2,4-TCBD in **Fig. 4.2** where two conformers corresponding

to minima in the potential energy curve (PEC) were found: The first conformer has a dihedral angle (i.e., the angle between the planes comprising the atoms C_1-C_2-C_3 and C_2-C_3-C_4 in **Fig. 4.2**, respectively) of 0° and the other 116° (Text S4 for more details). The planar *s-trans* global minimum conformer (φ=0°) of (*E*)-1,1,2,4-TCBD reads -11.50 eV and -12.77 eV of $E_{NBO,\ C\text{-}C(\pi)}$ (open circles) for the two C=C bonds, respectively. Based on a linear regression equation (log k_{O3} = 1.32×$E_{NBO,\ C\text{-}C(\pi)}$ +18.54 for the HF/6-311++G** method),(Lee et al., 2015) $k_{O3,\ global(C1=C2)}$ = 48 $M^{-1}s^{-1}$ and $k_{O3,\ global(C3=C4)}$ = 2265 $M^{-1}s^{-1}$ were obtained, respectively, resulting in 2314 $M^{-1}s^{-1}$ for a species-specific second-order rate constant ($k_{O3,\ global}$) for the global conformer based on Eq. S5. As expected, the C=C bond with a higher chlorine substitution had a lower k_{O3}. In the same manner, $k_{O3,\ local}$ of 1378 $M^{-1}s^{-1}$ was obtained for the *gauche* local minimum conformer (φ=116°). Applying Eq. S6 with k_{O3}-values for global and local conformers and their relative populations (p_i in Table S3), $k_{O3,pred}$ for (*E*)-1,1,2,4-CBD was predicted to be 2.3×10^3 $M^{-1}s^{-1}$ with a prediction error of a factor of ~ 3 from $k_{O3,\ exp}$ = 7.8×10^3 $M^{-1}s^{-1}$.

Similarly, $k_{O3,pred}$-values were obtained for all 9 CBDs for both the HF and the B3LYP methods (**Tab. 4.1**). The k_{O3} prediction was satisfactory for the 6 TCBDs: 5 out of 6 TCBDs were predicted within a factor of 4 for both methods (Figure S6). In contrast, an overestimation occurred for the two PCBDs and HCBD by more than an order of magnitude. This may be caused by steric hindrances by chlorine substituents for the orbital interaction between ozone and PCBD/HCBD, which are not taken into account in $E_{NBO,\ C\text{-}C(\pi)}$ calculations. Alternatively, the C=C bond is so electron-poor that the formation of a cyclic ozonide(Dowideit and von Sonntag, 1998; von Sonntag and von Gunten, 2012) is no longer dominant. Therefore, the reactivity of PCBDs and HCBD with ozone cannot be interpreted by only $E_{NBO,\ C\text{-}C(\pi)}$.

For CBDs with multiple conformers (Table S3), $k_{O3,pred}$-values in **Tab. 4.1** derived by considering both global and local minimum conformers (i.e., $k_{O3,global}$, $k_{O3,local}$, and their relative populations) based on Eq. S6 are almost the same as $k_{O3,global}$ in Table S4. This suggests that the contribution of a local minimum conformer (i.e., $k_{O3,local}$) to $k_{O3,pred}$ is insignificant, which is understood by the predominant population of a global minimum (Table S3). Moreover, the difference between $k_{O3,global}$ and $k_{O3,local}$ is less than a factor of 2 except for 1,1,4,4-TCBD (~3 and ~4 folds for HF and B3LYP method, respectively). Therefore, it seems that $k_{O3,global}$ can be used as a good approximation. However, it should be noted that this does not justify the general representability of $k_{O3,global}$ for other compounds.

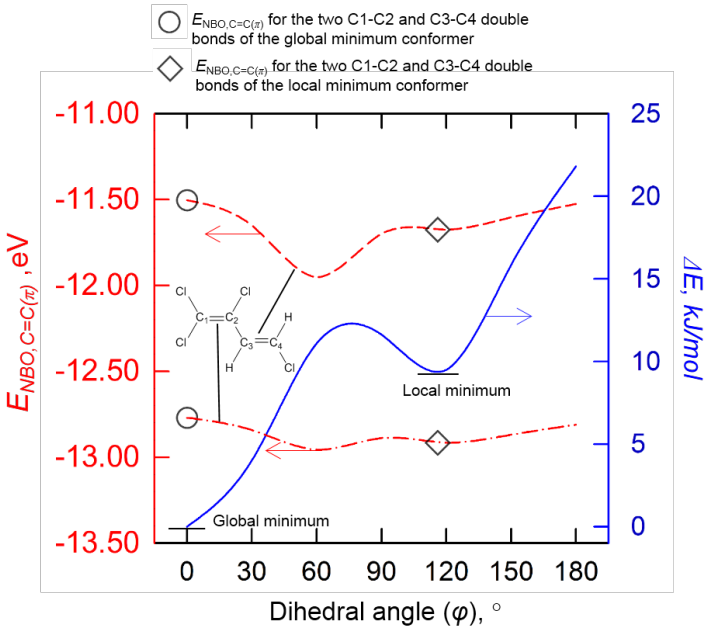

Fig. 4.2: *Profiles of the difference of a total electronic energy (blue solid line) (ΔE) of the (E)-1,1,2,4-TCBD conformers and the lowest energy of the (E)-1,1,2,4-TCBD conformer and the corresponding natural bond orbital energy ($E_{NBO,\ C\text{-}C(\pi)}$) (red dash-dot line and red dashed line for the C_1-C_2 and C_3-C_4 double bonds, respectively) of the π orbital of a C-C double bond of TCBD conformers as a function of the dihedral angle comprising the atoms C_1-C_2-C_3-C_4. All the energies were obtained at the HF/6-311++G** level.*

4.2.3 KINETICS FOR THE REACTION OF CBDS WITH HYDROXYL RADICAL ($K_{\bullet OH}$)

Experimenatlly determined $k_{\bullet OH}$-values for 9 CBDs are presented in **Tab. 4.1**. The determined $k_{\bullet OH}$-values are higher than 5×10^9 $M^{-1}s^{-1}$ for all TCBDs except 1,1,2,3-TCBD (3.4×10^9 $M^{-1}s^{-1}$). A lower reactivity with •OH was observed for the 2 PCBDs (2.1×10^9 $M^{-1}s^{-1}$ and 3.9×10^9 $M^{-1}s^{-1}$), followed by the lowest reactivity for HCBD (0.9×10^9 $M^{-1}s^{-1}$). Overall, a higher chlorine substitution of CBD leads to a lower reactivity with •OH. Decreased $k_{\bullet OH}$ with increasing chlorine substitution was also observed for chlorinated ethenes: 3.8×10^9 $M^{-1}s^{-1}$, 2.8×10^9 $M^{-1}s^{-1}$, and 2.0×10^9 $M^{-1}s^{-1}$ for *cis*-1,2-DCE, TCE, and PCE, respectively.(Getoff, 1991)

4.2.4 DETERMINATION OF FLUENCE-BASED FIRST-ORDER RATE CONSTANTS (K'), MOLAR ABSORPTION COEFFICIENTS (E), AND QUANTUM YIELDS (Φ)

4.2.4.1 FLUENCE-BASED FIRST-ORDER RATE CONSTANTS (K') AND PHOTOISOMERIZATION PROCESSES.

The determined k'-values based on Eq. 1 ranged from 210±30 m^2 $einstein^{-1}$ for 1,1,4,4-TCBD to 2730±440 m^2 $einstein^{-1}$ for (*Z*,*Z*)-1,2,3,4-TCBD, respectively. Two k'-values were reported for (*E*)-1,1,3,4- and (*Z*)-1,1,3,4-TCBDs for separate photoisomerization and other phototransformation processes (see below).

A noticeable formation of photo-products was detected by GC/MS analyses for (*E*)-1,1,2,4-, (*Z*)- and (*E*)-1,1,3,4- as a mixture, (*Z*,*Z*)-1,2,3,4-TCBD and (*Z*)-1,1,2,3,4-PCBD (**Fig. 4.3** and S7). Because of their identical mass fragmentation patterns to those of the parent compounds (Figure S7), these products are considered to be the isomers of the parent CBDs, and are termed as photoisomers hereafter. No other confirmative examinations of their molecular structure than the mass fragmentation were used.

Only relative responses of the photoisomers are presented in **Fig. 4.3** for (*E*)-1,1,2,4- and (*Z*,*Z*)-1,2,3,4-TCBD and (*Z*)-1,1,2,3,4-PCBD because there were no commercially available standards. The relative response was calculated as the peak area of the parent CBD or its photoisomers divided by the initial peak area of the parent CBD (all peak areas corrected by normalization to the internal standard).

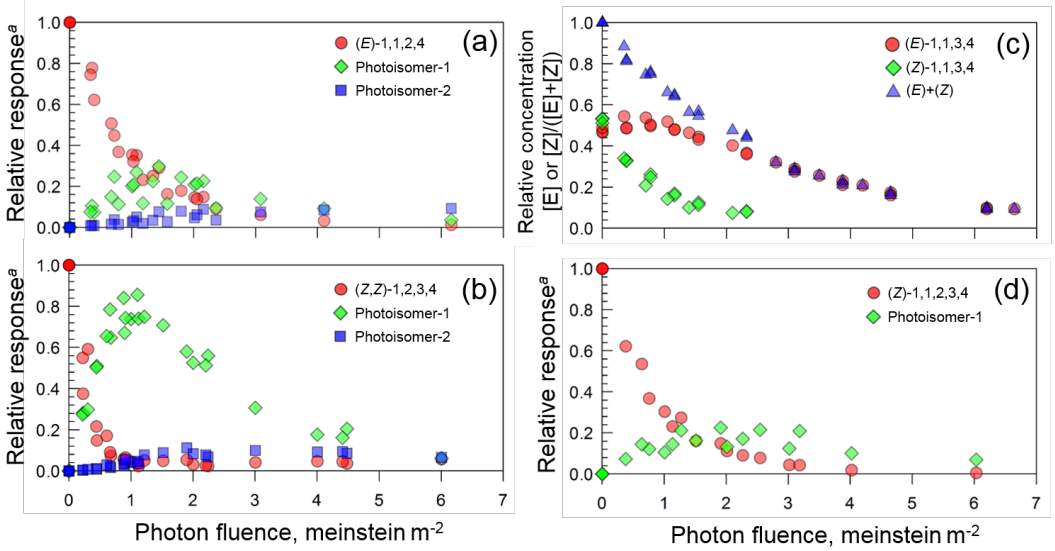

Fig. 4.3: *Evolution of (a) (E)-1,1,2,4-TCBD, (b) (Z,Z)-1,2,3,4-TCBD, (c) (E)-1,1,3,4- and (Z)-1,1,3,4-TCBD, and (d) (Z)-1,1,2,3,4-PCBD and their photoisomers as a function of the photon fluence (meinstein m^{-2}). [a]A relative response is the peak area of the parent CBDs or its photoisomers dividied by the initial peak area of the parent CBD. All peak areas are normalized by the internal standard.*

Photoisomerization of less than 40% relative to the parent CBD based on the relative response were observed for (*E*)-1,1,2,4-TCBD (**Fig. 4.3**a) and (*Z*)-1,1,2,3,4-PCBD (**Fig. 4.3**d), whereas a significant conversion of up to 85% was observed for (*Z*,*Z*)-1,2,3,4-TCBD (**Fig. 4.3**b). For UV irradiation (254 nm) of the mixture of (*E*)- and (*Z*)-1,1,3,4-TCBD (**Fig. 4.3**c), the (*E*)-1,1,3,4-TCBD concentration increased by ~10% compared to its initial concentration up to a UV photon fluence of 1 meinstein m^{-2}, while a significant degradation (>50%) of (*Z*)-1,1,3,4-TCBD occurred for the same UV dose. This indicates that a photoisomerization of the (*Z*)-1,1,3,4- to the (*E*)-1,1,3,4-TCBD occurs.

As rotation about a double bond is allowed in excited electronic states of organic compounds, all the CBDs with a *Z* or *E* configuration can undergo photoisomerization. Depending on the substitution pattern of the chlorine atoms, *Z* and *E* configuration pairs or (*Z*,*Z*), (*E*,*Z*) and (*E*,*E*) configuration triads are possible for photoisomerizable CBDs. In the case of (*Z*,*Z*)-1,2,3,4-TCBD, photoisomerization is proposed to occur following Scheme 1, which accounts for the formation of the two observed photoisomers (see **Fig. 4.3**b). Thereby, the peaks with a higher relative response (photoisomer-1 in (**Fig. 4.3**b and S7) and a lower relative response (photoisomer-2) were assigned to be the (*Z*,*E*)-photoisomer and the (*E*,*E*)-photoisomer, respectively, assuming a stepwise conversions (Scheme 4.1).

For (*E*)-1,1,2,4-TCBD two photoisomers were detected (**Fig. 4.3**a and S7), although only one photoisomer is predicted for an *E*-*Z* photoisomerization reaction. The additional photoisomer could be the result of a photocyclization reaction. Indeed, the formation of cyclobutene and cyclopropene isomers has been shown to occur upon direct UV irradiation of 1,3-dienes.(Boue and Srinivasan, 1970; Srinivasan, 1962) Only one photoisomer was observed for (*Z*)-1,1,2,3,4-PCBD, which was assigned to its *E* configuration.

$k_{CBD,254nm}$ in Eq. 1 determined for photo-isomerizable CBDs takes into account both photoisomerization and other phototransformations. This propagates into Φ_{254nm} and *k'* reported in **Tab 4.2** as those are determined based on $k_{CBD,254nm}$. Only for two 1,1,3,4-TCBD isomers, both photochemical processes could be differentiated by kinetic simulations because standards were available (see Text S5 and Figure S8 for more details), yielding the individual Φ_{254nm}- and *k'*-values in **Tab. 4.2**.

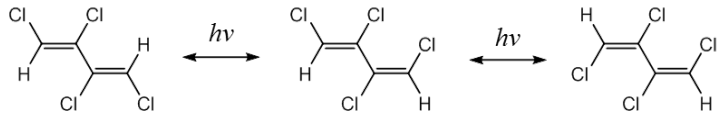

(*Z*,*Z*)-1,2,3,4 (*Z*,*E*)-1,2,3,4 (*E*,*E*)-1,2,3,4

Scheme 4.1: *Proposed photoisomerization of (Z,Z)-1,2,3,4-TCBD to (Z,E)-1,2,3,4-TCBD and (E,E)-1,2,3,4-TCBD.*

Tab. 4.2: ε_{254nm}, Φ_{254nm}, *and k' determined for the 9 selected CBDs*[a]

Compound	ε_{254nm}[a], m^2 mol^{-1}	Φ_{254nm}[b], mol $einstein^{-1}$	*k'* [a], m^2 $einstein^{-1}$
1,1,2,3-TCBD	620±80	0.22±0.04	310±40
(*E*)-1,1,2,4-TCBD	2490±140	0.14±0.04	820±370
(*E*)-1,1,3,4-TCBD	1580±140[c]	0.05±0.03[d], 0.07±0.04[e]	200±110[d], 270±150[e]
(*Z*)-1,1,3,4-TCBD		0.13±0.11[d], 0.27±0.06[e]	1000±180[d], 460±400[e]
1,1,4,4-TCBD	3210±100	0.03±0.004	210±30
(*Z*,*Z*)-1,2,3,4-TCBD	1620±140	0.73±0.13	2730±440
(*Z*)-1,1,2,3,4-PCBD	1110±470	0.32±0.26	810±560
1,1,2,4,4-PCBD	540±60	0.37±0.09	460±110
HCBD	230±60	0.95±0.28	510±110

[a]95% confidence intervals determined by the student's *t* test are given for all the reported values. [b]uncertainties estimated based on the error propagation through the multiplication of uncertainties in *k´* and ε_{254nm} for the respective CBDs. [c]average ε_{254nm} for the isomer mixture of (*E*)-1,1,3,4-TCBD (43%) and (*Z*)-1,1,3,4-TCBD (57%), [d]for photoisomerization, [e]for other phototransformations. The number of replicates for determination of *k'* for CBDs is 3 except for (*E*)-1,1,2,4- and (*Z*,*Z*)-1,2,3,4-TCBD for which the number is 4.

4.2.4.2 MOLAR ABSORPTION COEFFICIENTS (E).

The determined ε_{254nm} for the 9 selected CBDs are summarized in **Tab. 4.2**. The ε_{254nm}-values for 1,1,2,3-TCBD, 1,1,2,4,4-PCBD, and HCBD are in the order of 10^2 m^2 mol^{-1}, whereas they are in the order of 10^3 m^2 mol^{-1} for (*E*)-1,1,2,4-, 1,1,4,4-, and (*Z*,*Z*)-1,2,3,4-TCBD and (*Z*)-1,1,2,3,4-PCBD (**Tab. 4.2**). Note that since there were no separate standards available for the individual isomers, an average ε_{254nm} was determined for the isomer mixture of (*E*)-1,1,3,4- and (*Z*)-1,1,3,4-TCBDs.

4.2.4.3 QUANTUM YIELDS (Φ).

The determined Φ_{254nm} values based on Eq. 2 are presented in **Tab. 4.2**. They vary between 0.03 and 0.95, where the highest and the lowest Φ_{254nm} were determined for HCBD and 1,1,4,4-TCBD, respectively. Note that Φ_{254nm} for (*E*)-1,1,3,4- and (*Z*)-1,1,3,4-TCBD were determined using an average ε_{254nm} of their isomer mixture.

4.2.5 ABATEMENT OF CBDS AND MICROPOLLUTANTS AND BROMATE FORMATION IN A NATURAL GROUNDWATER DURING OZONATION, DIRECT UV PHOTOLYSIS, AND THE AOPS O_3/H_2O_2 AND UV/H_2O_2

4.2.5.1 OZONATION AND O_3/H_2O_2.

Fig. 4.4 shows the abatement of 7 selected CBDs and 3 micropollutants as well as the bromate formation during ozonation and the AOP O_3/H_2O_2 in Hardwald groundwater. For 0.5 mg O_3/L, >95% abatement (based on the calibration range) was observed for all TCBDs, whereas 47% and 16% abatement was obtained for (*Z*)-1,1,2,3,4-PCBD and HCBD, respectively. Note that the data for 0.25 mgO_3/L without H_2O_2 cannot be presented due to an analytical failure. A gradual increase in degradation was observed for (*Z*)-1,1,2,3,4-PCBD by increasing the ozone dose to 4.0 mgO_3/L achieving >95% abatement, while an abatement of up to 40% was observed for HCBD.

Among the 5 micropollutants investigated, carbamazepine and tramadol are not presented in **Fig. 4.4** because a complete abatement was always observed due to high k_{O3}-values of 3×10^5 $M^{-1}s^{-1}$ (Huber et al., 2003) for carbamazepine and 3.8×10^4 $M^{-1}s^{-1}$ (Zimmermann et al., 2012) for tramadol at pH 8.0, respectively. Benzotriazole shows overall similar degradation efficiencies as TCBDs, which can be explained by the similar k_{O3}-values (~1.0×10^3 $M^{-1}s^{-1}$ at pH 8.0 for benzotriazole(von Sonntag and von Gunten, 2012)). The degradation of iopamidol is comparable to (*Z*)-1,1,2,3,4-PCBD, which is consistent with rather similar k_{O3} and $k_{\cdot OH}$ (k_{O3} = <0.8 $M^{-1}s^{-1}$ (Huber et al., 2005) and $k_{\cdot OH}$ = 3.34×10^9 $M^{-1}s^{-1}$ (Jeong et al., 2010) for iopamidol and k_{O3} = 1.0 $M^{-1}s^{-1}$ and $k_{\cdot OH}$ = 2.2×10^9 $M^{-1}s^{-1}$ for (*Z*)-1,1,2,3,4-PCBD, this study). A higher abatement efficiency was observed for diatrizoate compared to HCBD. While two $k_{\cdot OH}$-values are reported for diatrizoate, namely, 0.5×10^9 $M^{-1}s^{-1}$ (Real et al., 2009) and 0.9×10^9 $M^{-1}s^{-1}$ (Jeong et al., 2010), 0.9×10^9 $M^{-1}s^{-1}$ was determined for HCBD in this study (**Tab. 4.1**).

Overall H_2O_2 addition led to a lower abatement efficiencies of the investigated compounds (**Fig. 4.4**). For ozone-reactive TCBDs and benzotriazole, it may be due to a decreased ozone exposure by a fast transformation of ozone to ·OH by hydrogen peroxide (mainly by HO_2^-).(von Sonntag and von Gunten, 2012) For ozone-resistant PCBD, HCBD, iopamidol, and diatrizoate, it may be due to an increased OH scavenging rate by added hydrogen peroxide (both H_2O_2 and HO_2^-) (e.g., about 8% increase of ·OH scanveging rate (s^{-1}) was estimated for H_2O_2/O_3 = 2.0 (w/w) and O_3 = 2.0 mg/L).

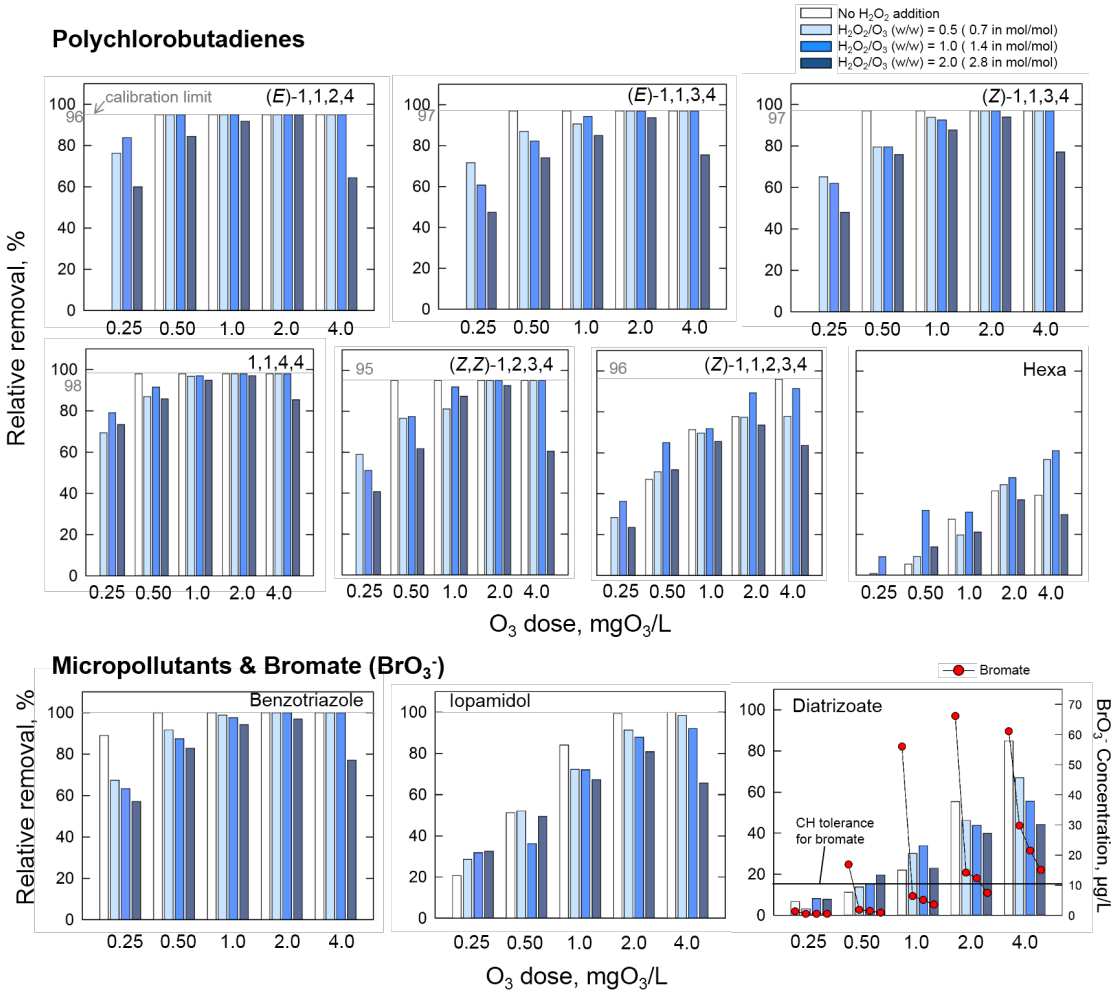

Fig. 4.4: *Abatement of CBDs and micropollutants and bromate formation during ozonation of Hardwald groundwater in the absence/presence of H_2O_2. The data for CBDs at 0.25 mgO_3/L without H_2O_2 are not presented due to an analytical failure. pH = 7.95 – 8.05, temperature = 25°C, and bromide concentration = 48 µg/L.*

Bromate formation dramatically increased with increasing ozone doses from 1.3 µg/L for 0.25 mgO_3/L to 56 – 66 µg/L for the higher ozone doses (1.0 - 4.0 mgO_3/L) (**Fig. 4.4**), which corresponds to 31-37% molar conversion from bromide. Upon H_2O_2 addition, the bromate formation was significantly reduced to below 10 µg/L, the drinking water standard in Switzerland,("Swiss Federal Department of the Interior (2000). Ordinance on Contaminants in Food., Bern, Switzerland," n.d.) EU,(EU, 1998) and USA.(USEPA, 1989), up to 1.0 mgO_3/L. The bromate concentrations remained above 10 µg/L for the higher ozone doses except for 2.0 mgO_3/L with H_2O_2/O_3=2.0 (w/w). The reduced bromate formation is attributable to the decreased ozone exposure caused by H_2O_2 addition, as explained above for TCBDs and benzotriazole.

4.2.5.2 Direct UV photolysis and UV/H_2O_2.

Direct UV photolysis for the 7 selected CBDs was compared with a simulated degradation based on the *k'*-values in 4.2 (**Fig. 4.5**). Overall, the model could predict the % abatement up to 50 % relatively well for all CBDs (lines in **Fig. 4.5**). For further degradation, relatively good predictions were observed for (*E*)-1,1,3,4- and 1,1,4,4-TCBD and HCBD. In contrast, poor predictions were obtained for (*E*)-1,1,2,4-, (*Z*)-1,1,3,4, and (*Z*,*Z*)-1,2,3,4-TCBD and (*Z*)-1,1,2,3,4-PCBD, which is due to an appearance of a plateau without further degradation. Interestingly, the CBDs with a poor prediction coincided with photo-isomerizable compounds except for (*E*)-1,1,3,4-TCBD. The concentration even slightly increased for (*Z*,*Z*)-1,2,3,4-TCBD. Concurrently with the appearance of a plateau, the enhanced formation of photoisomers was observed in a groundwater compared to a buffered purified water.

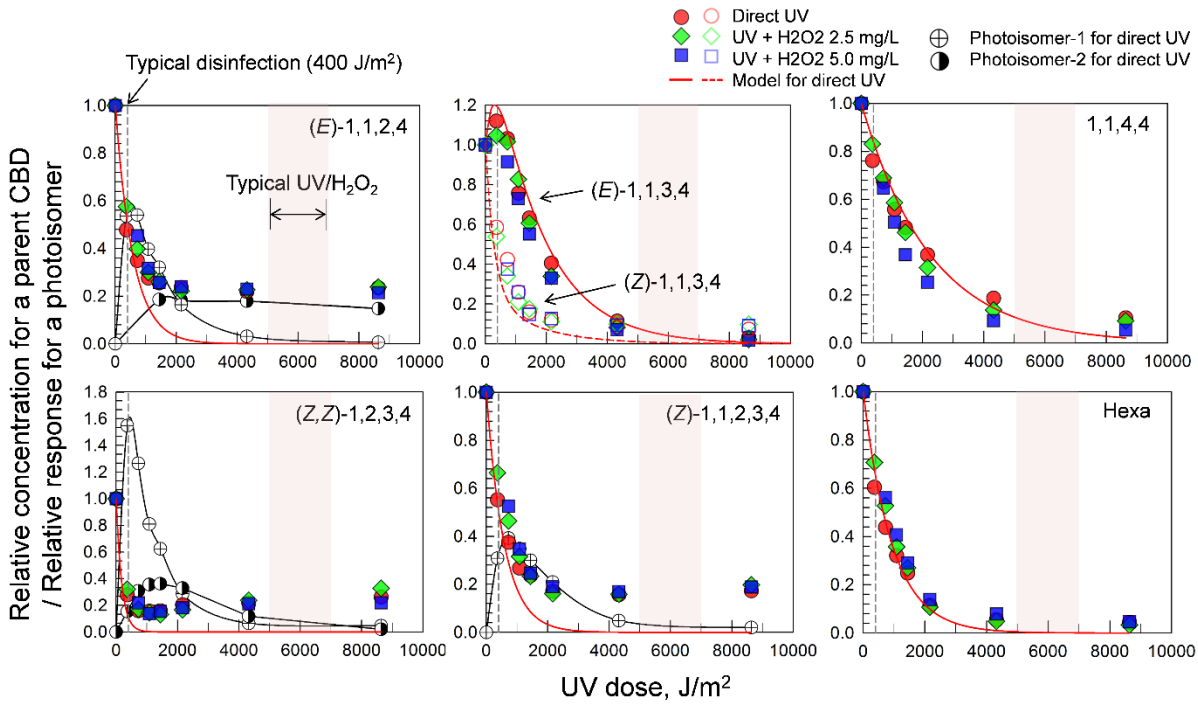

Fig. 4.5: *Abatement of CBDs during UV irradiation in absence/presence of H_2O_2 in Hardwald groundwater. A relative response is the peak area of the parent CBDs or its photoisomers dividied by the initial peak area of the parent CBD. All peak areas are normalized by the internal standard. UV dose (J/m²) was calculated by the equation: UV dose=E_p^0×irradiation time (seconds)×U, where U = 4.72×10⁵ J einstein⁻¹ at 254nm. pH = 7.95 – 8.05 and temperature = 25°C. Note the data for UV dose of about 360 J/m² for H_2O_2 = 5.0 mg/L are not presented due to an analytical failure.*

For example, the maximum relative response of the photoisomer-1 of (*Z,Z*)-1,2,3,4-TCBD was ~0.9 and ~1.6 in a buffered purified water (**Fig. 4.3**a) and a groundwater (**Fig. 4.5**), respectively. The interplay between CBDs and dissolved organic matter (DOM) present in a groundwater may be attributable to this phenomenon. Adsorption of CBDs to DOM could influence photoisomerization, inducing potentially a higher rotational barrier in the excited states. Moreover, the energy transfer between the species in the excited triplet states may play a role, especially when CBDs are adsorbed to DOMs. Further investigations to verify these hypotheses are necessary.

Although some enhancements (~10%) and inhibitions (~15%) were seemingly observed for (*E*)-1,1,3,4- and 1,1,4,4-TCBDs and (*Z*)-1,1,2,3,4-PCBD and HCBD (**Fig. 4.5**), respectively, overall no significant effect on the degradation of the investigated CBDs seemed to manifest upon H_2O_2 addition. This may be mainly due to the efficient UV phototransformation of CBDs. For non-photoisomerizable CBDs such as 1,1,4,4-TCBD and HCBD, the matrix effect of the groundwater seems to play a minor role because their degradation could be relatively well predicted using parameters determined in purified water.

4.2.6 PRACTICAL IMPLICATIONS

During ozonation 50-100% of the TCBDs were abated at ozone doses of 0.25-1.0 mgO_3/L. The abatement efficiencies were smaller for PCBD and HCBD. Overall abatement efficiencies were consistent between CBDs and other selected micropollutants when evaluated based on the corresponding experimental k_{O3} and $k_{\cdot OH}$. k_{O3} predictions for TCBDs by quantum chemical models can be an alternative to an empirical k_{O3} determination. H_2O_2 addition is advantageous for minimizing the bromate formation during ozonation, however, it may lead to a decreased abatement of CBDs or micropollutants. Therefore, the ozone and H_2O_2 doses have to be carefully optimized to maximize pollutant abatement and to minimize bromate formation. For a typical UV dose for disinfection (400 J/m²), various degrees of phototransformation could be achieved for the investigated CBDs from 10 % for 1,1,4,4-TCBD to 90% for (*Z,Z*)-1,2,3,4-TCBD. However, the photoisomer formation from

photoisomerizable CBDs and their biological effects must be taken into account for assessing the benefits of this treatment process. The beneficial effect of H_2O_2 addition on the UV-induced abatement of CBDs in the tested groundwater was observed to be minor (<10%).

4.3 REFERENCES

Agency for Toxic Substances and Disease Registry (ATSDR), 1994. Toxicological Profile for Hexachlorobutadiene.

Atlanta, GA: U.S. Department of Health and Human Services, P.H.S., 2006. Toxicological profile for Vinyl Chloride.

Banerjee, S., Yalkowsky, S.H., Valvani, S.C., Valvani, C., Valvani, S.C., 1980. Water Solubility and Octanol / Water Partition Coefficients of Organics . Limitations of the Solubility-Partition Coefficient Correlation. Environ. Sci. Technol. 14, 1227–1229. doi:10.1021/es60170a013

Barco-Bonilla, N., Plaza-Bolaños, P., Fernández-Moreno, J.L., Romero-González, R., Frenich, A.G., Vidal, J.L.M., 2011. Determination of 19 volatile organic compounds in wastewater effluents from different treatments by purge and trap followed by gas-chromatography coupled to mass spectrometry. Anal. Bioanal. Chem. 400, 3537–3546. doi:10.1007/s00216-011-5014-3

Bolton, J.R., Stefan, M.I., 2002. Fundamental photochemical approach to the concepts of fluence (UV dose) and electrical energy efficiency in photochemical degradation reactions. Res. Chem. Intermed. 28, 857–870. doi:10.1163/15685670260469474

Booker, R.S., Pavlostathis, S.G., 2000. Microbial reductive dechlorination of hexachloro-1,3-butadiene in a methanogenic enrichment culture. Water Res. 34, 4437–4445. doi:10.1016/S0043-1354(00)00214-1

Bosma, T.N., Cottaar, F.H., Posthumus, M.A., Teunis, C.J., van Veldhuizen, A., Schraa, G., Zehnder, A.J., 1994. Comparison of Reductive Dechlorination of Hexachloro-1,3-butadiene in Rhine Sediment and Model Systems with Hydroxocobalamin. Environ. Sci. Technol. 28, 1124–8. doi:10.1021/es00055a023

Botta, D., Dancelli, E., Mantica, E., 1996. A Case History of Contamination by Polychloro-1,3-butadiene Congeners. Environ. Sci. Technol. 30, 453–462. doi:10.1021/es9501575

Boue, S., Srinivasan, R., 1970. Differences in reactivity between excited states of cis- and trans-1,3-pentadiene. J. Am. Chem. Soc. 92, 3226–3227. doi:10.1021/ja00713a074

Brüschweiler, B.J., 2010. TTC-based risk assessment of tetrachlorobutadienes and pentachlorobutadienes--the in vitro genotoxic contaminants in ground and drinking water. Regul. Toxicol. Pharmacol. 58, 341–4. doi:10.1016/j.yrtph.2010.07.009

Burkhard, L.P., Sheedy, B.R., McCauley, D.J., DeGraeve, G.M., 1997. Bioaccumulation factors for chlorinated benzenes, chlorinated butadienes and hexachloroethane. Environ. Toxicol. Chem. 16, 1677–1686. doi:10.1897/1551-5028(1997)016<1677:BFFCBC>2.3.CO;2

Canonica, S., Meunier, L., von Gunten, U., 2008. Phototransformation of selected pharmaceuticals during UV treatment of drinking water. Water Res. 42, 121–8. doi:10.1016/j.watres.2007.07.026

Chaudhuri, R.K., Hammond, J.R., Freed, K.F., Chattopadhyay, S., Mahapatra, U.S., 2008. Reappraisal of cis effect in 1,2-dihaloethenes: an improved virtual orbital multireference approach. J. Chem. Phys. 129, 64101. doi:10.1063/1.2958284

Craig, N.C., Brandon, D.W., Stone, S.C., Lafferty, W.J., 1992. Partial structure for trans-1,2-difluoroethylene from high-resolution infrared spectroscopy. J. Phys. Chem. 96, 1598–1605. doi:10.1021/j100183a022

Dewulf, J., Van Langenhove, H., Everaert, P., 1999. Determination of Henry's law coefficients by combination of the equilibrium partitioning in closed systems and solid-phase microextraction techniques. J. Chromatogr. A 830, 353–363. doi:10.1016/S0021-9673(98)00877-2

Dowideit, P., von Sonntag, C., 1998. Reaction of Ozone with Ethene and Its Methyl- and Chlorine-Substituted Derivatives in Aqueous Solution. Environ. Sci. Technol. 32, 1112–1119. doi:10.1021/es971044j

E. D. Glendening, A. E. Reed, J. E. Carpenter, F.W., n.d. NBO Version 3.1.

EU, 1998. Official Journal of the European Community L 330: Directive 98/83/EG.

Fattore, E., Benfenati, E., Fanelli, R., 1996. Analysis of Chlorinated 1,3-Butadienes by Solid-Phase Microextraction and Gas Chromatography-Mass Spectrometry. J. Chromatogr. A 737, 85–91. doi:10.1016/0021-9673(95)01338-5

G. Oliver, Barry, L.E. Kaiser, K., 1986. Chlorinated organics in nearshore waters and tributaries of the St. Clair River. Water Poll. Res. J. Canada, 21, 344–350.

Getoff, N., 1991. Radiation- and photoinduced degradation of pollutants in water. A comparative study. Int. J. Radiat. Appl. Instrumentation. Part C. Radiat. Phys. Chem. 37, 673–680. doi:10.1016/1359-0197(91)90166-Y

Glaze, W.H., Kang, J.-W., Chapin, D.H., 1987. The Chemistry of Water Treatment Processes Involving Ozone, Hydrogen Peroxide and Ultraviolet Radiation. Ozone Sci. Eng. 9, 335–352. doi:10.1080/01919518708552148

Goldbach, R.W., Van Genderen, H., Leeuwangh, P., 1976. Hexachlorobutadiene residues in aquatic fauna from surface water fed by the river Rhine. Sci. Total Environ. 6, 31–40. doi:10.1016/0048-9697(76)90004-8

Hexachlorobutadiene in Drinking-water, Background document for development of WHO Guidelines for Drinking-water Quality, WHO/SDE/WSH/03.04/101, 2004.

Hoigné, J., Bader, H., 1983. Rate constants of reactions of ozone with organic and inorganic compounds in water—I. Non-dissociating organic compounds. Water Res. 17, 173–183. doi:10.1016/0043-1354(83)90098-2

Huber, M.M., Göbel, A., Joss, A., Hermann, N., Löffler, D., McArdell, C.S., Ried, A., Siegrist, H., Ternes, T. a, von Gunten, U., 2005. Oxidation of pharmaceuticals during ozonation of municipal wastewater effluents: a pilot study. Environ. Sci. Technol. 39, 4290–9.

Huber, M.M.M., Canonica, S., Park, G.-Y., von Gunten, U., 2003. Oxidation of Pharmaceuticals during Ozonation and Advanced Oxidation Processes. Environ. Sci. Technol. 37, 1016–1024. doi:10.1021/es025896h

Ianni, J.C., 2014. Kintecus, Windows Version 5.00.

Jeong, J., Jung, J., Cooper, W.J., Song, W., 2010. Degradation mechanisms and kinetic studies for the treatment of X-ray contrast media compounds by advanced oxidation/reduction processes. Water Res. 44, 4391–4398. doi:10.1016/j.watres.2010.05.054

Laska, A.L., Bartell, C.K., Laseter, J.L., 1976. Distribution of hexachlorobenzene and hexachlorobutadiene in water, soil, and selected aquatic organisms along the lower Mississippi River, Louisiana. Bull. Environ. Contam. Toxicol. 15, 535–542. doi:10.1007/BF01685701

Lee, M., Zimmermann-Steffens, S.G., Arey, J.S., Fenner, K., von Gunten, U., 2015. Development of Prediction Models for the Reactivity of Organic Compounds with Ozone in Aqueous Solution by Quantum Chemical Calculations: The Role of Delocalized and Localized Molecular Orbitals. Environ. Sci. Technol. 49, 9925–9935. doi:10.1021/acs.est.5b00902

Nikolaou, A.D., Golfinopoulos, S.K., Kostopoulou, M.N., Kolokythas, G.A., Lekkas, T.D., 2002. Determination of volatile organic compounds in surface waters and treated wastewater in Greece. Water Res. 36, 2883–2890. doi:10.1016/S0043-1354(01)00497-3

Pitzer, K.S., Hollenberg, J.L., 1954. cis- and trans-Dichloroethylenes. The Infrared Spectra from 130-400 Cm. -1 and the Thermodynamic Properties 1. J. Am. Chem. Soc. 76, 1493–1496. doi:10.1021/ja01635a010

Real, F.J., Benitez, F.J., Acero, J.L., Sagasti, J.J.P., Casas, F., 2009. Kinetics of the Chemical Oxidation of the Pharmaceuticals Primidone, Ketoprofen, and Diatrizoate in Ultrapure and Natural Waters. Ind. Eng. Chem. Res. 48, 3380–3388. doi:10.1021/ie801762p

Srinivasan, R., 1962. Kinetics of the Photochemical Dimerization of Olefins to Cyclobutane Derivatives. I. Intramolecular Addition. J. Am. Chem. Soc. 84, 4141–4145. doi:10.1021/ja00880a034

Stockholm Convention on Persistent Organic Pollutants, n.d.

Swiss Federal Department of the Interior (2000). Ordinance on Contaminants in Food., Bern, Switzerland, n.d.

Tomasi, J., Mennucci, B., Cammi, R., 2005. Quantum mechanical continuum solvation models. Chem. Rev. 105, 2999–3093. doi:10.1021/cr9904009

Trucks, G.W., Schlegel, H.B., Scuseria, G.E., Robb, M.A., Cheeseman, J.R., Scalmani, G., Barone, V., Mennucci, B., Petersson, G.A., Nakatsuji, H., 2009. Gaussian 09, revision C. 01; Gaussian, Inc. Wallingford, CT.

USEPA, 1989. National Primary Drinking Water Regulations (NPDWRs). Federal Register.

Vogel, T.M., McCarty, P.L., 1985. Biotransformation of tetrachloroethylene to trichloroethylene, dichloroethylene, vinyl chloride, and carbon dioxide under methanogenic conditions. Appl. Environ. Microbiol. 49, 1080–1083.

von Gunten, U., 2003. Ozonation of drinking water: part I. Oxidation kinetics and product formation. Water Res. 37, 1443–67. doi:10.1016/S0043-1354(02)00457-8

von Sonntag, C., von Gunten, U., 2012. Chemistry of ozone in water and wastewater treatment: From basic principles to applications. IWA publishing.

Wenk, J., von Gunten, U., Canonica, S., 2011. Effect of Dissolved Organic Matter on the Transformation of Contaminants Induced by Excited Triplet States and the Hydroxyl Radical. Environ. Sci. Technol. 45, 1334–1340. doi:10.1021/es102212t

Zimmermann, S.G., Schmukat, A., Schulz, M., Benner, J., von Gunten, U., Ternes, T.A., 2012. Kinetic and Mechanistic Investigations of the Oxidation of Tramadol by Ferrate and Ozone. Environ. Sci. Technol. 46, 876–84. doi:10.1021/es203348q

4.4 SUPPORTING INFORMATION

Text S1. Standards and reagents

6 Tetrachlorobutadiene (TCBD) isomers (1,1,2,3-, (*E*)-1,1,2,4-, (*Z*)-1,1,3,4-, (*E*)-1,1,3,4-, 1,1,4,4-, and 1,2,3,4-) and 2 pentachlorobutadiene (PCBD) isomers ((*Z*)-1,1,2,3,4- and 1,1,2,4,4-) (≥96%) were obtained from Neochema GmbH & Co. KG (Bodenheim, Germany). HCBD (98%), 4-chlorobenzoic acid (*p*CBA) (99%), *tert*-butanol (*t*-BuOH) (≥99.7%), hydrogen peroxide (≥35%), atrazine (98.8%), benzotraizole (99%), tramadol (≥99%), carbamazepine (99%) and sodium sulfite (≥98%) were obtained from Sigma Aldrich, and EPA 524 Internal Standard Mix containing fluorobenzene and 1,2-dichlorobenzene-d_4 were obtained from Supelco, respectively. Diatrizoic acid (92%) and iopamidol (99.6%) were purchased from Dr. Ehrenstorfer (Augsburg, Germany) and U.S. Pharmacopeia (MD, USA), respectively. Note that (*E*)- and (*Z*)-1,1,3,4-TCBD isomers were provided as a mixture, and their compositions were determined to be 43% and 57%, respectively, by ^{1}H and ^{13}C nuclear magnetic resonance (NMR) analysis (Table S1 and Figure S1). The fractions of (*E*)-1,1,3,4- and (*Z*)-1,1,3,4-TCBD were estimated by comparing the areas of two proton signals (22.85 and 29.91 for the proton attached to the C2 of (*E*)-1,1,3,4-TCBD and for the proton attached to the C4 of (*Z*)-1,1,3,4-TCBD, respectively). The *Z* configuration of 1,1,2,3,4-PCBD was confirmed by a ^{1}H NMR analysis (Table S2). All aforementioned chemicals were used without further purification. Solutions were prepared in purified water produced by the Milli-Q (Millipore) nanopure system for all experiments except for the experiments conducted in a natural groundwater.

Text S2. Analytical methods

The 9 CBDs were quantified by a purge and trap/gas chromatography/mass spectrometry (PT/GC/MS) system. The GC (Thermo Scientific Trace GC Ultra) equipped with Rts-VMS® capillary column (60m length, 0.32 mm i.d., 1.8µm film thickness; Restek) was connected to a MS (Thermo Scientific DSQ II). The CBDs were extracted from aqueous samples by the PT (Tekmar Dohrmann 3100 Sample Concentrator), which are then introduced with a splitless injection into the GC-MS system using helium (99.999%) as a carrier gas. Both a total ion current (TIC) chromatogram and a selected ion monitoring (SIM) chromatogram were employed depending on the purpose of the measurements. Note that the highest oven temperature and the MS source temperature were set to 220°C and 250°C, respectively, and no thermal isomerization was observed when CBDs were individually analyzed. *p*CBA (competition kinetics) and atrazine (UV dosimetry) were quantified using a high-performance liquid chromatography (HPLC) (Dionex Ultimate 3000) at 240 nm with an eluent of methanol and 20 mM phosphate buffer (pH 2) (60:40, v:v) and at 240 nm with an eluent of water and acetonitrile (50:50, v:v), respectively. A UV spectrophotometer (Cary 100, Varian) was used for various purposes: the determination of the ozone stock solution (molar extinction coefficient (ε) = 3200 M^{-1} cm^{-1} at 258 nm)(von Sonntag and von Gunten, 2012), the residual ozone concentration using the indigo method (ε = 20000 M^{-1} cm^{-1} at 600 nm)(Bader and Hoigné, 1981), the quantification of H_2O_2 stock solution (ε = 40 M^{-1} cm^{-1} at 240 nm)(Bader et al., 1988), and the determination of ε for 9 CBDs at 254 nm. The 5 micropollutants (benzotriazole, carbamazepine, diatrizoate, iopamidol, and tramadol) were quantified by a fully automated online solid phase extraction/liquid chromatography/mass spectrometry (online SPE/LC/MS/MS). In a first step, 20 mL of sample was loaded with a solution of acidic nanopure water (0.1 % formic acid) on a 2-layer extraction cartridge made of 8 mg OASIS HLB (15 µm, Waters) and 14 mg Isolute ENV+ (70 µm, Biotage, Uppsala, Sweden). Hence, the separation was performed at ambient temperature using an Atlantis T3 column (3.0 x 150 mm, 3 µm particle size) with a HPLC gradient containing acidic nanopure water (0.1% formic acid) and methanol. The detection was operated with a Thermo TSQ-Vantage equipped with an electrospray ionization probe (ESI). The method detection limits (MDL) were 1 ng L^{-1} for carbamazepine, 2 ng L^{-1} for tramadol and 5 ng L^{-1} for diatrizoate, iopamidol and benzotriazole. Bromate concentration was measured by capillary ion chromatography (Thermo Dionex ICS-4000) coupled with tandem mass spectrometry (Thermo TSQ-Vantage). The water samples were diluted 10 times prior to analysis and the MDL was 0.5 µg L^{-1}.

Text S3. Determination of second-order rate constants for the reactions of CBDs with ozone (k_{O3}) and hydroxyl radicals ($k_{\bullet OH}$)

k_{O3} for CBDs in aqueous solution were determined by simultaneously monitoring two terms in Eq. S1 during ozonation, i.e., the relative residual concentrations of CBDs at time, *t*, expressed as the natural logarithm and the corresponding ozone exposures, respectively.

$$-\ln\frac{[CBD]_t}{[CBD]_o} = k_{O3}\int [O_3]dt \qquad (S1)$$

An ozone stock solution was prepared in purified water cooled in an ice bath by sparging ozone-containing oxygen produced from an ozone generator using pure oxygen gas (>99.999%). The ozone concentration range in the stock solution was between 1 and 1.3 mM. For the determination of k_{O3}, an appropriate aliquot of the ozone stock solution, which renders always an excess of ozone to CBD, was transferred into the solution containing the individual CBDs (1.0 - 3.5 µM) at pH 2 in the presence of 5 mM *t*-BuOH as a scavenger for hydroxyl radicals. Samples from the ozonated CBD solution withdrawn at appropriate time intervals were quenched with sulfite. Thereafter, the CBDs were quantified with GC/MS and residual ozone was measured by the indigo method(Bader and Hoigné, 1981), respectively. The k_{O3}-values were determined separately for individual CBDs. The experimental data used to determine k_{O3} in **Tab. 4.1** are presented in Figure S2.

$k_{\bullet OH}$ for CBDs were determined by UV-photolysis of H_2O_2 by competition kinetics with *para*-chlorobenzoic acid (*p*CBA) ($k_{\bullet OH,pCBA} = 5\times10^9\ M^{-1}s^{-1}$)(Neta, P., 1968). A medium pressure (MP) mercury UV lamp housed in a Pyrex® cooling jacket with tap water as cooling water was used. The filtered MP-UV lamp, the main emission line responsible for H_2O_2 photolysis being centered at 313 nm, was placed in the center of a DEMA 125 merry-go-round photoreactor (MGRR) (Hans Mangels, Bornheim-Roisdorf, Germany) filled with purified water and constantly kept at 25°C. Details about the photoreactor are found elsewhere.(Canonica et al., 1995; Wegelin et al., 1994) The Pyrex® glass cooling jacket, which ensured that UV light with wavelength <290 nm was cut off, was chosen to minimize direct photolysis of the CBDs (Figure S4) while sustaining an acceptable rate of •OH production. A composite solution (pH 7, 5 mM phosphate buffer) of 20 mL containing CBD (1.0-3.5 µM), *p*CBA (0.2-2.0 µM) as a competitor, and H_2O_2 (10 mM) as •OH source in a quartz tube (ID: 15 mm and OD: 18 mm) was exposed to UV at 313 nm in the MGRR. Samples were collected at appropriate irradiation times for the quantification of the respective compounds. Despite the use of 313 nm to achieve exclusive degradation of CBDs by •OH, a loss of the target compound still occurred to some extent by direct photolysis at 313nm and volatilization. Therefore, the photo-degradation of CBDs in the absence of H_2O_2 was also monitored to correct the loss. The net degradation of CBDs by •OH after the correction was used to determine $k_{\bullet OH}$. The correction was in the range of 0~13%. Consequently, $k_{\bullet OH,CBD}$ could be determined based on Eq. S4 which is obtained by combining Eqs. S2 and S3. The slope of a linear regression line obtained by $\ln([CBD]_t/[CBD]_0)/\ln([pCBA]_t/[pCBA]_0)$ is multiplied by $k_{\bullet OH,pCBA}$ ($5\times10^9\ M^{-1}\ s^{-1}$)(Neta, P., 1968) to give rise to the corresponding $k_{\bullet OH,CBD}$.

$$-\ln\frac{[CBD]_t}{[CBD]_o} = k_{\bullet OH,\,CBD}\int [{}^\bullet OH]dt \qquad (S2)$$

$$-\ln\frac{[pCBA]_t}{[pCBA]_o} = k_{\bullet OH,\,pCBA}\int [{}^\bullet OH]dt \qquad (S3)$$

$$k_{\bullet OH,\,CBD} = k_{\bullet OH,\,pCBA}\ln\left(\frac{[CBD]_t}{[CBD]_o}\right)/\ln\left(\frac{[pCBA]_t}{[pCBA]_o}\right) \qquad (S4)$$

The ln term is a relative concentration of respective compounds at the time (*t*) with respect to its initial concentration (*t*=0), $k_{\bullet OH}$ is a second-order rate constant for the reaction of •OH for the respective

compounds in units of $M^{-1}s^{-1}$, and $\int[^{\bullet}OH]dt$ is the exposure to $^{\bullet}OH$ until t in units of M·s. The experimental data used to determine $k_{^{\bullet}OH,CBD}$ in **Tab. 4.1** are presented in Figure S3.

Text S4. Prediction of second-order rate constants for the reactions of CBDs with ozone (k_{O3}) using a previously developed quantum chemical prediction model.

The k_{O3} prediction for CBDs by a quantum chemical model was conducted and is of special interest for the following two reasons:

(*i*) Model applicability to non-planar dienes: (near)-Planar dienes such as sorbic acid and microcystin-LR were successfully included in a previously developed quantum chemical model.(Lee et al., 2015) Unlike those, CBDs manifest the high degree of a non-planarity driven by the steric repulsion between chlorine substituents (e.g., (*E*,*E*)-1,2,3,4-TCBD and HCBD were found to be in the *gauche* form with torsion angles of 75° and 83.6°, respectively.(Gundersen et al., 1988)) (Scheme S1). Therefore, the applicability of the model to non-planar dienes such as CBDs has to be tested.

(*ii*) Consideration of co-present CBD conformers: 1,3-butadiene, by virtue of facile rotation about a central C–C single bond, can exist in planar forms such as *s-trans* and *s-cis* and/or in a non-planar (i.e., *gauche*) form (Scheme S1). An unsubstituted 1,3-butadiene is known to predominantly exist in the *s-trans* form(Almenningen et al., 1958; Marais et al., 1962; Schomaker and Pauling, 1939) with the *gauche* form co-present(Boopalachandran et al., 2011; Furukawa et al., 1983) in a fraction of approximately ~2%(Craig and Sams, 2008) in the gas phase at room temperature.

In contrast to an experimental k_{O3}, which yields an overall value of aggregate reactions of all present conformers with ozone, the quantum chemical model allows to predict k_{O3} for a specific species under consideration. As conformers may have differing populations and reactivities with ozone, their role to a predicted k_{O3} is of interest when CBD conformers are present. Note that the previously developed prediction model was using only one local minimum conformer without considering multiple conformers. Thus, the prediction performance when considering multiple conformers is unknown. As such, there is an interest to explore the sensitivity of the model on the treatment of multiple CBD conformers. With these two facets in mind, a k_{O3} prediction for CBDs was performed.

A relaxed potential energy curve (PEC) scan with a dihedral angle comprising the atoms C_1-C_2-C_3-C_4 (φ) (Scheme S1) as a variable from the *s-trans* to the *s-cis* configuration was performed for nine CBDs to locate stationary points on the PEC for HF and B3LYP with the 6-311++G** basis set. Note that the *s-trans* configuration is adopted to be 0° as a convention throughout this study. In **Fig. 4.2** in the main manuscript, the profile of the relative total electronic energy of the (*E*)-1,1,2,4-TCBD rotamers is presented compared to the conformer with the lowest energy and the corresponding $E_{NBO,\ C\text{-}C(\pi)}$ of the two C=C bonds of (*E*)-1,1,2,4-TCBD computed at the HF/6-311++G**. Two minima were identified in the vicinity of 0° and 120° with the former being the lowest energy minimum, i.e., the global minimum. As the geometries obtained from the relaxed scan are approximate, two *s-trans* and *gauche* conformers were further optimized and confirmed to be the minimum structure by frequency analysis at the same level of theory. The dihedral angles of the two optimized minimum structures were 0° and 116°, respectively. With ΔG=7.63 kJ mol^{-1} calculated between the two minima, the calculation of the Boltzmann distribution at room temperature (298K) yielded the population (p) of two *s-trans* and *gauche* conformers to be 92% and 8%, respectively. Note that a frequency analysis for the optimized geometry was conducted to derive ΔG. The minimum structures for the 9 CBDs with their dihedral angles and populations obtained at HF/6-311++G** and B3LYP/6-311++G** level are summarized in Table S3. While the B3LYP method identified 6 CBDs with two minima among the 9 CBDs, the HF method could only identify 3 CBDs with two minima. For such CBDs, the population of the local minimum structures ranged from 1 – 43% over both methods. A geometry obtained by B3LYP is commonly known to be more accurate than HF,(Cramer, 2013) minimum structures obtained by B3LYP are considered more accurate. However, the HF method has not been excluded from further investigations because it was previously shown that the HF method does not necessarily yield a worse prediction performance, which is supposedly due to the fortuitous cancellation of errors in a relative correlation.(Lee et al., 2015)

For a CBD with two C-C double bonds, an overall species-specific $k_{O3,i}$ can be derived according to Eq. S5.

$$k_{O3,i} = k_{O3,\,i(C1=C2)} + k_{O3,\,i(C3=C4)} \qquad \text{(S5)}$$

$k_{O3,\,i(C1=C2)}$ and $k_{O3,\,i(C3=C4)}$ are the site-specific second-order rate constant for the reaction of ozone with C_1=C_2 and C_3=C_4 of the *i*-th CBD conformer, respectively. $k_{O3,\,i(C1=C2)}$ and $k_{O3,\,i(C3=C4)}$ are derived from using the respective $E_{NBO,\,C\text{-}C(\pi)}$ of the two C=C bonds of the optimized CBDs for the linear regression equation from the previous study.(Lee et al., 2015) The predicted $k_{O3,i}$ for the 9 CBDs are presented in Table S4.

Taking the presence of multiple conformers into account for the k_{O3} assessment, an overall second order rate constant for the reaction of ozone with all minimum conformers, denoted as $k_{O3,pred.}$, is represented by Eq. S6.

$$k_{O3,pred.} = \Sigma(p_i \times k_{O3,i}) \quad \text{over all conformers i} \qquad \text{(S6)}$$

p_i is the relative population of a *i*-th conformer derived from a Boltzmann distribution (Table S3) and $k_{O3,i}$ is the species-specific second-order rate constant for the reaction of ozone with an *i*-th conformer from Eq. S5, respectively. The predicted $k_{O3,pred.}$ for the 9 CBDs for both calculation methods are presented in **Tab. 4.1**.

Text S5. Estimation of time-based first-order rate constants (s^{-1}) for phototransformation and photoisomerization of (*E*)-1,1,3,4- and (*Z*)-1,1,3,4-TCBD during UV irradiation at 254 nm by kinetic simulation

A pseudo-first order rate constant for the phototransformation of a CBD, denoted as *k*, was obtained during direct UV photolysis, which was then used to determine Φ and *k'* in the main manuscript. However, for CBDs that undergo a photoisomerization, the derived *k*-value can contain errors because of a reversibility of the photoisomerization (Eqs. S7 and S8).

$$\frac{d[Z]}{dt} = -k_{Z\rightarrow P}[Z] - k_{Z\rightarrow E}[Z] + k_{E\rightarrow Z}[E] \qquad \text{(S7)}$$

$$\frac{d[E]}{dt} = -k_{E\rightarrow P}[E] - k_{E\rightarrow Z}[E] + k_{Z\rightarrow E}[Z] \qquad \text{(S8)}$$

[*Z*] and [*E*] are the concentrations (mol L^{-1}) of a CBD in the *Z* configuration or the *E* configuration, respectively. $k_{Z\rightarrow P}$, $k_{Z\rightarrow E}$, $k_{E\rightarrow P}$, and $k_{E\rightarrow Z}$ are the first-order rate constants (s^{-1}) for the corresponding processes of CBDs during UV irradiation at 254 nm. The subscripts before and after the arrow (→) indicate the initial configuration (*E* or *Z*) of the CBD before photoisomerization and the final configuration of the CBD after the photoreaction, respectively. Unknown products are collectively denoted as *P* and the photoisomer is denoted as *E* or *Z*, respectively. Note that Eqs. S7 and S8 above are shown as examples for the CBDs which yield one photoisomer, such as (*E*)-1,1,3,4-TCBD, (*Z*)-1,1,3,4-TCBD, and (*Z*)-1,1,2,3,4-PCBD.

Based on the measured concentrations of two 1,1,3,4-TCBD isomers as a function of the UV irradiation time, the differential equations above (Eqs. S7 and S8) could be numerically solved by a kinetics simulation software (Kintecus 5.00(Ianni, 2014), fitting/optimization algorithm: Nelder & Mead,(Nelder and Mead, 1965) comparison operator: standard least squares) to derive individual *k*-values (Figure S8). The average *k*-values from triplicates with 95% confidence interval were 0.061±0.017, 0.078±0.035, 0.009±0.004, and 0.038±0.013 (s^{-1}) for $k_{Z\rightarrow P}$, $k_{Z\rightarrow E}$, $k_{E\rightarrow P}$, and $k_{E\rightarrow Z}$, respectively. Based on the *k*-value (0.0032±0.00003, s^{-1}) for atrazine determined from the atrazine actinometery, the corresponding *k'*-values for photoisomerization and other phototransformations are calculated according to Eq. 1 and presented in **Tab. 4.2** in the main manuscript.

Tab. S1: *1H and 13C chemical shifts (δ) and coupling constants (J) of (E)-1,1,3,4-tetrachlorobutadiene (TCBD) and (Z)-1,1,3,4-TCBD measured by 1H NMR and 13C NMR for a mixture of (E)-1,1,3,4-TCBD and (Z)-1,1,3,4-TCBD prepared in deuterated tetrahydrofuran (THF-d8) at a concentration of 20 mg/mL.*

C position[a]	This study				Reference study(Botta et al., 1998)		*Δδ* (^{13}C), ppm
	δ (^{1}H), ppm	*J*(^{1}H, ^{1}H), Hz	*δ* (^{13}C), ppm	*J*(^{13}C, ^{1}H), Hz	*δ* (^{13}C), ppm	*J*(^{13}C, ^{1}H), Hz	
(*E*)-1,1,3,4-TCBD							
1			126.6	1.6, 0.5	126.0		0.6
2	6.78	1.40	123.3	170.1, 6.9[b]	122.1	169.0, 6.9[b]	1.2
3			129.3	1.4, 1.1	128.9		0.4
4	6.69	1.40	121.0	204.0, 4.2[c]	120.2	201.9, 4.4[c]	0.8
(*Z*)-1,1,3,4-TCBD							
1			126.2	1.3, 1.3	125.7		0.5
2	6.70	1.16	125.6	169.4, 3.4[b]	124.7	168.7, 3.5[b]	0.9
3			128.9	13.8[d], 0.7	128.2	13.9[d]	0.7
4	6.99	1.16	124.1	200.0, 5.9[c]	123.2	199.1, 5.7[c]	0.9

[a]The position of a terminal carbon with two chlorine substituents is defined as 1, [b]*J*(^{13}C-2,^{1}H-4), [c]*J*(^{13}C-4,^{1}H-2), [d]*J*(^{13}C-3,^{1}H-4).

Tab. S2: *Confirmation of the Z configuration for 1,1,2,3,4-PCBD by 1H NMR and 13C NMR for a sample solution of (Z)-1,1,2,3,4-PCBD prepared in deuterated acetone at a concentration of 15 mg/mL.*

C position[a]	This study		Reference study(Botta et al., 1998)		*Δδ* (^{13}C), ppm	*ΔJ*(^{13}C,^{1}H), Hz
	δ (^{13}C), ppm	*J*(^{13}C, ^{1}H), Hz	*δ* (^{13}C), ppm	*J*(^{13}C, ^{1}H), Hz		
1	126.1	0.9	125.5	-	0.6	0.9
2	126.0	3.0	125.6	2.9	0.4	0.1
3	128.1	13.4	127.9	13.2	0.2	0.2
4	127.2	202.2	126.2	200.7	1.0	1.5

[a]The position of a terminal carbon with two chlorine substituents is defined as 1.

Tab. S3: *Summary of minimum structures of CBDs*

Compound	HF/6-311++G**			B3LYP/6-311++G**		
	φ[a]	*ΔG*[b]	Pop.[c]	*φ*[a]	*ΔG*[b]	Pop.[c]
1,1,2,3-TCBD	103.3	0	1.00	105.9	0	1.00
(*E*)-1,1,2,4-TCBD	0	0	0.92	0	0	0.96
	116.0	7.6	0.08	126.1	12.3	0.04
(*E*)-1,1,3,4-TCBD	105.6	0	1.00	38.5	0	0.58
				114.7	0.8	0.42
(*Z*)-1,1,3,4-TCBD	118.0	0	1.00	0	3.1	0.11
				128.5	0	0.89
1,1,4,4-TCBD	0	0	1.00	0	0	1.00
	106.2	16.6	0.00	119.0	24.0	0.00
(*Z,Z*)-1,2,3,4-TCBD	0	6.6	0.03	0	2.7	0.15
	117.8	0	0.97	122.0	0	0.85
(*Z*)-1,1,2,3,4-PCBD	101.7	0	1.00	104.5	0	1.00
1,1,2,4,4-PCBD[d]	100	0	1.00	58.1	0	0.57
				109.3	0.7	0.43
HCBD	92.2	0	1.00	94.4	0	1.00

[a]Dihedral angle (°), [b]Relative Gibbs free energy (kJ/mol) of the conformers to the lowest energy conformer [c]Population of the conformers calculated by the Boltzmann distribution equation using *ΔG*.

Tab. S4: *Predicted second-order rate constant for the reactions of ozone with a global minimum CBD (kO3,global) and a local minimum CBD (kO3,local) for various CBDs*

Compound	$k_{O3,global}$[a]/$k_{O3,local}$[b]	
	HF/6-311++G**	B3LYP/6-311++G**
1,1,2,3-TCBD	1.4×10^3	1.6×10^3
(*E*)-1,1,2,4-TCBD	2.3×10^3 / 1.4×10^3	2.5×10^3 / 1.6×10^3
(*E*)-1,1,3,4-TCBD	3.4×10^2	4.5×10^2 / 5.4×10^2
(*Z*)-1,1,3,4-TCBD	3.6×10^2	5.2×10^2 / 8.7×10^2
1,1,4,4-TCBD	6.9×10^2 / 2.5×10^2	1.0×10^3 / 2.6×10^2
(*Z*,*Z*)-1,2,3,4-TCBD	5.2×10^2 / 4.2×10^2	5.9×10^2 / 7.0×10^2
(*Z*)-1,1,2,3,4-PCBD	1.5×10^2	2.4×10^2
1,1,2,4,4-PCBD	1.5×10^2	1.6×10^2 / 2.4×10^2
HCBD	25	47

[a]Predicted k_{O3}-values ($M^{-1}s^{-1}$) calculated by only considering the global minimum conformer. [b]Predicted k_{O3}-values ($M^{-1}s^{-1}$) calculated by only considering the local minimum conformer. Only one k_{O3} is presented for CBDs with only one conformer (Tab. S3).

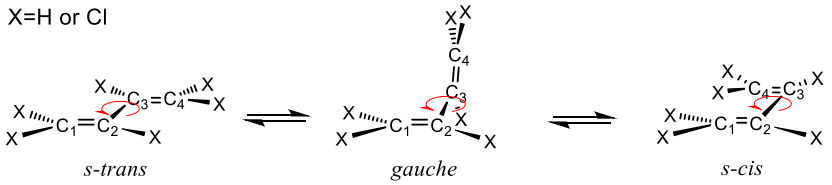

Scheme S1: *Conformations of (chloro)-1,3-butadiene*

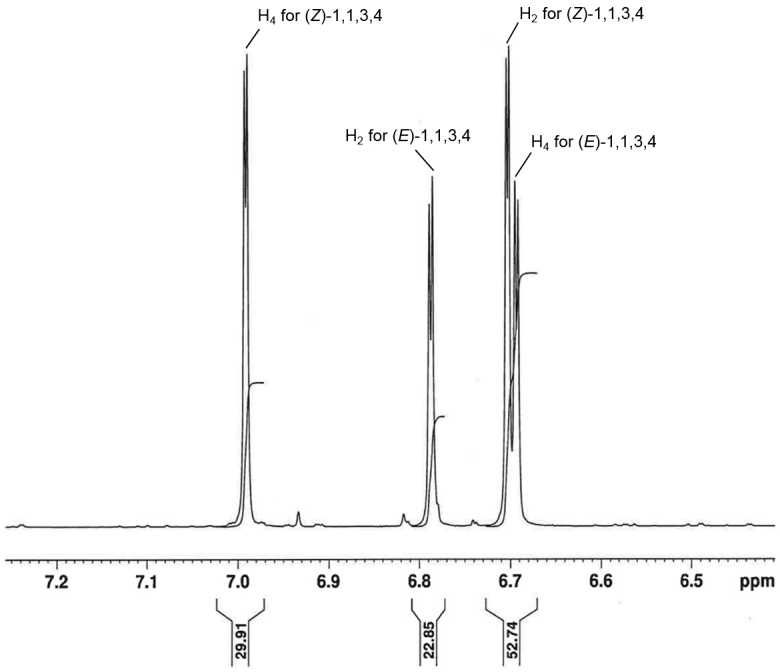

Fig. S1: *1H NMR of the mixture of (E)-1,1,3,4- and (Z)-1,1,3,4-TCBD prepared in THF-d8 at a concentration of 20 mg/mL. The areas of two proton signals (29.91 for (Z)-1,1,3,4-TCBD and 22.85 for (E)-1,1,3,4-TCBD) were used to estimate an isomer composition of 57 and 43 % for (Z)-1,1,3,4-TCBD and for (E)-1,1,3,4-TCBD, respectively.*

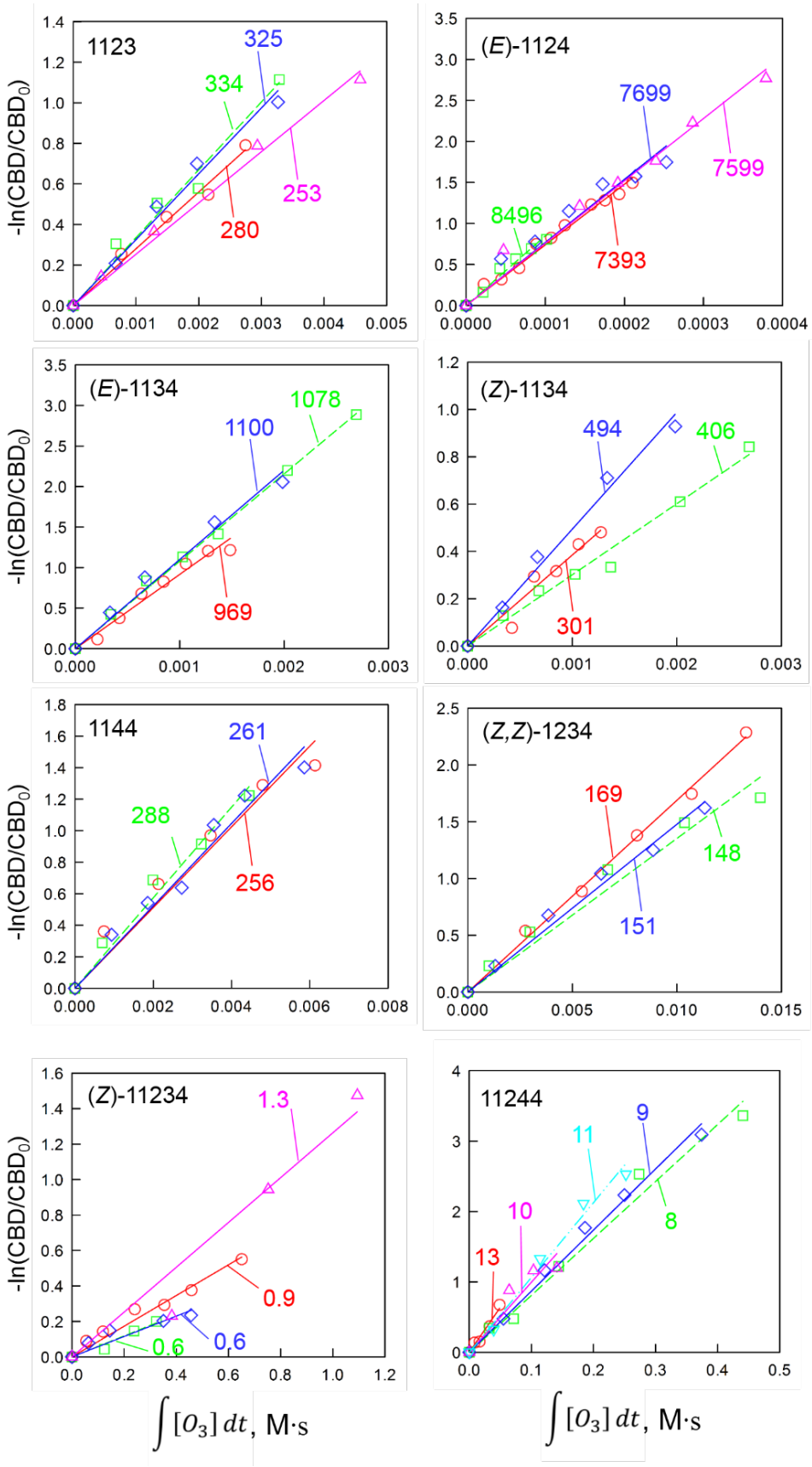

Fig. S2: *Second-order rate constants (kO3) for the reaction of CBDs with ozone. Natural logarithm of the relative decrease of CBDs as a function of the ozone exposures obtained from ozonation experiments. y-intercept was set to 0 for the linear regression. Experimental conditions: pH = 2, [CBDs]0 = 1.0 – 3.5 μM, and [t-BuOH] = 5mM. The number indicated to a slope of invididual linear regression lines represents the determined kO3.*

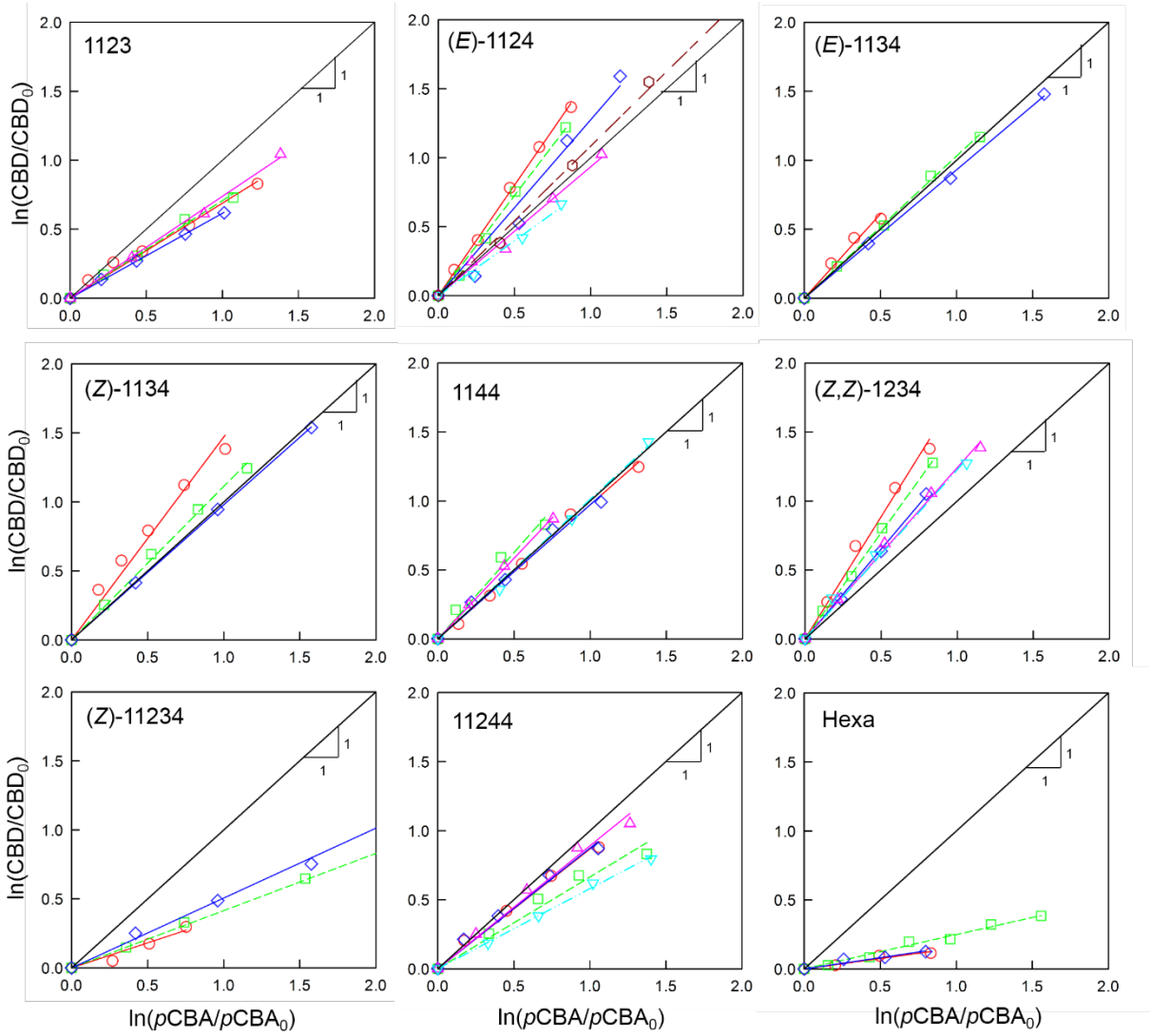

Fig. S3: *Competition kinetics to determine the second-order rate constants (k•OH,CBD)for the reactions of CBDs with hydroxyl radicals. Natural logarithm of the relative residual concentration of CBDs versus the corresponding natural logarithm of the relative residual concentration of pCBA during UV irradiation by the MP-UV (313nm). y-intercept was set to 0 for the linear regression. Experimental conditions: pH 7 buffered by 5 mM phosphate, [CBDs]0 = 1.0 – 3.5 µM, [pCBA]0 = 0.2 – 2.0 µM, and [H2O2]0 = 10 mM. The slopes of the straight lines represent k•OH,CBD/k•OH,pCBA*

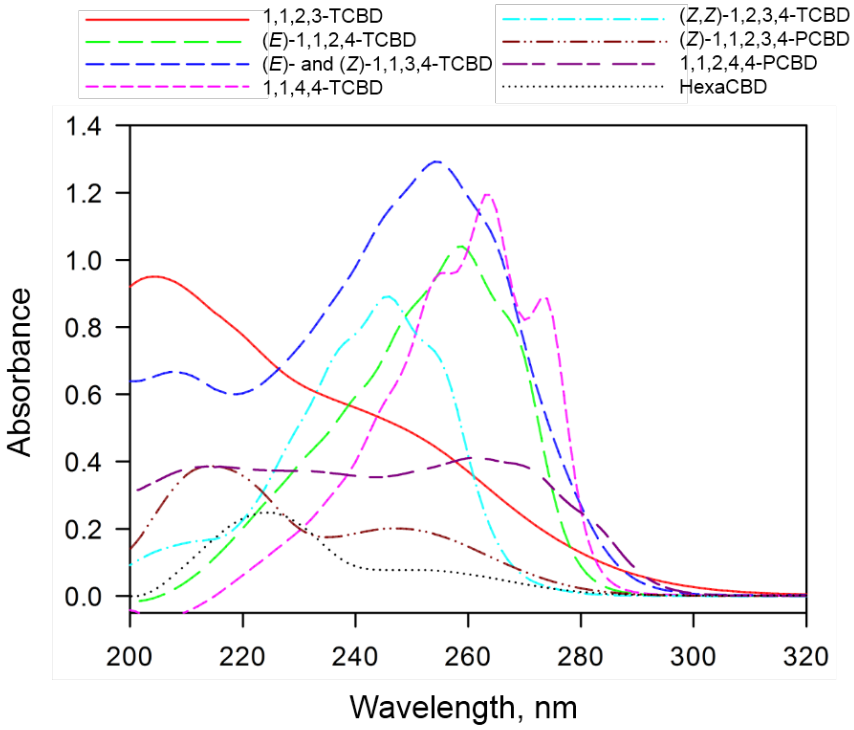

Fig. S4: *UV spectra between 200 and 320 nm for the selected chlorobutadienes (CBDs) (pathlength = 10 cm). 1,1,2,3- (7.2 µM), (E)-1,1,2,4- (3.8 µM), 1,1,3,4- (8.2 µM as the total concentration of the two isomer mixture), 1,1,4,4- (2.9 µM), and (Z,Z)-1,2,3,4-TCBD (4.5 µM), (Z)-1,1,2,3,4- (7.2 µM) and 1,1,2,4,4-PCBD (7.1 µM), and HCBD (3.2 µM)*

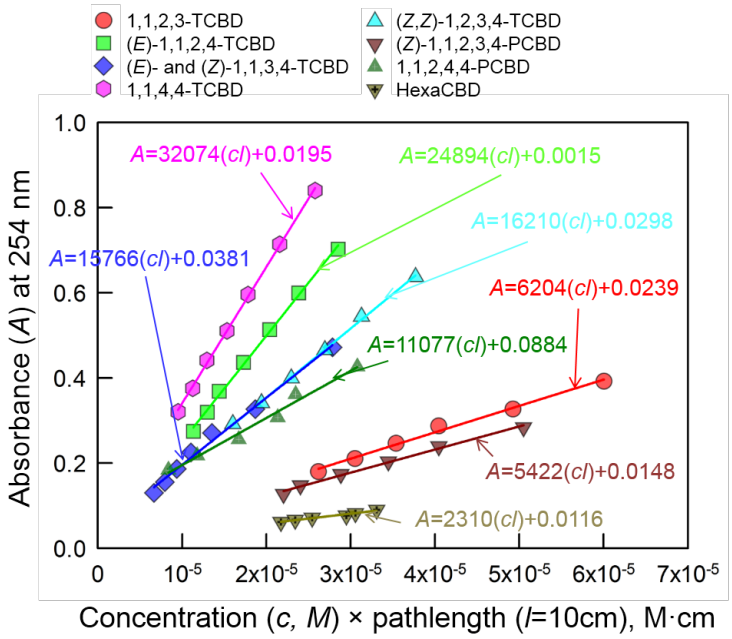

Fig. S5: *Determination of the molar absorption coefficients of the 9 selected CBDs (path length (l)=10 cm).*

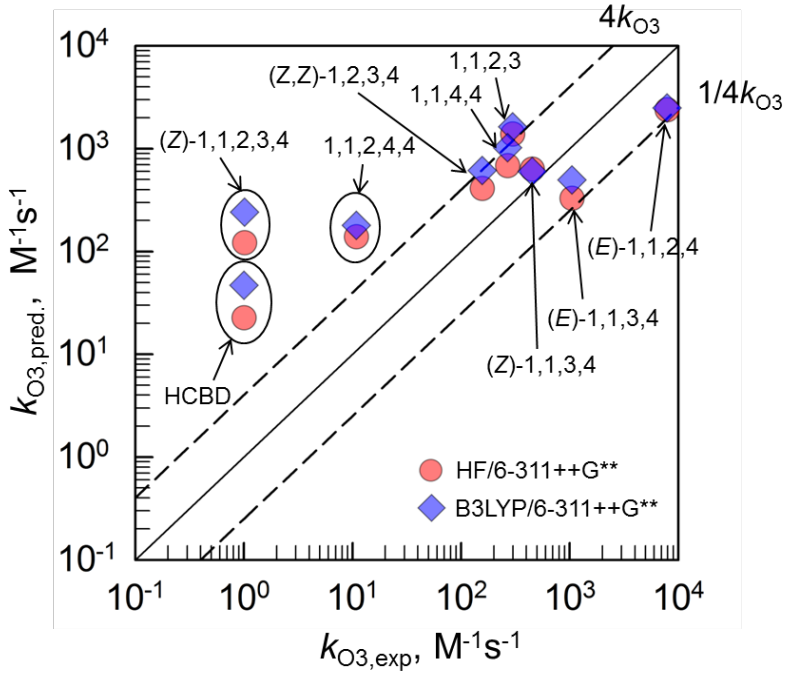

Fig. S6: *Predicted kO3 (kO3,pred.) versus experimental kO3 (kO3,exp) for the nine selected CBDs. Both kO3,exp- and kO3,pred.-values are from* ***Tab. 4.1****. The dotted line indicates an error of a factor of 4 of kO3,pred.*

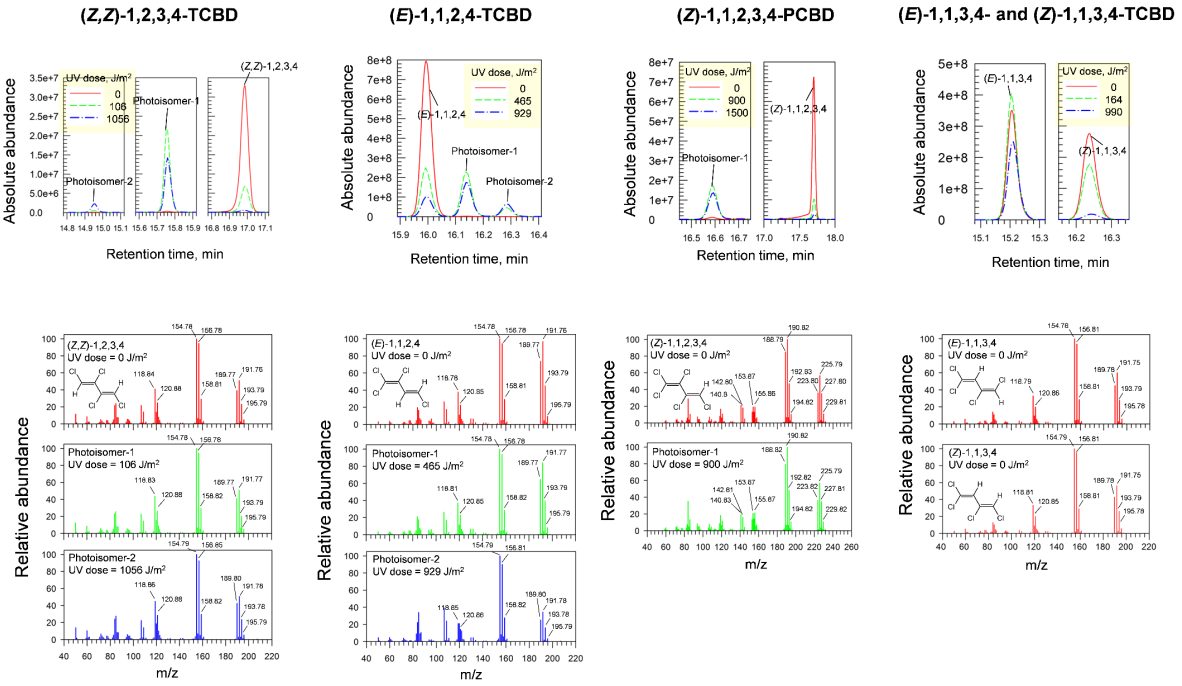

Fig. S7: *GC/MS chromatograms and mass spectra for photoisomerizable CBDs and their photoisomers. For the chromatograms, the peaks for parent and photoisomer CBDs are presented in an absolute abundance. This is only to visually guide their evolutions during UV irradiation. No quantitative information can be obtained because the repsonses from the three different samples were not corrected by an internal standard and no standards are available for photoisomers except for 1,1,3,4-TCBD.*

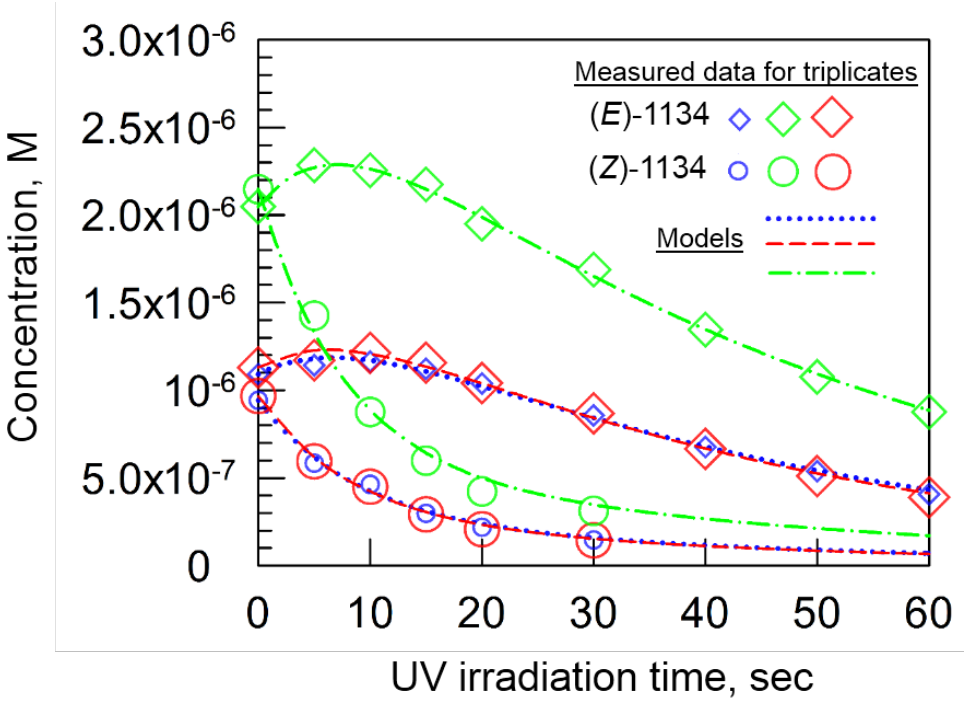

Fig. S8: *Experimental (symbols) and modeled (lines) evolution of a mixture of (E)-1,1,3,4- and (Z)-1,1,3,4-TCBDs (in triplicate) during UV irradiation at 254 nm. The modeled values (lines) were obtained based on Eqs. S7 and S8 by fitting of the experimental data.*

4.5 REFERENCES (SUPPORTING INFORMATION)

Almenningen, A., Bastiansen, O., Trætteberg, M., Grönvall, A., Zaar, B., Diczfalusy, E., 1958. An Electron Diffraction Reinvestigation of the Molecular Structure of 1,3-Butadiene. Acta Chem. Scand. doi:10.3891/acta.chem.scand.12-1221

Bader, H., Hoigné, J., 1981. Determination of ozone in water by the indigo method. Water Res. 15, 449–456. doi:10.1016/0043-1354(81)90054-3

Bader, H., Sturzenegger, V., Hoigné, J., 1988. Photometric method for the determination of low concentrations of hydrogen peroxide by the peroxidase catalyzed oxidation of N,N-diethyl-p-phenylenediamine (DPD). Water Res. 22, 1109–1115. doi:10.1016/0043-1354(88)90005-X

Boopalachandran, P., Craig, N.C., Laane, J., 2011. Gas-Phase Raman Spectra of s-trans- and s-gauche-1,3-Butadiene and Their Deuterated Isotopologues. J. Phys. Chem. A 116, 271–281. doi:10.1021/jp208739d

Botta, D., Mantica, E., Castellani, L., Dotelli, G., Zetta, L., 1998. 1H and 13C NMR study of some polychlorobuta-1,3-diene derivatives. Magn. Reson. Chem. 36, 885–891. doi:10.1002/(SICI)1097-458X(1998120)36:12<885::AID-OMR366>3.0.CO;2-Z

Canonica, S., Jans, U., Stemmler, K., Hoigne, J., 1995. Transformation Kinetics of Phenols in Water: Photosensitization by Dissolved Natural Organic Material and Aromatic Ketones. Environ. Sci. Technol. 29, 1822–1831. doi:10.1021/es00007a020

Craig, N.C., Sams, R.L., 2008. An investigation of the rotamers of butadiene by high-resolution infrared spectroscopy. J. Phys. Chem. A 112, 12637–12646. doi:10.1021/jp807677y

Cramer, C.J., 2013. Essentials of computational chemistry: theories and models. John Wiley & Sons.

Furukawa, Y., Takeuchi, H., Harada, I., Tasumi, M., 1983. Molecular Force Fields of s-trans-1,3-Butadiene and the Second Stable Conformer. Bull. Chem. Soc. Jpn. 56, 392–399. doi:10.1246/bcsj.56.392

Gundersen, G., Nielsen, C.J., Thomassen, H.G., Becher, G., 1988. Vibrational spectra of trans,trans-1,2,3,4-tetrachloro-1,3-butadiene; and the molecular structure of trans,trans-1,2,3,4-tetrachloro-1,3-butadiene and of hexachloro-1,3-butadiene (a reinvestigation) determined by gas-phase electron diffraction. J. Mol. Struct. 176, 33–60. doi:http://dx.doi.org/10.1016/0022-2860(88)80230-8

Ianni, J.C., 2014. Kintecus, Windows Version 5.00.

Lee, M., Zimmermann-Steffens, S.G., Arey, J.S., Fenner, K., von Gunten, U., 2015. Development of Prediction Models for the Reactivity of Organic Compounds with Ozone in Aqueous Solution by Quantum Chemical Calculations: The Role of Delocalized and Localized Molecular Orbitals. Environ. Sci. Technol. 49, 9925–9935. doi:10.1021/acs.est.5b00902

Marais, D.J., Sheppard, N., Stoicheff, B.P., 1962. An investigation of the structure of butadiene by high resolution infra-red and raman spectroscopy. Tetrahedron. doi:10.1016/S0040-4020(01)99016-7

Nelder, J.A., Mead, R., 1965. A Simplex Method for Function Minimization. Comput. J. 7, 308–313. doi:10.1093/comjnl/7.4.308

Neta, P., D.L.M., 1968. Pulse Radiolysis Studies XIII. Rate Constants for the Reaction of Hydroxyl Radicals with Aromatic Compounds in Aqueous Solutions, Advances in Chemistry Series. Radiat. Chem. 81, 222–230.

Schomaker, V., Pauling, L., 1939. The electron diffraction investigation of the structure of benzenne, pyridine, pyrazine, butadiene-1,3, cyclopentadiene, furan, pyrrole, and thiophene. J. Am. Chem. Soc. 61, 1769–1780. doi:10.1021/ja01876a038

von Sonntag, C., von Gunten, U., 2012. Chemistry of ozone in water and wastewater treatment: From basic principles to applications. IWA publishing.

Wegelin, M., Canonica, S., Mechsner, K., Fleischmann, T., Pesaro, F., Metzler, A., 1994. Solar water disinfection: Scope of the process and analysis of radiation experiments. Aqua J. Water Supply Res. Technol. 43, 154–169.

5 PILOT-SCALE TESTING

The pilot plant was designed and constructed between July 2014 and May 2015. It was operated between May 2015 and July 2016. This chapter will present the results of long- and short-term experiments. Long-term experiments were used to compare O_3/H_2O_2 or UV/H_2O_2 as pre-treatment before GAC filters in terms of the efficiency of micropollutant abatement. In these experiments the background concentrations of the micropollutants were used. The abatement of 8 micropollutants by oxidation, adsorption and biodegradation as well as the formation of transformation products were evaluated with short-term experiments for which micropollutants were spiked at µg/L levels. A special focus was put on the abatement of chlorobutadienes.

5.1 MATERIALS AND METHODS

5.1.1 DESCRIPTION OF THE PILOT-PLANT

The pilot plant was designed at Eawag and built by the company SIMA-tec (Schwamtal, Germany). It was delivered to the drinking water plant of Hardwasser AG in May 2015 and assembled by SIMA-tec.

The pilot plant was equipped with four fully automated treatment lines presented in **Fig. 5.3**: two for O_3/H_2O_2 treatment, one for UV/H_2O_2 treatment and one line for blank experiments. Three lines were dedicated to test advanced oxidation processes as pre-treatment before GAC adsorption using Hardwald groundwater before activated carbon filtration and one as post-treatment using Hardwald groundwater after activated carbon filtration.

In Line A1 (**Fig. 5.1**), O_3/H_2O_2 treatment was tested in a stainless steel plug-flow reactor with a volume of 17 L with a flow rate of 100 L/h (i.e., contact time of 10 min). H_2O_2 was injected in Hardwald groundwater before the reactor and ozone was then dosed with a static mixer system. After oxidation, the treated water was split and 2.7 L/h was transferred to a series of 10 columns filled with the granular activated carbon (GAC) Calgon F-400. The inside diameter and length of columns were 2.4 cm and 10 cm, respectively. This set-up mimicked the first meter of the full-scale GAC filters (2.5 m) and can be used to predict the adsorption capacity of GAC after pre-oxidation.

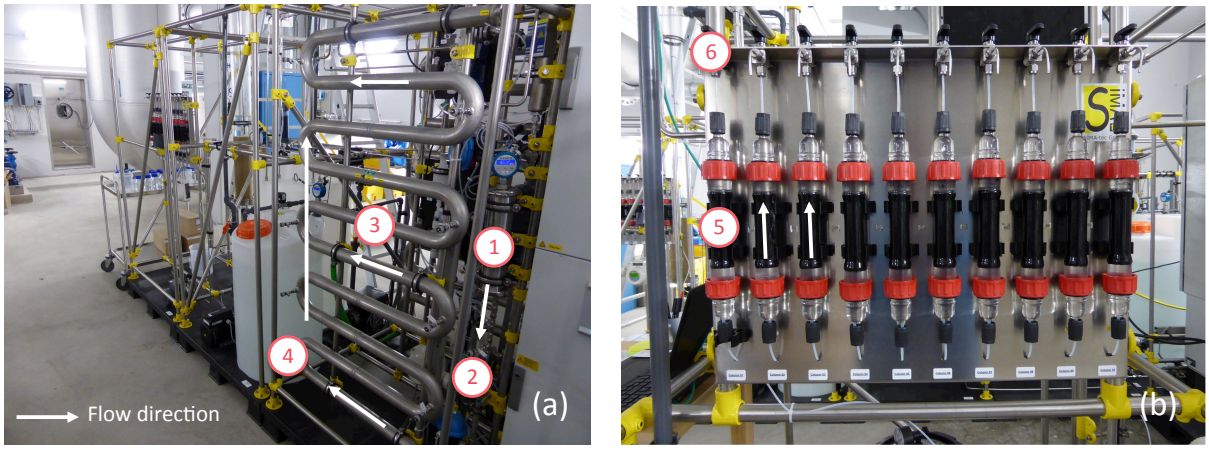

Fig. 5.1: *Pictures of line A1 (O_3/H_2O_2) combining (a) a plug-flow reactor followed by (b) 10 GAC columns in series – (1) ozone production system with an ozone gas injection and a degassing system, (2) H_2O_2 injection point directly after the ozone production system and before the entrance of the plug-flow reactor, (3) plug-flow reactor for oxidation reactions with dissolved ozone, (4) water sampling points located at each turn of the plug- flow reactor, (5) glass columns filled with GAC, (6) sampling points located after each column.*

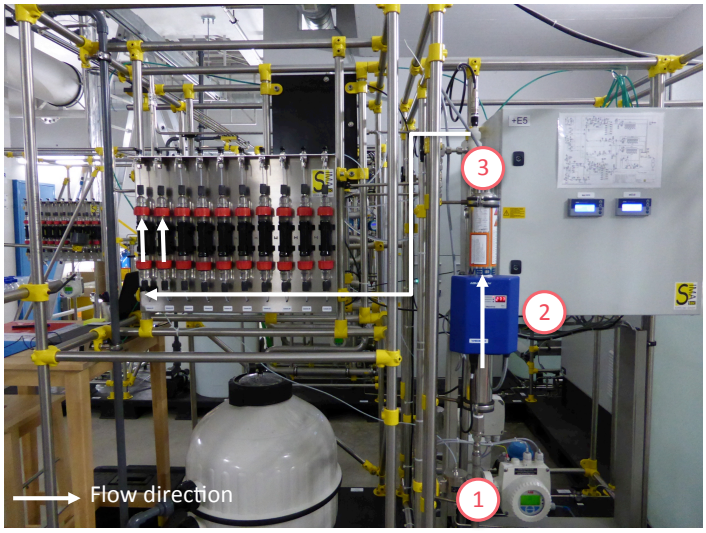

Fig. 5.2: *Picture of line B (UV/H_2O_2) combining the vertical UV reactor (right) with 10 GAC columns in series (left) – (1) H_2O_2 injection point just before the UV reactor, (2) UV reactor and (3) sampling point after the UV reactor.*

In Line B (**Fig. 5.2**), a low pressure UV reactor (254 nm) delivering 6800 J/m^2 at a flow rate of 100 L/h was assembled followed by the same series of GAC columns as in Line A1. H_2O_2 was injected in the Hardwald groundwater before the UV reactor.

Line C was implemented only with GAC columns. The test performed in this line, called “blank experiment”, was compared to the results obtained with Lines A1 and B.

Line A2 had the same configuration as line A1, however, it treated water collected from Hardwald groundwater after the full-scale GAC filters to assess the possibility of AOP as post-treatment. A sandfilter was placed after the oxidation reactor to ensure the degradation of assimilable organic carbon (AOC) and investigate the biodegradation of some transformation products.

The four treatment lines were run 24/7 from May 2015 to July 2016 with a flow of 100 L/h each. These tests were called “Long-term experiments” while “short-term experiments” (1h tests) were performed with differing oxidation conditions and spiking of selected micropollutants.

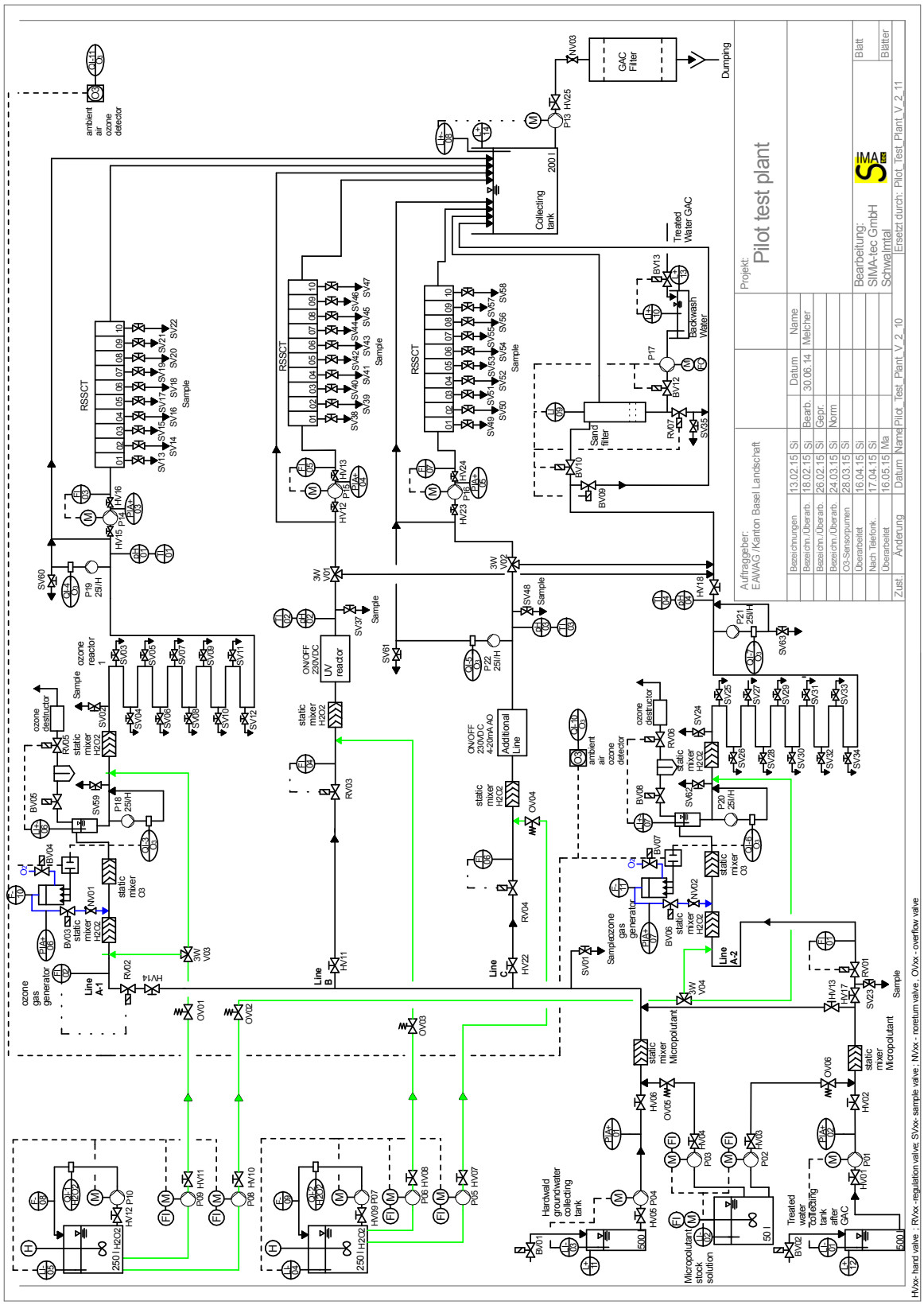

Fig. 5.3: *Pilot plant scheme presenting the four treatment lines (from top to bottom: lines A1, B, C and A2).*

5.1.1.1 LONG-TERM EXPERIMENTS

Long-term experiments were carried out 24/7 on the four treatment lines during about 8 months (220 days) (**Fig. 5.4**). Ozonation conditions were set to an ozone dose of 0.5 mg/L and a molar ratio for H_2O_2/O_3 of 1 for lines A1 and A2.

Line B was run with the standard conditions of 6800 J/m^2 for UV and a H_2O_2 dose of 5 mg/L. Line C was operated without pre-oxidation.

The water flow rate was 100 L/h for the pre-oxidation step and 2.7 L/h for the adsorption step on the small GAC columns.

The sand filter was designed for an empty bed contact time of 5 min and was backwashed during 20 min every day. These durations are usually applied in full-scale process to remove AOC from water.

Two types of sampling campaigns were performed for the activated carbon columns (**Tab. 5.1**). Firstly water was sampled after column 1 of lines A1, B and C at differing times (sampling dates, **Tab. 5.1**). This is based on the hypothesis that the adsorption is proportional to the filter depth in the RSSCT. If this phenomenon is confirmed with only one column of 10 cm, it might be worthwhile to develop such a small adsorption set-up to quickly predict the efficiency of full-scale filters. Secondly, water samples were collected after the columns 1, 2, 3, 4, 5, 7 and 10 after about 8 months (220 days) of operation (snapshot). Since the specific throughput is different for each column, a breakthrough curve can be drawn with these results. The main advantage of the second strategy is the lower effort for such a sampling. Basically, the whole breakthrough information can be obtained in one sampling campaign.

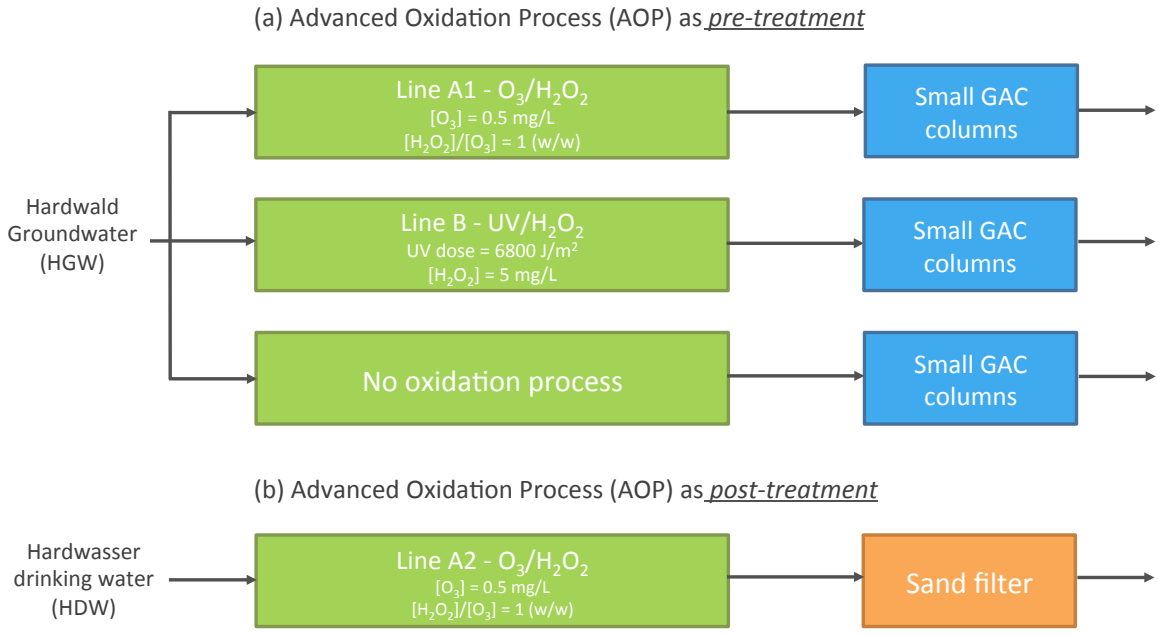

Fig. 5.4: *Configuration of the four treatment lines used during long-term experiments where AOPs were tested as (a) pre-treatment of GAC filters on Hardwald groundwater (HGW) and (b) post-treatment of GAC filters on Hardwasser drinking water (HDW).*

Tab. 5.1: *Selection of the sampling dates and points for the long-term observations of the GAC columns (bold values show the samples with comparable throughputs for the two sampling strategies).*

1st strategy: after 1st column		**2nd strategy: snapshot after 220 days**	
Day	**Throughput (m^3/kgGAC)**	**After Column**	**Throughput (m^3/kgGAC)**
20	**62**	10	**68**
35	**108**	7	**97**
70	**216**	5	136
110	**339**	4	170
150	463	3	**227**
220	**679**	2	**339**
		1	**679**

Line A2 was run 24/7 to develop the microbiology on the sand filter to assess the biodegradation of micropollutants and transformation products during the short-term tests. Therefore, the cell density was measured by flow cytometry in Hardwald groundwater, before and after the sand filter from May 2015 to November 2015

5.1.1.2 SHORT-TERM EXPERIMENTS

The short-term experiments were performed on selected days between October 2015 and March 2016. Each experiment lasted about 1h, which was the time to reach a steady-state in the treatment lines after changing the treatment conditions. The treatment conditions were selected according to the results obtained in section 3. As presented in **Fig. 5.5**, for O_3/H_2O_2 experiments, three ozone doses (i.e. 0.5, 1 and 2 mg/L) and four H_2O_2/O_3 mass ratios (i.e. 0, 0.25, 0.5, 1 and 4) were chosen. For UV/H_2O_2 experiments, five UV doses from 2500 to 13600 J/m^2 and three H_2O_2 doses (i.e., 0, 2 and 5 mg/L) were tested. One experiment was run with a combination of O_3/H_2O_2 and sand filtration for an ozone dose of 0.5 mg/L and a H_2O_2/O_3 mass ratio of 0.5.

Hardwald groundwater and treated water after GAC were spiked with the eight compounds presented in **Fig. 5.22**.

Water samples were collected before (SV48, **Fig. 5.3**) and after the two oxidation reactors (SV12 and SV37, **Fig. 5.3**). In addition, water was also sampled after 2 (SV04), 4 (SV06), 6 (SV08) and 8 min (SV10) in the ozonation plug-flow reactor to investigate the ozone and micropollutant depletions. Finally, 2 L of treated water (SV12) were collected for further PAC adsorption tests at Eawag. All water samples were stored at 4°C prior to analyses or further experiments. For samples collected in the ozonation line, the ozone residual was quenched with sulfite to stop the reaction.

One experiment was run with a combination of O_3/H_2O_2 followed by sand filtration for an ozone dose of 0.5 mg/L and a H_2O_2/O_3 mass ratio of 0.5. Samples were collected before (SV23) after the plug-flow reactor (SV34) and after the sand filter (SV35).

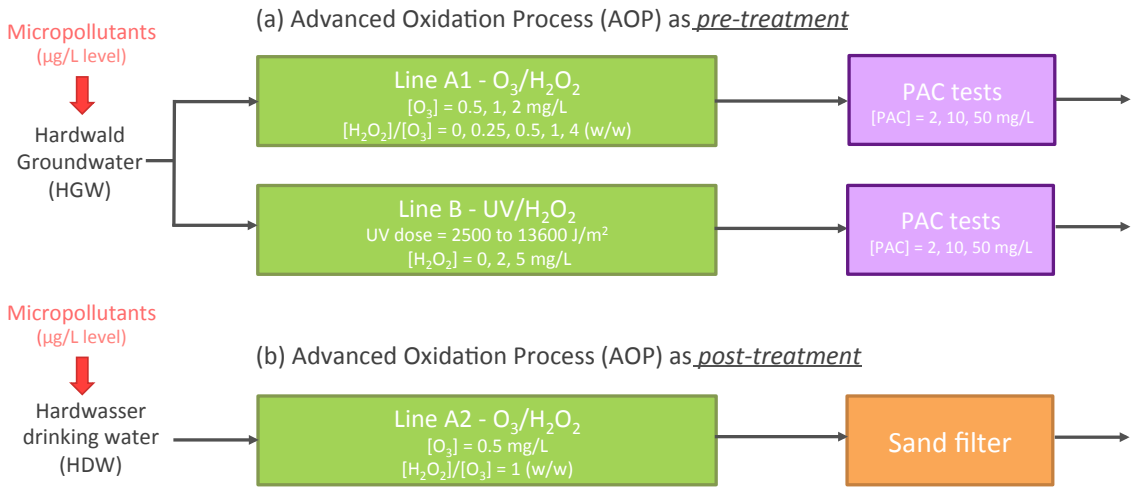

Fig. 5.5: *Configuration of the three treatment lines used during short-term experiments where the AOP was tested as (a) pre-treatment and (b) post-treatment of GAC filters.*

5.1.2 Analytical methods

5.1.2.1 Long-term experiments

The micropollutants were analysed according to the method presented in section 3.1.3.

Dissolved organic carbon (DOC) was measured using a size exclusion chromatography equipped with an organic carbon detector (DOC-labor, Germany).

Bacterial cells were counted with a BD Accuri C6 flow cytometry according to the method described by Hammes et al. (2008).

Ozone concentration was measured using the indigo method already described in section 4.4.

5.1.2.2 Short-term experiments

For measurements of micropollutants, 100 mL samples were stored at 4°C prior to analyses. After shaking and sedimentation, 1.0 mL of the supernatant was collected for each sample and 40 µL of internal standard was added. 100 µL samples were then directly injected the Dionex Ultimate 3000 RS HPLC combined with a Thermo Fisher Scientific Q-exactive plus mass spectrometer. Analyses were performed at 30°C with a Water Atlantis T3 (C18, 3.0 µm, 3.0 x 150 mm) and a gradient of nanopure water and methanol, both acidified with formic acid. The calibration was established between 1 and 10000 ng/L.

Ozone, *p*CBA and bromate were quantified according to the methods presented in section 3.1.3 and 4.4

5.2 Results and discussion

5.2.1 Long-term experiments with advanced oxidation processes as pre-treatment

5.2.1.1 Water qualities of Hardwald groundwater before and after advanced oxidation

pH, temperature and ozone concentrations were recorded with online sensors during the long-term experiments (**Fig. 5.6**). pH values show a low fluctuation from 7.58 to 7.71 whereas temperature varied from 12.7 to 17.6°C. The average ozone concentration measured before the addition of H_2O_2 was kept

constant between 0.50 and 0.51 mg/L, however, some values were measured between 0.47 and 0.54, which is an acceptable fluctuation.

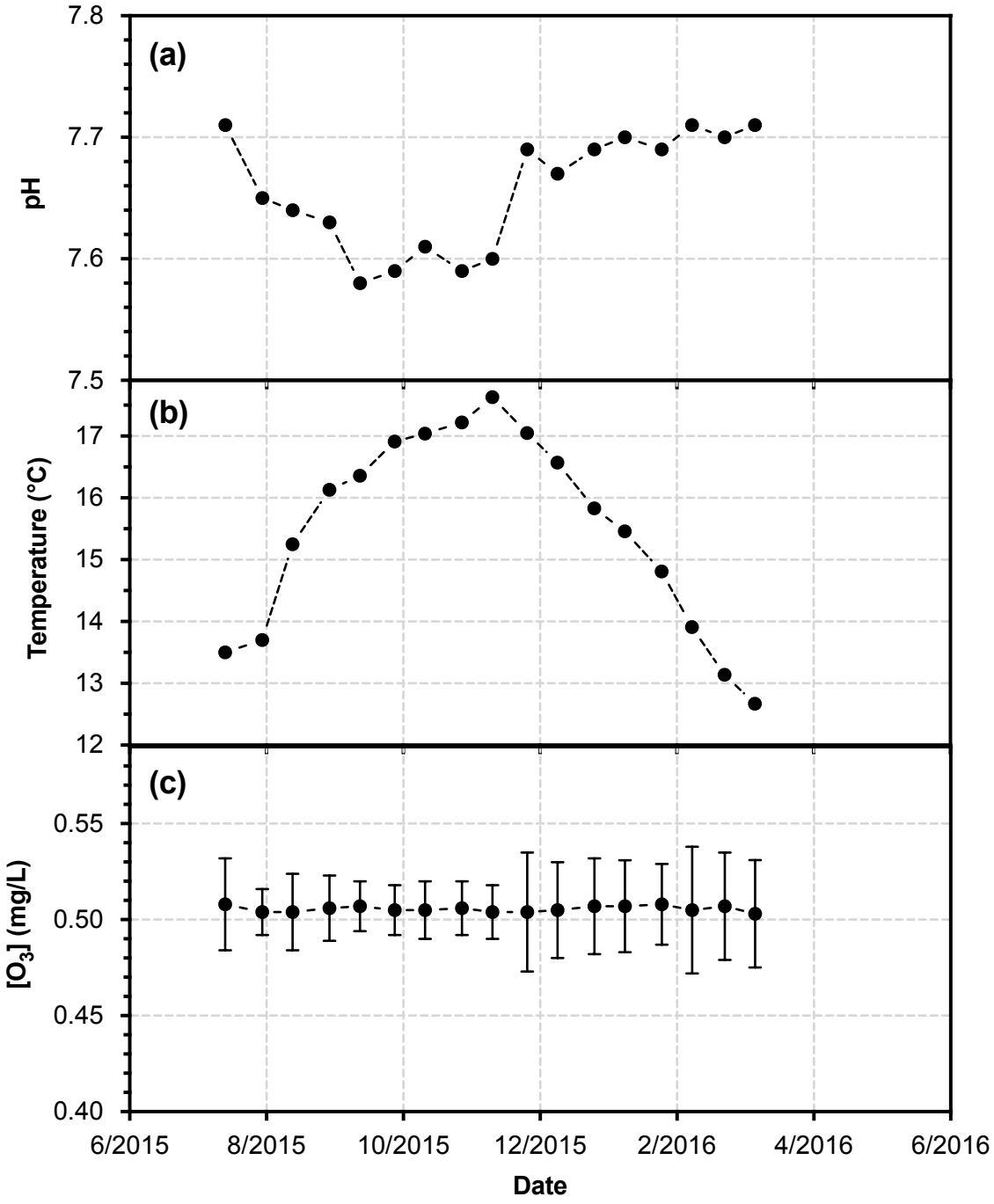

Fig. 5.6: *Long-term pilot-scale experiments. Variations of (a) pH, (b) temperature and (c) ozone concentrations measured before the addition of H_2O_2.*

5.2.1.2 MICROPOLLUTANT ABATEMENT IN AOPS

During the long-term experiments, micropollutants were not spiked to Hardwald groundwater for economical reason. Therefore, the micropollutant concentrations were very low and it was challenging to measure some of them, especially after pre-oxidation.

A slight seasonal effect can be observed for some compounds, during winter the concentrations of X-ray contrast media (**Fig. 5.7**) and sulfamethoxazole (**Fig. 5.10**) increased.

While X-ray contrast media and concentrations of artificial sweeteners are observed in concentrations of about 100 ng/L or higher (**Fig. 5.7** and **Fig. 5.8**), the concentrations of pesticides, pharmaceuticals and industrial compounds never exceeded 25 ng/L. Most of the pesticides (i.e., 5 out of 8) were measured below 5 ng/L (**Fig. 5.9**) and the average concentration of pharmaceuticals was around 12 ng/L (**Fig. 5.10**).

The micropollutant concentrations were also quantified after O_3/H_2O_2 and UV/H_2O_2 treatments. As expected, the abatement of X-ray contrast media was higher with UV/H_2O_2 (**Fig. 5.7**), because these compounds undergo direct photolysis. While the diatrizoate concentration decreased below 8 ng/L with UV/H_2O_2 during the testing period, concentrations ranged from 16 to 30 ng/L with O_3/H_2O_2. For iopamidol, the difference in terms of treatment performances is less pronounced since its abatement occurs both with O_3 (partially) and °OH.

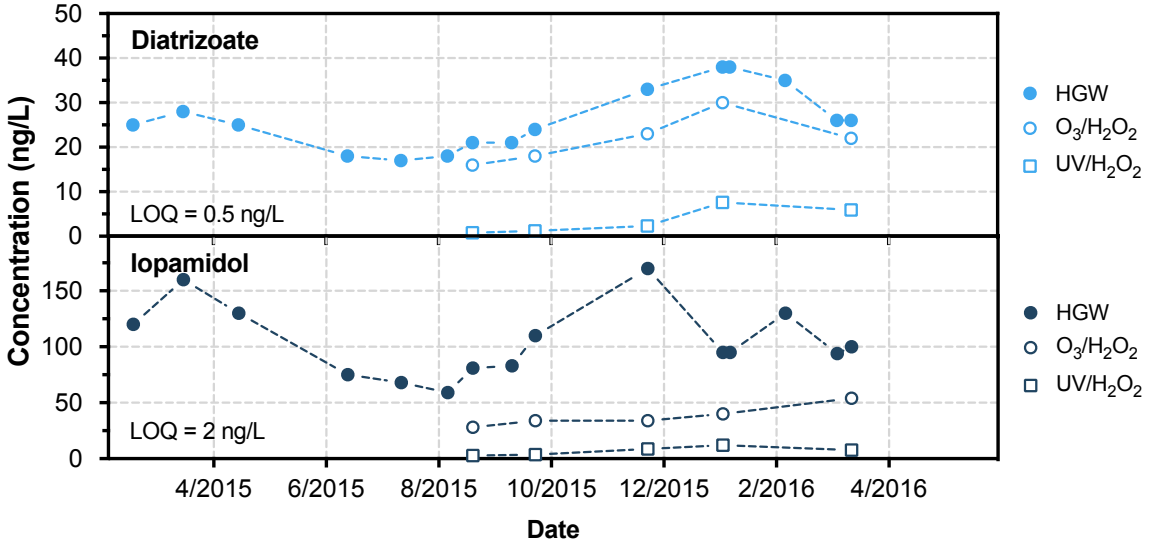

Fig. 5.7: *Concentrations of X-ray contrast media in Hardwald groundwater (HGW) and after treatment with the AOPs O_3/H_2O_2 or UV/H_2O_2 during the pilot testing period (August 2015 to March 2016). Concentrations measured in HGW before the pilot testing period are also shown - Conditions: O_3/H_2O_2 – $[O_3]$ = 0.5 mg/L, $[H_2O_2]$ = 0.5 mg/L; UV/H_2O_2 – UV dose = 6800 J/m², $[H_2O_2]$ = 5 mg/L.*

While sucralose results highlight the same abatement for both AOPs (**Fig. 5.8**), the concentrations recorded for acesulfame are below the limit of quantification (LOQ) for UV/H_2O_2 treatment and from 4 to 34 ng/L for O_3/H_2O_2. Consequently, it will be impossible to determine the adsorption of acesulfame onto GAC column filters after a UV/H_2O_2 as pre-treatment. Moreover, the abatement efficiency of sucralose decresead during the last four months of treatment for unknown reasons.

Fig. 5.9 shows the concentrations of pesticides before and after O_3/H_2O_2 or UV/H_2O_2 treatment. The concentrations of metolachor ESA, diuron and simazine after both AOPs were all below the LOQ. As per acesulfame, breakthrough curves could not be studied. Regarding the other pesticides, a concentration of 7 ng/L was never exceeded after the AOPs. Moreover, no significant difference is observed between both AOP treatments except for atrazine and desethylatrazine for which photodegradation provides higher abatement in the UV-based process. Metolachlor ESA increased dramatically from February-April 2016 and desphenylchloridazon and 2,6-dichlorobenzamide, to a lesser extent, whereas atrazine and its metabolites do not show the same trend. This might be due to the use of the former pesticides, whereas, atrazine is prohibited .

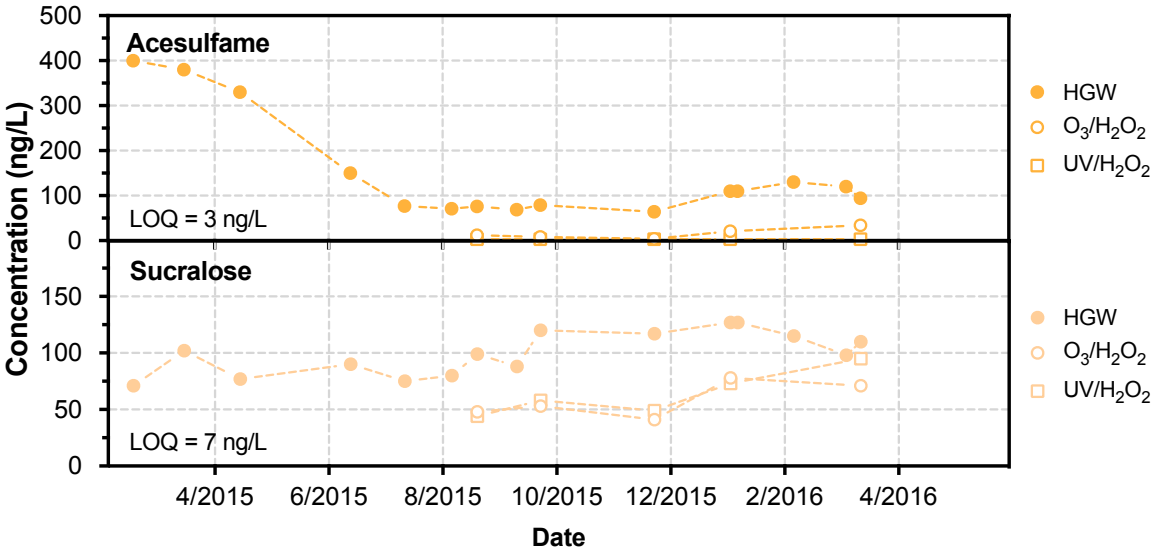

Fig. 5.8: *Concentrations of artificial sweeteners in Hardwald Groundwater (HGW) and after treatment with the AOPs O_3/H_2O_2 or UV/H_2O_2 during the pilot testing period (August 2015 to March 2016). Concentrations measured in HGW before the pilot testing period are also shown - Conditions: O_3/H_2O_2 – $[O_3]$ = 0.5 mg/L, $[H_2O_2]$ = 0.5 mg/L; UV/H_2O_2 – UV dose = 6800 J/m², $[H_2O_2]$ = 5 mg/L.*

For pharmaceutical compounds sulfamethoxazole, candesartan, carbamazepine and hydroxychlorothiazide (**Fig. 5.10**), both AOPs are powerful treatments for their oxidation and the residual concentrations were below 1 ng/L or below the LOQs. The elimination of lamotrigine and dihydroxycarbamazepine is also satisfactory, especially with UV/H_2O_2 treatment with resulting concentrations < 8 ng/L.

The abatement of 5-methylbenzotriazole and benzotriazole is depicted in **Fig. 5.11**. The two compounds were efficiently abated by both AOPs (i.e. residual concentration < 10 ng/L) even though the elimination was higher for 5-methylbenzotriazole.

Overall, the oxidative pre-treatments with O_3/H_2O_2 or UV/H_2O_2 considerably decreased the concentrations of micropollutants in Hardwald groundwater, except for diatrizoate and sucralose.

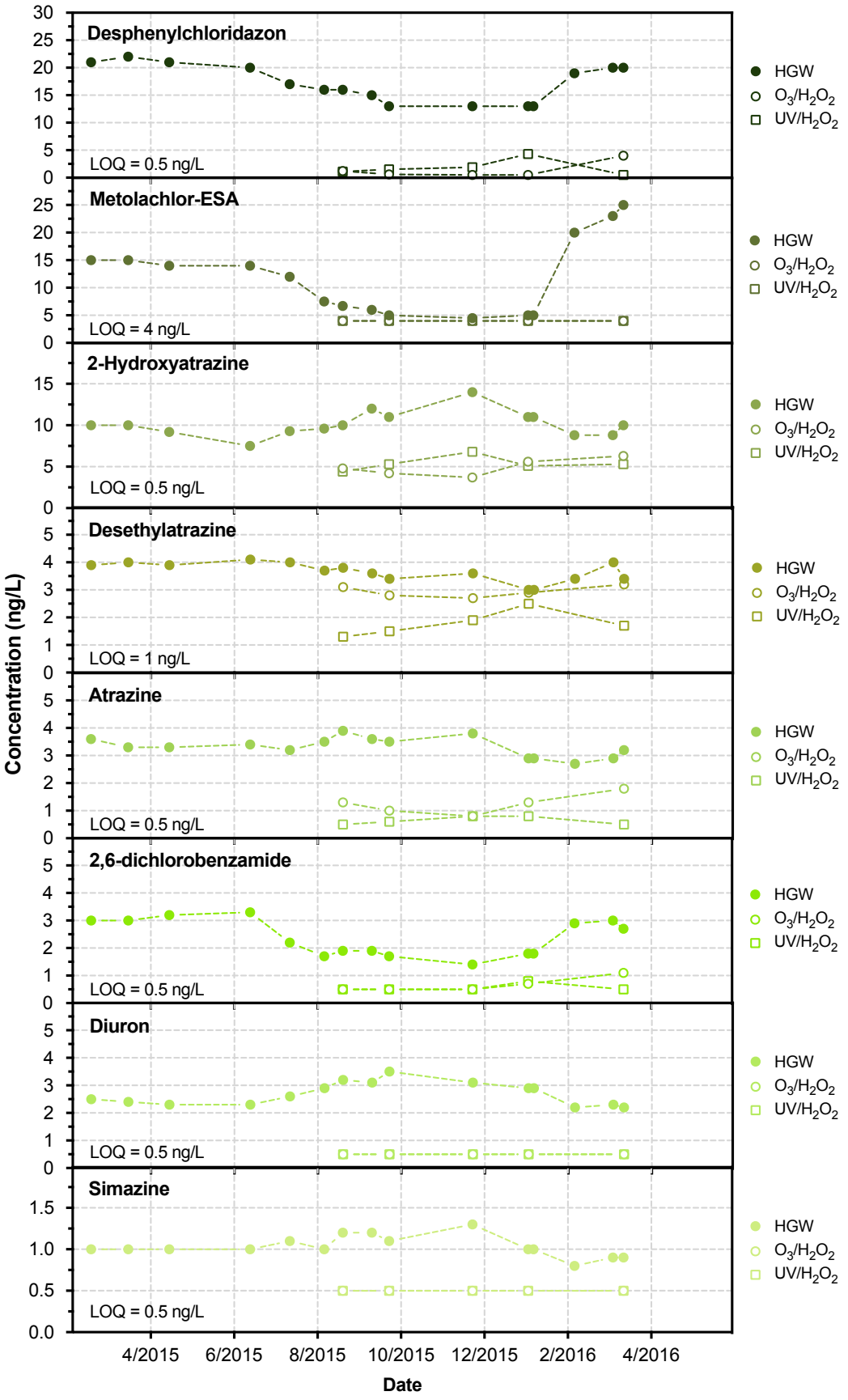

Fig. 5.9: *Concentrations of pesticides in Hardwald Groundwater (HGW) and after treatment with the AOPs O_3/H_2O_2 or UV/H_2O_2 during the pilot testing period (August 2015 to March 2016). Concentrations measured in HGW before the pilot testing period are also shown - Conditions: O_3/H_2O_2 – $[O_3]$ = 0.5 mg/L, $[H_2O_2]$ = 0.5 mg/L; UV/H_2O_2 – UV dose = 6800 J/m², $[H_2O_2]$ = 5 mg/L.*

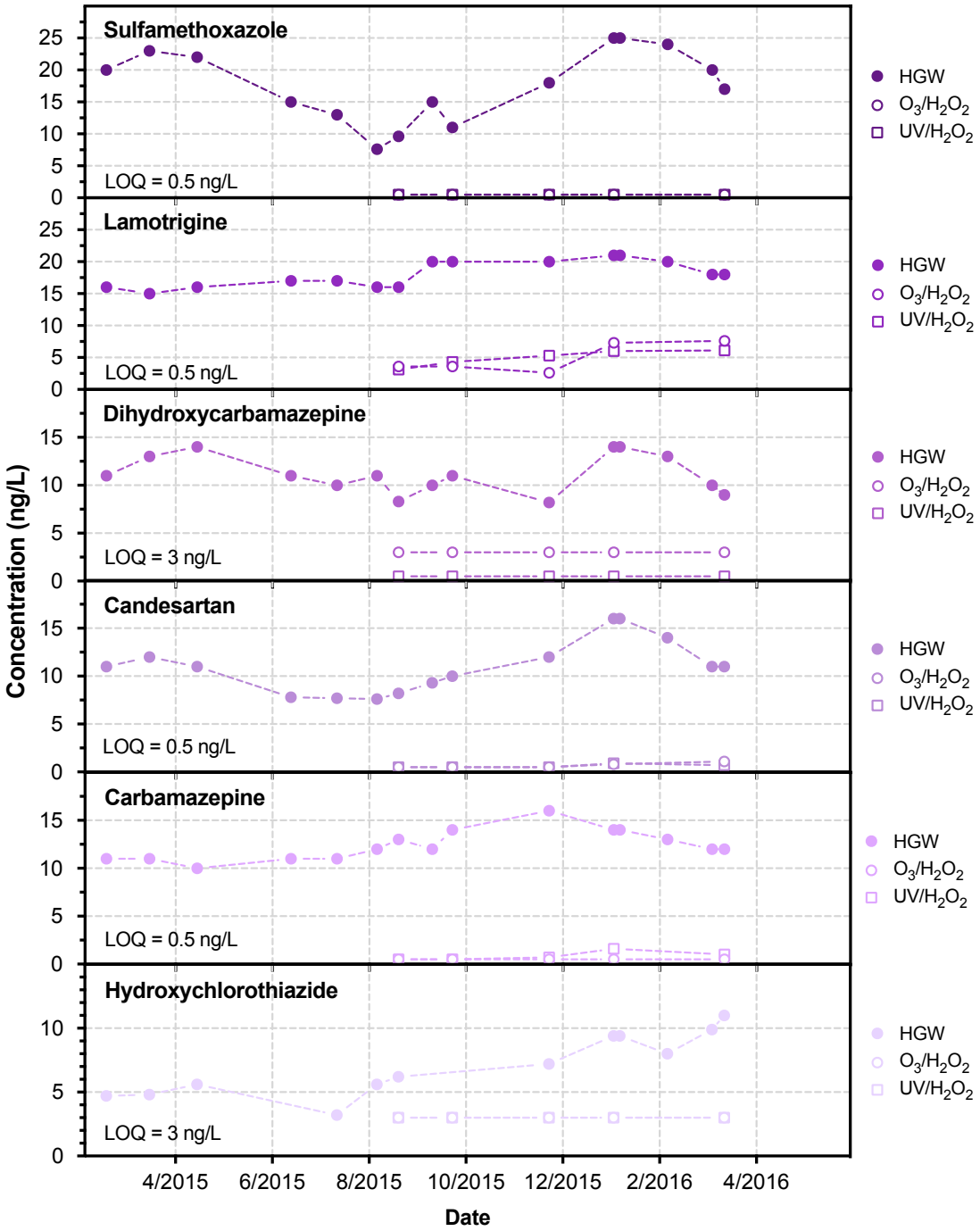

Fig. 5.10: *Concentrations of pharmaceuticals in Hardwald Groundwater (HGW) and after treatment with the AOPs O_3/H_2O_2 or UV/H_2O_2 during the pilot testing period (August 2015 to March 2016). Concentrations measured in HGW before the pilot testing period are also shown - Conditions: O_3/H_2O_2 – $[O_3]$ = 0.5 mg/L, $[H_2O_2]$ = 0.5 mg/L; UV/H_2O_2 – UV dose = 6800 J/m², $[H_2O_2]$ = 5 mg/L.*

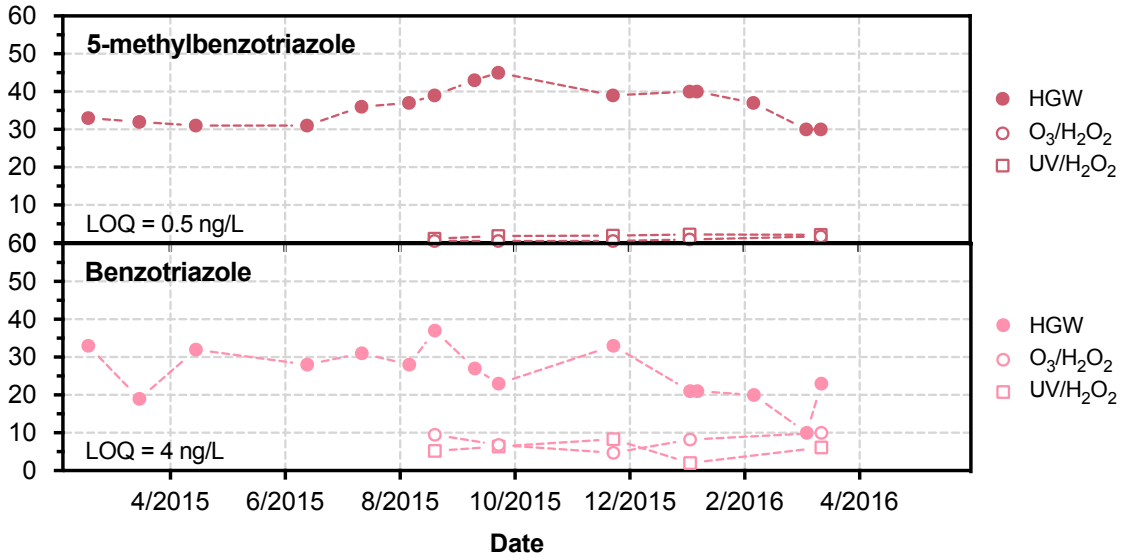

Fig. 5.11: *Concentrations of industrial compounds in Hardwald Groundwater (HGW) and after treatment with the AOPs O_3/H_2O_2 or UV/H_2O_2 during the pilot testing period (August 2015 to March 2016). Concentrations measured in HGW before the pilot testing period are also shown Conditions: O_3/H_2O_2 – $[O_3]$ = 0.5 mg/L, $[H_2O_2]$ = 0.5 mg/L; UV/H_2O_2 – UV dose = 6800 J/m², $[H_2O_2]$ = 5 mg/L.*

5.2.1.3 Adsorption of micropollutants with and without pre-oxidation treatment using small-scale columns in series

O_3/H_2O_2 and UV/H_2O_2 are two powerful treatment options to abate most of the micropollutants (see above). In this study, diatrizoate and sucralose were the only two exceptions. Therefore, for such compounds oxidative treatments cannot be considered alone and an additional adsorption step would be needed. Since AOP pre-treatments reduce the concentrations of micropollutants, we hypothesized that a pre-oxidation step could increase the lifetime of GAC filters. This hypothesis was tested comparing two sampling strategies (see section 5.1.1.1)

The 20 micropollutants previously described were analyzed before and after the full-scale filters to evaluate their breakthrough under real conditions and and a comparison was made with the adsorption column set-up from Line C (i.e., without pre-oxidation). Unfortunately, the testing period was too short for a breakthrough of many compounds and only diatrizoate, iopamidol, sucralose and acesulfame provided a sufficient data set.

Fig. 5.12 compares the adsorption performances of the full-scale filters with results from treatment line C (i.e., without preoxidation). For the results in treatment line C, we selected two options: (1) sampling after column 1 during the entire testing period by assuming that the adsorption is proportional to the column length or (2) sampling after the columns 1, 2, 3, 4, 5, 7, and 10 after about 8 months (220 days) of operation (i.e., snapshot). For diatrizoate, iopamidol and sucralose, the two methods show similar breakthrough curves whereas acesulfame data shows a better prediction for the snapshot method. Moreover, compared to the full-scale data, diatrizoate and iopamidol breakthrough curves can be predicted with a good accuracy without any fitting. For an unexplained reason, the small column set-up was not able to reproduce the values of C/C_0 above 1. For instance, the breakthrough curves of acesulfame reached a C/C_0 of 4.1 for the full-scale conditions. This means that acesulfame is replaced at the GAC surface by compounds having a higher affinity with the adsorbent. Somehow, this phenomenon was not observed with the Line C data set. Nevertheless, the most important part of breakthrough curve is generally the one below C/C_0 = 50% since this part is often used to decide at which point the GAC filter should be replaced to guarantee a certain water quality.

Although the two methods provide quite similar results, the “snapshot” strategy seems to be the best option. It requires less sampling efforts since only one sampling campaign is necessary and there is no need to collect samples over several months.

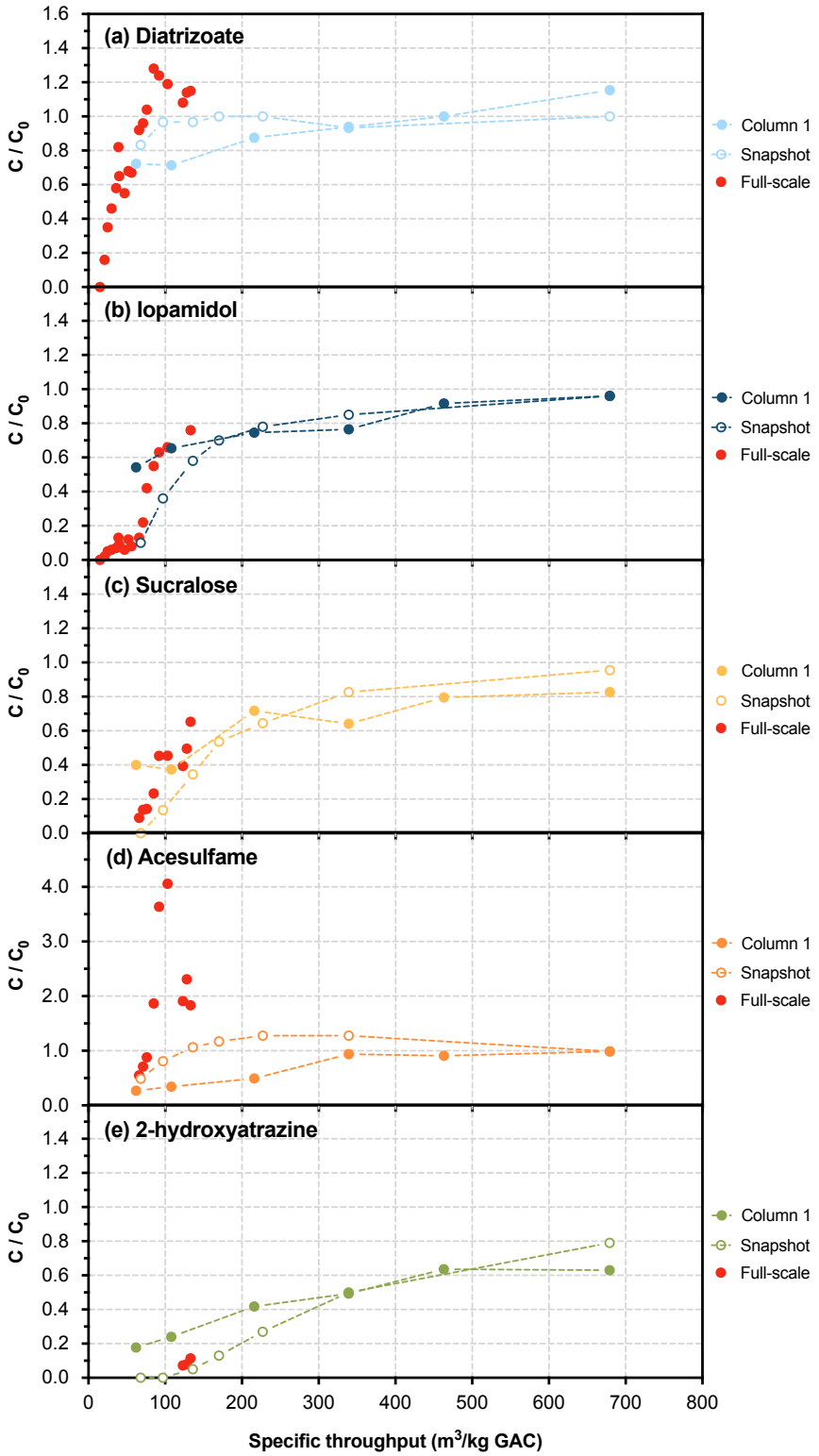

Fig. 5.12: *Breakthrough curves of various micropollutants in pilot plant small-scale GAC filters (without pre-oxidation, various colors) and the full-scale GAC filter (red symbols) as a function of the specific throughput. (a) diatrizoate, (b) iopamidol, (c) sucralose and (d) acesulfame. Two approaches were used: (i) Water was sampled after column 1 at differing times during about 8 months (220 days) (column 1),(ii) water samples were taken only at one time point after columns 1, 2, 3, 4, 5, 7 and 10 after about 8 months (220 days) of operation (snapshot)).*

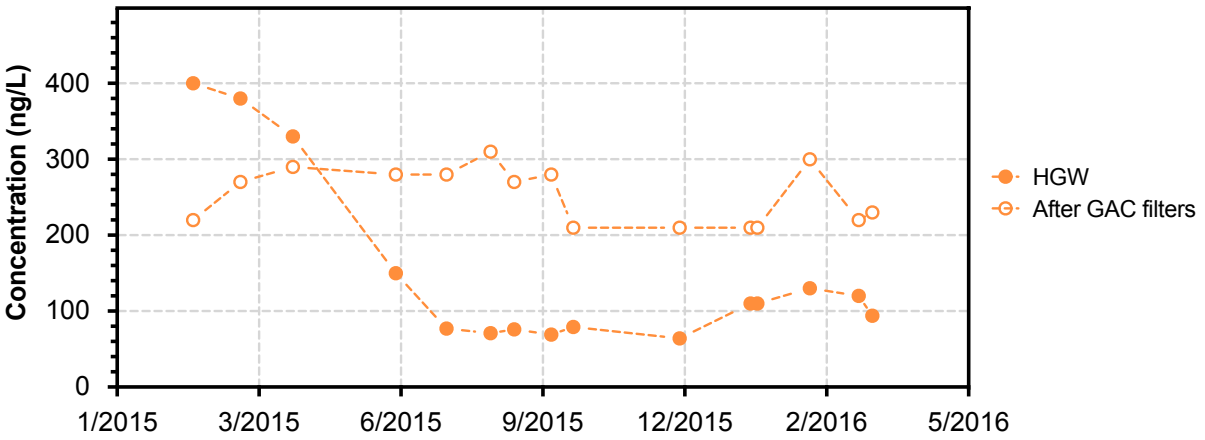

Fig. 5.13: *Concentration of acesulfame in Hardwald groundwater (HGW) and after the full-scale GAC filters during the pilot testing period.*

Even though ratio C/C_0 above 1 is feasible, the ratio of 4.1 as observed for acesulfame is very unusual. Indeed, as shown in **Fig. 5.13**, the concentration of acesulfame after the full-scale GAC filters was more or less constant during the pilot testing period (i.e., about 250 ng/L in average) while the concentration in Hardwald groundwater decreased dramatically. Therefore, it might be possible that full-scale filters ran with a high load before the testing period and the sudden concentration decrease in the untreated water provoqued the unusually high ratio C/C_0.

Fig. 5.14 presents the breakthrough curves of five micropollutants recorded in treatment line A (O_3/H_2O_2 as pre-treatment), line B (UV/H_2O_2 as pre-treatment) and line C (w/o pre-treatment) during the snapshot campaign.

As expected, a pre-oxidation increases the breakthrough time of the micropollutants. The best performances were observed with UV/H_2O_2 as pre-treatment except for 2-hydroxyatrazine for which O_3/H_2O_2 was slightly better. For acesulfame, it is not possible to draw conclusions due to its complete abatement after UV/H_2O_2. As expected, the breakthrough curves depend on the concentration at the entrance of the GAC column. The GAC adsorbents have a maximum adsorption capacity directly linked to the micropollutant load. With waters containing low micropollutant concentrations, GAC filters could last longer since the breakthrough will occur later.

Tab. 5.2 shows the time gain by pre-oxidation treatments in terms of weeks for 50% breakthrough. This time saved can go from 43 weeks for acesulfame using O_3/H_2O_2 as pre-treatment to 328 weeks for iopamidol using UV/H_2O_2 as pre-treatment.

Tab. 5.2: *Comparison of the throughputs observed for a 50% breakthrough with or without pre-oxidation and equivalent of time saved in weeks considering an average hydraulic rate of 7.8 m/h.*

	Throughput (m^3/kgGAC) observed for a 50% breakthrough (+ number of weeks saved by applying a preoxidation step)		
	w/o preoxidation	**O_3/H_2O_2**	**UV/H_2O_2**
Diatrizoate	n.a.	n.a.	n.a.
Iopamidol	120	200 (+ 70 weeks)	500 (+ 328 weeks)
Sucralose	160	350 (+ 164 weeks)	530 (+ 319 weeks)
Acesulfame	70	120 (+ 43 weeks)	n.a.
2-hydroxyatrazine	340	680 (+ 293 weeks)	650 (+ 267 weeks)

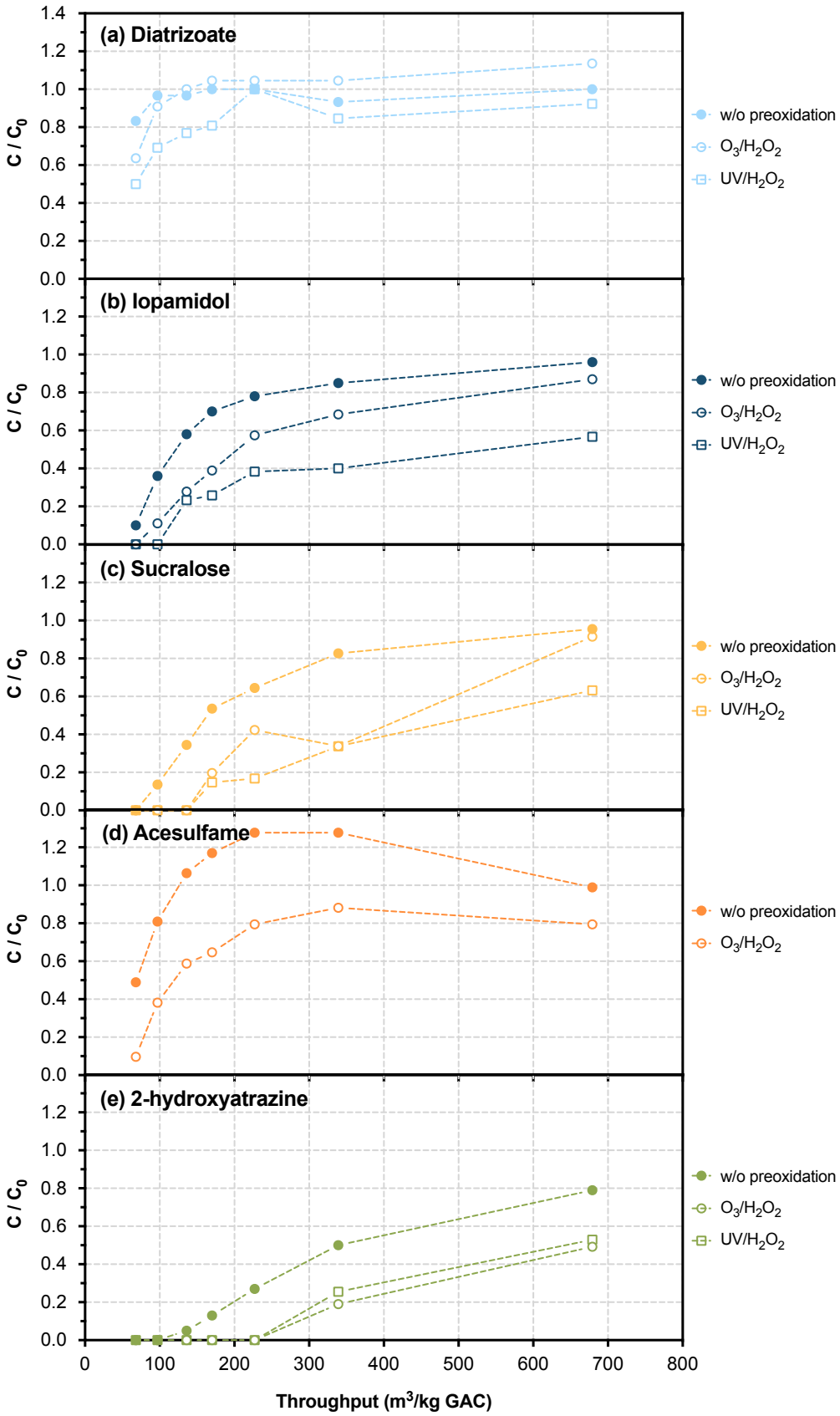

Fig. 5.14: *Comparison of breakthrough curves without (closed symbols) and with pre-oxidation (open symbols) of Hardwald groundwater with O_3/H_2O_2 (circles) or UV/H_2O_2 (squares). (a) diatrizoate, (b) iopamidol, (c) sucralose, (d) acesulfame and (e) 2-hydroxyatrazine Conditions: O_3/H_2O_2 – $[O_3]$ = 0.5 mg/L, $[H_2O_2]$ = 0.5 mg/L; UV/H_2O_2 – UV dose = 6800 J/m², $[H_2O_2]$ = 5 mg/L.*

5.2.1.4 ADSORPTION OF CHLOROBUTADIENES WITHOUT PRE-OXIDATION TREATMENT USING SMALL-SCALE COLUMNS IN SERIES

Chlorobutadienes (CBDs) were also measured during the snapshot sampling campaign (**Tab. 5.3**). Most of the values were below the quantification limit and it was difficult to evaluate individual breakthrough curves. Only 16 ng/L of 1,1,4,4-TCB was measured after column 1 (679 m^3/kgGAC). Moreover, 1,1,4,4,-TCB was not detected after column 2 (339 m^3/kgGAC). Therefore, the breakthrough of 1,1,4,4-TCB would start between 339 and 679 m^3/kgGAC. If we consider that full-scale filters will be run with an average constant hydraulic rate of 7.8 m/h (i.e. the current hydraulic rate), this should occur between August 2019 and March 2025.

From a practical point of view, the sum of CBDs is considered as the best indicator to follow the breakthrough of CBDs. In this study, a total of 21 ng/L of CBDs (C/C_0 = 0.29) was measured after column 1 and no CBDs were released from column 2. Because 1,1,4,4-CBD is the main representative, the previous conclusion can be extrapolated to CBDs in general. For instance, the concentration of hexachlorobutadiene (HCB) in Hardwald groundwater was only 9 ng/L. Since the LOQ for the individual CBDs is 8 ng/L, it is impossible to evaluate the breakthrough lower than C/C_0 = 0.9, which is close to the GAC saturation for this compound. Overall, this conclusion is based on the extrapolation of a 10 cm column, which is the filter part that is most affected by organic material fouling. It is expected that the fouling of GAC by organic material leads to a reduction of adsorption capacity and the prediction might be an underestimation and the breakthrough could occur even later.

The breakthrough of CBDs was not investigated with pre-oxidation (lines A1 and B) because less than 10 ng/L of CBDs was measured after O_3/H_2O_2 or UV/H_2O_2, in agreement with the data in chapter 4. These concentrations were too low to compile accurate adsorption data.

Tab. 5.3: *Fractions (C/C_0) and concentrations of chlorobutadienes breaking through the columns 1, 2, 3, 4, 5, 7 and 10 placed in series for treatment line C during the snapshot sampling campaign (23/03/2016).*

	C/C_0 for differing throughputs (m^3/kg GAC) (with measured outlet concentration)						
compounds	**68** (column 10)	**97** (column 7)	**136** (column 5)	**170** (column 4)	**227** (column 3)	**339** (column 2)	**679** (column 1)
1,1,2,3-TCB (C_0 < 8 ng/L)	n.a. (< 8 ng/L)	n.a. (< 8 ng/L)	n.a. (< 8 ng/L)	n.a. (< 8 ng/L)	n.a. (< 8 ng/L)	n.a. (< 8 ng/L)	n.a. (< 8 ng/L)
1,1,3,4-TCB (C_0 = 13 ng/L)	< 0.6 (< 8 ng/L)	< 0.6 (< 8 ng/L)	< 0.6 (< 8 ng/L)	< 0.6 (< 8 ng/L)	< 0.6 (< 8 ng/L)	< 0.6 (< 8 ng/L)	< 0.6 (< 8 ng/L)
1,1,4,4-TCB (C_0 = 39 ng/L)	< 0.2 (< 8 ng/L)	< 0.2 (< 8 ng/L)	< 0.2 (< 8 ng/L)	< 0.2 (< 8 ng/L)	< 0.2 (< 8 ng/L)	< 0.2 (< 8 ng/L)	**0.41 (16 ng/L)**
1,1,2,4-TCB (C_0 = 11 ng/L)	< 0.7 (< 8 ng/L)	< 0.7 (< 8 ng/L)	< 0.7 (< 8 ng/L)	< 0.7 (< 8 ng/L)	< 0.7 (< 8 ng/L)	< 0.7 (< 8 ng/L)	< 0.7 (< 8 ng/L)
1,2,3,4-TCB (C_0 = 10 ng/L)	< 0.8 (< 8 ng/L)	< 0.8 (< 8 ng/L)	< 0.8 (< 8 ng/L)	< 0.8 (< 8 ng/L)	< 0.8 (< 8 ng/L)	< 0.8 (< 8 ng/L)	< 0.8 (< 8 ng/L)
1,1,2,4,4-PCB (C_0 < 8 ng/L)	n.a. (< 8 ng/L)	n.a. (< 8 ng/L)	n.a. (< 8 ng/L)	n.a. (< 8 ng/L)	n.a. (< 8 ng/L)	n.a. (< 8 ng/L)	n.a. (< 8 ng/L)
1,1,2,3,4-PCB (C_0 < 8 ng/L)	n.a. (< 8 ng/L)	n.a. (< 8 ng/L)	n.a. (< 8 ng/L)	n.a. (< 8 ng/L)	n.a. (< 8 ng/L)	n.a. (< 8 ng/L)	n.a. (< 8 ng/L)
HCB (C_0 = 9 ng/L)	< 0.9 (< 8 ng/L)	< 0.9 (< 8 ng/L)	< 0.9 (< 8 ng/L)	< 0.9 (< 8 ng/L)	< 0.9 (< 8 ng/L)	< 0.9 (< 8 ng/L)	< 0.9 (< 8 ng/L)
Sum CBDs (C_0 = 73 ng/L)	< 0.1 (< 8 ng/L)	< 0.1 (< 8 ng/L)	< 0.1 (< 8 ng/L)	< 0.1 (< 8 ng/L)	< 0.1 (< 8 ng/L)	< 0.1 (< 8 ng/L)	**0.29 (21 ng/L)**

5.2.1.5 ADSORPTION OF DISSOLVED ORGANIC CARBON (DOC) WITH AND WITHOUT PRE-OXIDATION TREATMENT USING SMALL-SCALE COLUMNS IN SERIES

Dissolved organic carbon (DOC) was followed after all the small-scale columns during the first months of experiments and the breakthrough was plotted over the specific throughput for each column (**Fig. 5.15**). Contrary to micropollutants, pre-oxidation does not improve the adsorption efficiency of organic matter on GAC. This was expected since the structure of organic compounds is not significantly modified for the applied oxidation conditions. Therefore, no change of its adsorbability was expected.

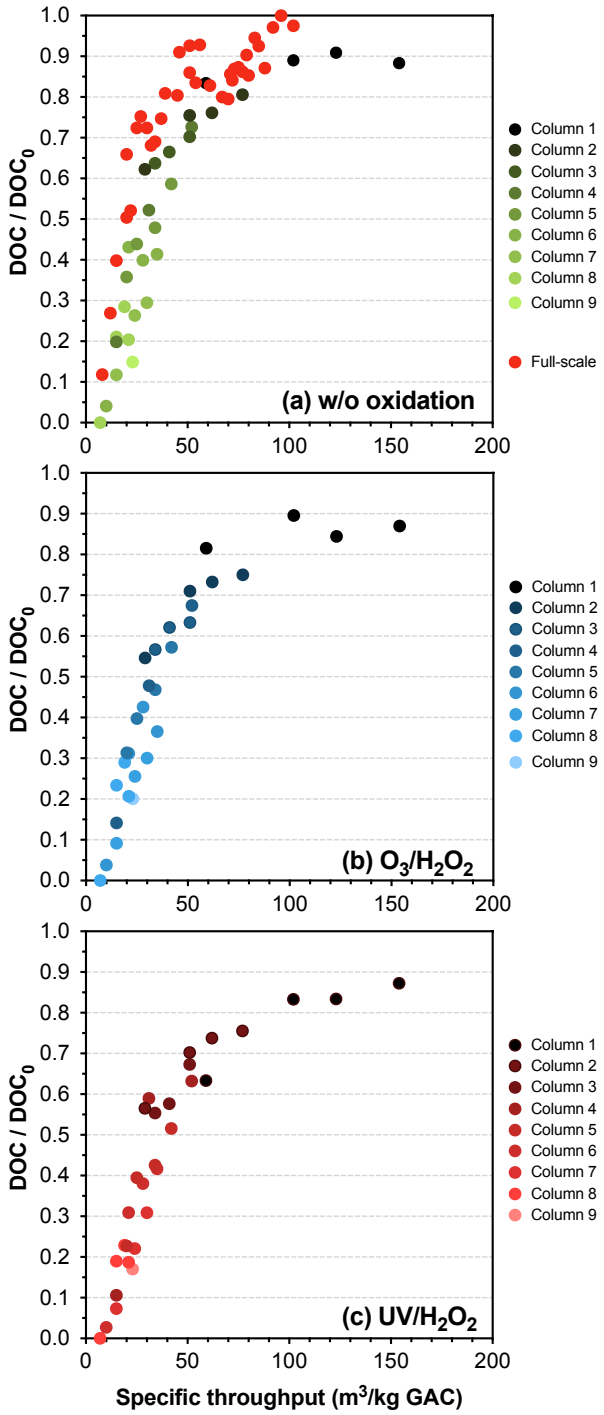

Fig. 5.15: *Comparison of breakthrough curves for dissolved organic carbon (DOC) for the GAC columns in series for Hardwald groundwater (a) without and with (b) O_3/H_2O_2 or (c) UV/H_2O_2 - Conditions: O_3/H_2O_2 – $[O_3]$ = 0.5 mg/L, $[H_2O_2]$ = 0.5 mg/L; UV/H_2O_2 – UV dose = 6800 J/m², $[H_2O_2]$ = 5 mg/L.*

5.2.1.6 ELIMINATION OF H_2O_2 RESIDUAL IN THE SMALL-SCALE COLUMNS IN SERIES

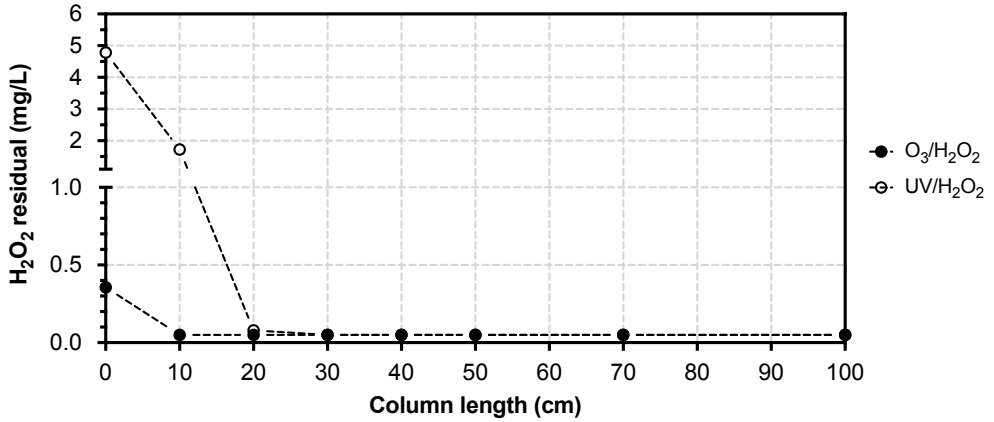

Fig. 5.16: *Abatement of the H_2O_2 residual concentration in the column set-up in line A1 (O_3/H_2O_2) and line B (UV/H_2O_2) – treatment conditions: line A1 – $[O_3]$ = 0.5 mg/L, $[H_2O_2]_0$ = 0.5 mg/L; line B – UV dose = 6800 J/m², $[H_2O_2]_0$ = 5.1 mg/L; Hardwald GW not spiked with micropollutants – pH = 7.71, T = 12.7°C.*

Fig. 5.16 shows significant H_2O_2 residual concentrations in AOP treated water before entering the AC columns. However, the residual concentrations are quickly degraded to below the detection limit at a GAC column length of 20 cm even for the UV/H_2O_2 line where the H_2O_2 residual concentration was about 5 mg/L after the UV reactor.

5.2.2 LONG-TERM EXPERIMENTS WITH ADVANCED OXIDATION AS POST-TREATMENT

When the pilot testing period started in May 2015, the organic matter from Hardwald groundwater was not retained anymore on the full-scale filters. Consequently, the DOC concentration was the same in Hardwald groundwater and in the treated drinking water (i.e. about 0.5 mg/L) and the efficiency of O_3/H_2O_2 process was similar when applied as pre-treatment to Hardwald groundwater (HGW) or post-treatement on Hardwasser drinking water (HDW) during this period as shown in **Tab. 5.4**.

Tab. 5.4: *Comparison of O_3/H_2O_2 treatment used as pre-treatment on Hardwald groundwater (HGW) and post-treatment on Hardwasser drinking water (HDW) to abate four micropollutants - treatment conditions: $[O_3]$ = 0.5 mg/L, $[H_2O_2]/[O_3]$ = 0.5.*

	Micropollutant abatement - % (concentration HGW (Pre.) and HDW (Post.) / concentration after O_3/H_2O_2 – ng/L)							
	Diatrizoate		**Iopamidol**		**Acesulfame**		**Sucralose**	
Date	**Pre.**	**Post.**	**Pre.**	**Post.**	**Pre.**	**Post.**	**Pre.**	**Post.**
24/08/2015	23.8 (21/16)	34.6 (26/17)	65.4 (81/28)	77.8 (45/10)	84.2 (76/12)	91.1 (270/24)	51.5 (99/48)	78.1 (32/7)
28/09/2015	25.0 (24/18)	31.8 (22/15)	70.9 (110/32)	73.9 (36/9.4)	89.4 (79/8.4)	92.9 (210/15)	55.8 (120/53)	67.6 (37/12)
30/11/2015	30.3 (33/23)	29.6 (27/19)	80.0 (170/34)	78.4 (43/9.3)	93.9 (64/3.9)	93.3 (210/14)	65.0 (117/41)	64.3 (42/15)
11/01/2016	21.1 (38/30)	19.4 (31/25)	57.9 (95/40)	48.8 (43/22)	80.9 (110/21)	72.9 (210/57)	38.6 (127/78)	38.0 (50/31)
23/03/2015	15.4 (26/22)	14.3 (28/24)	46.0 (100/54)	54.2 (59/27)	63.8 (94/34)	78.3 (230/50)	35.5 (110/71)	34.9 (43/28)
Average	**23.1 +/- 5.5**	**25.9 +/- 8.7**	**64.0 +/- 12.9**	**66.6 +/- 14.0**	**82.4 +/- 11.5**	**85.7 +/- 9.5**	**49.3 +/- 12.2**	**56.6 +/- 19.1**

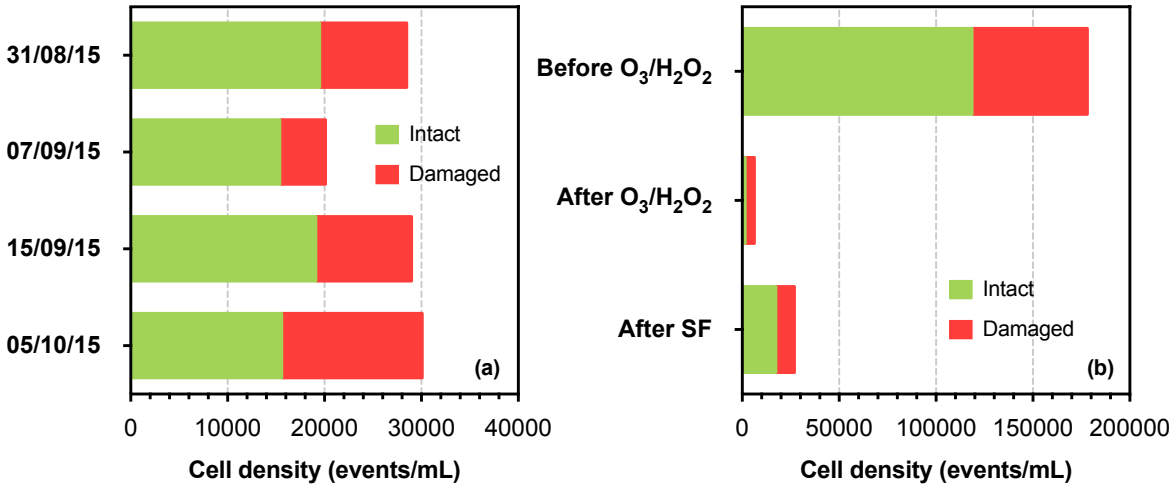

Fig. 5.17: *Intact and damaged cell counts measured (a) after the sand filter during the period from August to October 2015 and (b) along line A2 (i.e. O_3/H_2O_2 used as post-treatment) on 15/09/15.*

Before making tests on micropollutant biodegradation with the sand filter, the biology should be more or less stable in the filter. For that, the cell count was followed during the first months of testing and results show a low but constant cell count averaging 17000 intact cells/mL after three months of tests (**Fig. 5.17**a). Moreover, it was clear that ozone-based oxidation killed a lot of cells and a cell growth occurred in the sand filter (**Fig. 5.17**b)

When the short-term test was performed with the sand filter in March 2016, the number of intact cells was 14000 cells/mL.

5.2.3 SHORT-TERM EXPERIMENTS

Due to the limited testing period, short-term and long-term experiments were run in parallel. For this reason, long-term experiments were run with the expected optimum conditions. However, it was necessary to run short-term tests under differing treatment conditions to assess the limitations of the two oxidation processes in terms of micropollutant abatement, transformation product formation and bromate formation.

5.2.3.1 OPTIMISATION OF THE PEROXONE PROCESS (O_3/H_2O_2)

O_3 depletion, BrO_3^- formation and *p*CBA abatement

O_3, BrO_3^- and *p*CBA concentrations were measured along the ozone plug-flow reactor during the short-term experiments. The ozone depletion was more influenced by the H_2O_2/O_3 ratio than by the O_3 dose (**Fig. 5.18**). For the three ozone doses, the ozone depletion was above 90% after a contact time of 2 min with a molar H_2O_2/O_3 ratio of 1 and 4 while it was less than 50% after a contact time of 10 min without H_2O_2.

The ozone residual had a direct influence on the bromate formation. As shown in **Fig. 5.19**, O_3 will react with Br^- to HOBr/OBr^-, which further slowly reacts with O_3 to BrO_3- (green reaction pathway). An additional reaction between Br^- and °OH yields Br°, which reacts with O_3 to BrO° and finally bromate (blue reaction pathway). If H_2O_2 is added to the solution, HOBr can be reduced to Br^- but more importantly, the lifetime of ozone becomes smaller so that the reaction of Br° with O_3 is (partially) hindered. Consequently, as depicted in **Fig. 5.20**, the bromate formation is mitigated in the peroxone process but if the ozone dose is too high (e.g., 2 mg/L), bromate formation exceeds 20 µg/L even with a molar H_2O_2/O_3 ratio of 1. For a molar H_2O_2/O_3 ratio of 4, the bromate formation is close to 10 µg/L meaning that an ozone dose of 2 mg/L could not be applied in a full-scale application if one doesn't want to use the full margin for bromate.

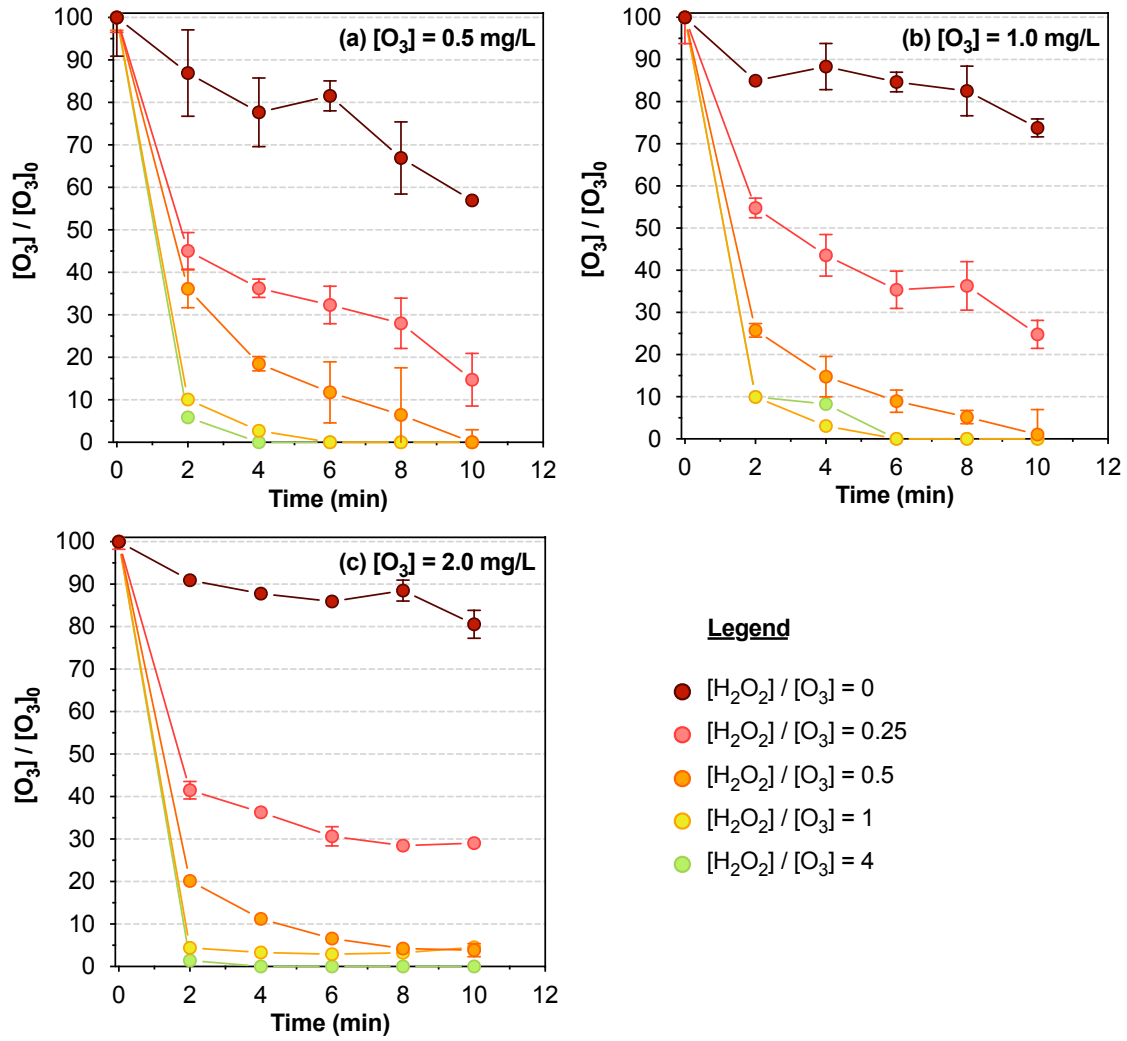

Fig. 5.18: *Ozone depletion along the plug flow reactor of treatment line A1 for three ozone doses (a) 0.5, (b) 1.0 and (c) 2.0 mg/L and molar $[H_2O_2]/[O_3]$ = 0, 0.25, 0.5, 1 and 4. Hardwald groundwater: pH 7.72 ± 0.05, [Br] = 82.3 ± 18.5 µg/L*

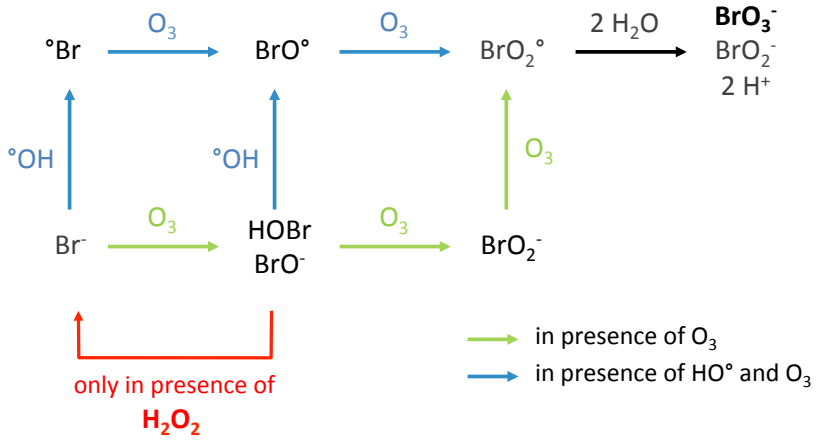

Fig. 5.19: *Simplified bromate formation mechanism in bromide-containing waters during ozonation (according to von Sonntag and von Gunten (2012))*

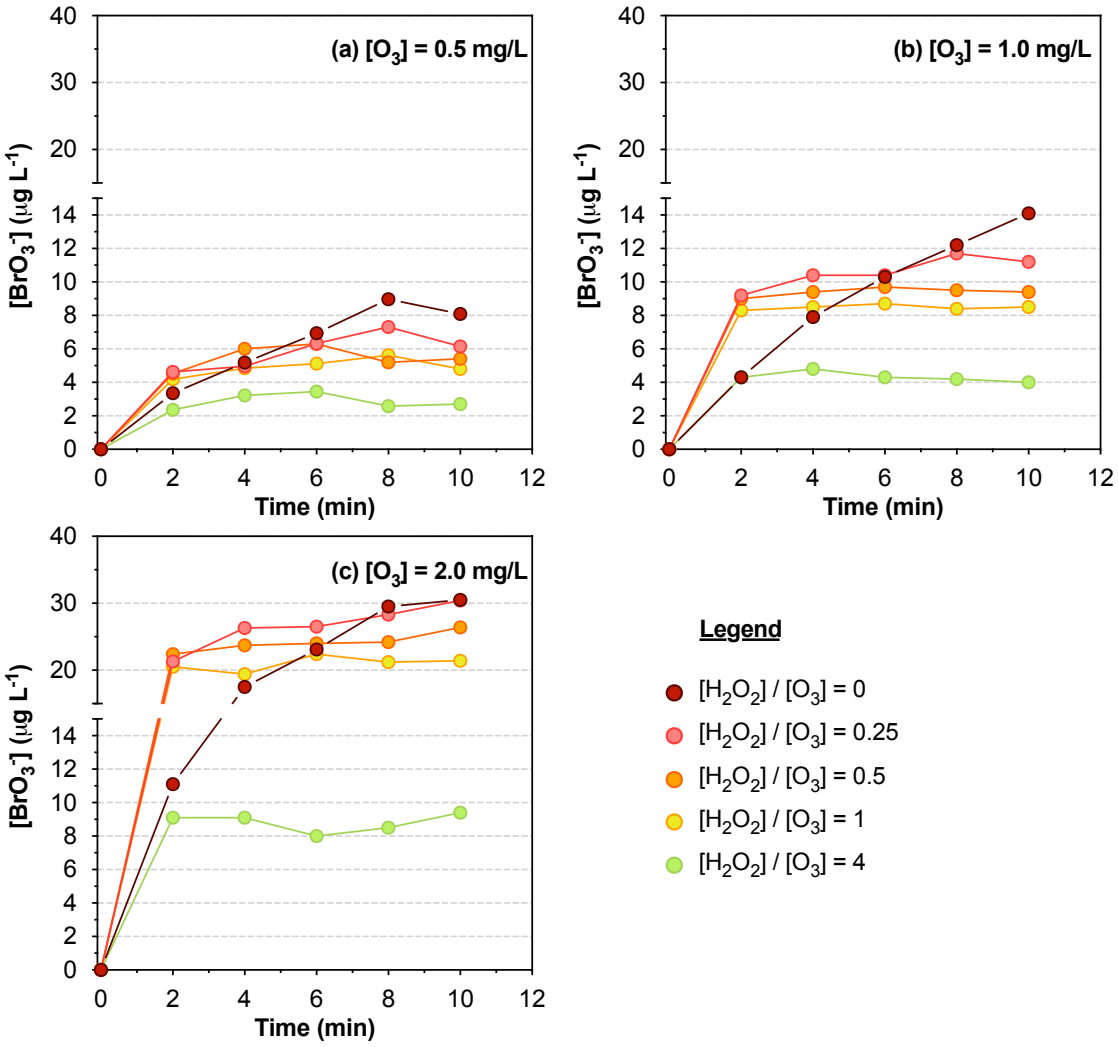

Fig. 5.20: *Bromate formation along the plug flow reactor of treatment line A1 for three ozone doses (a) 0.5, (b) 1.0 and (c) 2.0 mg/L and molar [H_2O_2]/[O_3] = 0, 0.25, 0.5, 1 and 4. Hardwald groundwater: pH 7.72 ± 0.05, [Br^-] = 82.3 ± 18.5 µg/L*

Bromate formation is a limiting parameter when dealing with ozonation processes since the drinking water standard is 10 µg/L. Therefore, an optimum has to be found between micropollutant abatement and bromate formation. To assess the possible range of operation, we compared the formation of bromate with the abatement of *p*CBA (an ozone-resistant model compound) after the ozone reactor for experiments with or without H_2O_2 addition (**Fig. 5.21**).

The use of an ozone dose higher than 0.5 mg/L seems to be problematic. For an ozone dose of 1 mg/L, a molar H_2O_2/O_3 ratio of at least 0.5 is necessary to ensure a bromate formation below 10 µg/L. However, even for a molar H_2O_2/O_3 ratio of up to 1, the formation of bromate stays close to the drinking water standard (about 9 µg/L) and it is not recommended to apply such treatment conditions. For a higher ozone dose of of 2 mg/L the bromate formation was up to 31 µg/L without H_2O_2 addition and a bromate concentration of about 10 µg/L was reached only with a high H_2O_2/O_3 molar ratio of 4.

Consequently, for an applied ozone dose of 0.5 mg/L and a H_2O_2/O_3 molar ratio of 1, the maximum pCBA abatement was 71% (**Fig. 5.21**b). This abatement might be considerably increased if the ozone dose is set to 1 mg/L. However, in this case a molar H_2O_2/O_3 ratio of 2 or higher would be necessary to avoid too much bromate.

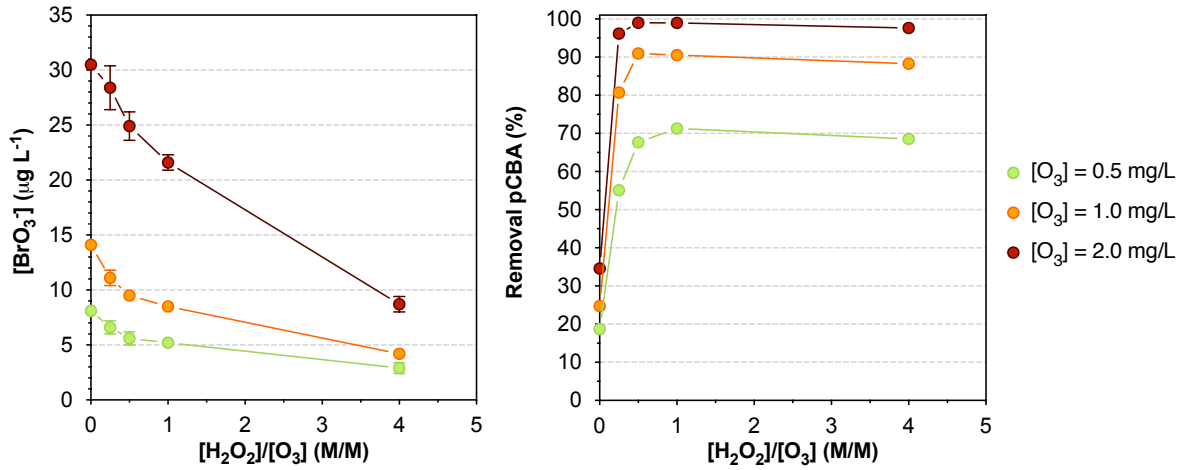

Fig. 5.21: *Comparison of (a) bromate formation and (b) pCBA abatement after 10 min contact time for three ozone doses 0.5, 1.0 and 2.0 mg/L and molar [H_2O_2]/[O_3] = 0, 0.25, 0.5, 1 and 4. Hardwald groundwater: pH 7.72 ± 0.05, [Br] = 82.3 ± 18.5 µg/L*

Micropollutant abatement

Eight micropollutants (**Fig. 5.22**) were selected to assess the efficiency of the O_3/H_2O_2 process for their abatement. These compounds were spiked in Hardwald groundwater with an online injection system at concentrations ranging from 2.2 to 11.9 µg/L. Chlorobutadienes, "naturally" present in low concentrations (i.e., below 56 ng/L) in Hardwald groundwater, were also analyzed (**Fig. 5.23**).

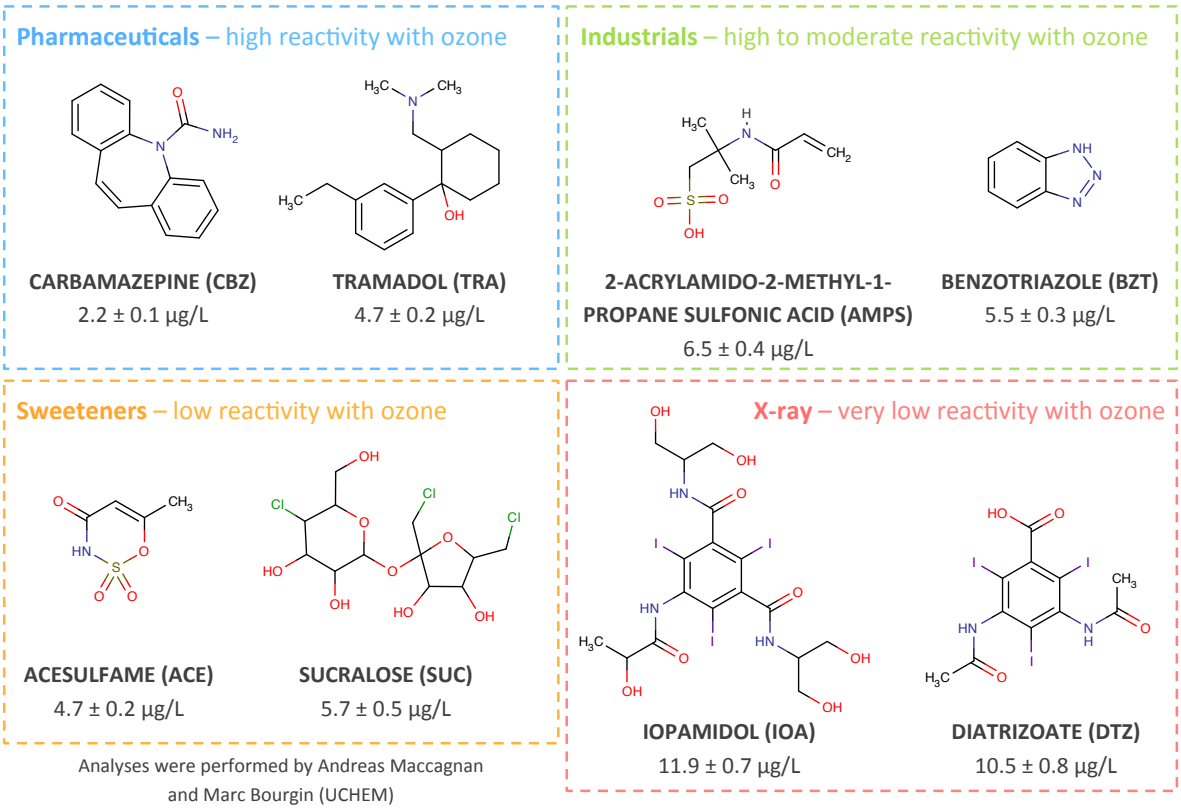

Fig. 5.22: *Chemical structures and spiked concentrations of the eight selected compounds.*

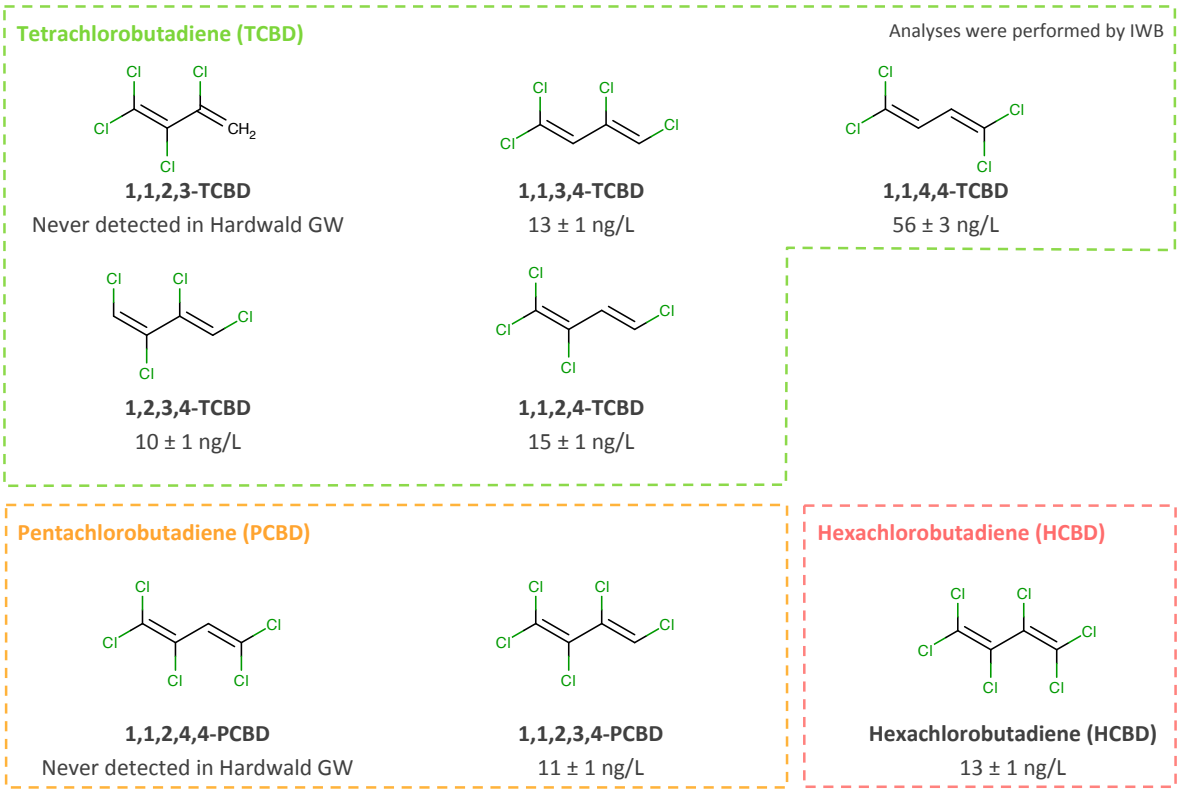

Fig. 5.23: *Chemical structures of the eight chlorobutadienes "naturally" present in Hardwald groundwater.*

With an ozone dose of 0.5 mg/L, the abatement of carbamazepine, tramadol and AMPS was > 95% with or without H_2O_2 addition (symbols on top of **Fig. 5.24** a-c). Moreover, a molar H_2O_2/O_3 ratio of about 1 seems to be optimal providing a reasonable abatement for all spiked micropollutants. With an ozone dose of 1 mg/L, it was possible to abate > 95% of benzotriazole and > 80% of acesulfame in presence of H_2O_2. Unfortunately, the abatement of sucralose and X-ray contrast media did not reach 80% under these conditions. Seven out of the eight spiked compounds reach > 80% abatement for an ozone dose of 2 mg/L (i.e., only diatrizoate was poorly degraded). Nevertheless, as previously discussed, this ozone dose should not be applied to a full-scale process since the drinking water standard for bromate is exceeded significantly for these conditions.

Three CBDs (i.e., 1,1,2,4,-TCBD, 1,1,2,4-TCBD, 1,2,3,4-TCBD) were measured below the LOQ with an O_3 dose of 0.5 mg/L and with or without H_2O_2 addition. However, H_2O_2 addition was necessary to achieve the same goal for 1,1,2,3,4-PCBD. The most abundant CBDs in Hardwald groundwater 1,1,4,4-TCBD was abated by 81% with the O_3/H_2O_2 process but its abatement to < LOQ was feasible only with an O_3 dose of 1.0 mg/L. HCBD was barely removed for any conditions. Even with an ozone dose of 2 mg/L, this compound was still detected. These results are in agreement with the specific study made on CBDs oxidation in chapter 4. They match very well with those presented in **Fig. 4.4**.

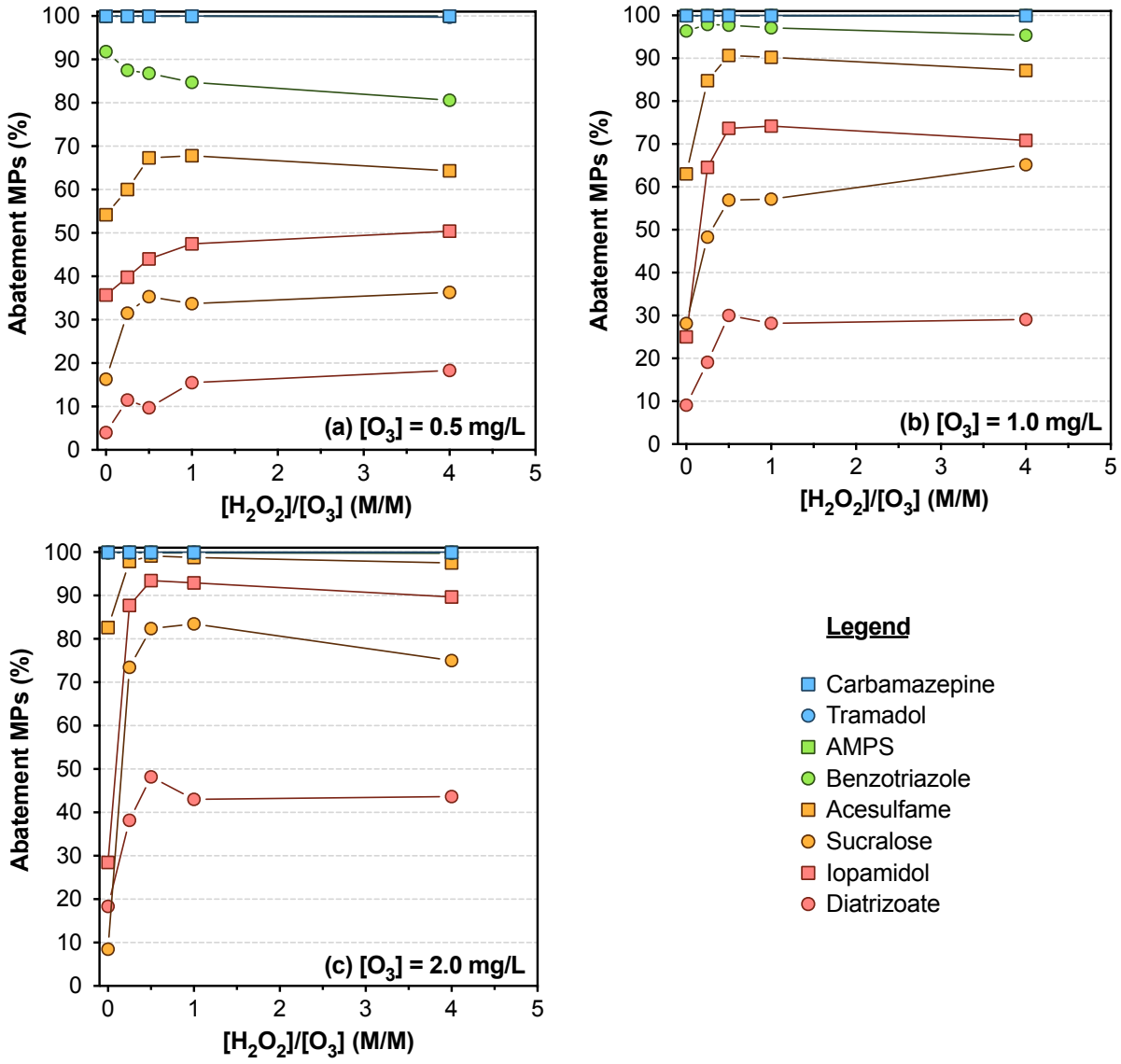

Fig. 5.24: *Abatement of eight micropollutants after 10 min contact time in Line A1 for three ozone doses (a) 0.5, (b) 1.0 and (c) 2.0 mg/L and a molar $[H_2O_2]/[O_3]$ = 0, 0.25, 0.5, 1 and 4. Hardwald groundwater: pH 7.72 ± 0.05, [Br] = 82.3 ± 18.5 µg/L.*

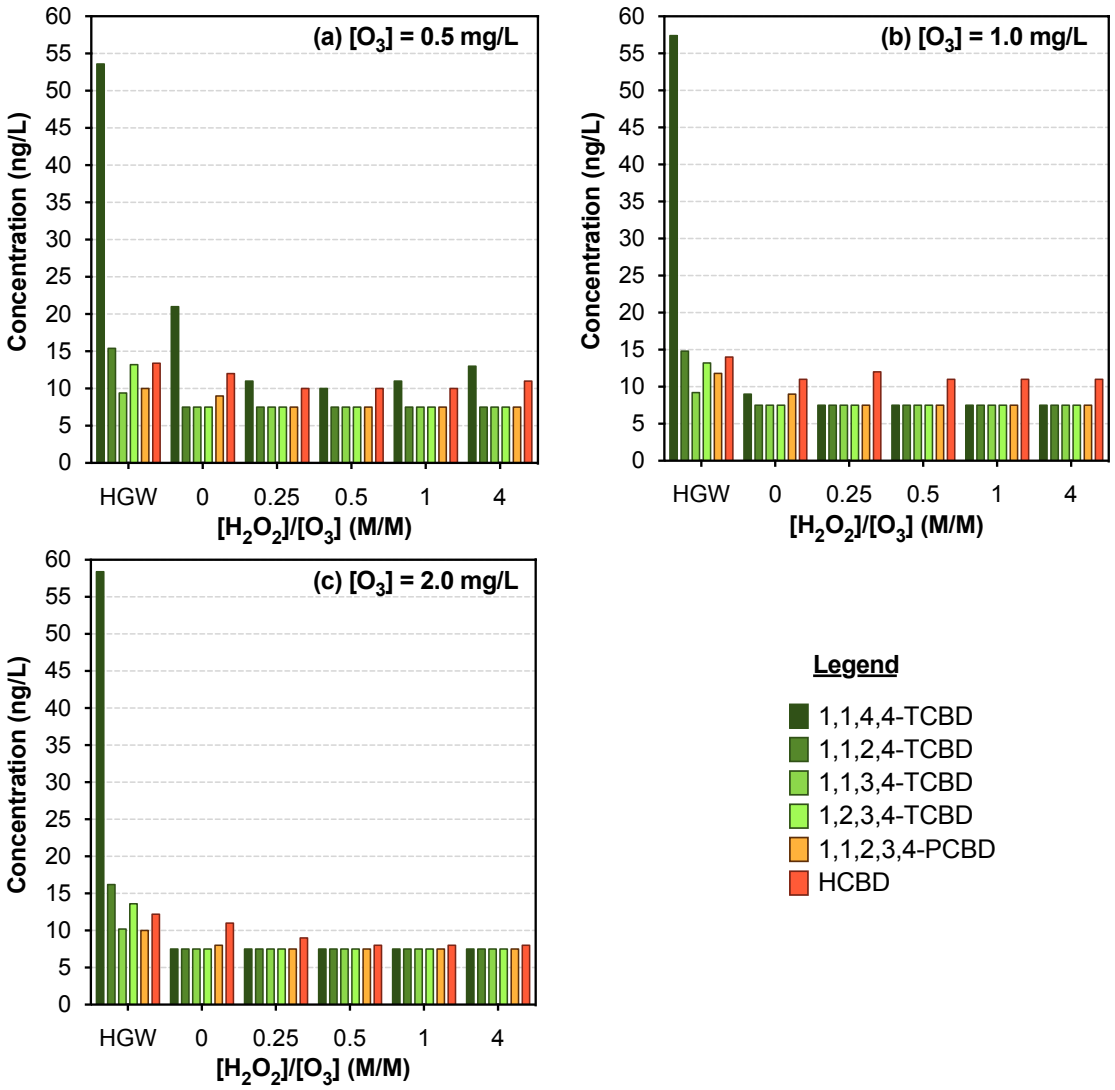

Fig. 5.25: *Abatement of six chlorobutadienes (CBDs) after 10 min contact time for three ozone doses (a) 0.5, (b) 1.0 and (c) 2.0 mg/L and a molar $[H_2O_2]/[O_3]$ = 0, 0.25, 0.5, 1 and 4 (LOQ = 7.5 ng/L for all CBDs). Hardwald groundwater: pH 7.72 ± 0.05, $[Br^-]$ = 82.3 ± 18.5 µg/L.*

5.2.3.2 Optimisation of the UV/H_2O_2 process

_p_CBA abatement

Fig. 5.26 presents the abatement of pCBA by direct photooxidation and UV/H_2O_2. Only 25% of *p*CBA was transformed by direct photolysis with a high UV dose of 13600 J/m^2. However, with an addition of H_2O_2, an abatement of 80% can be achieved for a UV dose of 12000 J/m^2 and 2 mg/L of H_2O_2. The UV dose might be decreased to 6000 J/m^2 if the concentration of H_2O_2 is increased to 5 mg/L. These conditions are in agreement with those applied during the long-term experiments.

X-ray contrast media were well degraded by direct photolysis, while they were poorly degraded by O_3/H_2O_2, especially diatrizoate. The addition of H_2O_2 in the UV process did not improve their abatement. Acesulfame degradation showed a similar trend as X-ray contrast media. Direct photolysis of carbamazepine, tramadol, AMPS, benzotriazole and sucralose was below 52% even with a UV dose of 13600 J/m^2, In contrast, their abatement was clearly improved with a H_2O_2 addition of 5 mg/L. Only AMPS and sucralose was not abated to 80% with a UV dose of 6000 J/m^2 and a H_2O_2 dose of 5 mg/L.

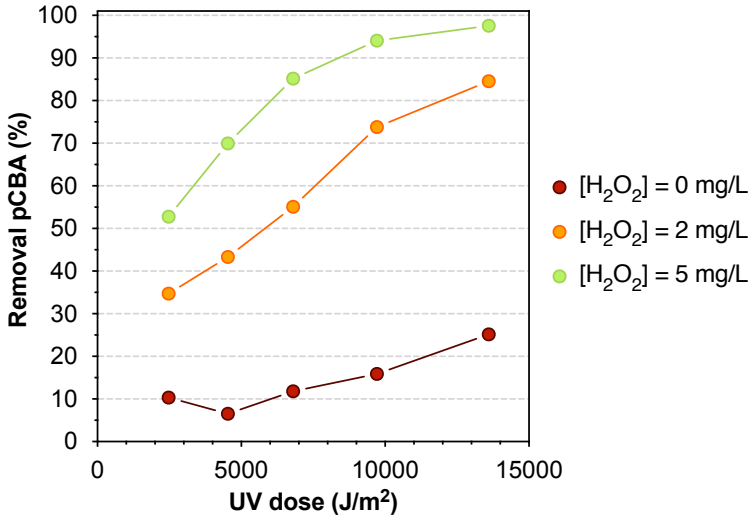

Fig. 5.26: *Abatement of pCBA by direct photolysis and the AOP UV/H_2O_2 as a function of the UV dose and the hydrogen peroxide concentration - [H_2O_2] = 0, 2 and 5 mg/L.*

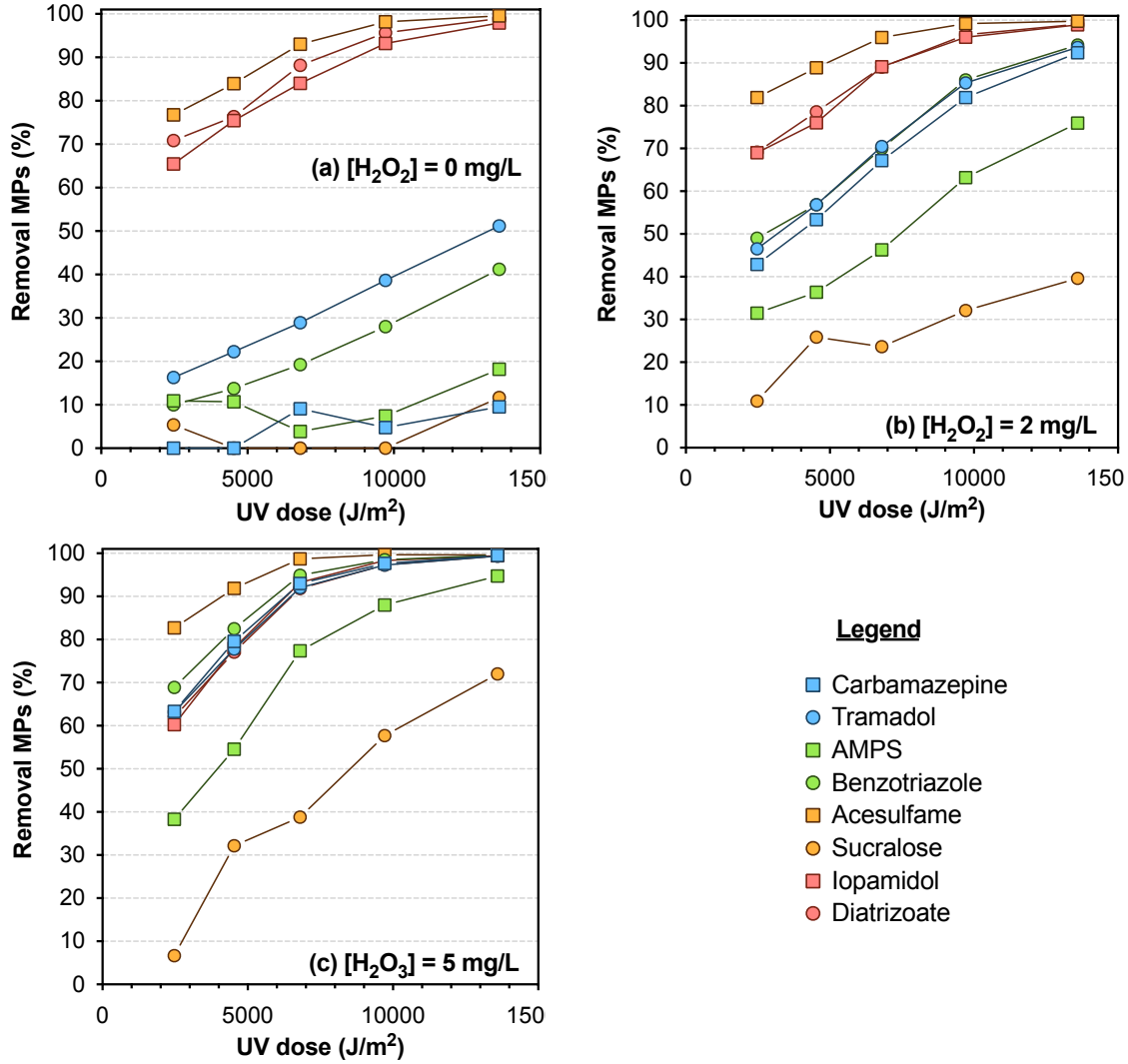

Fig. 5.27: *Abatement of eight micropollutants by direct photolysis and the AOP UV/H_2O_2 as a function of the UV dose and the hydrogen peroxide concentration - [H_2O_2] = (a) 0 mg/L, (b) 2 mg/L and (c) 5 mg/L.*

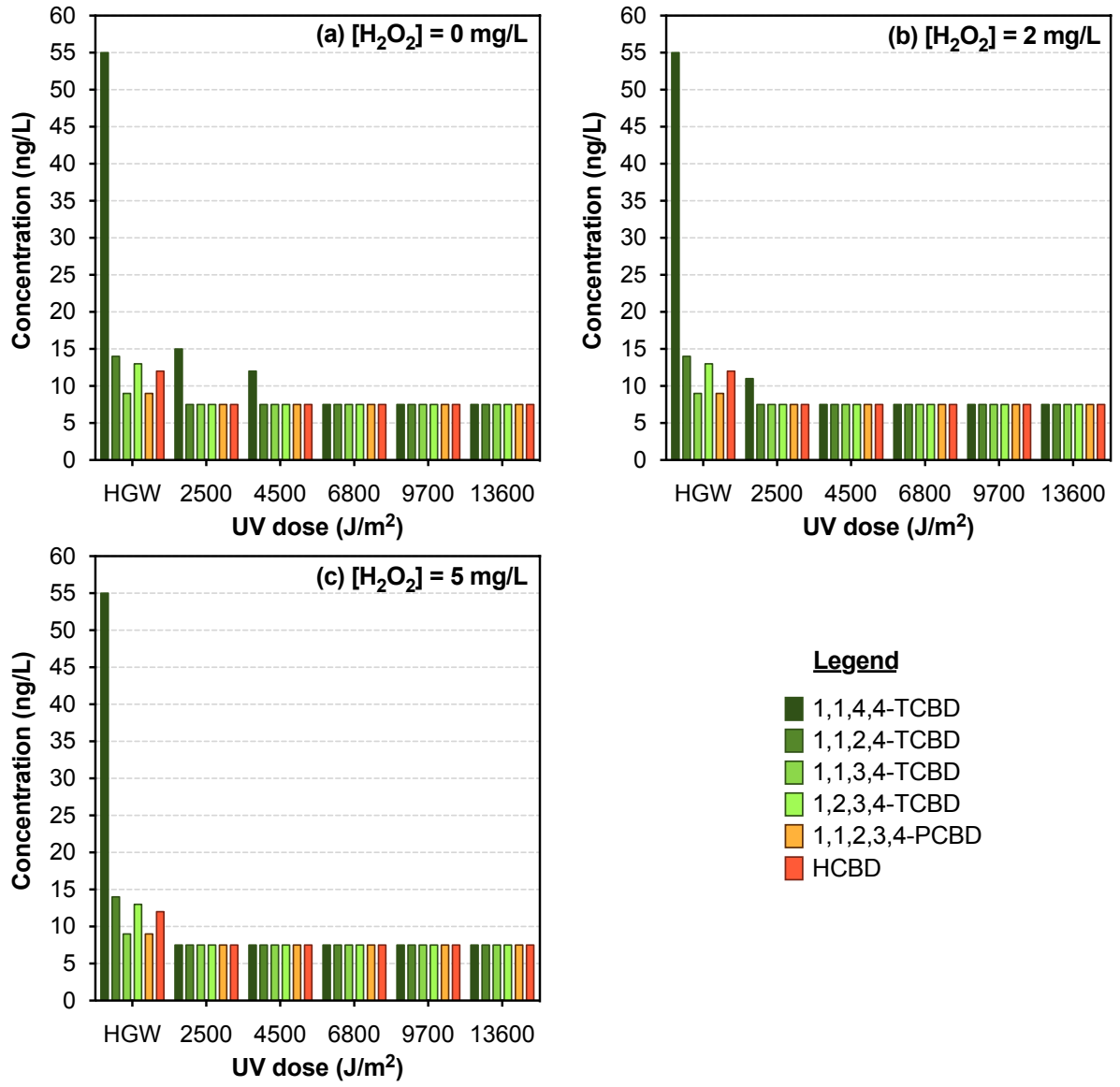

Fig. 5.28: *Abatement of chlorobutadienes (CBD) by direct photolysis and UV/H_2O_2 as a function of the UV dose and the hydrogen peroxide concentration - [H_2O_2] = (a) 0 mg/L, (b) 2 mg/L and (c) 5 mg/L.*

The abatement of CBDs by direct photolysis and UV/H_2O_2 is presented in **Fig. 5.28**. As shown in chapter 4, UV alone or UV/H_2O_2 are ideal processes to degrade CBDs. However, the formation of potential photoisomerization products has to be considered. Under conventional conditions (UV dose = 6800 J/m^2, [H_2O_2] = 5 mg/L), CBDs concentrations including HCB were below LOQs.

5.2.3.3 COMBINATION OF AOPS AND PAC ADSORPTION TO REMOVE MICROPOLLUTANTS

Adsorption without preoxidation

First of all, the adsorption of the eight micropollutants previously described was evaluated (**Fig. 5.29**). To reach the equilibrium, the adsorption tests were run with PAC during 5 days under mixed conditions. It appears that most of the micropollutants are adsorbed by up to 80% with an adsorbent dose lower than 3 mg PAC/L. Diatrizoate, acesulfame and AMPS required 7.4, 14.4 and 17.5 mg PAC/L, respectively, to reach the same performance.

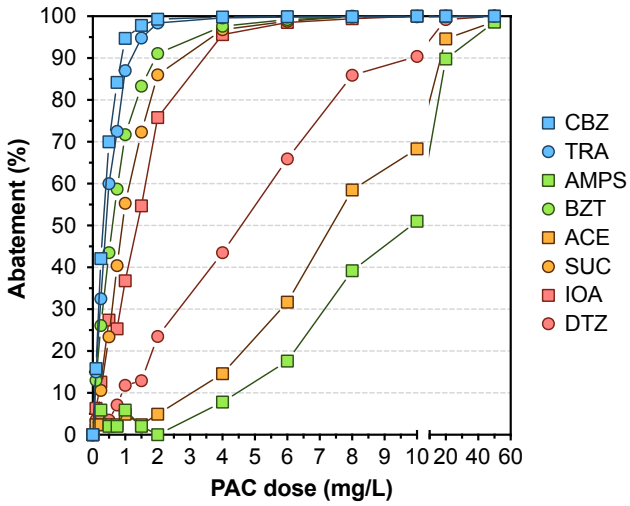

Fig. 5.29: *Adsorption of eight micropollutants on PAC (0 to 50 mg/L) without preoxidation – treatment conditions: Hardwald groundwater, [micropollutants] = 1.9 to 9.5 µg/L, contact time: 5 days, T = 12°C. Hardwald groundwater: pH 7.72 ± 0.05, [Br⁻] = 82.3 ± 18.5 µg/L.*

O_3/H_2O_2 and adsorption on PAC

Fig. 5.30 presents the abatement of the eight target micropollutants by O_3 or O_3/H_2O_2 followed by adsorption on PAC.

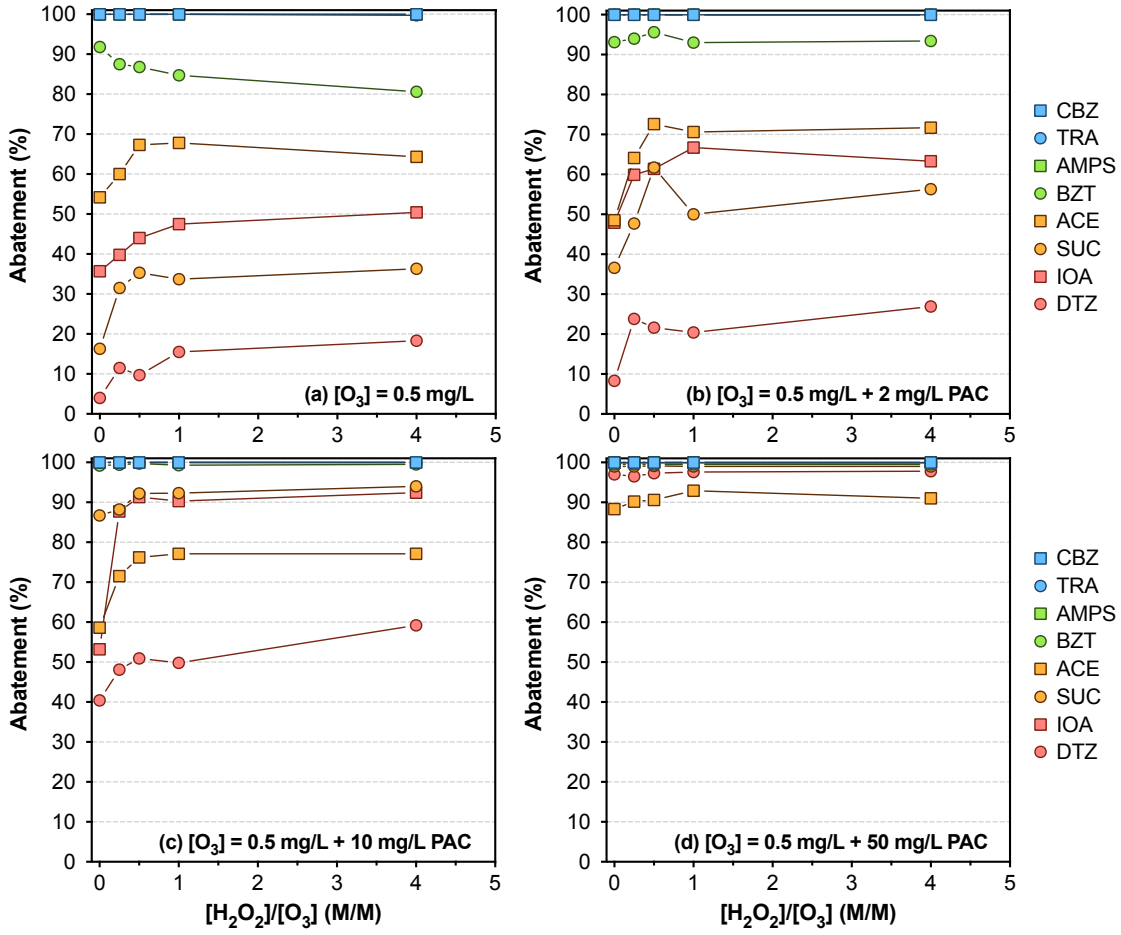

Fig. 5.30: *Combination of O_3/H_2O_2 and PAC adsorption to abate eight micropollutants – treatment conditions: Hardwald groundwater, oxidation - [O_3] = 0.5 mg/L, molar ratios [H_2O_2]/[O_3] = 0, 0.25, 0.5, 1 and 4, adsorption - [PAC] = (a) 0 mg/L, (b) 2 mg/L, (c) 10 mg/L and (d) 50 mg/L, contact time: 1 h.*

Basically, only 4 micropollutants were abated up to 80% by oxidation (with or without H_2O_2) and the adsorption treatment with 2 mg PAC/L did not improve their elimination. However, acesulfame and diatrizoate removal was still < 80% for 10 mg PAC/L. For this PAC dose, sucralose also reached 80% elimination but only if H_2O_2 was present during oxidation. AMPS, which is poorly adsorbable on PAC, is well oxidized in presence of O_3. Therefore, an oxidation step is recommended if this compound is selected to design the treatment scheme. With 50 mg PAC/L, the abatement is at least 90% for all compounds independently of the presence of H_2O_2 during ozonation. Even though diatrizoate was less oxidized by O_3/H_2O_2 than acesulfame, it is more adsorbable. Consequently, the combination O_3/H_2O_2 followed by adsorption with 50 mg PAC/L leads to a better elimination of diatrizoate (more than 96%) compared to acesulfame (88 to 93%). However, a dose of 50 mg PAC/L is extreme and beyond a realistic application. A dose of 10 mg PAC/L is more appropriated meaning that diatrizoate and acesulfame would be eliminated by 55% and 75%, respectively, and the six other compounds would be eliminated by at least 80%.

UV/H_2O_2 + adsorption on PAC

Similar experiments were performed with UV/H_2O_2 treatment and results are presented in **Fig. 5.31**. As for the O_3/H_2O_2 experiments, the addition of 2 mg PAC/L did not significantly improved the treatment and more than 90% elimination is achieved for all compounds with a dose of 50 mg PAC/L. The oxidation of AMPS is higher than for sucralose but it is less adsorbable than the latter. Therefore, if 10 mg PAC/L is applied as adsorbent dosage, the abatement of acesulfame is higher than for AMPS. This difference is negligible if a dosage of 50 mg PAC/L is applied. All micropollutants could be abated by 80% if a UV dose of at least 6000 J/m^2 is applied with a H_2O_2 dose of 5 mg/L followed by a PAC dose of 10 mg/L (realistic PAC dose for a full-scale application).

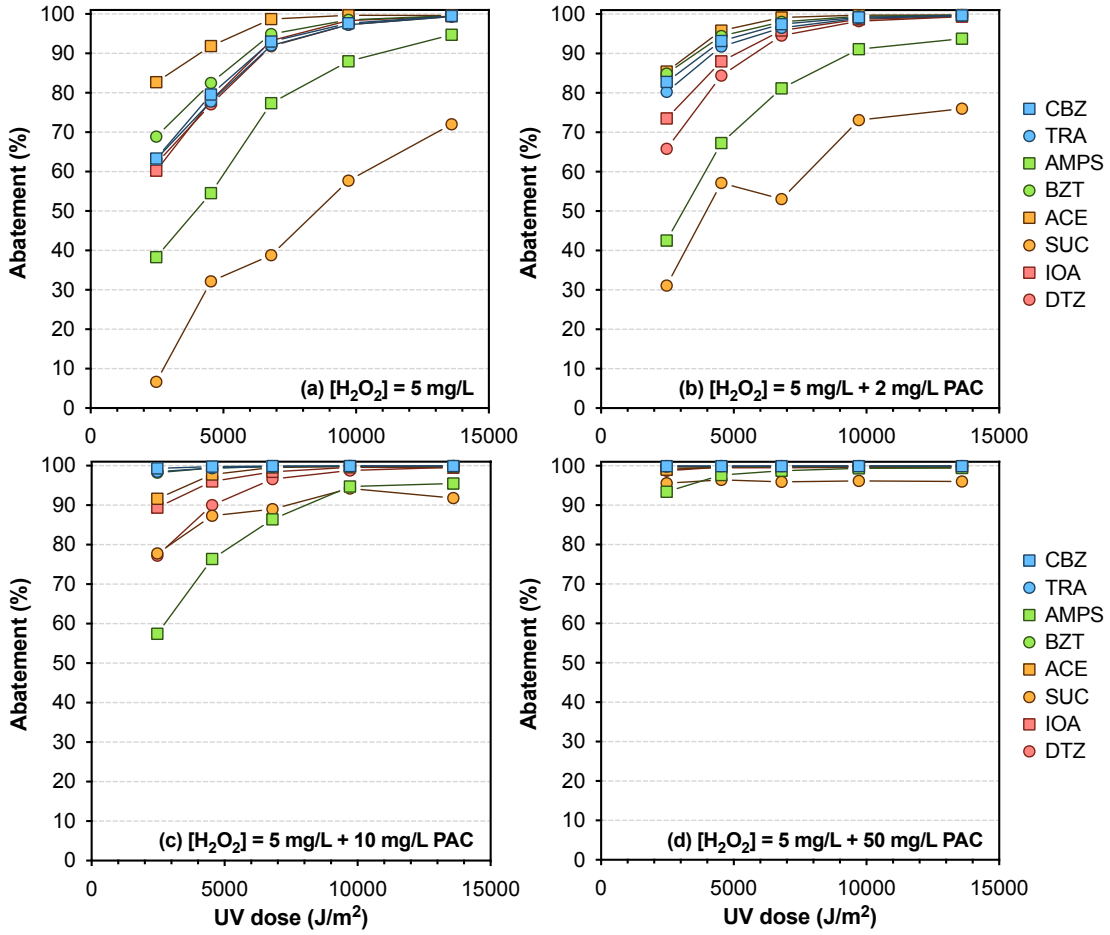

Fig. 5.31: *Combination of UV/H_2O_2 and PAC to abate the selected eight micropollutants – treatment conditions: Hardwald groundwater, oxidation - UV dose = from 2500 to 13600 J/m^2, [H_2O_2] = 5 mg/L, adsorption - [PAC] = (a) 0 mg/L, (b) 2 mg/L, (c) 10 mg/L and (d) 50 mg/L, contact time: 1 h.*

5.2.3.4 FORMATION OF TRANSFORMATION PRODUCTS DURING AOP TREATMENTS

Tab. 5.5 presents the masses (m/z) of transformation products detected in water samples after O_3/H_2O_2 and UV/H_2O_2 treatments. The detected masses for transformation products of carbamazepine (CBZ), tramadol (TRA), benzotriazole (BZT), acesulfame (ACE) and iopamidol (IOA) were already identified in previous studies while those for AMPS, sucralose (SUC) and diatrizoate (DTZ) were found with preliminary laboratory-scale experiments performed at Eawag by Marc Bourgin.

Overall, 26 transformation products were detected but only 15 were semi-quantified (except for the two transformation products of tramadol for which standards were available). The semi-quantification was done by calculating the ratio between the peak area of the transformation product and the peak area of an internal standard of the parent compounds (except for AMPS for which the internal standard of hydrochlorothiazide was used).

Tab. 5.5: *List of transformation products detected after O_3/H_2O_2 and/or UV/H_2O_2 treatment of 7 micropollutants (see above). The compounds in grey were detected but not semi-quantified. It is also indicated whether or not the transformation products were detected during the laboratory-scale experiments (section 3.2.2.2). Notation: CBZ_TP1 = transformation product 1 of carbamazepine.*

Compounds	m/z (polarity)	Presence after		Detected in laboratory-scale experiments	Remark
		O_3/H_2O_2	UV/H_2O_2		
CBZ_TP1	251.0815 (+)	Yes	Yes	Yes	
CBZ_TP2	267.0764 (+)	Yes	Yes	Yes	
CBZ_TP3	283.0713 (+)	Yes	No	Yes	
CBZ_TP4	208.0757 (+)	Yes	Yes	Yes	
CBZ_TP5	253.0972 (+)	No	Yes	Yes	
CBZ_TP6	271.1077 (+)				In-source fragment of CBZ_TP1
CBZ_TP7	196.0767 (+)				In-source fragment
TRA_TP1	290.1907 (+)	Yes	No	Yes	Identified as tramadol *N*-oxide
TRA_TP2	250.1802 (+)	No	Yes	Yes	Identified as *N*-desmethyl tramadol
AMPS_TP1	226.0390 (-)	Yes	Yes	Not studied	
AMPS_TP2	224.0230 (-)	Yes	Yes	Not studied	
AMPS_TP3	210.0430 (+)				In-source fragment of AMPS_TP2
AMPS_TP4	240.0548 (-)				In-source fragment of AMPS_TP2
AMPS_TP5	226.0379 (+)				AMPS_TP1 in positive mode
AMPS_TP6	182.0130 (-)				Low intensity
AMPS_TP7	176.0550 (+)				Low intensity
BZT_TP1	124.0150 (-)	Yes	Yes	No	
BZT_TP2	166.0255 (-)	Yes	Yes	Yes	
BZT_TP3	150.0306 (-)	Yes	Yes	No	
BZT_TP4	168.0404 (+)				BZT_TP2 in positive mode
BZT_TP5	170.0560 (+)				Low intensity
ACE_TP1	179.9968 (-)	No	Yes	No	
SUC_TP1	376.0563 (+)	Yes	Yes	Not studied	
SUC_TP2	403.0208 (-)	Yes	Yes	Not studied	
IOA_TP1	775.8457 (+)	Yes	Yes	No	
IOA_TP2	717.8039 (+)	Yes	No	No	

The analytical protocol (i.e. sample preparation and analyses) and the initial concentrations were different from the laboratory-scale experiments. Consequently, the list of transformation products slightly differs from the one shown in **Table. 3.3**. The transformation products of compounds easily oxidisable by ozone (i.e. carbamazepine and tramadol) were similar while the transformation products of ozone-resistant compounds (i.e., acesulfame, iopamidol) were either not detected or different. For benzotriazole, only BZT_TP2 was common in both experiments.

Carbamazepine (CBZ)

Fig. 5.32 presents the abatement of carbamazepine and the abundance of transformation products formed during O_3/H_2O_2. It is shown that all indentified transformation products are in higher concentrations when conventional ozonation is performed (i.e., without H_2O_2). However, with a molar H_2O_2/O_3 ratio of 0.5, their concentrations are close to the mimimum observed under the studied conditions. An increase of the molar H_2O_2/O_3 ratio to 4 did not demonstrate significant improvements. Moreover, with an ozone dose of 2 mg/L, the four transformation products are present in very low concentrations since they are certainly further oxidised to other transformation products. This leads to a further “oxidative dilution” to other transformation products and eventually these products might not be measurable anymore.

These results are not directly comparable to laboratory-scale results presented in section 3.2.2.2 even though the same transformation products were detected because the ozone doses were totally different (i.e., up to 0.09 mg/L for laboratory-scale experiments while the mimimum ozone dose was 0.5 mg/L in pilot plant test). However, it seems that the addition of H_2O_2 (i.e. molar H_2O_2/O_3 ratio of 0.5) had a small effect on the concentrations of transformation products for an ozone dose of 0.05 and 0.09 mg/L while their concentrations decreased if the ozone dose is set to 0.5 mg/L. This phenomenon was even more pronounced for higher ozone doses (i.e., 1 and 2 mg/L).

The oxidation pathway seems more complex for UV/H_2O_2 treatments (**Fig. 5.33**). While carbamazepine was weakly transformed by direct photolysis, the presence of CBZ_TP1, CBZ_TP2 and CBZ_TP4 increased with increasing UV doses in absence of H_2O_2. A new transformation product (CBZ_TP5) was also detected while CBZ_TP3 was not detected in these experiments.

The abundance trends were different after adding 2 and 5 mg/L of H_2O_2. For CBZ_TP1 and CBZ_TP2 a maximum was observed for a UV dose of about 7000 or 10000 J/m^2, respectively with 2 mg/L H_2O_2, or 4000 J/m^2 with 5 mg/L H_2O_2. These conditions correspond to a carbamazepine abatement of about 55-60%. For CBZ_TP4, this maximum was observed with a UV dose below 5000 J/m^2 for both H_2O_2 doses. For higher UV doses, the concentration decreased independently of the compounds. The CBZ_TP5 concentration increased with increasing UV doses in presence of H_2O_2. Therefore, it might be a secondary transformation product.

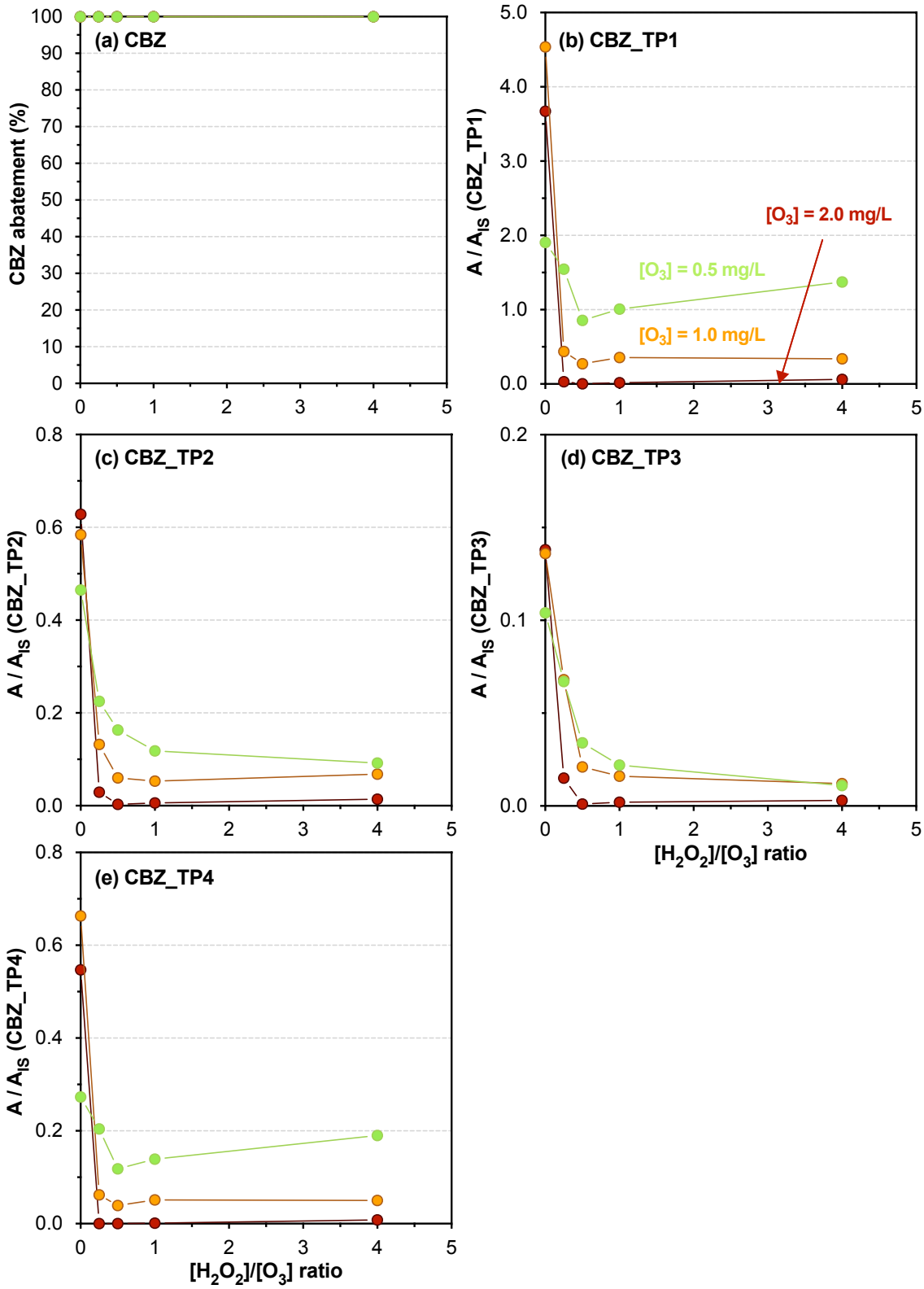

Fig. 5.32: *Abatement of (a) carbamazepine (CBZ) and the evolution of four transformation products during ozonation and the AOP O_3/H_2O_2 as a function of the ozone dose and the H_2O_2:O_3 ratio: (b) CBZ_TP1, (c) CBZ_TP2, (d) CBZ_TP3, and (e) CBZ_TP4 (according to Tab.* ***5.5****). Conditions: Hardwald groundwater, $[O_3]$ = 0.5, 1.0 and 2.0 mg/L, $[H_2O_2]/[O_3]$ = 0, 0.25, 0.5, 1 and 4 (M/M).*

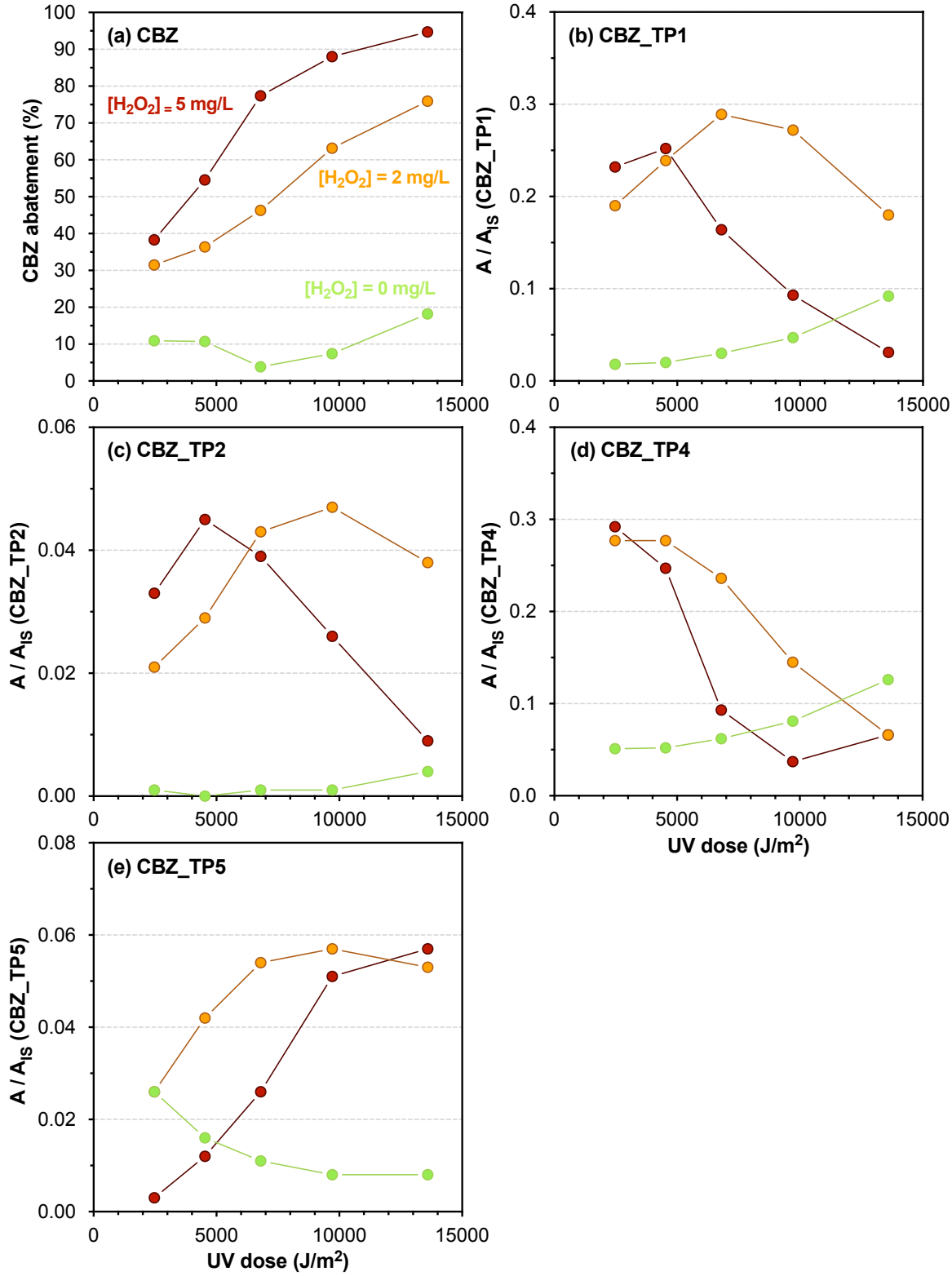

Fig. 5.33: *Abatement of (a) carbamazepine (CBZ) and the evolution of four transformation products for UV/H_2O_2-treatment as a function of the UV and the hydrogen peroxide dose: (b) CBZ_TP1, (c) CBZ_TP2, (d) CBZ_TP4, and (e) CBZ_TP5 (according to Tab.* ***5.5****). Conditions: Hardwald groundwater, UV doses = from 2500 to 13600 J/m², [H_2O_2] = 0, 2 and 5 mg/L.*

Tramadol (TRA)

For tramadol, two transformation products were followed after O_3/H_2O_2 (**Fig. 5.34**) and UV/H_2O_2 (**Fig. 5.35**) treatment.

It is known that TRA_TP1 (tramadol *N*-oxide) resulted from the direct reaction of tramadol with ozone at the tertiary amine group. This compound was not detected after UV/H_2O_2 treatment. Without H_2O_2, for an ozone dose of 0.5 mg/L, the minimum formation of TRA_TP1 is 690 ng/L for an initial tramadol concentration of 4450 ng/L. The concentration decreased to 3.8 ng/L when the ozone dose was increased to 2 mg/L. The concentration of TRA_TP1 unexpectedly increased with a molar $[H_2O_2]/[O_3]$ > 0.5. A reason might be the high concentration of H_2O_2 consuming the oxidant species present in solution. TRA_TP2 was also present in solution but only for an ozone dose of 0.5 mg/L and a molar $[H_2O_2]/[O_3]$ ratio of 1 and 4 with concentrations of 12 and 33 ng/L, respectively. For all other treatment conditions, its concentration was below the LOQ of 5 ng/L.

As for carbamazepine, it is difficult to correlate the pilot plant data with the results from the laboratory-scale experiments since the tests were performed with differing ozone doses. However, due to a higher initial tramadol concentration during the laboratory-scale experiments (i.e., 300 µg/L), it was possible to measured TRA_TP3 and TRA_TP4 while they were not detected during the pilot plant tests performed with an initial tramadol concentration of 4.7 µg/L.

The formation of TRA_TP2 (*N*-desmethyltramadol) is up to 46 ng/L with UV/H_2O_2 and it might be minimized by increasing the H_2O_2 dose to 5 mg/L and the UV dose to 13600 J/m^2. The abundance of TRA_TP2 starts decreasing (i.e., TRA_TP2 is further oxidized) when the elimination of tramadol exceeds 80%. This is because under these conditions it is not formed significantly anymore and its abatement becomes the most important process. For a UV dose of 6800 J/m^2, only 19 ng/L of TRA_TP2 was formed. In addition, as expected, TRA_TP1 was not formed in the UV-based process.

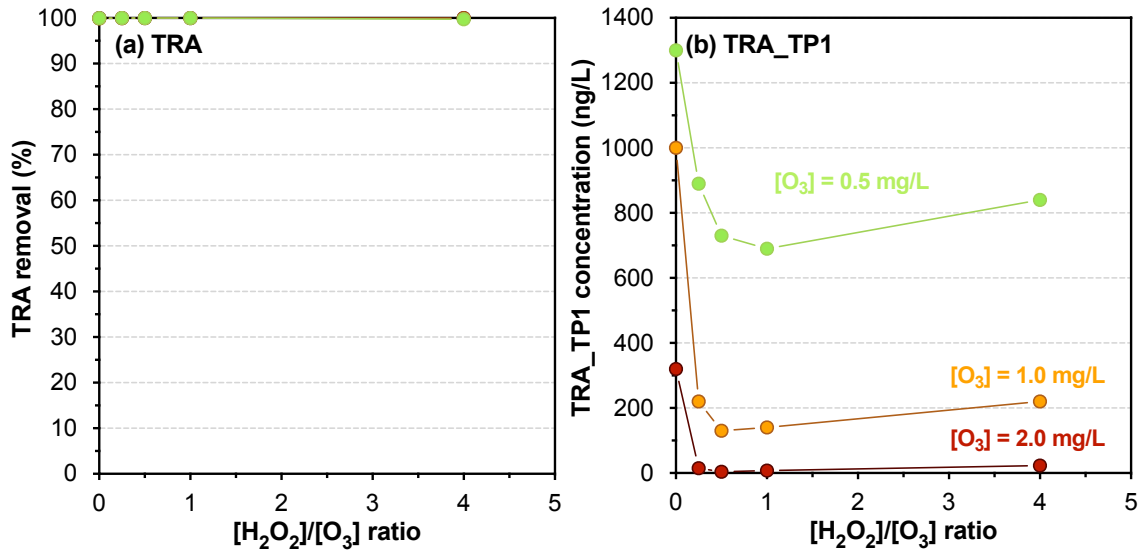

Fig. 5.34: *Abatement of (a) tramadol (TRA) and the evolution of one transformation product during ozonation and the AOP O_3/H_2O_2 as a function of the ozone dose and the molar H_2O_2:O_3 ratio: (b) TRA_TP1 (according to Tab.* ***5.5****). Conditions: Hardwald groundwater, $[O_3]$ = 0.5, 1.0 and 2.0 mg/L, $[H_2O_2]/[O_3]$ = 0, 0.25, 0.5, 1 and 4 (M/M).*

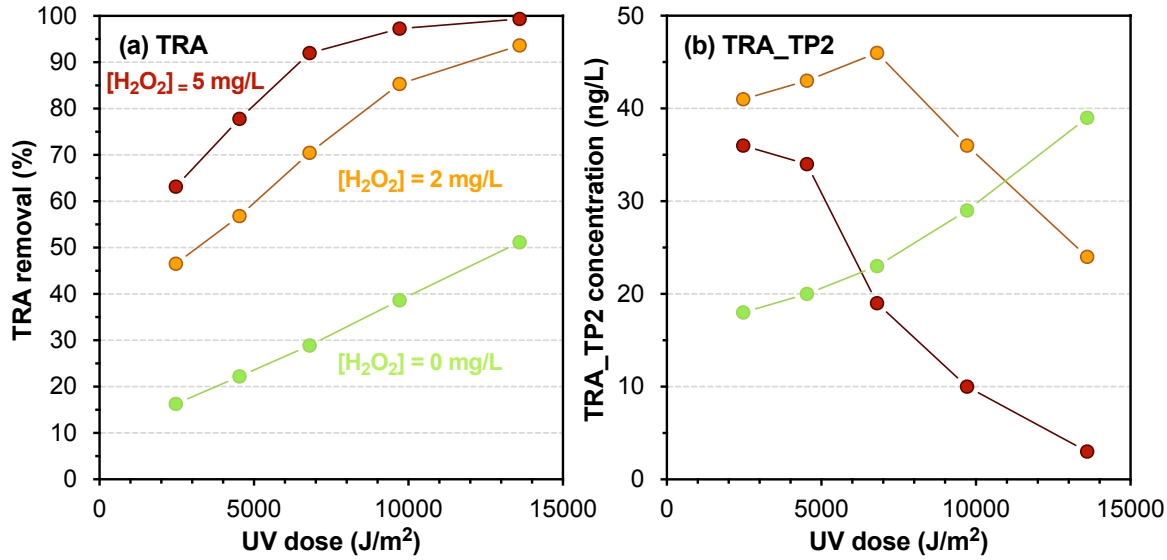

Fig. 5.35: *Abatement of (a) tramadol (TRA) and the evolution of one transformation product for UV/H_2O_2-treatment as a function of the UV and the hydrogen peroxide dose: (b) TRA_TP2 (according to Tab.* ***5.5****). Conditions: Hardwald groundwater, UV doses = from 2500 to 13600 J/m², [H_2O_2] = 0, 2 and 5 mg/L.*

2-Acrylamido-2-methylpropane sulfonic acid (AMPS)

As shown in **Fig. 5.36**a, AMPS is completetly degraded during ozonation and ozone-based advanced oxidation. Indeed, the C=C double bond present in the structure is a very reactive site for ozone attack. From this oxidation, AMPS_TP1 and AMPS_TP2 were detected. A structural elucidation led to two potential structures: AMPS_TP1 would be the aldehyde of AMPS after cleavage of the double bond according to the Criegee mechanism, while AMPS_TP2 would be the acid form ensuing of the AMPS_TP1 oxidation. This oxidation pathway seems to be confirmed by results presented in **Fig. 5.36**b and c. Indeed, minimum concentrations of AMPS_TP1 were observed for molar H_2O_2/O_3 ratios of 0.25 and 0.5 when maximum concentrations was observed for AMPS_TP2 and vice versa. This molar H_2O_2/O_3 ratio optimum was also observed for TRA_TP1 and has stayed unexplained so far. Moreover, it seems that the ozone dose did not influence the abundance of AMPS_TP1 while AMPs_TP2 was produced in higher concentration with an ozone dose of 2 mg/L.

AMPS_TP1 and AMPS_TP2 were also detected with UV/H_2O_2 treatment (Fig. 5.37). However, the concentration was 15 times lower for AMPS_TP1 than for O_3/H_2O_2 treatment while AMPS_TP2 concentration was in the same order of magnitude. It should also be noted that direct photolysis does not lead to a significant AMPS elimination (below 20%) and AMPS_TP1 and AMPS_TP2 were therefore not detected after treatment. In addition, when H_2O_2 is added, both transformation products seem to be formed proportionaly to the AMPS elimination and their concentrations increased with increasing UV doses.

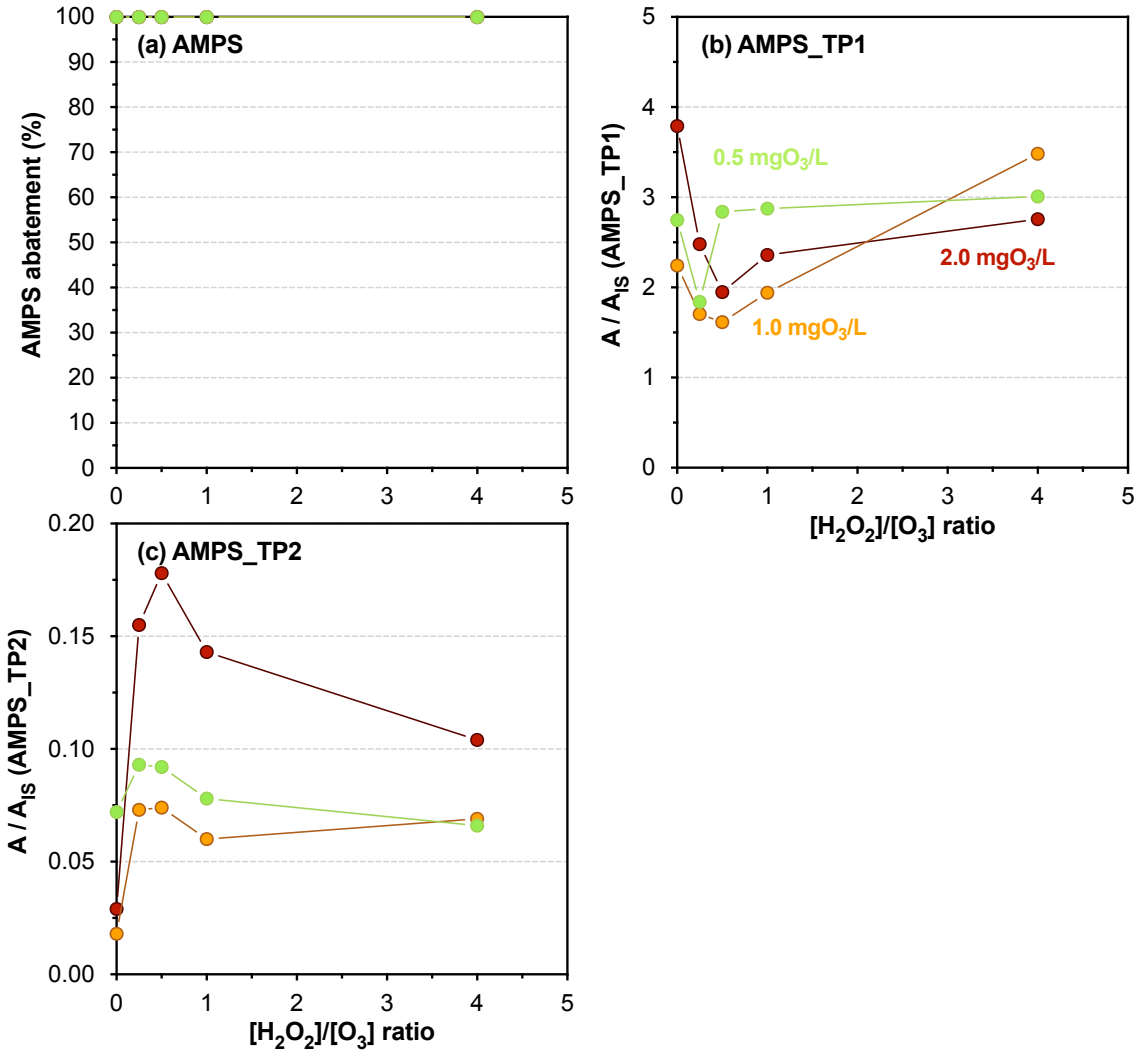

Fig. 5.36: *Abatement of (a) AMPS and the evolution of two transformation products during ozonation and the AOP O_3/H_2O_2 as a function of the ozone dose and the molar H_2O_2:O_3 ratio: ((b) AMPS_TP1, (c) AMPS_TP2 (according to Tab.* ***5.5****). Conditions: Hardwald groundwater, $[O_3]$ = 0.5, 1.0 and 2.0 mg/L, molar $[H_2O_2]/[O_3]$ = 0, 0.25, 0.5, 1 and 4.*

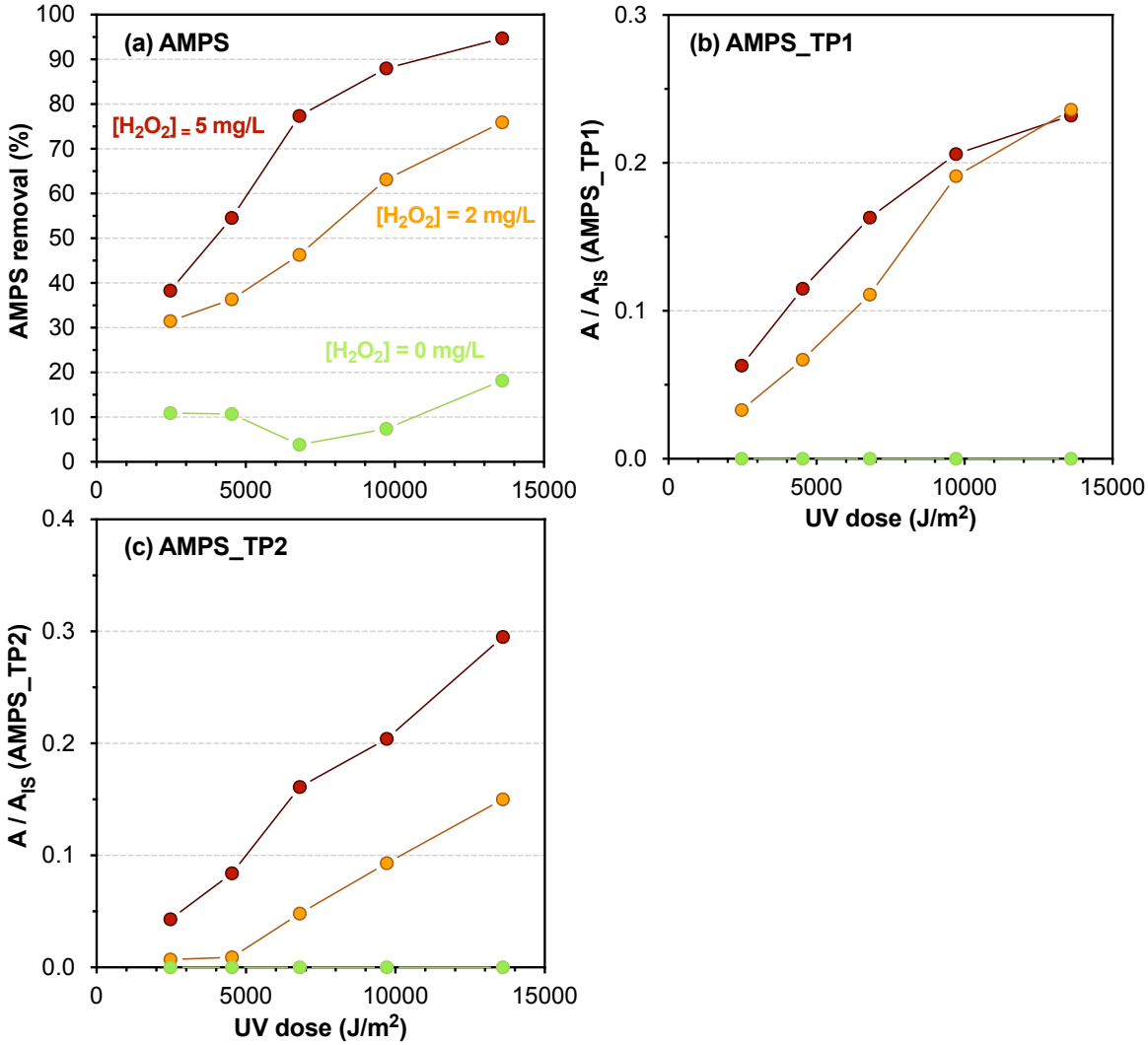

*Fig. 5.37 – Abatement of (a) AMPS and the evolution of two transformation products for UV/H_2O_2-treatment as a function of the UV and the hydrogen peroxide dose: (b) AMPS_TP1 and (c) AMPS_TP2 (according to **Tab. 5.5**). Conditions: Hardwald groundwater, UV dose = from 2500 to 13600 J/m², [H_2O_2] = 0, 2 and 5 mg/L.*

Benzotrizole (BZT)

As shown in **Fig. 5.38**, BZT_TP1 is a transformation product preferentially formed during conventional ozonation while BZT_TP2 is formed in higher concentration in presence of H_2O_2. The third transformation product BZT_TP3 was only detected during tests with an ozone dose of 0.5 mg/L and increased with increasing molar H_2O_2/O_3 ratios.

During UV/H_2O_2 treatment, the maximum concentration of transformation products was observed with a dose of H_2O_2 of 2 and 5 mg/L (Fig. 5.39). However, these transformation products are further oxidized when increasing the UV dose.

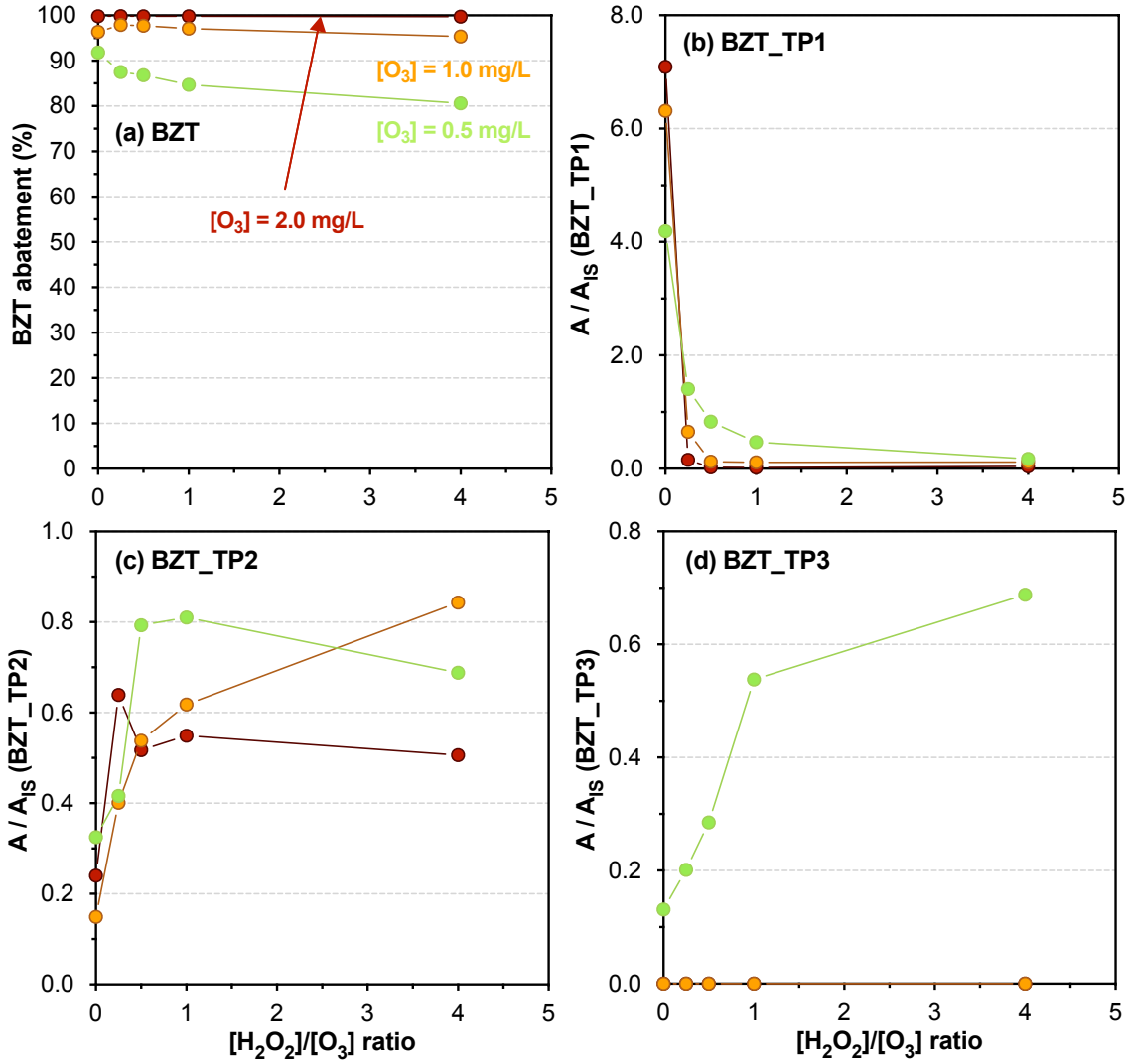

Fig. 5.38: *Abatement of (a) benzotriazole (BZT) and the evolution of three transformation product during ozonation and the AOP O_3/H_2O_2 as a function of the ozone dose and the molar H_2O_2:O_3 ratio: (b) BZT_TP1, (c) BZT_TP2, and (d) BZT_TP3 (according to Tab.* ***5.5****). Conditions: Hardwald groundwater, $[O_3]$ = 0.5, 1.0 and 2.0 mg/L, $[H_2O_2]/[O_3]$ = 0, 0.25, 0.5, 1 and 4 (M/M).*

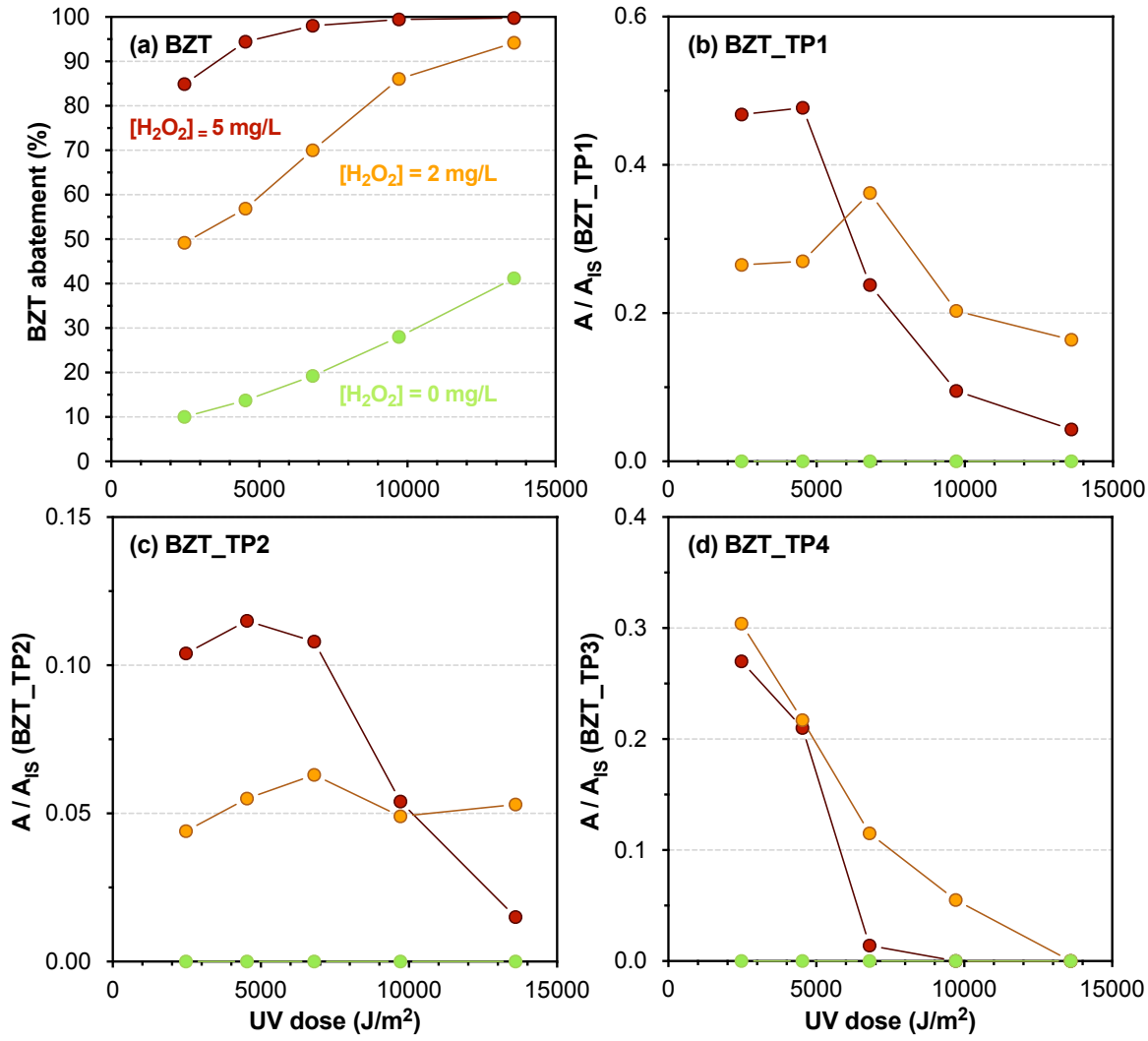

*Fig. 5.39 – Abatement of (a) benzotriazole (BZT) and the evolution of three transformation products for UV/H_2O_2-treatment as a function of the UV and the hydrogen peroxide dose: (b) BZT_TP1, (c) BZT_TP2 and (d) BZT_TP3 (according to **Tab. 5.5**). Conditions: Hardwald groundwater, UV doses = from 2500 to 13600 J/m², [H_2O_2] = 0, 2 and 5 mg/L.*

Acesulfame (ACE)

No transformation products were detected after O_3/H_2O_2 while one was measured during oxidation of acesulfame by UV/H_2O_2 treatment (**Fig. 5.40**). Its presence was decreased when increasing the H_2O_2 dose. However, the UV dose has no significant influence on its formation and degradation.

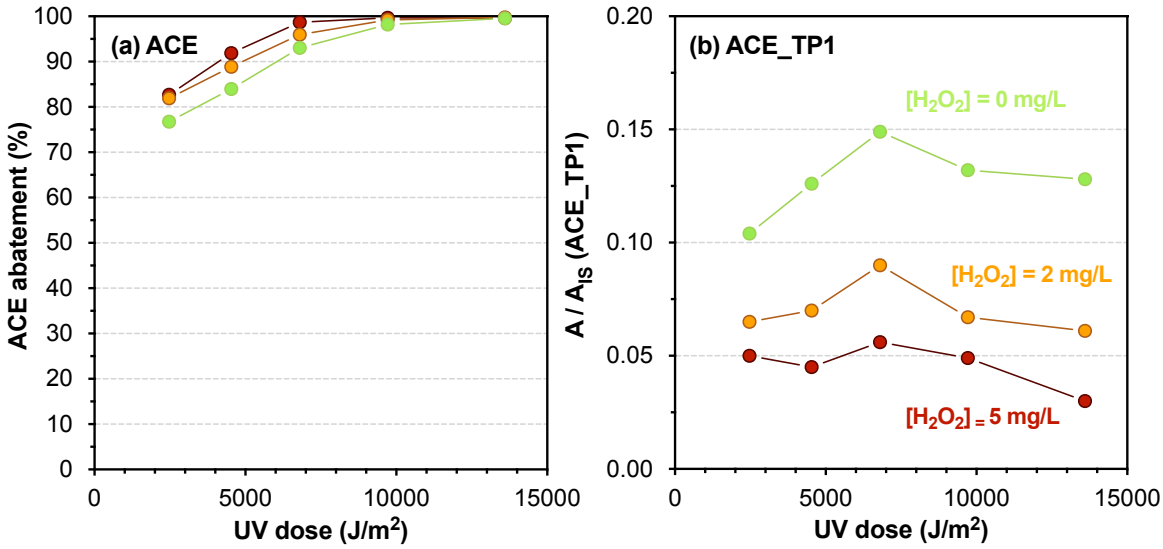

Fig. 5.40: *Abatement of (a) acesulfame (ACE) and the evolution of one transformation product for UV/H_2O_2-treatment as a function of the UV and the hydrogen peroxide dose: (b) ACE_TP1. Conditions: Hardwald groundwater, oxidation - UV doses = from 2500 to 13600 J/m², [H_2O_2] = 0, 2 and 5 mg/L.*

Sucralose (SUC)

Two transformation products were quantified when sucralose was oxidized by O_3/H_2O_2. As expected, no transformation products could be detected during ozonation without H_2O_2, since sucralose has a very low reactivity with ozone. With the addition of H_2O_2, their formation increased, however, the influence of the ozone dose is unclear. The formation of the transformation products is higher for 0.5 mg/L of ozone compare to a dose of 1.0 mg/L, however, the highest ozone dose (i.e., 2.0 mg/L) provided the highest concentrations of transformation products.

The direct photolysis of sucralose was almost negligible and consequently, as shown in **Fig. 5.42**, no transformation products were detected. Nevertheless, sucralose was oxidized to up to 73% with the maximum H_2O_2 and UV doses tested (i.e., 5 mg/L H_2O_2 and 13600 J/m²). Consequently, SUC_TP1 and SUC_TP2 were formed and a maximum relative concentration was observed for a H_2O_2 dose of 5 mg/L and a UV dose of 9600 J/m² for both transformation products. This corresponds to an abatement of about 60-65% of sucralose.

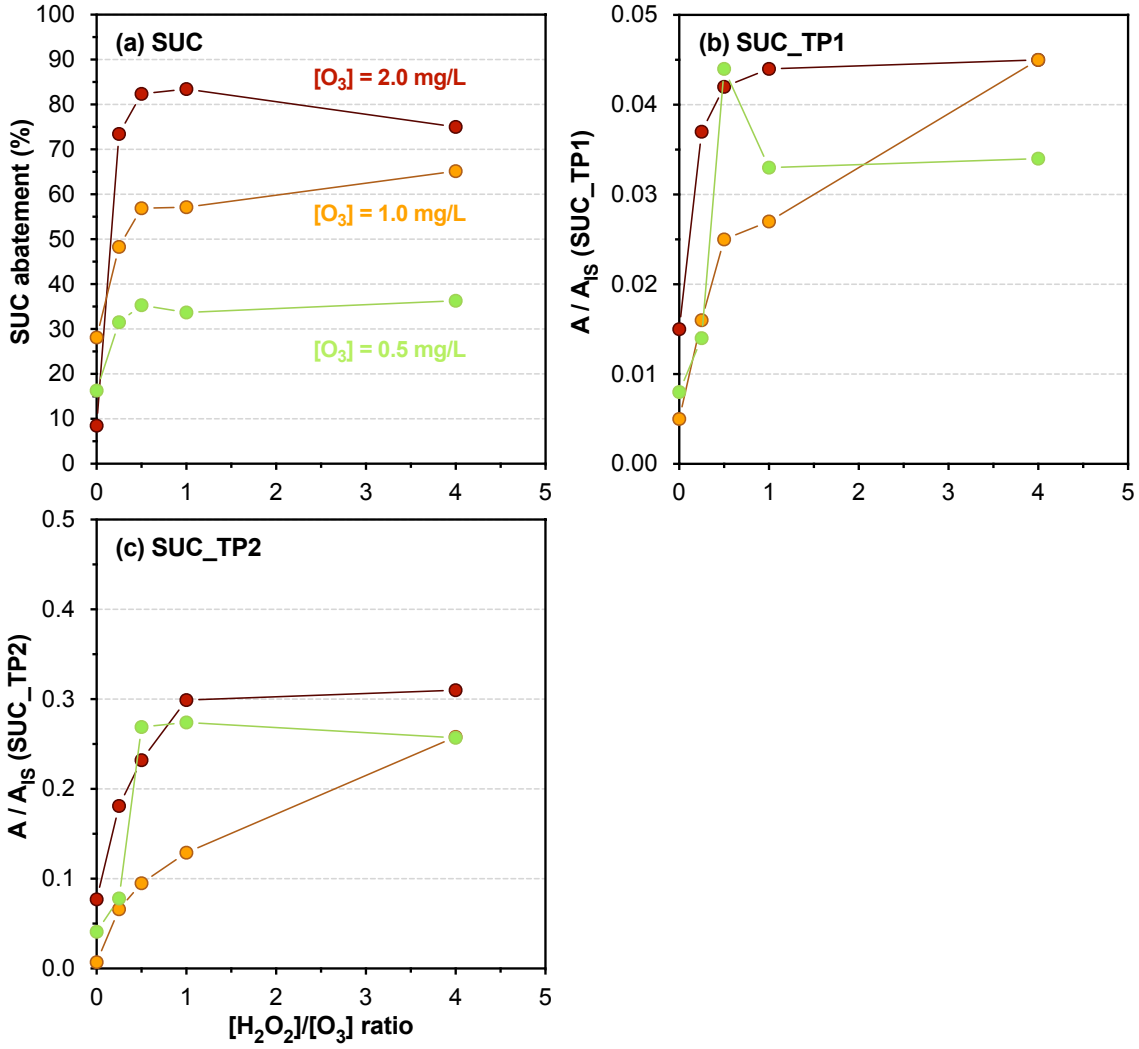

Fig. 5.41: *Abatement of (a) sucralose (SUC) and the evolution of two transformation products during ozonation and the AOP O_3/H_2O_2 as a function of the ozone dose and the H_2O_2:O_3 ratio: (b) SUC_TP1 and (c) SUC_TP2 (according to Tab.* ***5.5****). Conditions: Hardwald groundwater, $[O_3]$ = 0.5, 1.0 and 2.0 mg/L, molar $[H_2O_2]/[O_3]$ = 0, 0.25, 0.5, 1 and 4.*

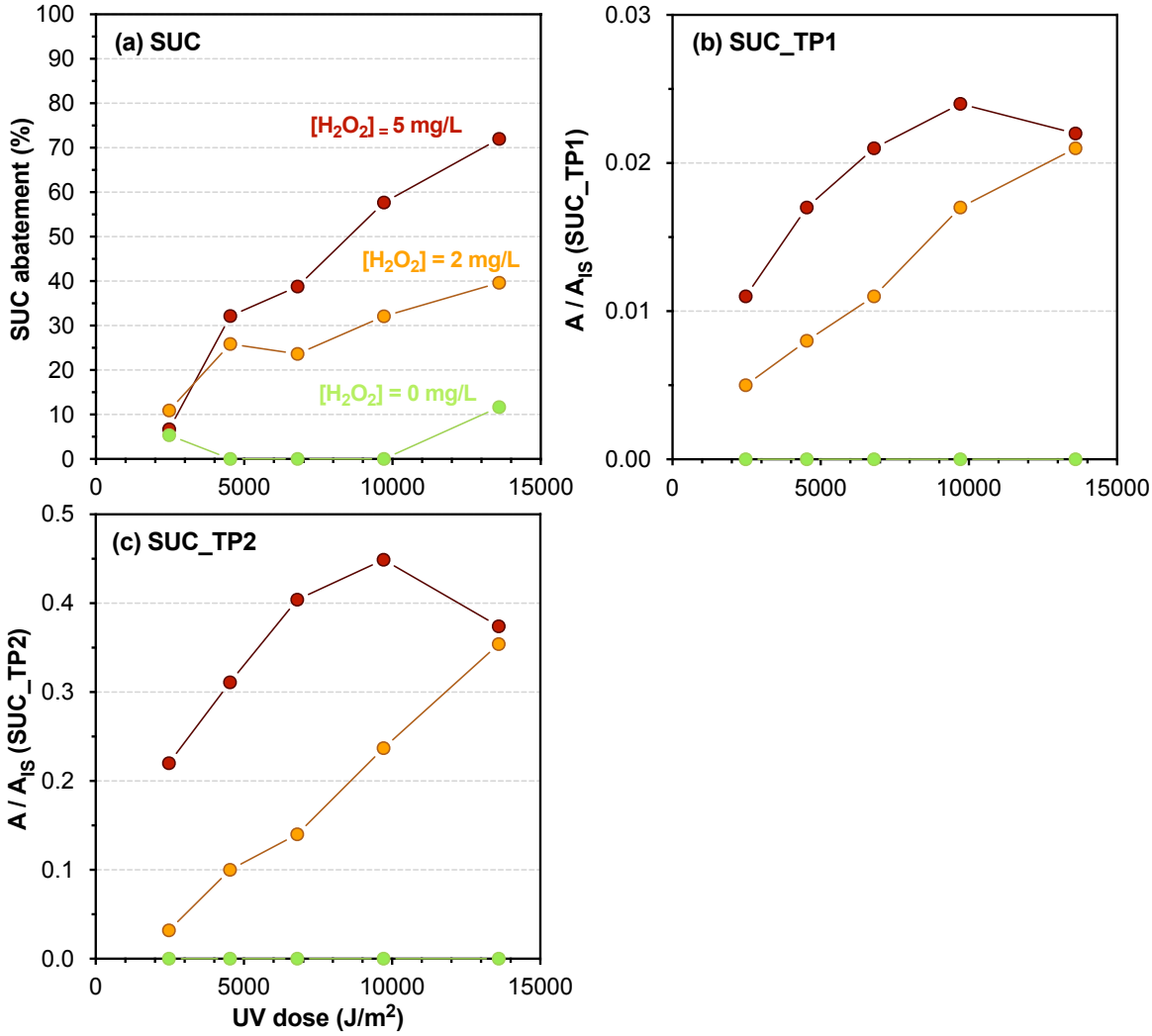

Fig. 5.42: *Abatement of (a) sucralose (SUC) and the evolution of one transformation product for UV/H_2O_2-treatment as a function of the UV and the hydrogen peroxide dose: (b) SUC_TP1 and (c) SUC_TP2) (according to Tab.* ***5.5****). Conditions: Hardwald groundwater, UV doses = from 2500 to 13600 J/m², [H_2O_2] = 0, 2 and 5 mg/L.*

Iopamidol (IOA)

Two transformation products from iopamidol oxidation by O_3/H_2O_2 treatment were quantified (Fig. 5.43). IOA_TP1 seems to be formed to a higher extent in presence of H_2O_2 but the molar H_2O_2/O_3 ratio did not have a consistent influence on its formation. The concentration of IOA_TP2 increased with increasing ozone doses. This compound was not detected for an elimination of iopamidol < 50%.

For the UV/H_2O_2 process, the elimination of iopamidol and IOA_TP1 were significant. For a low UV dose of 2500 J/m², iopamidol was oxidized at least by 60% even in absence of H_2O_2. An icrease of the H_2O_2 dose led to a higher formation of IOA_TP1, which is attenuated when the UV dose increased. For instance, its formation is attenuated by a factor of 20 when the UV dose was raised from 2500 to 9700 J/m².

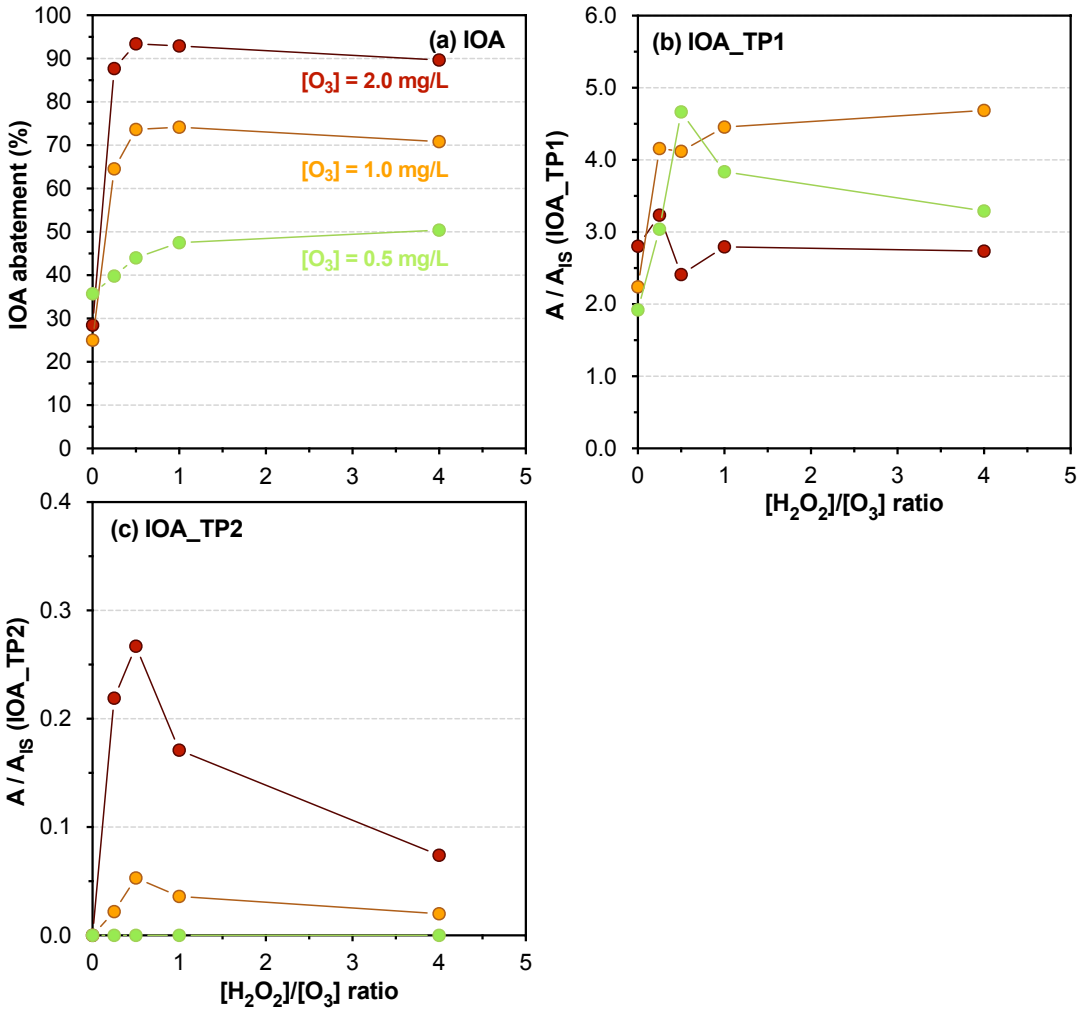

Fig. 5.43 – Abatement of (a) iopamidol (IOA) and the evolution of two transformation products during ozonation and the AOP O_3/H_2O_2 as a function of the ozone dose and the molar H_2O_2:O_3 ratio: (b) IOA_TP1 and (c) IOA_TP2 (according to Tab. ***5.5****). Conditions: Hardwald groundwater, $[O_3]$ = 0.5, 1.0 and 2.0 mg/L, molar $[H_2O_2]/[O_3]$ = 0, 0.25, 0.5, 1 and 4.*

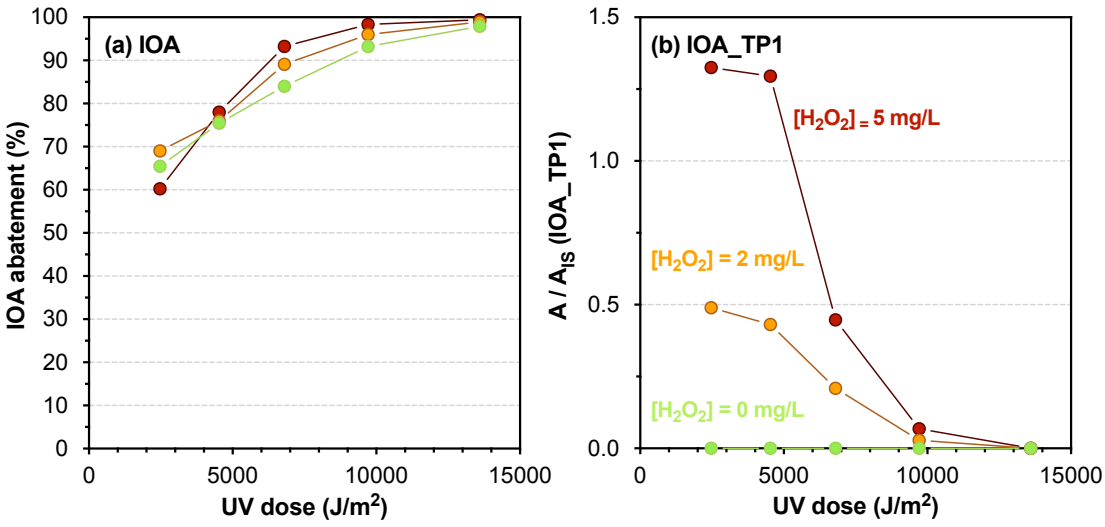

Fig. 5.44: *Abatement of (a) iopamidol (IOA) and the evolution of one transformation product for UV/H_2O_2-treatment as a function of the UV and the hydrogen peroxide dose: (b) IOA_TP) (according to Tab.* ***5.5****). Conditions: Hardwald groundwater, UV dose = from 2500 to 13600 J/m², $[H_2O_2]$ = 0, 2 and 5 mg/L.*

5.2.3.5 ADSORPTION OF TRANSFORMATION PRODUCTS ON PAC

It can be expected that transformation products would be less adsorbable on PAC than the corresponding parent compounds because transformation products are typically more polar. An adsorption experiment with several doses of PAC was performed after O_3/H_2O_2 and the results were compared with the data in **Fig. 5.29** showing the adsorption of the parent compounds (**Fig. 5.45**).

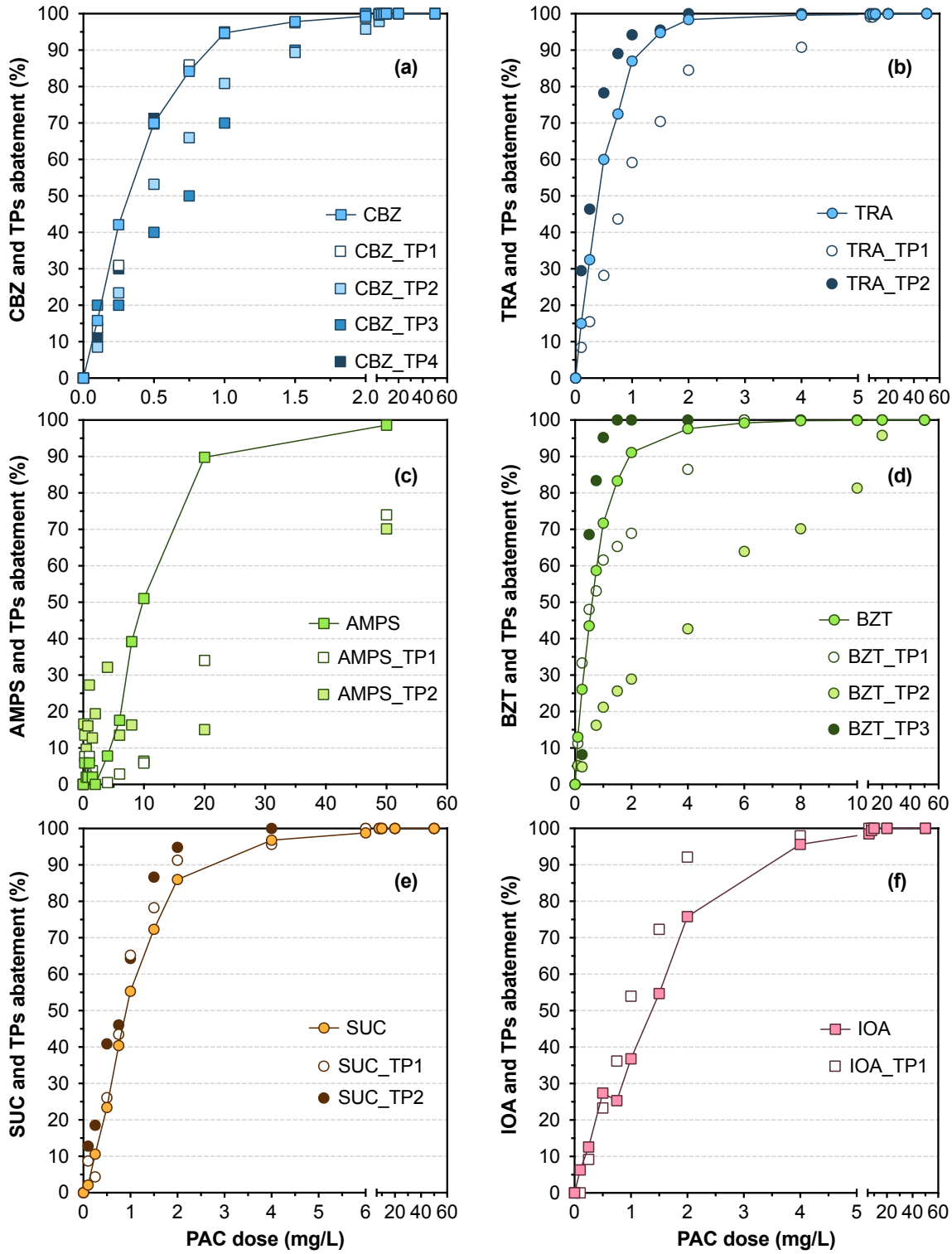

Fig. 5.45: *Adsorption of micropollutants and transformation products on PAC. (a) Carbamazepine, (b) tramadol, (c) AMPS, (d) benzotriazole, (e) sucralose and (f) iopamidol and their associated transformation products. Treatment conditions: Hardwald groundwater, oxidation - [O_3] = 0.5 mg/L, molar [H_2O_2]/[O_3] = 1; adsorption - [PAC] = 0 to 50 mg/L, contact time: 5 days, T = 12°C.*

For carbamazepine, the adsorption of transformation products was similar as for the parent compounds (CBZ_TP1 and CBZ_TP4) or lower (CBZ_TP2 and CBZ_TP3). For tramadol and benzotriazole, one transformation product for each was more adsorbable than the parent compounds (TRA_TP2 and BZT_TP3) while one was less adsorbable for tramadol (TRA_TP1) and two for benzotriazole (BZT_TP1 and BZT_TP2). BZT_TP2 shows a higher difference of adsorbability between transformation product and parent compound. For sucralose and iopamidol, the targeted transformation products were more adsorbable than the parent compounds. Results are more scattered for AMPS (especially for small PAC doses) but overall its transformation products are less retained on activated carbon.

5.2.3.6 BIODEGRADATION OF TRANSFORMATION PRODUCTS DURING SAND FILTRATION

Short-term experiments were also run with the sand filter. Micropollutants and transformation products were analysed before and after the sand filter and the abatements are reported in **Tab. 5.6**. Except for iopamidol, all transformation products were better biodegraded than the parent compounds. However, this abatement was only up to 64% for BZT_TP1. We expect that a longer contact time in the sand filter might improve the biodegradation.

Tab. 5.6: *Abatement of parent compounds and transformation products during the sand filtration - treatment conditions: oxidation - $[O_3]$ = 0.5 mg/L, molar $[H_2O_2]/[O_3]$ = 1; biofiltration – contact time = 5 min.*

	Biodegradation during sand filtration (%)
CBZ	0
CBZ_TP1	27
CBZ_TP2	15
CBZ_TP3	n.a.(1)
CBZ_TP4	28
TRA	0
TRA_TP1	25
TRA_TP2	30
AMPS	0
AMPS_TP1	18
AMPS_TP2	13
BZT	0
BZT_TP1	64
BZT_TP2	34
SUC	0
SUC_TP1	n.a.(1)
SUC_TP2	37
IOA	8
IOA_TP1	0

(1) values too low

5.3 REFERENCES

von Sonntag, C., von Gunten, U., 2012. Chemistry of ozone in water and wastewater treatment: From basic principles to applications. IWA publishing.

6 A NOVEL OXIDATION PROCESS FOR MICROPOLLUTANT ABATEMENT UNDER MINIMAL FORMATION OF BROMATE: O_3/H_2O_2/MEMBRANE

A patent has been submitted for this novel process: Ozone-based advanced oxidation process, 02.02.2016

This chapter is in preparation for publication: Merle, T.; Pronk, W.; von Gunten, U., Association of membrane and oxidation (O_3/H_2O_2) technologies to minimize the bromate formation (MOxiMiB) and abate micropollutants, **2017**, in preparation.

A novel oxidative treatment combining O_3, H_2O_2 and a membrane contactor was developed during this project. This novel technology aims to abate micropollutants with minimal bromate formation during ozonation. In this chapter, the performances of this new system will be compared to the conventional peroxone system. pCBA was used as a target compound and bromate formation was selected as the limiting parameter (i.e., the concentration of bromate after oxidation should not exceed 10 μg/L according to the Swiss drinking water standard).

6.1 MATERIALS AND METHODS

6.1.1 O_3/H_2O_2

Results presented for the O_3/H_2O_2 experiment are the same as those already presented in chapter 3.

6.1.2 O_3/H_2O_2/MEMBRANE

A scheme of the reactor is shown in **Fig. 6.1** and a picture of the set-up is presented in **Fig. 6.2**.

For the gaseous part, ozone was generated with a Triogen ozone generator (Ozonia) (1 in **Fig. 6.2**) fed with oxygen gas. The ozone gas concentration was measured directly after the ozone generator and regulated from 0.5 to 10 g/Nm^3 by changing the voltage of the ozone generator. For ozone concentrations < 5 g/Nm^3, the ozone gas was diluted using a second oxygen gas cylinder. The ozone gas was then introduced in a 2 L glass reactor (2 in **Fig. 6.2**) containing PTFE hollow fiber membranes (4 in **Fig. 6.2**). The gas flow rate was adjusted to get a residence time in the reactor of < 30 s. With that, the ozone consumption was considered as negligible and the ozone gas concentration in the reactor was assumed to be constant and equal to the initial concentration measured before the reactor. After the reactor, an ozone destructor was used to avoid ozone residual in the hood.

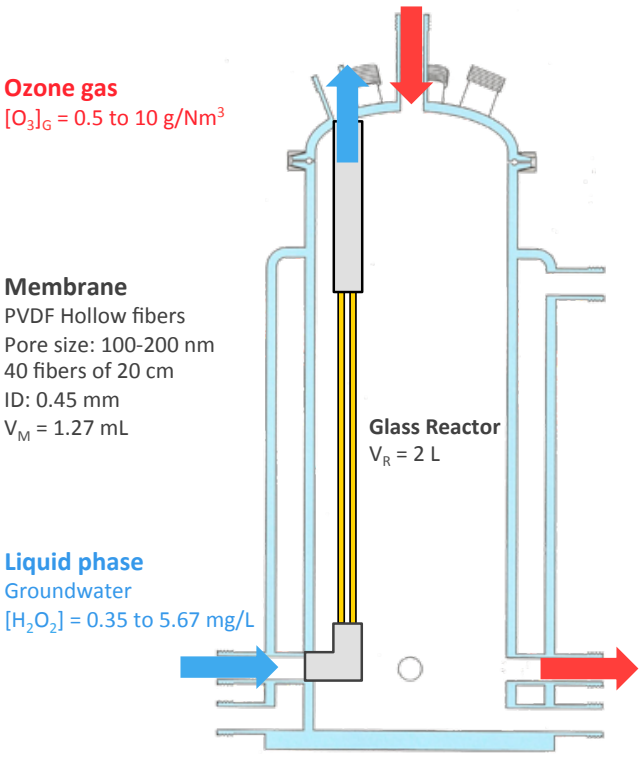

Fig. 6.1: *Scheme of the glass reactor used to perform the O_3/H_2O_2/membrane experiments*

Regarding the liquid part, Hardwald groundwater water was first spiked with differing concentrations of H_2O_2 (i.e., from 0.35 to 5.67 mg/L) and 100 µg/L of bromide. Then, a syringe pump was used to introduce the water inside the fibers located in the glass reactor. During the experiments, the water only flew inside the fibers, no water permeation across the membrane occurred. Only ozone gas permeated from the outside to the inside of the fibers by diffusion.

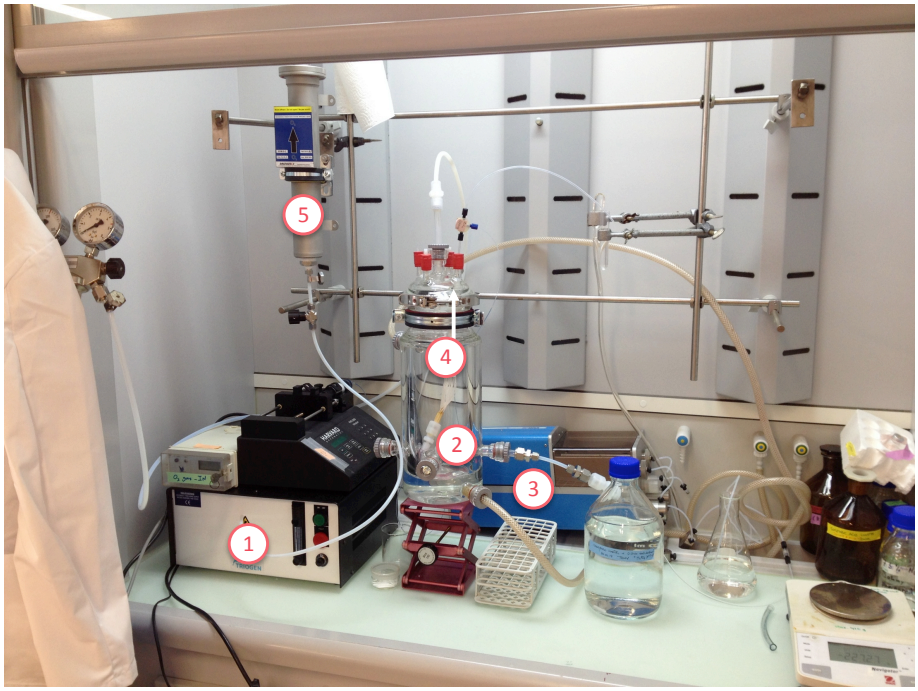

Fig. 6.2: *Picture of the set-up used to perform O_3/H_2O_2/membrane experiments. (1) ozone generator, (2) 2 L glass reactor, (3) syringe pump to inject water inside the fibers, (4) bundle of hollow fibers, (5) ozone destructor.*

6.2 RESULTS AND DISCUSSION

The main interest of the O_3/H_2O_2/membrane process is the possibility to inject ozone gas in small portions along the entire membrane fibers. In a conventional O_3/H_2O_2 process, H_2O_2 is injected before the ozonation reactor and O_3 is injected at once or at a few points into the reactor. Consequently, the dissolved ozone concentration is quite high in some zones of the reactor and BrO_3^- formation is favored because both ozone and °OH are present in relatively high concentrations. In the novel system described here, hollow fiber membranes are used as diffusors with almost an infinite number of gas injection points. Thereby, ozone can be dosed to reach a minimal dissolved concentration by optimizing the ozone gas concentration and the residence time of water in the fibers. Ozone will react with H_2O_2 to form °OH as soon as it will be introduced into aqueous phase. Under these conditions (low ozone concentrations and high formation of °OH), bromate formation is expected to be minimimal.

This hypothesis was confirmed by the results presented in **Fig. 6.3**. For a H_2O_2 dose of 5.67 mg/L, it was possible to abate 94% of *p*CBA using an ozone gas concentration of 0.5 g/Nm^3 and no bromate was detected after oxidation (i.e., below the limit of quantification of 0.5 µg/L). For the same pCBA abatement, a minimum of 8 µg/L was formed with the conventional O_3/H_2O_2 process. When the ozone gas concentration was increased to 1 g/Nm^3, the elimination of *p*CBA raised to more than 98% but 7.5 µg/L of bromate was formed in the O_3/membrane system. This concentration is still below the Swiss tolerance value and 45 µg/L of bromate was formed with the conventional O_3/H_2O_2 process.

For ozone gas concentrations higher than 1.0 g/Nm^3, the performances of O_3/H_2O_2/membrane process were worse than for the conventional O_3/H_2O_2 process.

It can be concluded that this novel process can be relevant to reduce bromate formation during ozonation, but further investigations are required for full-scale applications.

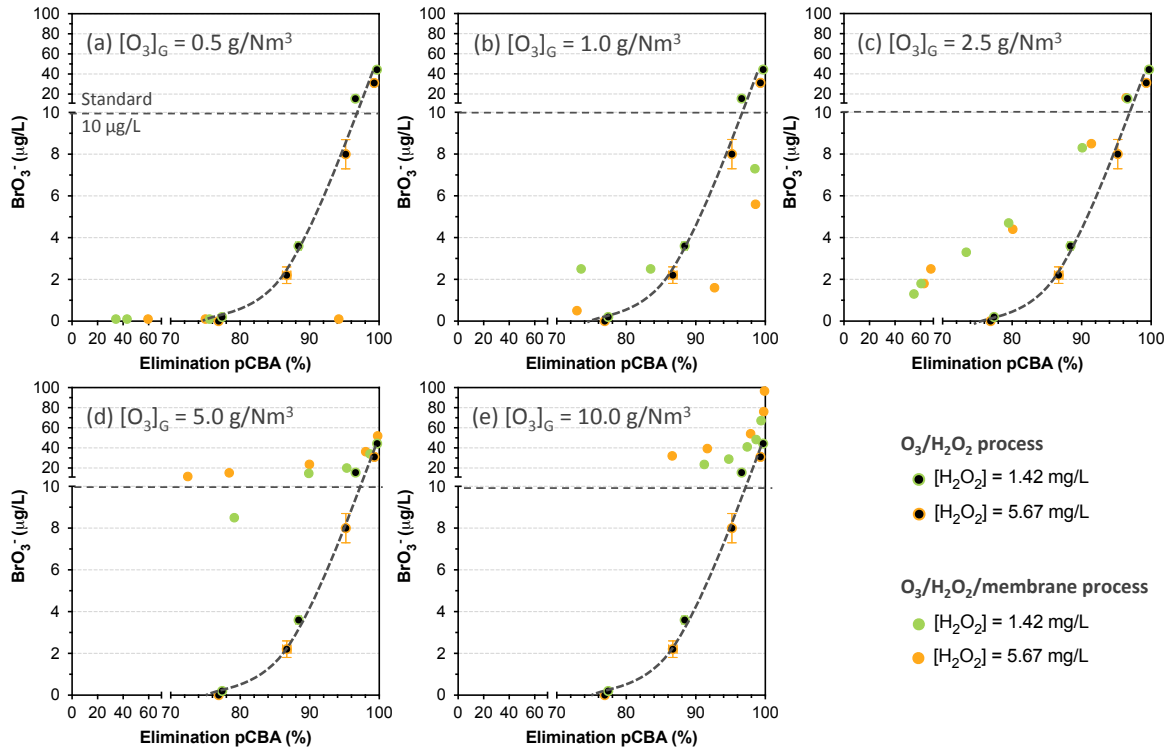

Fig. 6.3: *Abatement of para-chlorobenzoic acid (pCBA) and bromate formation by the conventional O_3/H_2O_2 process ([O_3] = 0.2 to 2 mg/L) and the O_3/H_2O_2/membrane process $[O_3]_G$ = (a) 0.5, (b) 1.0, (c) 2.5 (d) 5.0 and (e) 10.0 g/Nm^3 - Q_L = 0.25 to 1.5 mL/min) with Hardwald groundwater spiked with bromide. (Br = 170 +/- 5 µg/L, pH 8.1, DOC = 0.5 mgC/L).*

7 COMPARISON OF THE TREATABILITY OF HARDWALD GROUNDWATER AND RHINE RIVER WATER USING AOPS

The oxidation experiments performed with Hardwald groundwater and presented in sections 3.2 and 6.2 were also performed with Rhine river water to assess the possibility to directly treat this water instead of Hardwald groundwater in case of critical contaminations.

7.1 O_3/H_2O_2

As shown in **Fig. 7.1**, *p*CBA abatement in the O_3/H_2O_2 process was similar for both water qualities during ozonation without H_2O_2. However, the formation of bromate was much higher for Hardwald groundwater due to a lower DOC content (**Fig. 7.2**). In presence of H_2O_2, the degradation of *p*CBA was slightly better in Hardwald GW due to a lower quenching of hydroxyl radicals by natural organic matter but consequently the formation of bromate was still higher in this case (more O_3 available). The addition of H_2O_2 had no influence on *p*CBA abatement since the abatement was already high, however, with increasing H_2O_2 concentrations, bromate formation decreases.

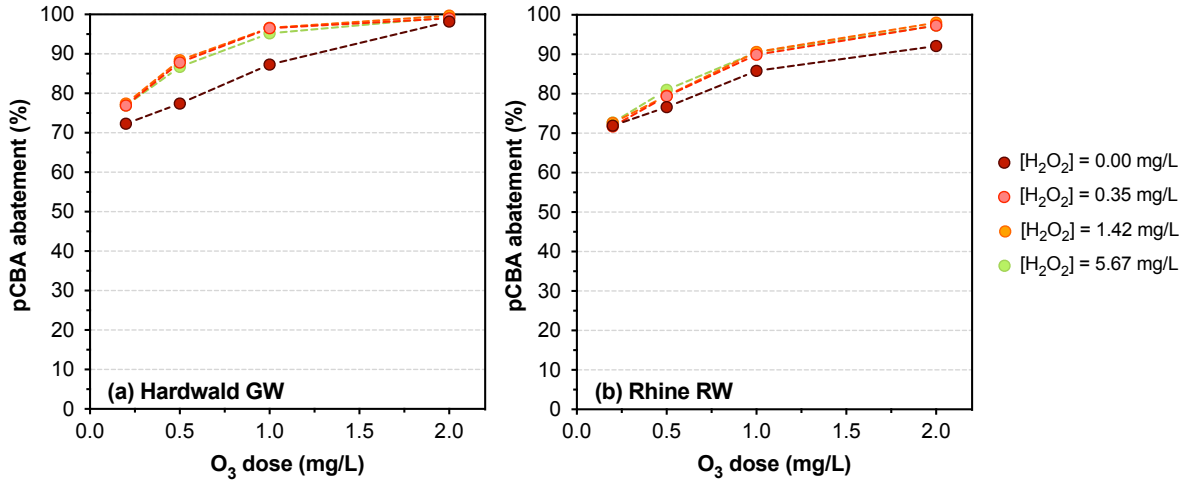

Fig. 7.1: *Comparison of pCBA abatement in (a) Hardwald GW and (b) Rhine RW by ozonation and O_3/H_2O_2. Conditions: [O_3] = 0.25 to 2.0 mg/L, [H_2O_2] = 0 to 5.67 mg/L; Hardwald GW: pH 8.13, [Br⁻] = 170 µg/L, [DOC] = 0.5 mgC/L; Rhine RW: pH 8.08, [Br⁻] = 205 µg/L, [DOC] = 1.3 mgC/L.*

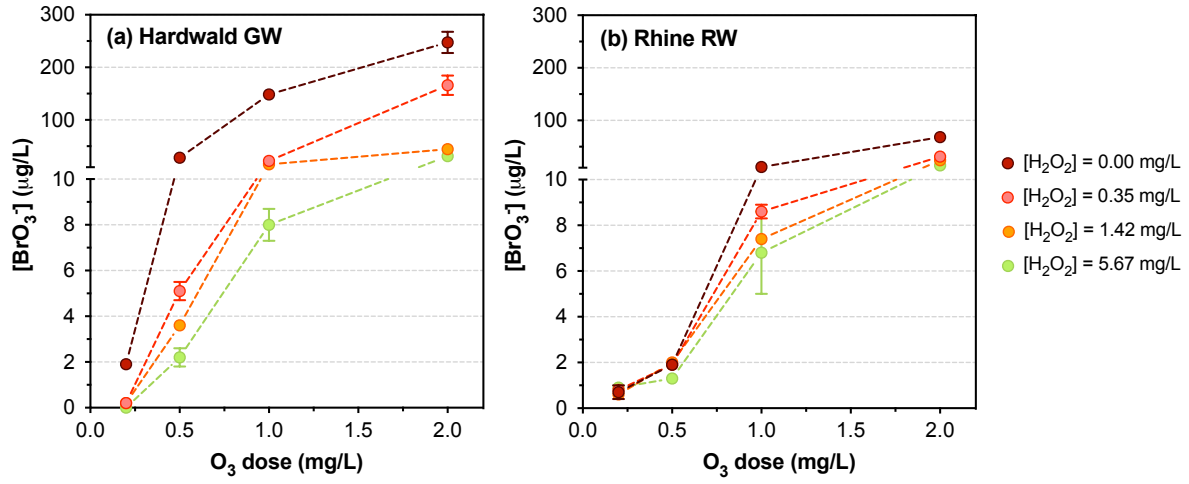

Fig. 7.2: *Comparison of bromate formation in (a) Hardwald GW and (b) Rhine RW for ozonation and O_3/H_2O_2. Conditions: [O_3] = 0.25 to 2.0 mg/L, [H_2O_2] = 0 to 5.67 mg/L; Hardwald GW: pH 8.13, [Br⁻] = 170 µg/L, [DOC] = 0.5 mgC/L; Rhine RW: pH 8.08, [Br⁻] = 205 µg/L, [DOC] = 1.3 mgC/L.*

7.2 UV/H_2O_2

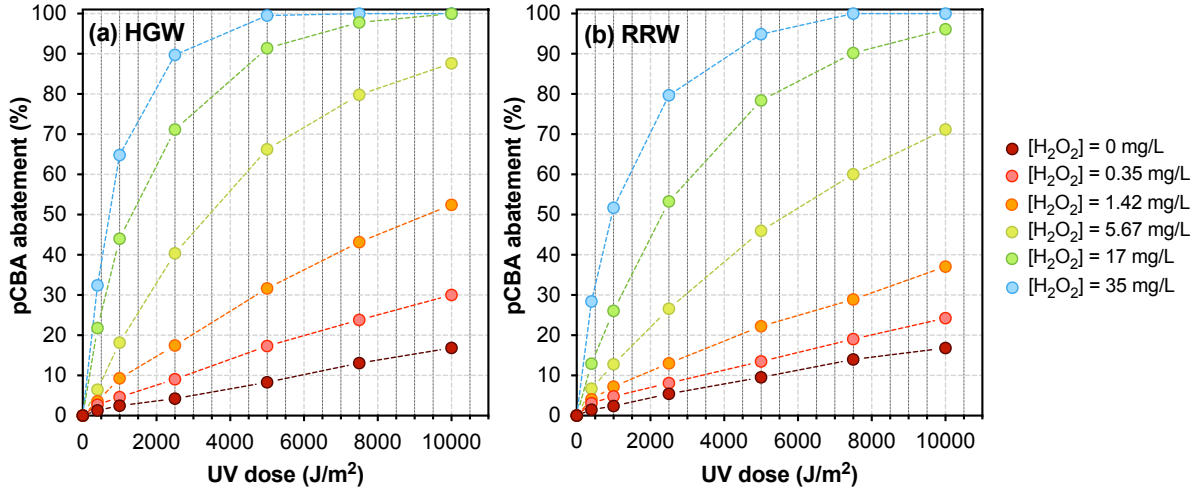

Fig. 7.3: *Comparison of pCBA abatement in (a) Hardwald GW (HGW) and (b) Rhine RW (RRW) by UV and UV/H_2O_2. Treatment conditions: UV doses = 400 to 10000 J/m², [H_2O_2] = 0 to 5.67 mg/L; Hardwald GW: pH 8.13, [DOC] = 0.5 mgC/L; Rhine RW: pH 8.08, [DOC] = 1.3 mgC/L.*

Overall, photooxidation was more efficient in Hardwald GW (**Fig. 7.3**). A *p*CBA abatement of 70% was obtained with a UV dose of 5600 J/m² and a H_2O_2 concentration of 5.67 mg/L while the UV dose (i.e., the energy demand) was 1.7 times higher to achieve the same abatement in Rhine RW. This was caused by the difference of the DOC concentration, which was higher in Rhine RW and led to a lower UV efficiency (light absorption) and a quenching of part of the °OH produced by photolysis of H_2O_2 with UV light.

7.3 O_3/H_2O_2/MEMBRANE

Fig. 7.4 compares the oxidation of *p*CBA with the O_3/H_2O_2/membrane process in Hardwald groundwater and Rhine river water. Under the same treatment conditions, the performance in terms of *p*CBA abatement and bromate formation with Rhine RW were as good as with Hardwald GW. Indeed, it was possible to achieve high *p*CBA elimination (up to 99% for an ozone gas concentration of 1 g/Nm³) and form less than 10 µg/L bromate. As for Hardwald GW, the *p*CBA abatement and the formation of bromate increased when the ozone gas concentration increased but results obtained for the ozone gas concentration of 1 g/Nm³ were still better than for the conventional O_3/H_2O_2.

It can be concluded that advanced oxidation processes can also be used with Rhine water instead of Hardwald groundwater. For ozone-based AOPs, the energy demand in the Hardwald groundwater is about 10% lower, whereas the bromate formation is smaller in Rhine river water. For UV/H_2O_2 the treatment of Hardwald groundwater requires about 60% of the energy, which is required in Rhine river water to achieve the same level of micropollutant abatement.

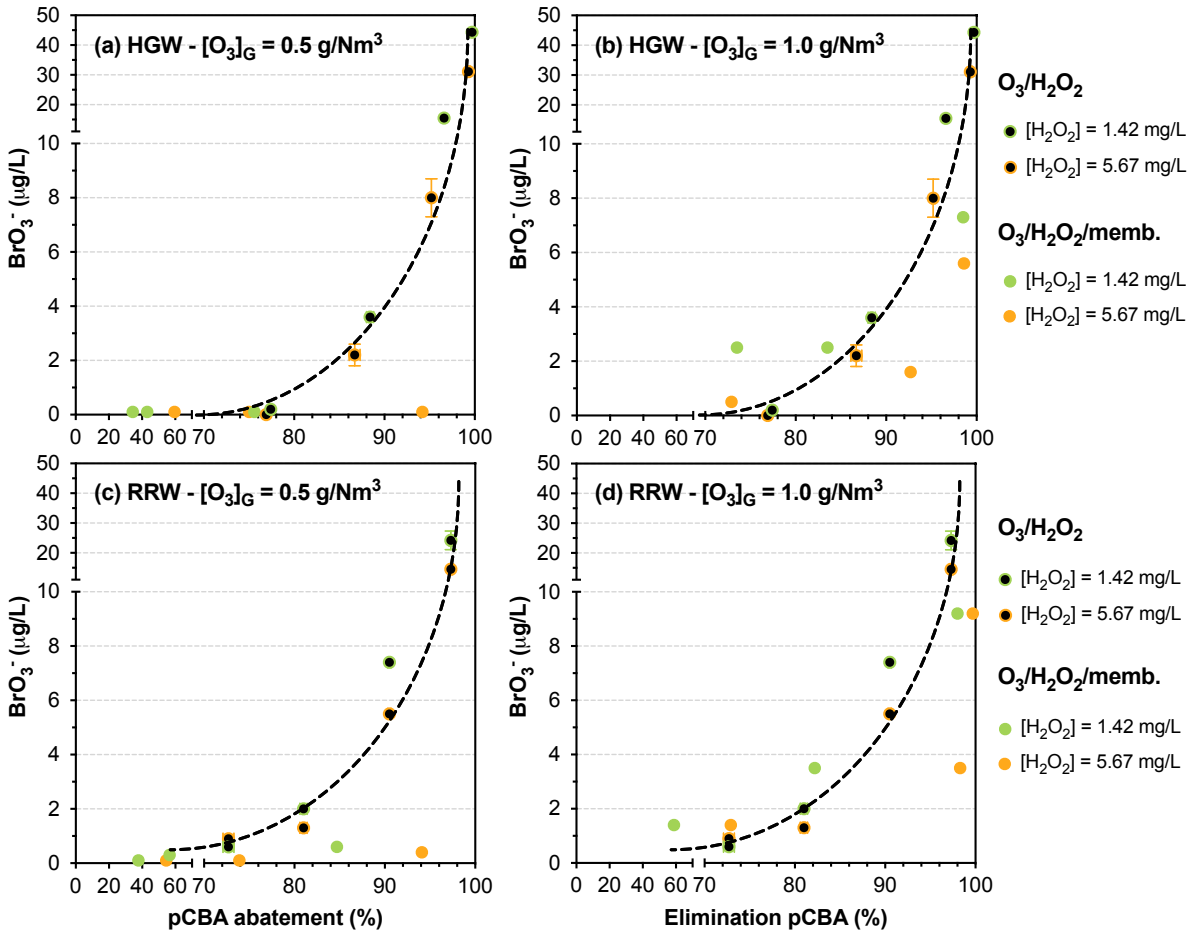

Fig. 7.4: *Comparison of bromate formation versus pCBA abatement in (a, b) Hardwald GW and (c, d) Rhine RW using O_3/H_2O_2 and O_3/H_2O_2/membrane. Conditions - O_3/H_2O_2: $[O_3]$ = 0.25 to 2.0 mg/L, $[H_2O_2]$ = 0 to 5.67 mg/L; O_3/H_2O_2/membrane: $[O_3]_G$ = 0.5 g/Nm³, Q_L = 0.25 to 1.5 mL/min; Hardwald GW: pH 8.13, [Br⁻] = 170 µg/L, [DOC] = 0.5 mgC/L; Rhine RW: pH 8.08, [Br⁻] = 205 µg/L, [DOC] = 1.3 mgC/L.*